Technical Report
TR-19-25
December 2019

Development and testing of methods suitable for quality control of bentonite as KBS-3 buffer and backfill

Daniel Svensson
Peter Eriksson
Lars-Erik Johannesson
Christel Lundgren
Terese Bladström

SVENSK KÄRNBRÄNSLEHANTERING AB

SWEDISH NUCLEAR FUEL
AND WASTE MANAGEMENT CO

Box 3091, SE-169 03 Solna
Phone +46 8 459 84 00
skb.se

SVENSK KÄRNBRÄNSLEHANTERING

ISSN 1404-0344
SKB TR-19-25
ID 1608673

December 2019
Updated 2021-01

Development and testing of methods suitable for quality control of bentonite as KBS-3 buffer and backfill

Daniel Svensson, Peter Eriksson, Lars-Erik Johannesson,
Christel Lundgren, Terese Bladström

Svensk Kärnbränslehantering AB

Keywords: Bentonite, Quality control, Error estimations, XRD, XRF, CEC, Swelling pressure, Thermal conductivity, Unconfined compression test, KBP1015.

Update notice

The original report, dated December 2019, was found to contain factual errors which have been corrected in this updated version. The corrected factual errors are presented below.

Updated 2021-01

Location	Original text	Corrected text
Page 91–93 and 95, Figure 6-10 – 6-14 and 6-17 – 6-18	Wrong values on y-axis	Figures updated with correct value on y-axis

Abstract

Development and testing of methods suitable for quality control of bentonite as KBS-3 buffer/backfill was performed. A number of different bentonite batches were also analysed, and some relations between the bentonite content (e.g. montmorillonite content) and its properties were studied.

The methods included in the report are targeting the following technical design requirements:

The installed buffer shall have a density that (1) have a swelling pressure when determined with a specific laboratory test procedure between 3 and 10 MPa, (2) have a hydraulic conductivity in saturated state < 10^{-12} m/s when determined with a specific laboratory test procedure, (3) yield an unconfined compressive strength at failure < 4 MPa at a deformation rate of 0.8 %/min when determined with a specific laboratory test procedure, and for material specimens in contact with waters with less favourable characteristics than site-specific groundwater, (4) have content of organic carbon < 1 wt%, sulfide ≤ 0.5 wt%, and total sulfur ≤ 1 wt%, (5) have a thermal conductivity over the installed buffer that, given the allowed decay power in the canister, the thermal properties of the canister and the rock and the canister spacing, yields a buffer temperature < 100 °C. The backfill shall (1) have a swelling pressure > 1 MPa when determined with a specific laboratory test, (2) have a hydraulic conductivity < 10^{-10} m/s when determined with a specific laboratory test, and (3) have impurities at a low enough level that they do not provide a significant source of sulfide, as this may corrode the copper canister.

The swelling pressure and hydraulic conductivity of Wyoming MX-80 was studied as a function of the montmorillonite content (the most common smectite in bentonite) by diluting the selected bentonite with different proportions of finely milled sand (representing naturally present accessory minerals in bentonite). The result showed that a montmorillonite decrease of 5 % by weight significantly lowered the swelling pressure and increased the hydraulic conductivity. Hence, the aim of the quality control of the bentonite buffer was decided from this observation to at least be able to detect relative differences in montmorillonite content somewhere in the range of 3–5 wt% to ensure predictability of buffer performance in terms of swelling pressure and hydraulic conductivity.

The methods included were X-ray diffraction (XRD), X-ray fluorescence spectroscopy (XRF), cation exchange capacity (CEC), interchangeable cations (EC), analysis of carbon and sulfur by evolved gas analysis (EGA), determination of swelling pressure, hydraulic conductivity, water content, density, unconfined compression test, compaction properties and thermal conductivity.

The following bentonite batches were examined:

Milos	2017	20 kg
Morocco	2017	20 kg
Bulgaria	2017	20 kg
Bulgaria	2018	20 tonnes
Bulgaria F	2017	200 kg
Turkey	2016	3 cans
Turkey	2017	200 kg
India	2018	20 tonnes
Wyoming B-K	2017	200 kg
Sardinia	2017	200 kg

XRD showed a repeatability for MX-80 bentonite of approximately ± 2.0 wt% montmorillonite (n = 3). However, more complex bentonites (several clay minerals) are expected to show higher scattering due to the more complex evaluation. XRD determination of montmorillonite in MX-80 as a function of added sand was highly linear (R^2 = 0.99). Exact identification of all mineral phases present in the bentonites was not always possible, and the Rietveld refinement fittings used for quantification were

not perfect, however, the quantified amount of montmorillonite and major phases was reasonable when compared to CEC and XRF, and relative changes in montmorillonite content in the target range seems reasonable to detect. The main factor affecting the variation in the quantification was neither the evaluation, nor the orientation of the montmorillonite, but the sample inhomogeneity and minor larger grains gave rise to strong individual reflections. This problem was solved by averaging results of 3 or more measurements. In the future the sample preparation will be further improved.

XRF showed different repeatability for each element, but was generally very good. Determinations of chemical indexes or ratios were tested as indirect measures of the montmorillonite content in a bentonite. To be useful this requires knowledge about the chemical composition of the accessory minerals, hence the same ratio is not usable in all types of bentonites. The XRF bias was determined by comparing the results of recent MX-80 analysis with ICP-AES analysis at an accredited external laboratory, and found to be acceptable. The XRF response was linear to sand ($R^2 = 0.99$) and feldspar additions ($R^2 = 0.99$). The standard deviation of the XRF data was very low, and somewhat different for different elements (e.g. Na_2O 0.008; MgO 0.008; Al_2O_3 0.019; SiO_2 0.013).

The CEC method showed good repeatability but less good reproducibility (measurements at different occasions). Hence, it is recommended to analyse all samples that are to be compared at once and to average triplicate samples in order to quantify small relative changes. The CEC was linear towards the function of added sand (Wyoming $R^2 = 0.99$; Indian bentonite $R^2 = 0.99$; Milos $R^2 = 0.99$).

XRD and CEC confirmed all bentonites to be of high montmorillonite or other smectite content, except the Milos bentonite that purposely was selected to have lower montmorillonite content. There are several possibilities for artefacts or man made errors in the XRD and the CEC method, however, by combining XRD, CEC, XRF and evolved gas analysis it is possible to minimise this risk from individual mistakes. These methods are the basis for quality control regarding the material content, and other techniques come in as a complement (e.g. EC).

EC typically showed somewhat larger sum than the CEC, this is common because of the minor dissolution of e.g. gypsum. In some cases EC-sum was much larger than CEC, this was attributed to the presence of clinoptilolite, a zeolite that can exchange with ammonium ions used in the EC measurement, but that cannot exchange with the Cu-tri complex. Presence of clinoptilolite is expected to lead to an over estimation of the montmorillonite (or other smectite) content if the supplier is using methylene blue or ammonium ions to quantify the CEC instead of Cu-tri. The repeatability of EC was found to be different for different elements, but was in the range of 0–9.6 % of relative duplicate difference.

Evolved gas analysis (EGA) showed some spread in the data. The testing of the EGA method was also done with different pre-treatments in order to remove carbonates, organic carbon or to add something.

Pre-treatment with hot acid worked very well to remove carbonates from Milos bentonite. Hydrogen peroxide (H_2O_2) did not remove organic carbon from MX-80, the content even seemed to increase, which was unexpected, most likely due to the uncertainty of the method at lower levels. Added organic carbon was detected at the largest addition. Samples with added carbonate seem to have been overestimated with regards to carbonate and may need further attention. Addition of sulfide was found, however it also gave rise to minor increase in the sulfate values, most likely an effect of oxidation of sulfide to sulfate. The Milos material was relatively high in sulfide and total sulfur, while the others all were low. All tested bentonites were low in organic carbon.

The swelling pressure and the hydraulic conductivity measurements involved measurements with both de-ionized water and with a 1 M $CaCl_2$-solution. The measured swelling pressure and hydraulic conductivity were depending on the dry density of the specimen and the type of bentonite. At the determinations the standard deviation of the method was also calculated, which reflects the accuracy in the measurements and also this varied between the bentonites. Most bentonites showed similar swelling pressure curves, however, the bentonite Bulgaria 2017 was significantly different from the others, showing higher swelling pressures at comparable densities.

The physical strength of the compacted bentonites was determined with a so called unconfined compression test. The strength was measured on total eight different bentonites and was very much depending on the dry density of the specimens. The variation between the different bentonites was small except for one bentonite, Bulgaria 2017, which had a much higher strength compared to rest

of the investigated bentonites. The standard deviation of the measurement was also calculated, which reflects the accuracy in the measurements. The standard deviation varied between the investigated bentonites and was highest for the bentonite Morocco 2017 and lowest for Turkey 2017.

The compaction properties of a bentonite are important as input for the design of the buffer and the backfill blocks but also at the production of them. The compaction properties were investigated with a laboratory test and the outcome of the test were, what dry density was possible to achieve and at what water content and compaction stress this could be made. An estimation of the accuracy of the determination was also made by repeating the compaction 30 times at the same conditions i.e. the same bentonite type, water content and compaction pressure.

The thermal properties of the bentonite have been determined with a transient plane source (TPS) sensor. The result shows that there is not a very large difference in the thermal conductivity between the different bentonite types measured in this report. The result is similar to measurements on thermal conductivity that have been done earlier. However, the thermal conductivity shows a quite large anisotropy were the thermal conductivity is larger perpendicular to the compaction direction.

The overall impression from the testing of the methods was that the included methods were relevant, their performance was suitable for the application, and seems to cover what is needed. However, further development and optimisations are expected in the future. All included bentonites seem to be potential candidates for use as buffer and/or backfill, with the exception of the included Milos bentonite that intentionally was lower in montmorillonite. Other qualities higher in montmorillonite from Milos would also be useful candidate materials.

Sammanfattning

Utveckling och testning av metoder för kvalitetskontroll av bentonit som KBS-3 buffert genomfördes. Ett antal olika bentoniter analyserades, och vissa relationer mellan bentonitinnehåll och egenskaper studerades, t ex effekten av montmorillonitinnehåll (den vanligaste smektiten i bentonit) på svälltrycket och den hydrauliska konduktiviteten.

Metoderna i rapporten är inriktade på följande tekniska designkrav:

Bufferten ska installeras med en densitet som (1) har ett svälltryck när det bestäms med ett specifikt laboratorietest mellan 3 och 10 MPa, (2) har en hydraulisk konduktivitet i mättat tillstånd < 10^{-12} m/s när den bestäms med ett specifikt laboratorietestförfarande. (3) enaxlig tryckhållfasthet < 4 MPa vid en deformationshastighet av 0.8 %/min vid bestämning med en specifik laboratorietestprocedur och för materialprover i kontakt med vatten med mindre gynnsamma egenskaper än platsspecifikt grundvatten, (4) ha ett innehåll av organiskt kol < 1 viktprocent, sulfid ≤ 0.5 viktprocent och total svavel ≤ 1 viktprocent, (5) ha en värmeledningsförmåga över den installerade bufferten, med tanke på det tillåtna sönderfallet i kapseln, kapslarnas och bergens egenskaper och kapselavståndet, vilket ger en buffertemperatur < 100 °C. Återfyllningen ska (1) ha ett svällningstryck > 1 MPa vid bestämning med ett specifikt laboratorietest, (2) ha en hydraulisk konduktivitet < 10^{-10} m/s när den bestäms med ett specifikt laboratorietest, och (3) inte vara en signifikant sulfidkälla, eftersom detta kan korrodera kopparkapseln.

Svälltrycket och den hydrauliska konduktiviteten hos MX-80 studerades som en funktion av montmorillonitinnehållet genom att späda MX-80 med olika mängder av finmald sand (vilket simulerade accessoriska mineral i en bentonit). Resultatet visar att en minskning av montmorillonit med 5 viktprocent signifikant gav ett lägre svälltryck och en högre hydraulisk konduktivitet. Därför gjordes bedömningen att kvalitetskontrollen av bentonitbufferten från denna observation åtminstone bör kunna detektera relativa skillnader i montmorillonithalt någonstans inom intervallet 3–5 vikt%.

Metoderna som inkluderades var röntgendiffraktion (XRD), röntgenfluorescensspektroskopi (XRF), katjonutbyteskapacitet (CEC), utbytbara katjoner (EC), analys av kol och svavel, svälltryck, hydraulisk konduktivitet, vattenhalt, densitet, hållfasthet, kompakteringsegenskaper och värmeledningsförmåga.

Följande bentonitbatcher undersöktes:

Milos	2017	20 kg
Morocco	2017	20 kg
Bulgaria	2017	20 kg
Bulgaria	2018	20 ton
Bulgaria F	2017	200 kg
Turkey	2016	3 burkar
Turkey	2017	200 kg
India	2018	20 ton
Wyoming B-K	2017	200 kg
Sardinia	2017	200 kg

XRD uppvisade en repeterbarhet för MX-80-bentonit på ungefär ± 2.0 viktprocent montmorillonit (n = 3). Men mer komplexa bentoniter (flera lermineraler) förväntas visa högre spridning. Exakt identifiering av alla mineralfaser som fanns närvarande i bentoniterna var inte alltid möjlig och Rietveldförfiningarna som genomfördes för kvantifiering var inte perfekta. Men den kvantifierade mängden montmorillonit och övriga huvudmineral var rimlig jämfört med CEC och XRF, och relativa förändringar i montmorillonitinnehållet i målområdet kunde detekteras på ett bra sätt. XRD-bestämning av montmorillonit i MX-80 som en funktion av tillsatt sand var linjär (R^2 = 0.99).

XRD-repeterbarhet var mycket hög. Den huvudsakliga faktorn som påverkade repeterbarheten i kvantifieringen var inte utvärderingen eller orienteringen av montmorilloniten, utan provhomogeniteten då mindre enstaka större korn gav upphov till starka individuella reflektioner. Detta problem löstes genom medelvärdesbildning av flera mätningar, men i framtiden kommer provprepareringen att förbättras.

XRF visade olika repeterbarhet för respektive element, men var generellt mycket bra. Bestämning av kemiska index eller förhållanden testades som indirekta mått av montmorillonithalten i en bentonit. För att vara användbar krävs det kunskap om den kemiska sammansättningen bimineralen. XRF bias bestämdes genom att jämföra resultaten med ICP-AES-analys vid ett ackrediterat externt laboratorium och befanns vara acceptabelt låg. XRF-responsen var linjär mot spädningar med sand ($R^2 = 0.99$) och fältspat ($R^2 = 0.99$). Standardavvikelsen för XRF-data var mycket låg och skiljde sig något för olika element (t ex Na_20 0.008; MgO 0.008; Al_20_3 0.019; SiO_2 0.013 vikt%).

CEC visade på hög repeterbarhet men lägre reproducerbarhet (mätning vid olika tillfällen). Genom att mäta på trippelprover och att alltid inkludera materialet man vill jämföra mot vid samma mätning bedöms metoden fylla ovan antagna krav. CEC var linjär mot funktionen av tillsatt sand (Wyoming $R^2 = 0.99$; indisk bentonit $R^2 = 0.99$; Milos $R^2 = 0.99$).

EC visade vanligen något större summa än CEC, detta är vanligt på grund av en mindre upplösningen av t ex gips. I vissa fall var EC betydligt större än CEC, vilket berodde på närvaron av clinoptilolit, en zeolit som kan jonbyta med ammoniumjoner (som används EC), men som inte kan jonbyta med Cu-trikomplexet. Närvaro av clinoptilolit förväntas leda till en överskattning av montmorillonitinnehållet om metylenblå eller ammoniumjoner används för att kvantifiera CEC istället för Cu-tri. Repeterbarheten hos EC visade sig vara annorlunda för olika element, men var inom intervallet 0–9.6 % av den relativa dubbla differensen.

Det finns flera möjligheter för artefakter eller misstag i XRD och CEC-metoden, men genom att kombinera XRD, CEC, XRF och kol och svavelanalyser är det möjligt att minimera denna risk. Dessa metoder utgör grunden för kvalitetskontroll avseende materialinnehållet och andra tekniker kommer in som ett komplement när det behövs (t ex EC).

Kvantifieringen av organiskt kol, karbonat, sulfid och sulfat testades genom tillsatser till bentoniten eller genom avlägsnande genom olika förbehandlingar. Kol och svavel analyser visade viss spridning i data, användandet av medelvärdesbildning av triplikat är också här ett bra val för pålitliga resultat. Förbehandling med varm syra fungerade mycket bra för att avlägsna karbonater från Milos bentonit. Väteperoxid (H_2O_2) avlägsnade inte organiskt kol från MX-80, innehållet verkade till och med öka, vilket sannolikt var en effekt av metodens osäkerhet vid låga nivåer. Tillagd organiskt kol detekterades vid den högsta tillsatsen. Prover med tillsatt karbonat verkar ha överskattats med avseende på karbonat vilket bör kontrolleras ytterligare. Addition av sulfid hittades, men det gav också upphov till mindre ökning av sulfatvärdena, sannolikt en effekt av oxidation av sulfid till sulfat. Milosbentoniten hade ett relativt högt innehåll av sulfid och totalt svavel, medan resterande bentoniter hade låga nivåer. Alla testade bentoniter hade lågt innehåll av organiskt kol.

Materialegenskaperna studerades också, och de är också viktiga kvalitetskontrollparametrar. Svälltrycket och den hydrauliska konduktiviteten bestämdes både med avjonat vatten och med en 1 M $CaCl_2$-lösning. Det uppmätta svälltrycket och den hydrauliska konduktiviteten var beroende av provets torrdensitet och bentonittyp. Vid bestämningarna beräknades också standardavvikelsen för metoden, vilket avspeglar noggrannheten i mätningarna. Standardavvikelsen varierade mellan de olika bentoniterna. De flesta av de undersökta bentoniterna uppvisade liknande svälltryck med undantag för bentoniten Bulgaria 2017 som var signifikant annorlunda. Den hade betydligt högre svälltryck vid jämförbara densiteter.

Hållfastheten hos de kompakterade bentoniterna bestämdes med ett så kallat enaxligt tryckförsök. Hållfastheten mättes på totalt åtta olika bentoniter och var mycket beroende på provets torrdensitet. Skillnaden mellan de olika bentoniterna var liten med undantag för Bulgaria 2017, som hade en mycket högre hållfasthet jämfört med resten av de undersökta bentoniterna. Standardavvikelsen på utförda mätningar beräknades också,. Den varierade mellan de undersökta bentoniterna och var högst för Marocco 2017 och lägst för Turkey 2017.

Kompakteringsegenskaperna hos en bentonit är viktiga att känna till vid designen av buffert- och återfyllningsblocken men också vid produktionen av dem. Kompakteringsegenskaperna undersöktes med ett laboratorieförsök där de olika bentoniterna kompakterades med varierande vatteninnehåll och kompakteringsspänning varefter bentonitens torrdensitet bestämdes. En uppskattning av noggrannheten hos bestämningen gjordes också genom att kompakteringen upprepades 30 gånger under samma betingelser, dvs med samma bentonit, vattenhalt och kompakteringsspänning.

De termiska egenskaperna hos bentoniten har bestämts med en TPS-sensor. Resultatet visar att det inte finns någon väldigt stor skillnad i värmeledningsförmågan mellan de olika bentonittyperna som mäts i denna rapport. Resultatet liknar mätningar på värmeledningsförmåga som tidigare gjorts. Den termiska konduktiviteten visar emellertid en ganska stor anisotropi, då värmeledningsförmågan är större vinkelrätt mot komprimeringsriktningen.

Intrycket från testningen av metoderna var att de inkluderade metoderna var relevanta, deras prestanda var lämplig för applikationen och verkar täcka vad som behövs. Ytterligare utveckling och optimering av metoderna förväntas i framtiden. Alla inkluderade bentoniter verkar vara potentiella kandidater för användning som buffert och/eller återfyllning, med undantag för den inkluderade Milosbentoniten, som avsiktligt hade lägre montmorillonithalt. Andra kvaliteter högre i montmorillonit från Milos skulle också vara användbara kandidatmaterial.

Contents

1 Introduction

Bentonite has been selected as a suitable buffer and backfill material in the KBS-3 concept (Figure 1-1) for its sealing properties such as: high swelling pressure, low hydraulic conductivity, appropriate plasticity and high long term stability. The active component in the bentonite are smectites (swelling clay minerals), most commonly the mineral montmorillonite. Montmorillonite swells (expands) upon hydration, and contracts upon dehydration. Bentonites from different parts of the world typically contain more or less unique montmorillonites (or other smectite), each with a specific chemical composition, grain density, particle size, surface charge etc (e.g. Karnland et al. 2006, Karnland 2010, Svensson et al. 2017). This leads to that different bentonites as well as different montmorillonites (or smectites) have different properties.

The purpose of this report is to summarise our recent development in methodology as well as the recent outcome of the analytical work performed during the time period of 2016–2018. The goal is increased understanding of the differences in important properties between the selected bentonites, as well as how they are affected by a change in the montmorillonite content, and how well this change in montmorillonite can be captured with the selected methods for quality control. The swelling pressure data is input for the target designed buffer dry density for the specific bentonites.

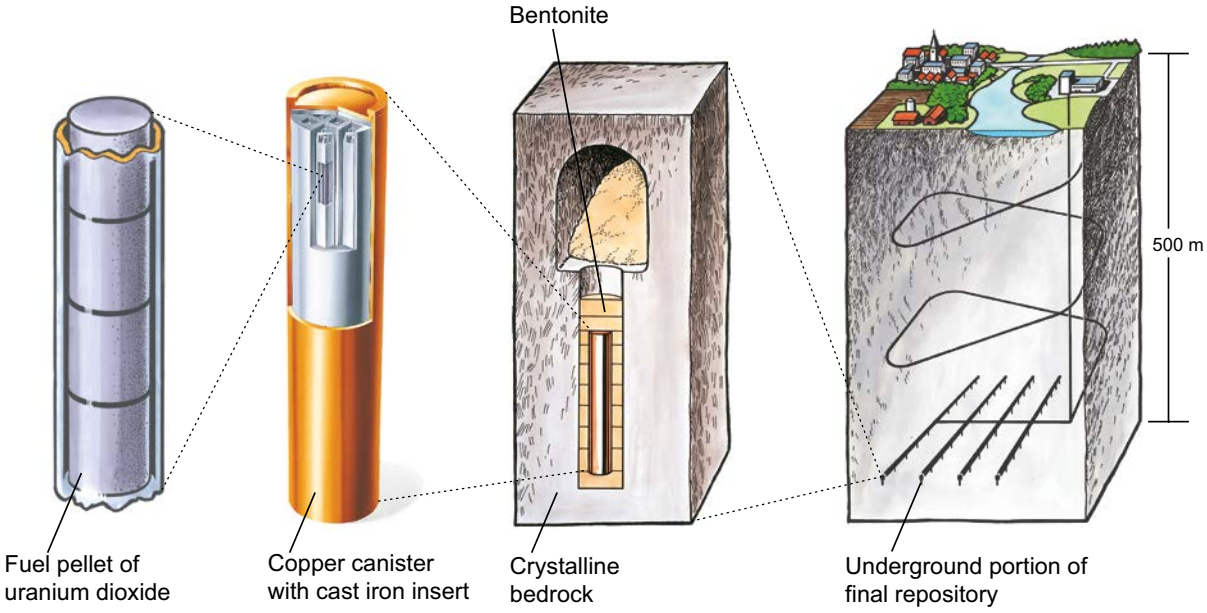

Figure 1-1. *Bentonite in the KBS-3 system.*

The structure of the report

The purpose of Chapter 2 is to give an overview of the relation between some of the bentonite technical requirements and central properties. Chapter 3 and 4 are describing recent method development of methods in Table 1-2. Some complementary methods are also used for some selected bentonites. Additionally method uncertainty estimations are included, as well as some method validation. The method uncertainties are critical during the quality control of the bentonite buffer. Chapter 5 and 6 describes the results from the characterisation of the selected bentonite batches (Table 1-1). This information can be usable for screening of bentonite properties, as background information during scientific or technical testing, or for further detailed design of buffer and backfill components.

Strategy for sampling and analysis

Each batch (Table 1-1) was sampled into 20 sub-batches where each one was analysed with XRF to give information about the homogeneity of the batch with regards to the chemical content. The 20 sub-batches were mixed and homogenised to a blend of 10 kg (composite sample), and this blend was characterised using the methods listed in Table 1-2. The methods were based on the work by Svensson et al. (2017), where justification for method selection is presented.

Wyoming MX-80 was analysed in parallel as an internal reference, and for some selected methods data for some odd samples were also included. During the testing of the methods some additional bentonites were sometimes also added sporadically.

The selected bentonites where included because of (i) large production capabilities, (ii) previously well described, or (iii) special properties such as very low iron content (Marocco).

Table 1-1. Overview of the characterised bentonite batches.

Bentonite	Year	Amount
Milos	2017	20 kg
Morocco	2017	20 kg
Bulgaria	2017	20 kg
Bulgaria	2018	20 tons
Bulgaria F	2017	200 kg
Turkey (3 types)	2016	3 jars
Turkey	2017	200 kg
India (Kutch)	2018	20 tons
Wyoming (B-K)	2017	200 kg
Sardinia	2017	200 kg

Table 1-2. Methods selected for main characterisation of bentonite batches. Based on Svensson et al. (2017).

Method	Abbreviation	Information/purpose
X-ray diffraction	XRD	Mineralogical content
X-ray fluorescence	XRF	Chemical content
Cation exchange capacity	CEC	Wet chemical technique for montmorillonite quantification
Exchangeable cations	EC	Montmorillonite interlayer composition
Evolved gas analysis	EGA	Carbon and sulfur quantification of different types.
Swelling pressure	SP	Inhibit microbiological activity while not impacting the canister. Self-sealing
Hydraulic conductivity	HC	Ensure slow water transport
Water content	WC	Important for the dry mass of the bentonite
Density	D	E.g. SP and HC are functions of the density
Unconfined compression test	UCT	Physical strength of compacted bentonite
Thermal conductivity	TC	Keeping the temperature of the bentonite low
Grain density		To calculate void ratio
Compaction properties		For designing components
Granular size distribution		Important for compaction

2 Bentonite technical design requirements and central properties

Most of the buffer and backfill requirements (Section 2.1) are related somehow to the content of the bentonite. In this section attempts are made to link the swelling and sealing (hydraulic conductivity) properties of the bentonite clay to the montmorillonite content and/or type. The montmorillonite content in weight percent (Section 2.2), the type of montmorillonite (origin), and the type of interlayer cations are discussed (Section 2.3). Chapter 2 is not intended to be fully comprehensive but rather to give a background, context and motivation to the work presented in the following chapters.

The experimental work with different montmorillonite contents were performed during this project, while the experimental work with different montmorillonites and interlayer cations is summarised and reproduced from Svensson (2015), with permission from the author. In the current work, swelling was measured as swelling pressure, while in Svensson (2015) swelling was measured as interlayer basal spacing's using synchrotron X-ray diffraction with the clay suspended in liquid water. These different ways of measuring the swelling are not identical, but are expected to show similar trends.

2.1 Current buffer and backfill requirements

The following technical design requirements are from the Posiva SKB (2017):

Buffer

1. The minimum dry density yielding a swelling pressure > 3 MPa when determined with a specific laboratory test procedure. The maximum dry density yielding a swelling pressure < 10 MPa when determined with a specific laboratory test procedure.
2. The minimum dry density yielding a hydraulic conductivity in saturated state < 10^{-12} m/s when determined with a specific laboratory test procedure.
3. The maximum dry density yielding an unconfined compressive strength at failure < 4 MPa at a deformation rate of 0.8 %/min when determined with a specific laboratory test procedure, and for material specimens in contact with waters with less favourable characteristics than site-specific groundwater.
4. The content of **organic carbon** shall be **< 1 wt%, sulfide ≤ 0.5 wt%** (of the total mass; corresponding to approximately 1 wt% of pyrite), and **total sulfur ≤ 1 wt%**.
5. The **thermal conductivity** over the installed buffer shall, given the allowed decay power in the canister, the thermal properties of the canister and the rock and the canister spacing, yield a **buffer temperature < 100 °C**.

Backfill

1. An acceptable dry density is one giving a swelling pressure > 1 MPa when determined with a specific laboratory test.
2. The minimum dry density yielding a hydraulic conductivity < 10^{-10} m/s when determined with a specific laboratory test.
3. **Impurities** in the backfill shall **not provide a significant source of sulfide**, as this may corrode the copper canister.

2.2 Bentonite swelling pressure

The swelling pressure is a central technical design requirement. In addition to continuously monitor the swelling pressure, it is important to know what parameters that affects it, and control those parameters. The swelling pressure is affected by a multitude of parameters (Figure 2-1). Two of the most critical ones are the montmorillonite content and the density. The swelling pressure discussed here is regarding water saturated samples in contact with an external water or solution.

If the buffer expands into the deposition tunnel (e.g. by water saturation in the lower part of the hole) the buffer bentonite density is expected to decrease. If the buffer is eroded into the minor fractures in the rock, the density also decreases. However, if montmorillonite is altered into another non-swelling mineral, the density remains intact, while the montmorillonite content decrease. The montmorillonite content can also decrease due to variations in the delivery. In order to predict the outcome of these factors the swelling pressure (Figure 2-2), and the hydraulic conductivity (Figure 2-3) has to be described as a function of density and montmorillonite content. These relations are also central when developing methods for bentonite quality control (what to control, and how well must it be done). E.g. a 5 % decrease in montmorillonite of the bentonite will somewhat decrease the swelling pressure (Figure 2-2).

The salinity can increase or decrease in the repository with time as well as the type of interlayer cation, which is why the swelling pressure is measured using the most extreme cases expected, deionised water and a 1 M $CaCl_2$-solution.

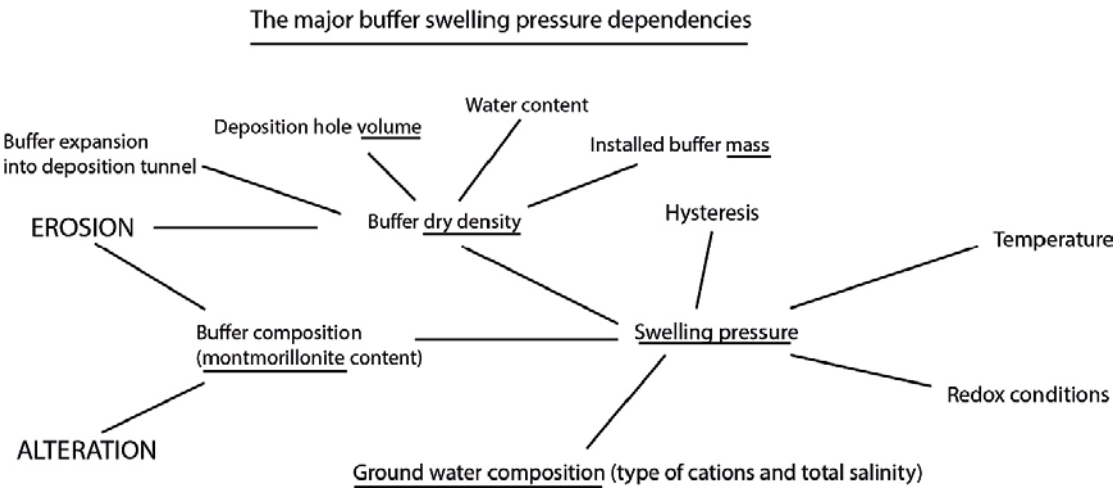

Figure 2-1. *Overview of the major swelling pressure dependencies. Other properties such as sealing capacity have similar dependencies.*

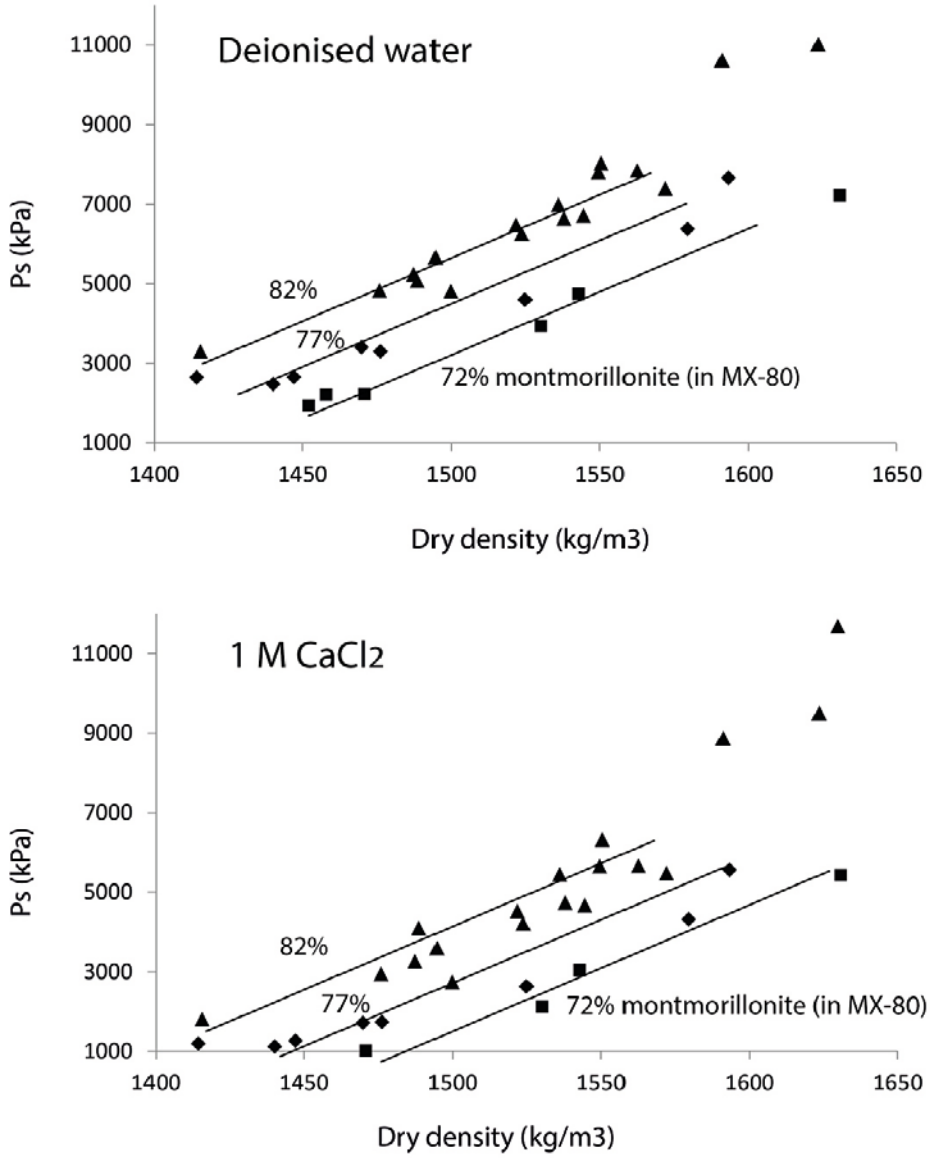

Figure 2-2. *The swelling pressure in MX-80 bentonite as a function of montmorillonite content (by dilution with milled sand) and density using deionised water and 1 M $CaCl_2$ solution. The density in this dataset was not corrected for its salt content. Lines are added as guides for the eyes.*

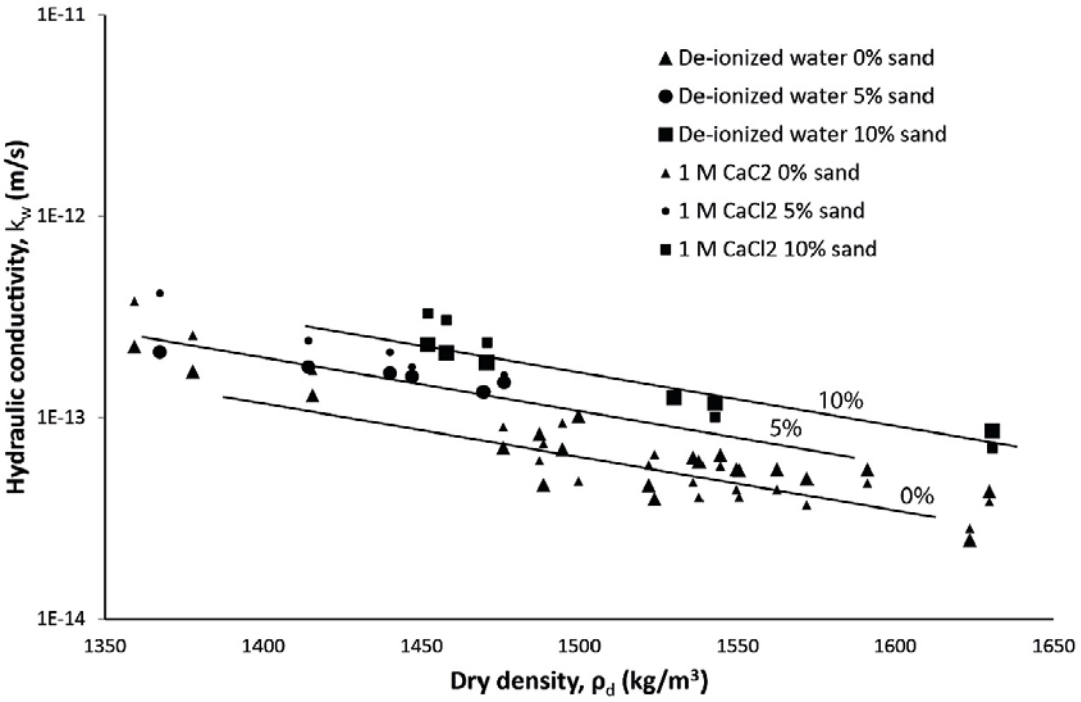

Figure 2-3. *The hydraulic conductivity in MX-80 bentonite as a function of sand dilution (affecting the montmorillonite content) and density using deionised water and 1 M $CaCl_2$ solution. The density in this dataset was not corrected for its salt content. Lines are added as guides for the eyes.*

2.3 Interlayer cation and swelling properties

Montmorillonite with a monovalent interlayer cation such as Na^+ have at low ionic strength more or less infinite swelling possibilities (osmotic swelling) only restricted by the liquid/solid ratio (Figure 2-4). While montmorillonites with divalent interlayer cations such as Ca^{2+} and Mg^{2+} have a restricted swelling (crystalline swelling) typically in the range of 3–4 layers of hydration water depending on the temperature (Svensson and Hansen 2010). This leads to that sodium dominated bentonites have higher swelling pressures at low densities, however at high densities, this may no longer be the case as it is not the restricted amount of swelling that sets the swelling pressure but rather the total balance between the hydration energy and the contractive forces in the clay such as Coulombic and van der Waals interactions and ion-ion correlation effects. For a specific montmorillonite the swelling in terms of basal spacing in water seems to generally increase when increasing the Gibbs hydration energy of the interlayer cation and to decrease when increasing the layer charge hence increasing the attractive Coulombic layer-layer interaction (Svensson 2015).

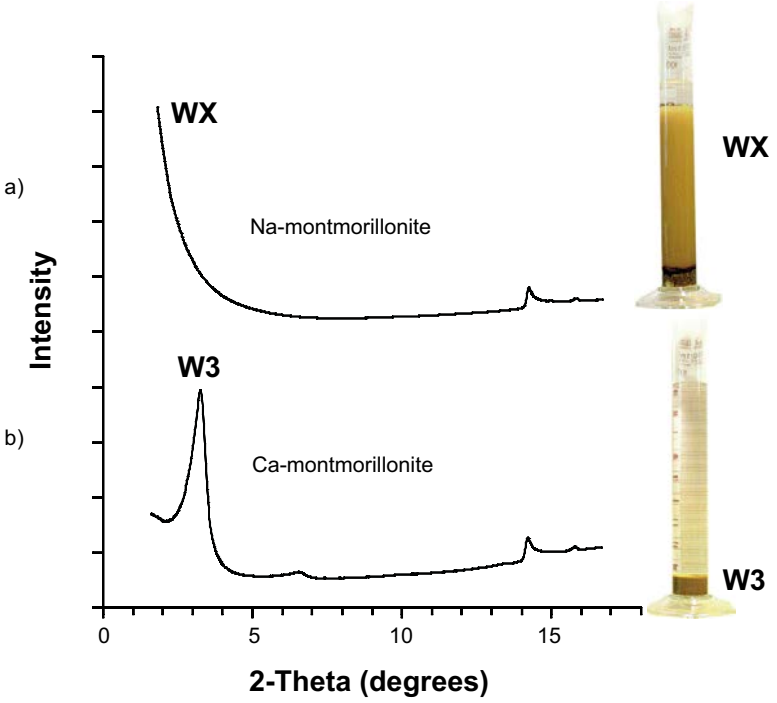

Figure 2-4. *X-ray diffractograms of wet clays (left) and swelling tests (right). (a) Wyoming Na-montmorillonite in water showing osmotic swelling (WX). In the glass cylinder is a natural sodium-dominated bentonite from the Kutch area, India. (b) Wyoming Ca-montmorillonite in water. In the glass cylinder is a natural calcium-dominated bentonite from Rokle, Czech Republic. (reproduced with permission from Svensson 2015).*

3 Chemistry and mineralogy method development

This work is a continuation of the work reported in Svensson et al. (2017), were a selection of methods was done for quality control of bentonite for the KBS-3 system. The selection was based partly on older work e.g. Karnland et al. (2006), and partly on for SKB new methods. Some methods that were used previously were excluded, e.g. free swelling; based on the limited value of that kind of data for the KBS-3 application. The main focus of the methods and their development is for their suitability for quality control of the bentonite buffer, however, if they work for the buffer, they will work for the backfill as well. The control of the buffer is much more complicated compared to the backfill, based on the requirements listed in Section 2.1, specifically the buffer has a lower and an upper limit for the swelling pressure, while the backfill only has a lower limit. The combination of a lower and an upper limit creates a density window for each bentonite where the swelling pressure is acceptable. The complexity of dependencies of the swelling pressure (Figure 2-1) and the strong dependence of the montmorillonite (or other smectite) content of the bentonite is the background and motivation for the use of methods such as XRD, CEC, EC and XRF, described below in further detail.

During this work (2016–2018) some methods have been added, while most of the work has been done in estimation of measurement uncertainties of each method. In some methods, the total error (bias) as well as the repeatability has been the focus, while in others focus has been on estimating the repeatability. This basis for the last ones is that the absolute content of montmorillonite of a specific bentonite is not that important, however, relative changes within a given bentonite or between different shipments are important, as it has a direct consequence on the buffer performance. To handle lack of reproducibility or methods dependency, it is important to always include a reference bentonite that the result can be compared to.

By increasing the number of measurements (n), it is possible to create an average with an increasingly higher repeatability. Hence, if a higher repeatability is needed based on the requirements, the number of measurements can be increased. This is however costly as an increase in the number of measurements leads to an increase in time and cost. Higher requirements are expected to increase the needed quality and quantity on the sampling and the analysis. How the sampling is done, how many samples are collected, and how they are blended together to get an overall representative sample (composite sample; CS).

3.1 Mineralogy (X-ray diffraction/XRD)

Powder X-ray diffraction (XRD) is a very useful method for qualitative and quantitative determination of the mineralogy of bentonites. Clay minerals such as montmorillonite have a platy habitus and hence become highly oriented in standard XRD powder mounts for measurements. Additionally the clay minerals are soft, while some of the accessory minerals are hard, making it difficult to get a homogenously milled material in the µm-range without destroying the clay minerals, hence, the presence of minor single crystals of the accessory minerals leads to sporadic very strong reflections in the data sets. To minimise the effect from this, a number of samples can be analysed and averaged. The method used is described in further detail in Svensson et al. (2017).

Estimation of method requirement mainly based on the swelling pressure relation with MX-80 (Figure 2-2) and practical arguments:

(i) Low bias. Give a reasonably correct value (e.g., U = ± 8 %) for montmorillonite (or other smectite).

(ii) Proportional. Give a value that is linear to the montmorillonite or smectite content.

(iii) High repeatability. Have a sufficiently high repeatability (e.g., U_r requirement = ± 3 %) for montmorillonite or other smectite.

3.1.1 Bias U

Measured values of MX-80 within this work are at approximately the same level as previously reported data on similar samples (e.g., Karnland et al. 2006). Measured values are in good agreement with montmorillonite levels calculated from other methods such as cation exchange capacity (CEC). XRD showed montmorillonite content of 80–84 % and CEC about 76/88 = 86 % (ratio of bulk sample / clay fraction; Karnland et al. 2006). This indicates that the bias is lower than the expected requirement. In the future, a complementary Rietveld software is suggested to be added to further evaluate the bias.

3.1.2 Linearity

By mixing sand (free of montmorillonite) with bentonite in known proportions it was possible to make synthetic qualities with known differences in montmorillonite content. Determination of the montmorillonite content using XRD (Siroquant version 3) showed that the measured montmorillonite was linearly proportional to the amount of bentonite in the sample (Figure 3-1). This indicated that the method was suitable for detecting an increase or decrease in montmorillonite content, at least when the difference was large enough.

This indicated that one can distinguish between samples that had higher and lower montmorillonite content, respectively. How small differences can be detected depends on the spread of the method, and whether the samples differ in some way in their nature that it introduces an error.

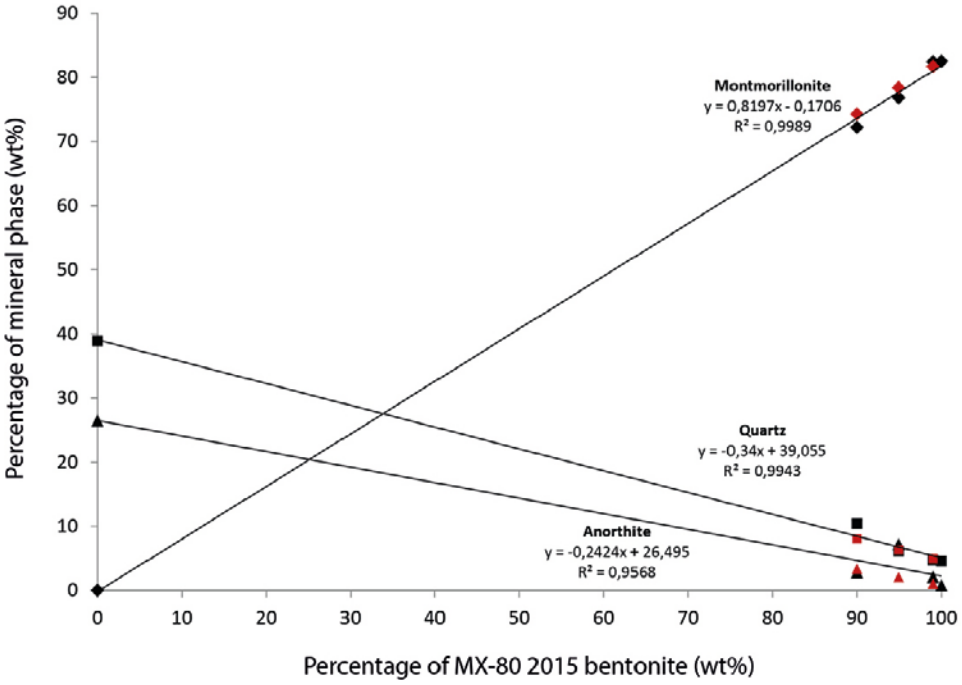

Figure 3-1. *Montmorillonite quantified using XRD in a selection of simulated qualities made from MX-80 and milled sand. Each value represents one measurement (not based on averaged values).*

3.1.3 Repeatability U_r

The repeatability is different for different bentonites, and depends on the bentonite content (e.g. type and number of clay minerals), how well it is characterized (missing phases, phases below 1 wt%), how even it is blended (milling, blending), preparation of XRD mount and also the data evaluation.

In Table 3-1, 10 samples were taken from the same can with MX-80 (samples 1 to 10). Each sample mount was measured twice (montmorillonite1 and montmorillonite2).

All the XRD mounts and all the evaluation was made by the same person at the same time for all measurements.

The difference (diff) was calculated as the difference in results between measurements 1 and 2 for the same sample. The difference between the different measurements and evaluations is between −0.5 to +0.1 = 0.6 wt%, which is less than the difference between the different samples spreading between 82.6 to 85.1 = 2.5 wt%. That indicates that it is not meaningful to measure the same sample mount several times, but to instead measure on several samples (or remount the same sample, exposing a new sample volume to the X-ray beam).

Table 3-1. Montmorillonite content (wt%) measured with XRD for 10 samples with MX-80. Each sample mount was measured twice (Montmorillonite 1, Montmorillonite 2).

MX-80 c65dae	**September 2017**		
Sample	Montmorillonite 1	Montmorillonite 2	Diff
1	84	84.5	−0.5
2	83	82.8	0.2
3	82.6	82.2	0.4
4	84.2	83.9	0.3
5	85.1	85	0.1
6	84.5	84.4	0.1
7	83.8	83.4	0.4
8	84.2	83.8	0.4
9	84.7	84.9	−0.2
10	84.9	85.2	−0.3
Average	84.1	84.01	
Std Dev (10)	0.80	0.99	
Std Dev of average	0.25	0.31	

The difference between the samples depends on (i) different sample contents (inhomogeneity) and (ii) the sample preparation. One can qualitatively observe differences between the different samples in that certain accessory minerals come and go, which indicates that it is inhomogeneity in the composition that primarily contributes to the spread. Variation in the sample preparation would rather give rise to different degrees of orientation of the sample which would be seen as a changed relationship between the 001 basal reflection and the 4.48 Å reflection, which was not really the case, and minor variation in the orientation parameter can also partly be corrected for by the Siroquant software.

More efficient grinding (e.g. longer time) would probably improve homogeneity, but would also risk destroying the clay mineral's crystallinity and properties. Instead, it is necessary to measure several samples and averages to obtain more representative values.

Depending on the requirements for the U_r requirements you set on the method, you have to measure different number of samples (n). It may also be that a poorly ground (inhomogeneous) clay demands higher n. Things to further explore in the future are wet milling, sieving and spray drying, that are expected to produce more homogenously milled material as well as a more randomly oriented sample (spray drying).

Currently it is not fully known which requirement will be placed on Ur in the application, so the goal here was to:

(i) Estimate how U_r may look as a function of n (number of samples measured) for the measured MX-80 series (Table 3-1).

(ii) Show that U_r (n = 3) < Ur-requirements, i.e. the uncertainty in the mean of a triple sample for sample data is less than the example requirement specified above.

From Table 3-1:

Mean = 84.1 %

The standard deviation SD = 0.80 (n = 10).

Simplified, you get the uncertainty in the mean as:

$S_{average(n)} = S / \sqrt{n}$

Hence:

$S_{average(n = 2)} = 0.80/\sqrt{2} = 0.57$ %

$S_{average(n = 3)} = 0.80/\sqrt{3} = 0.46$ %

$S_{average(n = 6)} = 0.80/\sqrt{6} = 0.33$ %

$S_{average(n = 10)} = 0.80/\sqrt{10} = 0.25$ %

U_r with 95 % confidence is given by multiplication with $T_{critical}$ which is a function of n, from Magnusson et al. (2013):

$T_{critical (n = 2)} = 12.7$

$T_{critical (n = 3)} = 4.3$

$T_{critical (n = 6)} = 2.57$

$T_{critical (n = 10)} = 2.26$

$T_{critical (n = 20)} = 2.09$

$T_{critical (n=\infty)} = 2$

$U_r = S_{average(n)} \times T_{critical (n)}$

$U_{r(n = 2)} = 0.57 \times 12.7 = \pm 7.2$ %

$U_{r(n = 3)} = 0.46 \times 4.3 = \pm 2.0$ %

$U_{r(n = 6)} = 0.33 \times 2.57 = \pm 0.85$ %

$U_{r(n = 10)} = 0.25 \times 2.26 = \pm 0.57$ %

U_r decreases dramatically between n = 2 to n = 3. Should one then further reduce significantly, one goes to n = 6 etc.

The calculated repeatability at triplicate (n = 3) is U_r (n = 3) = ± 2.0 % which is less than Ur requirements as assumed here to ± 3.0 %. Duplicate samples do not meet this fictitious requirement, which is a qualified guess on what is reasonable.

The measurement time for 3 samples is by the current method 9 hours. It means 3 samples of the unknown clay and 3 samples of the known clay compared to be measured. This will be a total of 18 hours of measurement time. It is then possible to measure and evaluate a new delivery against an old one in 24 hours. Most likely this can be shortened further e.g. by lowering the measurement time and by achieving a better milling and sample mount. This is the same magnitude of time required for other methods such as CEC measurement and water content determination of bentonite, which makes it a reasonable scope.

Sample preparation

The sample preparation is crucial for the powder X-ray diffraction method. The amount of milling should be long enough to produce a fine powder with no large grains, however short enough to not destroy the clay mineral crystal structures. As the clay minerals have a platy habitus, they strongly orient themselves during compaction or even under the slight pressure used to flatten a sample for the XRD measurement. Differences in how different operators mount the samples may have an impact on the repeatability of the method. This has not been evaluated in this study. Another important factor is the water content of the sample, the relative humidity when prepared and when measured (Figure 3-2). The 001 reflections at low angle change as the clay hydrate/dehydrate with various ambient relative humidity in the laboratory. A two water layer hydrate is preferred for the Rietveld data evaluation used for quantification of the minerals. As the bentonite hydrate/dehydrate it will physically expand or contract. This will affect the height of the sample, and hence the sample-detector distance, and hence the two theta values will be shifted to higher or lower angles depending on expansion or contraction.

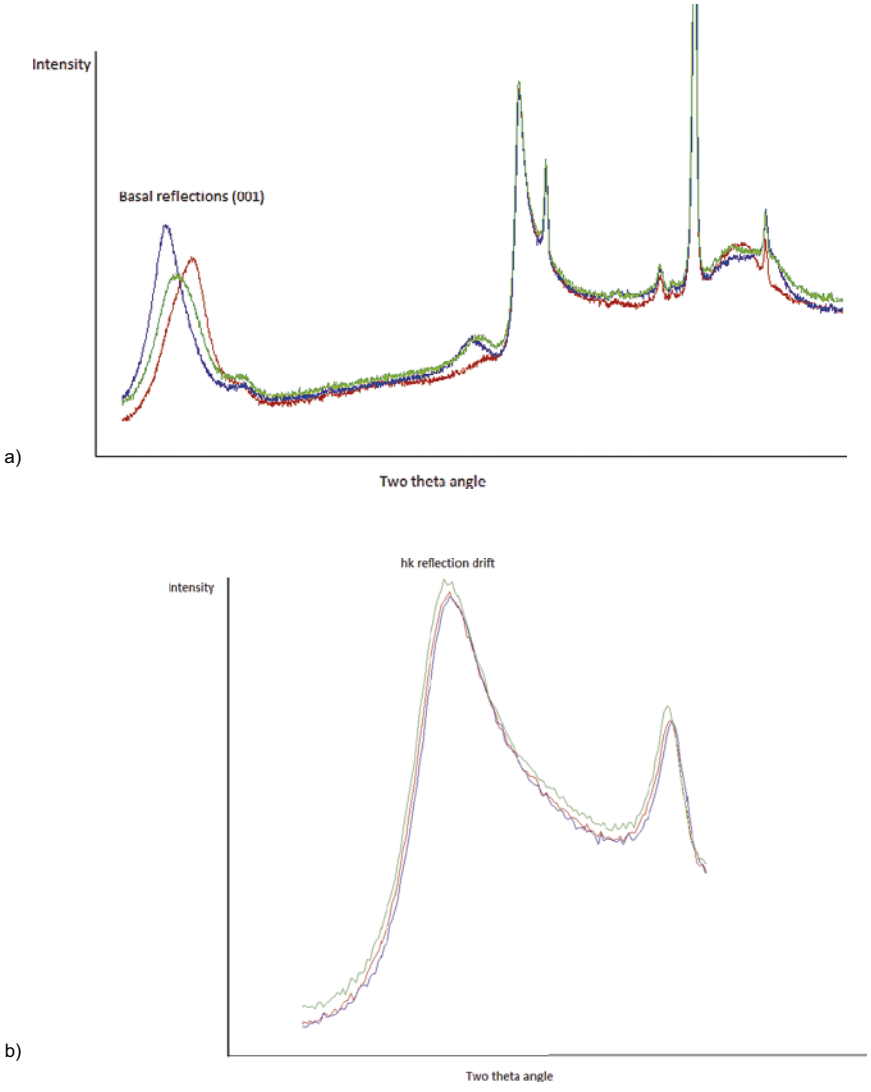

Figure 3-2. *(a) XRD pattern (intensity as a function of the two theta angle) collected at three occasions during one week for the same sample mount. Notice how the montmorillonite 001 reflections at low angle change as the clay hydrate/dehydrate with various ambient relative humidity in the laboratory. (b) Two theta shift error due to sample hydration/dehydration between preparation and measurement of the reflections of montmorillonite at 4.48 Å and cristobalite at 4.05 Å. This is a zoomed in dataset not showing the X- or Y-axis but as all diffractograms, it is intensity versus two theta angle (degree).*

3.2 Chemistry (X-ray fluorescence spectroscopy/XRF)

X-ray Fluorescence spectroscopy (XRF) is a very useful method for quantitative determination of the elemental composition of bentonites. The bentonite is compacted to discs and is rapidly measured (approximately 15 minutes) in the XRF equipment with very little impact from the user. The method used is described in further detail in Svensson et al. (2017).

3.2.1 Bias U

XRF and ICP-AES data for ABM MX-80 from 2006 are compared in Table 3-2. The ICP-AES analysis was performed by Acmelab, Canada (ISO 9002 accredited laboratory). The absolute values from XRF and from the ICP-AES are very close. Possibly Na is underestimated somewhat, which is not unexpected based on the low atomic number of Na (weak low energy X-rays).

Table 3-2. XRF versus ICP-AES for ABM MX-80 (2006) bentonite.

Bentonite	Method	Na_2O	CaO	K_2O	MgO	Al_2O_3
ABM MX-80	ICP-AES Acmelab (Svensson et al. 2011)	2.2	1.6	0.67	2.9	21.2
ABM MX-80	XRF SKB Äspö	1.7	1.6	0.55	2.5	21.6
		SiO_2	Fe_2O_3	TiO_2	MnO	P_2O_5
ABM MX-80	ICP-AES Acmelab (Svensson et al. 2011)	66.8	4.4	0.22	0.022	0.095
ABM MX-80	XRF SKB Äspö	66.7	4.4	0.18	0.013	0.007

3.2.2 Linearity

By mixing sand (free of montmorillonite) with bentonite in known proportions it is possible to make synthetic qualities with known differences in montmorillonite content and/or chemical content.

Determination of the chemical content, and calculating chemical indexes such as (Mg+Al)/Si is one way to indirectly monitor the montmorillonite content. Another useful ratio is Na/Ca which in general will reflect differences in the interlayer cation composition, and hence also affect some initial properties of the bentonite. If Mg is also present in the interlayer or in accessory minerals such as dolomite, one has to be careful and may have to use another chemical ratio.

Calculation of (Mg+Al)/Si ratio for bentonite-sand mixtures and bentonite-feldspar mixtures show that the measured ratios are linearly proportional to the amount of bentonite in the sample and the measured values are very close to the interpolated values (Figure 3-3). This indicates that the method is suitable for detecting an increase or decrease in e.g. montmorillonite content, or interlayer composition, etc.

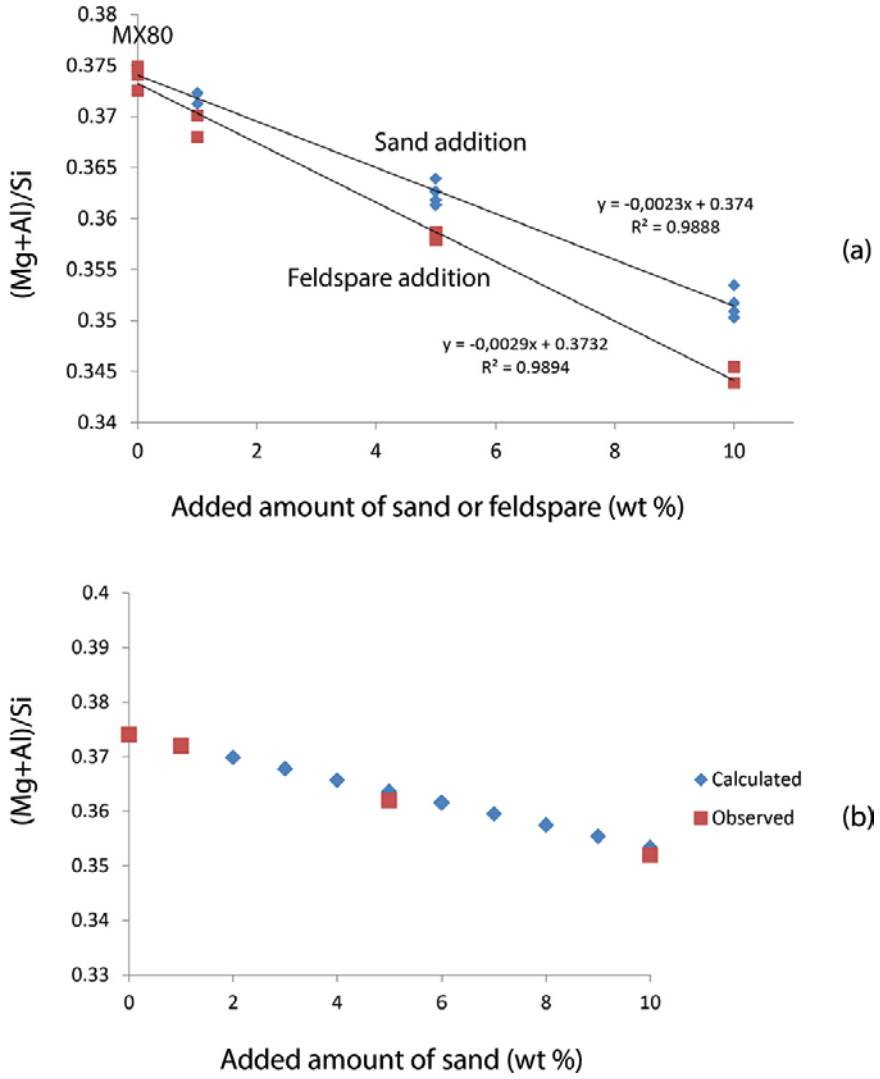

Figure 3-3. *Montmorillonite indirectly semi-quantified using chemical data. The (Mg+Al)/Si ratio is plotted as a function of the added amount of sand (decreasing montmorillonite content).*

3.2.3 Repeatability U_r

The repeatability of the method is very high and is good enough for the purpose. This is important for detecting small variations in the content, however, much more difficult to actually assess what the variation comes from (if it has an impact on the bentonite properties or not). The standard deviation and the repeatability are different for different elements or ratios (Table 3-3).

In this example U_r will be estimated for (Mg+Al)/(Si+K) for n = 2 and n = 3:
0.00069 is the standard deviation for the measurements of the chemical ratio in this example.

For n = 2 or 3, S becomes:

$S_{average(n = 2)} = 0.00069/\sqrt{2} = 0.049$ %

$S_{average(n = 3)} = 0.00069/\sqrt{3} = 0.040$ %

U_r with 95 % confidence is given by multiplication with $T_{critical}$ which is a function of n (Magnusson et al. 2013):

$T_{critical\ (n = 2)} = 12.7$

$T_{critical\ (n = 3)} = 4.3$

$U_r = S_{average(n)} \times T_{critical\ (n)}$

$U_{r(n = 2)} = 0.049 \times 12.7 = \pm 0.62$ %

$U_{r(n = 3)} = 0.040 \times 4.3 = \pm 0.17$ %

To summarise, the repeatability and the bias for the XRF method are in line with the expected performance for the method.

Table 3-3. Repeatability test (n = 11) using XRF on three samples of bentonite-sand mixtures (1, 5 and 10 % sand) in MX-80.

Sand wt%	Na_2O	MgO	Al_2O_3	SiO_2	P_2O_5	SO_3	Cl	K_2O	CaO	TiO_2	MnO	Fe_2O_3	(Mg+Al)/(Si+K)
1 % Av	1.70	2.40	21.90	65.97	0.01	0.53	0.01	0.69	1.62	0.21	0.02	4.95	0.365
1 % SD	0.013	0.007	0.026	0.024	0.001	0.002	0.001	0.003	0.005	0.001	0.001	0.014	
5 % Av	1.770	2.30	21.46	66.23	0.01	0.55	0.01	0.90	1.64	0.22	0.02	4.90	0.354
5 % SD	0.012	0.007	0.023	0.020	0.001	0.001	0.001	0.003	0.003	0.001	0.001	0.011	
10 % Av	1.810	2.20	20.89	66.68	0.02	0.55	0.01	1.09	1.71	0.23	0.02	4.80	0.340
10 % SD	0.008	0.008	0.019	0.013	0.001	0.003	0.002	0.003	0.002	0.001	0.001	0.011	

3.3 Cation Exchange Capacity (CEC)

The CEC of the bulk bentonite divided by the CEC of the pure montmorillonite give a good indication about the montmorillonite content of the bentonite and is a very good complement to other methods such as XRD. The CEC method is fairly quick and normally easy to interpret, but differences in the sample preparation and in the method itself can, if they are not well controlled, reduce the reproducibility of the method.

The specific cation exchange capacity (CEC) of a bentonite depends on the number of cation exchangers in the clay and the specific cation exchange capacity of the smectite itself in terms of charge per gram. The exchangeable cations are compensating two types of negative charges in the smectite; (1) permanent charge from layer (isomorphous) substitution, (2) variable edge charges depending on the pH. If the CEC of the smectite is known, the bulk CEC of a bentonite is a good measure of the smectite content, as long as no other cation exchangers are present.

The CEC can be determined in several ways. One method is to extract the cations with an NH_4Cl (or NH_4OAc) solution. Analysis of the extract gives information regarding the type and number of the cations present. One disadvantage with this method is that dissolvable phases (e.g. gypsum) also contribute to the result. This can however be minimized with an 80 % ethanol solution instead of water (Belyayeva 1967). Another method is to exchange with a Cu^{2+}-triethylenetetramine complex (Meier and Kahr 1999, Ammann et al. 2005). As the Cu-tri complex has a very strong blue colour this reaction can be rapidly quantified by using spectrophotometry. The exchange reaction is fast and is normally completed in 15 to 30 minutes. The measured CEC on pure montmorillonite (or other smectite) correspond very well to the calculated layer charge on Wyoming montmorillonite based on chemical composition (Karnland et al. 2006) hence it is very well established that Cu^{2+} is absorbed as a divalent cation in amounts corresponding to the permanent charge. The ratio of the CEC of the bulk bentonite and the clay fraction normally correspond very well to the montmorillonite content determined by methods such as XRD (Karnland et al. 2006) indicating that no other significant cation exchangers are present.

In Chapter 5 CEC data of composite samples (CS) and clay fractions (CF) of different bentonites analysed by the copper-tri method are presented. The method determines the total CEC (permanent layer charge and variable edge charge). Milled bentonite (CS and CF 400 mg ± 10 mg) is dispersed in deionised water (33 ml) on a vibrating table for 30 minutes followed by ultrasonic treatment (15 minutes). The bentonite is then equilibrating with Cu (II)-triethylenetetramine solution (7 ml; 45 mM) and left on a vibrating table for 30 minutes. After 5 minutes of centrifugation at 3 000 RCF (relative centrifugal force) spectrophotometer measurement at 583 nm of the supernatant is performed against a calibration curve. The CEC is calculated by the difference in the copper concentration before and after ion exchange with the clay and is reported as the mean CEC of two separate determinations (i.e. mean CEC of two separate samples) expressed as cmol(+)/kg dry weight. As the CEC is reported in relation to the dry weight of a bentonite sample the water content of the material is determined by weighing a separate bentonite sample before and after drying at 105 °C for 24 h. The weighing procedure of bentonite for CEC and water content is carried out at the same time and under the same conditions. The copper-tri method is described in further detail in Svensson et al. (2017).

3.3.1 Estimation of measurement uncertainty

An estimation of the expanded measurement uncertainty (U) close to 95 %confidence interval of the copper-tri method has been carried out in accordance with methodology described by Magnusson et al. (2013) using the software application MUkit.

The expanded measurement uncertainty was estimated in the following steps:

- Quantifying within-laboratory reproducibility, u(Rw) using standard deviation for:
  - Control samples of Wyoming bentonite MX-80 were n = 162 for a 3-year period of time (Figure 3-4). The measurements were carried out by different operators, at different times and in the same laboratory.
  - Routine replicate samples of bentonites from India, Greece, USA, Bulgaria and Turkey were n = 45 for a 3-year period of time. Number of parallel measurement is two. The measurements were carried out by different operators, at different times and in the same laboratory.

u(Rw) was calculated to 2.65 %.

- Quantifying method and laboratory bias, u(bias) using standard deviation for:
  - Data of a copper triethylenetetramine solution were n = 149 for a 3-year period of time. The measurements were carried out by different operators, at different times and in the same laboratory.

u(bias) was calculated to 0.75 %.

Combining u(Rw) and u(bias) and calculating expanded measurement uncertainty U using a coverage factor of 2 to achieve about 95 % confidence.

The expanded measurement uncertainty U of the copper-tri method was estimated to 6 %.

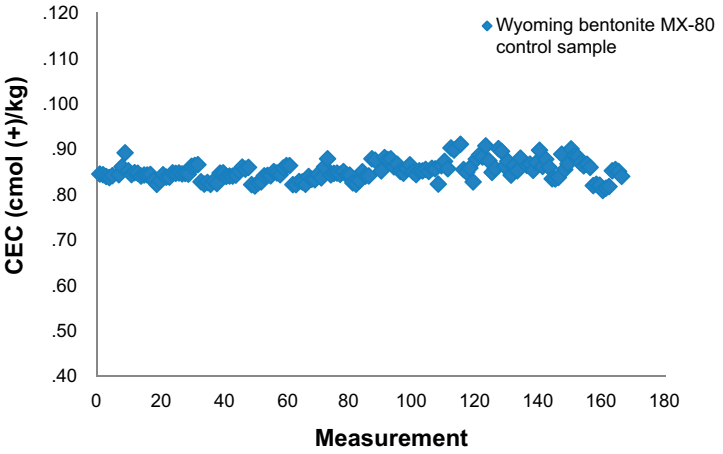

Figure 3-4. *Wyoming bentonite MX-80 analysed as control sample of the copper-tri method for a 3-year period of time. A linear increase in CEC over time is observed for control samples where the same batch Cutri solution has been used. A new batch was prepared every three weeks.*

3.3.2 Challenges

A contributing factor to the spread in the CEC for duplicates may be due to difficulty in dispersing the bentonite in water. Several samples were not completely dispersed after 15 minutes in ultrasonic batch (about 1–2 mm lumps were visually observed). When comparing CEC results between duplicates, slightly lower results are seen for non-completely dispersed samples, see CEC data for bentonites in Chapter 5. The relative standard deviation (RSD or CV) between these duplicates is between 1 to 3 % which is within the expanded measurement uncertainty of the method (U = 6 %, with 95 % confidence).

3.3.3 Linearity

Different proportions of natural sand were added and mixed with bentonite (0, 1, 5, 10, 25, 50 and 80 wt%). Both sand and bentonite were milled separate with a planetary ball mill (Retsch PM400; 10 minutes, 200 rpm) prior mixing. CEC was then determined for the different sand/bentonite mixtures according to the copper-tri method. In Figure 3-5 duplicate determinations of CEC are plotted as a function of the added amount of sand. CEC for all three sand/bentonite mixtures (MX-80 2015, Asha 2012 and Ibeco backfill) show linearity proportional to the amount of bentonite in the samples. The repeatability standard deviation of duplicates is less than 3 %. Reference sample of bentonite MX-80 2015 (without addition of sand) received a slightly higher CEC value than normal (Figure 3-5).

3.3.4 Alternatives for optimization

In the current CEC method (described above), 7 ml of 45 mM Cu-tri was used together with 33 ml water and 400 mg of bentonite. An alternative setup was worked out with the aim of being quicker and easier, requiring less work and to give data in shorter time, a gain in time with a sacrifice in a larger bias (but with the aim of an equal or better repeatability). The purpose of this alternative setup is to quickly being able to compare selected different bentonites internally with each other, with as simple laboratory glass ware as possible.

By changing the solutions to 10 ml of 45 mM Cu-tri and 25 ml water and the bentonite to 500 mg, the volumes are easier to measure using standard glassware, increasing flexibility and possibly also the repeatability. To increase the speed of drying (for the water content measurement) a temperature of 260 °C was chosen instead of 105 °C, and the water content was taken after 2 h and after 3 days (very little difference), making it possible to get quick results, as well as more correct results some days later. The Cu-tri solution was added to the dry bentonite directly, the high salt content of the solution made dissolution of the clay faster compared to prior addition of water that typically creates a very dense gel, difficult to disperse in the water. From Cu-tri addition to the measurement an hour passed, and the first results were available after a total of 2 h. This “quick method” gave somewhat lower CEC compared to the standard method, due to the faster exchange and lack of ultra-sonic treatment, but with a very comparable repeatability (see Figure 5-5 for a comparison).

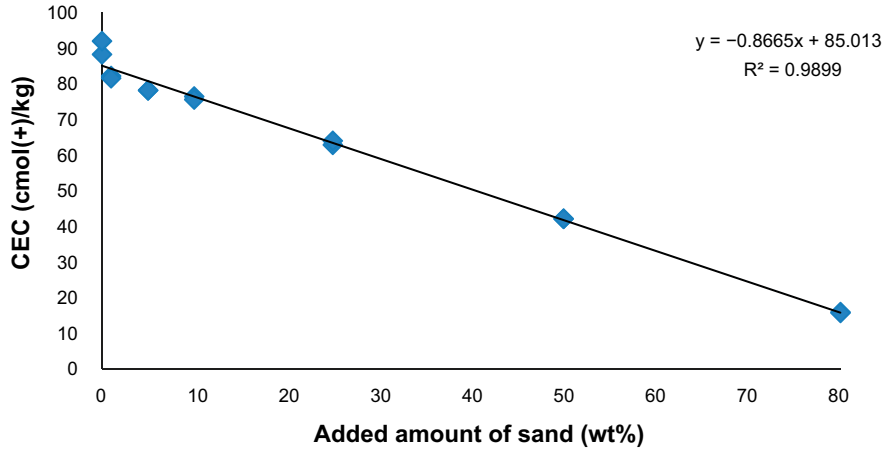

Wyoming bentonite (MX-80 2015; internal reference material)

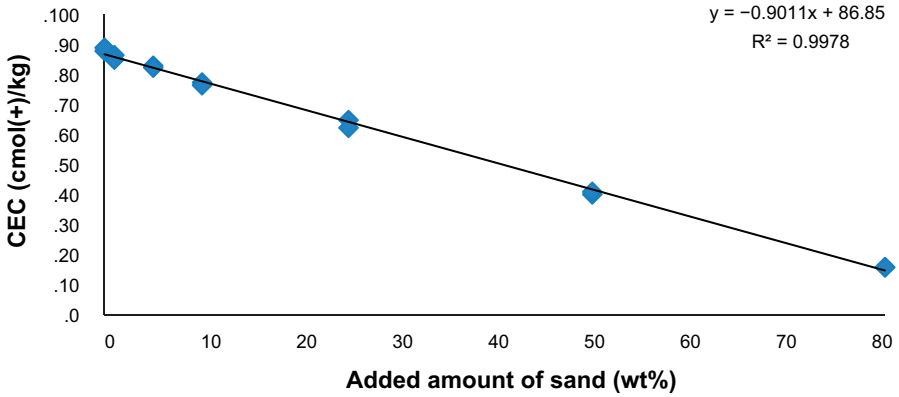

Indian bentonite (Asha 2012; internal reference material)

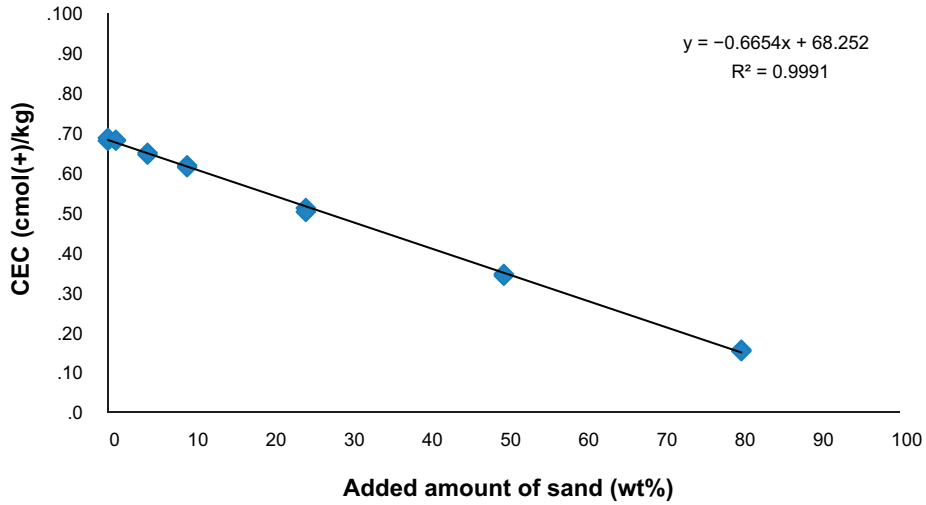

Greek bentonite (Ibeco backfill; internal reference material)

Figure 3-5. *CEC of bentonite-sand mixtures. CEC of duplicates are plotted as a function of the added amount of sand.*

3.4 Exchangeable Cations (EC)

Exchangeable cations refer to the amount of each type of the exchangeable cations initially present in the interlayer space of the bentonite (Karnland 2010). These interlayer cations are charge compensating for the negative charge of the montmorillonite layers. In natural bentonite, the charge compensating cations are rarely of one element alone, but a mixture of both mono and divalent ions. The most common cations are Na^+, Ca^{2+}, Mg^{2+} and K^+. The swelling properties are to a large extent dependent on the magnitude and the position of the layer charge, but also on the type of charge compensating cation (Karnland et al. 2006).

One method for extracting exchangeable cations is to use ammonium (NH_4^+) ions in an alcoholic solution to exchange with Na^+, Ca^{2+}, Mg^{2+} and K^+ (Jackson 1975). An alcoholic solution reduces dissolution errors (Belyayeva 1967), however easily soluble salts, such as chlorides and carbonates of alkali metals, will still dissolve in this extractant. The sum of the exchangeable cations therefore often exceeds the measured cation exchange capacity (copper-tri method, Section 3.3) of the sample (Karnland et al. 2006). Concentrations of the different extracted cations can be determined by using inductively coupled plasma (ICP) as analysis technique. The exchange capacity of each cation is calculated and expressed in milliequivalent (meq)/100 g dry weight. Total sum EC is then given by combining the calculated EC for each cation. The unit of EC, meq/100 g, is numerically equivalent to cmol(+)/kg (the unit of CEC, see Section 3.3) the latter is used in this report when comparing CEC and EC data of different bentonites.

In Chapter 5 EC data of composite samples (CS) of different bentonites are presented. The method used is based on scientific article by Jackson (1975). Exchangeable cations are extracted by shaking milled bentonite (CS 1 000 g ± 10 mg) in ammonium chloride solution in 76 % ethanol (saturated 1 M NH_4Cl; 12.5 ml) on a vibrating table for 30 minutes. After 5 minutes centrifugation at 2 700 RCF (relative centrifugal force) the supernatant is separated from the bentonite by decanting the extract to a sample tube. The extraction is repeated totally three times (i.e. same sample is extracted three times with a total volume of approximately 38 ml). After evaporation of the alcohol, the extract is filtrated (0.45 µm filter) and volume corrected with deionised water to 50 ml. For each composite sample, two separate extractions are performed (i.e. duplicate of extract for ICP analysis). The cations are analysed by inductively coupled plasma (ICP) at external laboratory. The alcohol is evaporated due to recommendations by the external laboratory for chosen analyse technique. As EC are reported in relation to the dry weight of a bentonite sample water content of the material is determined by weighing a separate bentonite sample before and after drying at 105 °C for 24 h. The weighing procedure of bentonite for EC and water content determination is carried out at the same time and under the same conditions. The water content is reported as the mass ratio between the water and the moist material, expressed in weight percent. The exchange capacity of each cation is calculated and total sum EC is then given by combining the calculated EC for each cation (Na^+, Ca^{2+}, Mg^{2+} and K^+). The method used is described in further detail in Svensson et al. (2017).

3.4.1 Estimation of measurement uncertainty

The method for determining exchangeable cations involves two steps; (1) extracting step at internal laboratory including duplicate sample, and (2) cation analysis by ICP at external laboratory. No measurement uncertainty was reported together with data from ICP analysis by the external laboratory.

When estimating expanded measurement uncertainty *U* from data obtained in the individual laboratory two factors are important; bias (trueness) and precision (within-lab reproducibility) (Magnusson et al. 2013). Usually bias is estimated from data of certified reference material (commercial sample from accredited laboratory) or data from ring tests (comparison from different laboratories). Unfortunately no ring tests have been performed and no certified reference material was available, therefore bias could not be estimated for the method. When analysing routine samples a control sample (Wyoming bentonite) also is analysed i.e. the control sample is undergoing the entire analytical process (step 1 and 2 above) and is representative for the matrix of the routine sample. However, only a few data were obtained for the control sample over a shorter period of time. Therefore, data is not entirely representative of estimating the precision of the method. Instead the standard deviation of repeatability (RSDr) of the method was estimated on the basis of the duplicate differences of routine bentonite samples (CS), i.e. duplicate differences of calculated concentration of Na^+, Ca^{2+}, Mg^{2+} and K^+ (given in meq/100 g). This was performed in following steps;

Calculating the relative range %d (relative duplicate differences of each routine sample).

$\%d = 100 \times (x_1 - x_2)/X$

Where x_1 and x_2 are the individual measured values of the duplicate determination and X is the average of these values.

Calculating relative standard deviation (RSD) from the mean relative range ($\%R_{mean}$):

$RSD_r = \%R_{mean}/1.128$

The calculated RSD_r for Na^+, Ca^{2+}, Mg^{2+} and K^+ in routine samples of bentonite are presented in Table 3-4 to Table 3-7.

The EC method repeatability and bias are regarded to be good enough in relation to the expected performance of the method.

Table 3-4. Calculated standard deviation of the repeatability (RSDr) for Na+ in routine samples, when extracted with ammonium chloride and detected by inductively coupled plasma (ICP-AES, *ICP-SFMS).

	Na^+ (meq/100 g)		Mean $_{X1, X2}$		Relative duplicate difference
Bentonite (CS)	x_1	x_2	X	$d = x_{(1.2)} - x_{(1.2)}$	$\%d = 100 \times (d/X)$
MX-80 2012 (control sample)	58.50	55.60	57.05	2.90	5.1
Bulgaria 2017 (20 kg)	19.60	19.80	19.70	0.20	1.0
Milos 2017	11.60	11.90	11.75	0.30	2.6
Morocco 2017	33.40	32.70	33.05	0.70	2.1
Turkey 2017	71.00	72.00	71.50	1.00	1.4
Wyoming BARA-KADE 2017	55.20	55.10	55.15	0.10	0.2
Bulgaria F 2017 (200 kg)	24.60	24.60	24.60	0.00	0.0
*Wyoming MX-80 P 2014 (control sample)**	57.60	52.30	54.95	5.30	9.6
*Sardinia 2017**	37.70	38.80	38.25	1.10	2.9
*India 2018**	57.40	53.50	55.45	3.90	7.0
Relative mean range ($\%R_{mean}$)					3.2
d2 (n = 2)					1.128
Relative standard deviation of the repeatability (RSD_r)					**2.8**

Table 3-5. Calculated standard deviation of the repeatability (RSDr) for Ca2+ in routine samples, when extracted with ammonium chloride and detected by inductively coupled plasma (ICP-AES, *ICP-SFMS).

	Ca^{2+} (meq/100 g)		Mean $_{X1, X2}$		Relative duplicate difference
Bentonite (CS)	x_1	x_2	X	$d = x_{(1.2)} - x_{(1.2)}$	$\%d = 100 \times (d/X)$
Wyoming MX-80 2012 (control sample)	22.40	20.80	21.60	1.60	7.4
Bulgaria 2017 (20 kg)	50.10	49.70	49.90	0.40	0.8
Milos 2017	28.10	28.00	28.05	0.10	0.4
Morocco 2017	20.30	19.90	20.10	0.40	2.0
Turkey 2017	13.60	13.80	13.70	0.20	1.5
Wyoming BARA-KADE 2017	25.70	26.00	25.85	0.30	1.2
Bulgaria F 2017 (200 kg)	47.40	47.10	47.25	0.30	0.6
*Wyoming MX-80 P 2014 (control sample)**	20.00	18.90	20.00	1.10	5.5
*Sardinia 2017**	32.60	33.10	32.60	0.50	1.5
*India 2018**	19.70	18.10	19.70	1.60	8.1
Relative mean range ($\%R_{mean}$)					2.1
d2 (n = 2)					1.128
Relative standard deviation of the repeatability (RSD_r)					**1.8**

Table 3-6. Calculated standard deviation of the repeatability (RSDr) for Mg2+ in routine samples, when extracted with ammonium chloride and detected by inductively coupled plasma (ICP-AES, *ICP-SFMS).

	Mg^{2+} (meq/100 g)		Mean $_{X1, X2}$		Relative duplicate difference
Bentonite (CS)	x_1	x_2	X	$d = x_{(1.2)} - x_{(1.2)}$	$\%d = 100 \times (d/X)$
Wyoming MX-80 2012 (control sample)	7.56	7.10	7.33	0.46	6.3
Bulgaria 2017 (20 kg)	7.88	7.76	7.82	0.12	1.5
Milos 2017	18.10	18.30	18.20	0.20	1.1
Morocco 2017	28.00	27.30	27.65	0.70	2.5
Turkey 2017	2.72	2.80	2.76	0.08	2.9
Wyoming BARA-KADE 2017	5.13	5.37	5.25	0.24	4.6
Bulgaria F 2017 (200 kg)	7.60	7.69	7.65	0.09	1.2
*MX-80 P 2014 (control sample)**	8.90	8.00	8.45	0.90	10.7
*Sardinia 2017**	48.80	51.00	49.90	2.20	4.4
*India 2018**	17.80	16.70	17.25	1.10	6.4
Relative mean range ($\%R_{mean}$)					4.2
d2 (n = 2)					1.128
Relative standard deviation of the repeatability (RSD_r)					**3.7**

Table 3-7. Calculated standard deviation of the repeatability (RSDr) for K+ in routine samples, when extracted with ammonium chloride and detected by inductively coupled plasma (ICP-AES, *ICP-SFMS).

	K^+ (meq/100 g)		Mean $_{X1, X2}$		Relative duplicate difference
Bentonite (CS)	x_1	x_2	X	$d = x_{(1.2)} - x_{(1.2)}$	$\%d = 100 \times (d/X)$
Wyoming MX-80 2012 (control sample)	1.47	1.36	1.42	0.11	7.8
Bulgaria 2017 (20 kg)	4.35	4.45	4.40	0.10	2.3
Milos 2017	3.05	3.23	3.14	0.18	5.7
Morocco 2017	1.46	1.51	1.49	0.05	3.4
Turkey 2017	5.32	5.25	5.29	0.07	1.3
Wyoming BARA-KADE 2017	1.50	1.56	1.53	0.06	3.9
Bulgaria F 2017 (200 kg)	4.02	4.03	4.03	0.01	0.2
*Wyoming MX-80 P 2014 (control sample)**	1.80	1.60	1.70	0.20	11.8
*Sardinia 2017**	1.70	1.70	1.70	0.00	0.0
*India 2018**	0.60	0.50	0.55	0.10	18.2
Relative mean range ($\%R_{mean}$)					5.5
d2 (n = 2)					1.128
Relative standard deviation of the repeatability (RSD_r)					**4.8**

3.5 Analysis of carbon and sulfur

Carbon is in bentonite in the form of inorganic and organic carbon. SKB is particularly interested in organic carbon from the perspective of whether it can be an energy source for microbes. Inorganic carbon compounds in the bentonite are especially carbonates (calcite, dolomite, etc) but the presence of graphite probably cannot be completely excluded. The carbonates are more or less water-soluble and in field tests they sometimes can be seen to accumulate towards a heater. Organic carbon compounds that may be relevant are coal, bitumen and humic substances. Some of the organic carbon compounds are soluble in organic solvent, whereupon they can be extracted from the bentonite and analysed, which can give qualitative information about the types of compounds present, and thus information on the clay origin and formation environment.

Sulfur is found in bentonite especially as sulfide (pyrite) and sulfate (gypsum), but elemental sulfur and possibly other forms of sulfur cannot be totally excluded. Ca-sulfates (e.g. gypsum) are soluble in water and in field experiment are often transported and enriched. Sulfates are themselves not reactive

to the copper canister, but under the right circumstances they can be converted to sulfide by sulfate-reducing bacteria, and therefore sulfates still has some relevance. Water soluble sulfides can attack the copper canister and therefore focus is more on sulfides than on the sulfates. The solubility of sulfides is very low and it is uncertain how well sulfides can be transported in bentonite in gas or liquid.

A number of different bentonite types are going to be analysed to see the variations in the different bentonite types with different origin. Every bentonite is analysed with three repetitions. Some samples are prepared with known amount of sucrose, calcium carbonate or zinc sulfide to test the validity of the method. Some additional bentonites or other clays were included in these tests, not further described or analysed in the report.

3.5.1 Procedure

Carbon series (Total, Organic C, Inorganic C and Graphite C) and Sulfur (Total S, sulfate and sulfide) were investigated using evolved gas analysis (EGA). LECO combustion analysis instruments were used. These analyses are done at external laboratories i.e. Bureau Veritas Commodities Canada Ltd. Samples were prepared at the Äspö Hard Rock Laboratory. Some samples were prepared at BV i.e milled to a mesh size of 200 prior to the analyse requirements.

3.5.2 Results

The analyses of carbon and sulfur show that none of the examined clays are above the required limit of carbon and sulfur (Table 3-8; Table 3-9). Carbon and sulfur data are reported for the selected and some additional bentonites. In Table 3-8 the highest reported organic carbon content was 0.37 wt% (Bulgarian bentonite), but the scattering of the data was high in some cases, which confirms the need of several samples (triplicates). The highest reported sulfide content was 0.43 wt% (Milos bentonite).

Table 3-8. EGA data. Content of carbon and sulfur components in bulk materials (wt%).

Id	Sample	Tot/C (%)	Tot/S (%)	C/ORG (%)	C/GRA (%)	CO_2 (%)	S/S^{2-} (%)	SO_4 (%)
c65e20	Bulgaria	0.58	0.03	0.08	< 0.02	1.86	< 0.02	0.13
c65e20	Bulgaria	0.86	0.04	0.37	< 0.02	1.79	< 0.02	0.16
c65e20	Bulgaria	0.59	0.03	< 0.02	< 0.02	2.81	< 0.02	0.18
c65e9f	Bulgaria	0.74	0.05	0.19	< 0.02	2.01	< 0.02	0.22
c65e9f	Bulgaria	0.72	0.04	0.10	< 0.02	2.26	< 0.02	0.18
c65e9f	Bulgaria	0.73	0.05	0.07	< 0.02	2.41	< 0.02	0.24
c65e22	Milos 2017	0.23	0.87	0.07	< 0.02	0.58	0.43	1.34
c65e22	Milos 2017	0.25	0.79	0.07	< 0.02	0.64	0.36	1.26
c65e22	Milos 2017	0.24	0.73	0.06	< 0.02	0.63	0.29	1.32
c65e24	Marocco 2017	0.06	0.03	0.02	< 0.02	0.12	< 0.02	0.12
c65e24	Marocco 2017	0.03	0.05	< 0.02	< 0.02	< 0.02	< 0.02	0.21
c65e24	Marocco 2017	0.03	0.03	< 0.02	< 0.02	0.03	< 0.02	0.09
c65e26	Turkey 2017	0.61	0.02	0.06	< 0.02	1.97	< 0.02	0.11
c65e26	Turkey 2017	0.62	< 0.02	0.11	< 0.02	1.86	< 0.02	0.11
c65e26	Turkey 2017	0.64	0.02	0.10	< 0.02	1.94	< 0.02	0.12
c65e89	India 2018	0.14	0.14	0.04	< 0.02	0.35	< 0.02	0.51
c65e89	India 2018	0.14	0.15	0.07	< 0.02	0.24	< 0.02	0.48
c65e89	India 2018	0.15	0.15	0.07	< 0.02	0.31	< 0.02	0.88
c65e3b	Bara-Kade 2017	0.44	0.21	0.18	< 0.02	0.90	0.03	0.56
c65e3b	Bara-Kade 2017	0.42	0.21	0.26	< 0.02	0.53	0.04	0.52
c65e3b	Bara-Kade 2017	0.42	0.21	0.24	< 0.02	0.62	0.04	0.50
c65e50	Bulgaria 2017	0.82	0.05	0.26	< 0.02	2.04	< 0.02	0.26
c65e50	Bulgaria 2017	0.78	0.05	0.09	< 0.02	2.54	< 0.02	0.26
c65e50	Bulgaria 2017	0.89	0.06	0.25	< 0.02	2.35	< 0.02	0.29
c65e6f	Sardinia 2017	0.18	0.03	0.04	< 0.02	0.52	< 0.02	0.14
c65e6f	Sardinia 2017	0.19	0.03	0.05	< 0.02	0.50	< 0.02	0.17
c65e6f	Sardinia 2017	0.18	0.03	0.05	< 0.02	0.48	< 0.02	0.17

Analyses performed with samples of 200 mesh size. Bureau Veritas Commodities Canada Ltd.

The analyses of carbon and sulfur show that none of the examined clays have a very high content of carbon and sulfur. Carbon and sulfur data are reported for different bentonites. In Table 3-9 the highest reported organic carbon content was 0.54 wt% and sulfide 0.09 wt%.

Table 3-9. EGA data. Content of carbon and sulfur components in bulk materials (wt%).

Id	Sample	Tot/C (%)	Tot/S (%)	C/ORG (%)	C/GRA (%)	CO_2 (%)	S/S^{2-} (%)	SO_4 (%)
C65e06	MX-80 P	0.29	0.31	0.18	< 0.02	0.36	0.06	0.74
C65e06	MX-80 P	0.30	0.32	0.17	< 0.02	0.45	0.08	0.73
C65e06	MX-80 P	0.29	0.32	0.16	< 0.02	0.43	0.08	0.72
c65d46	MX-80	0.40	0.28	0.21	0.04	0.55	0.02	0.76
c65d46	MX-80	0.40	0.26	0.20	0.04	0.59	< 0.02	0.77
c65d46	MX-80	0.41	0.27	0.21	0.03	0.58	0.07	0.61
c65def	MX-80	0.37	0.31	0.19	< 0.02	0.62	0.08	0.71
c65def	MX-80	0.36	0.29	0.19	< 0.02	0.60	0.07	0.67
c65def	MX-80	0.36	0.31	0.19	< 0.02	0.58	0.09	0.68
c65dd4	Milos	3.11	< 0.02	< 0.02	< 0.02	11.50	< 0.02	0.20
c65dd4	Milos	3.26	0.02	0.07	< 0.02	11.70	< 0.02	0.19
c65dd4	Milos	3.42	0.04	0.22	< 0.02	11.74	< 0.02	0.21
c65df4	Milos	3.29	0.14	0.24	< 0.02	11.19	< 0.02	0.52
c65df4	Milos	3.60	0.10	0.54	< 0.02	11.18	< 0.02	0.37
c65df4	Milos	3.19	0.10	0.36	< 0.02	10.35	< 0.02	0.45
c96a9f	Kutch	1.12	< 0.02	0.18	< 0.02	3.46	< 0.02	0.06
c96a9f	Kutch	1.19	< 0.02	0.18	< 0.02	3.69	< 0.02	0.13
c96a9f	Kutch	1.17	< 0.02	0.18	< 0.02	3.62	< 0.02	0.68
c96b27	Kutch	0.56	0.16	0.10	< 0.02	1.70	< 0.02	0.67
c96b27	Kutch	0.53	0.13	0.07	< 0.02	1.73	< 0.02	0.61
c96b27	Kutch	0.57	0.11	0.10	< 0.02	1.76	< 0.02	0.51
c65e1c	Nanocore	0.70	0.24	0.44	0.19	0.24	< 0.02	0.77
c65e1c	Nanocore	0.73	0.24	0.45	0.22	0.24	< 0.02	0.77
c65e1c	Nanocore	0.70	0.25	0.41	0.21	0.26	< 0.02	0.77
c65ef8	Kiruna	1.53	0.13	0.38	< 0.02	4.21	0.06	0.23
c65ef8	Kiruna	1.53	0.09	0.28	< 0.02	4.59	0.02	0.21
c65ef8	Kiruna	1.59	0.16	0.24	< 0.02	4.95	0.08	0.22
c65e85	Japan	0.04	0.45	< 0.02	< 0.02	0.14	< 0.02	1.47
c65e85	Japan	0.04	0.44	0.02	< 0.02	0.09	< 0.02	1.43
c65e85	Japan	0.05	0.45	0.03	< 0.02	0.08	< 0.02	1.35

Analyses performed with samples of 200 mesh size. Prepared at Äspö hard rock laboratory and-/or Bureau Veritas Commodities Canada Ltd.

3.5.3 Pre-treatments

Analysis of data- sample with preparation

MX-80 bentonite (c65f3a) was extracted with hydrogen peroxide (H_2O_2) to see the possibility of "wash out" of organic carbon. Milos bentonite (c65e22) was extracted with hydrochloric acid (HCl) to see the possibility of "wash out" of inorganic carbon (for testing the method).

MX-80 bentonite (c65f3a) were also prepared with known amount sucrose, calcium carbonate, and zinc sulfide, to test the method.

The initial water content (wc) for MX-80 bentonite (c65f3a) was 8.2 % and for Milos bentonite 14.6 %

Extraction procedure with hydrogen peroxide

40 g MX-80 bentonite (milled 10 min 200 rpm) was diluted with 300 ml Milliq (purified DI water) In a borosilicate container, after swelling MX-80 was diluted with another 300 ml H_2O_2 (12 %) and allocated in falcon tubes (16 pieces). Extraction was repeated with H_2O_2 in falcon tubes for another two repetitions with centrifugation between each. H_2O_2 were applied with the same volume as clay in the tube (i.e. if 10 ml bentonite clay + 10 ml H_2O_2). After stirring with a borosilicate stirrer bentonite were diluted with Milliq to the 45 ml mark before centrifugation.

Three repetitions of extractions with Milliq in falcon tubes filled up to the 45 ml mark. Stirring with a borosilicate stirrer before centrifugation.

After extraction bentonite are dried in oven for 40 °C for 2 days and placed in falcon tubes for further distribution to external laboratory.

Extraction procedure with hydrochloric acid

4 g × 12 of Milos bentonite was diluted with 10 % HCl in falcon tubes (12 pieces).

Extraction was performed with HCl in falcon tubes for three repetitions and HCl filled up to the 45 ml mark. Stirring with a borosilicate stirrer before centrifugation between each dilution with HCl and placed in water bath (50 °C for 10 minutes).

Three repetitions of extractions with Milliq in falcon tubes filled up to the 45 ml mark. Stirring with a borosilicate stirrer before centrifugation.

After extraction bentonite are dried in oven for 40 °C for 2 days and placed in falcon tubes for further distribution to external laboratory.

All centrifugation was performed with a rotor 5.1, RCF 3 000, 18 °C for 5 minutes and Acc9. The fluid is separated from the bentonite by decanting or pipetting.

Results

Evolved gas analysis (EGA) showed some spread in the data. Pre-treatment with hot acid worked very well to remove carbonates from Milos bentonite. Hydrogen peroxide (H_2O_2) did not remove the organic carbon from MX-80, the content even seemed to increase, possibly a minor dissolution of something else or due to the method uncertainty. The largest addition of organic carbon was detected, however the smaller additions seems to be within the uncertainty of the method. Samples with added carbonate seems to have been overestimated with regards to carbonate and may need further attention. The additions of sulfides were captured well both as total S and as sulfide.

Table 3-10. EGA data of pre-treated samples. Content of carbon and sulfur components in bulk materials (wt%).

Bentonite	Preparation	Tot/C (%)	Tot/S (%)	C/ORG (%)	C/GRA (%)	CO_2 (%)	S/S^{2-} (%)	SO_4 (%)
MX-80 P	wH_2O_2	0.44	0.36	0.25	< 0.02	0.62	0.19	0.53
MX-80 P	wH_2O_2	0.43	0.30	0.32	< 0.02	0.33	0.12	0.55
MX-80 P	wH_2O_2	0.50	0.40	0.35	< 0.02	0.50	0.19	0.62
Milos	wHCl	0.02	0.59	< 0.02	< 0.02	< 0.02	0.51	0.24
Milos	wHCl	0.02	0.53	< 0.02	< 0.02	0.03	0.45	0.25
Milos	wHCl	0.02	0.64	0.02	< 0.02	< 0.02	0.56	0.24
MX-80 P	c65f3a	0.25	0.24	0.14	< 0.02	0.37	< 0.02	0.75
MX-80 P	c65f3a	0.23	0.25	0.10	0.03	0.37	< 0.02	0.80
MX-80 P	c65f3a	0.24	0.23	0.12	< 0.02	0.39	< 0.02	0.75
MX-80 P	oc0.02	0.26	0.23	0.14	< 0.02	0.39	< 0.02	0.77
MX-80 P	oc0.02	0.27	0.24	0.15	< 0.02	0.40	< 0.02	0.77
MX-80 P	oc0.02	0.25	0.23	0.14	< 0.02	0.38	< 0.02	0.77
MX-80 P	oc0.1	0.32	0.23	0.20	< 0.02	0.39	< 0.02	0.72
MX-80 P	oc0.1	0.35	0.23	0.23	< 0.02	0.42	< 0.02	0.78
MX-80 P	oc0.1	0.32	0.23	0.21	< 0.02	0.39	< 0.02	0.72
MX-80 P	oc1	1.09	0.23	0.98	< 0.02	0.36	< 0.02	0.70
MX-80 P	oc1	1.05	0.23	0.93	< 0.02	0.37	< 0.02	0.68
MX-80 P	oc1	1.18	0.21	1.07	0.03	0.31	< 0.02	0.63
MX-80 P	ic0.1	0.32	0.23	0.15	< 0.02	0.63	< 0.02	0.76
MX-80 P	ic0.1	0.35	0.23	0.14	< 0.02	0.73	< 0.02	0.73
MX-80 P	ic0.1	0.34	0.23	0.15	< 0.02	0.69	< 0.02	0.77
MX-80 P	ic1	1.17	0.21	0.10	< 0.02	3.89	< 0.02	0.71
MX-80 P	ic1	1.23	0.21	0.20	< 0.02	3.74	< 0.02	0.75
MX-80 P	ic1	1.32	0.20	0.28	< 0.02	3.77	< 0.02	0.61
MX-80 P	ic5	5.11	0.12	0.13	< 0.02	18.23	< 0.02	0.37
MX-80 P	ic5	5.40	0.12	0.54	< 0.02	17.80	< 0.02	0.33
MX-80 P	ic5	5.15	0.13	0.03	< 0.02	18.76	< 0.02	0.49
MX-80 P	s0.1	0.25	0.33	0.15	< 0.02	0.32	0.07	0.79
MX-80 P	s0.1	0.24	0.32	0.16	< 0.02	0.24	0.05	0.82
MX-80 P	s0.1	0.25	0.32	0.14	< 0.02	0.39	0.06	0.79
MX-80 P	s1	0.23	1.17	0.12	< 0.02	0.38	0.86	0.94
MX-80 P	s1	0.25	1.19	0.14	< 0.02	0.35	0.89	0.87
MX-80 P	s1	0.25	1.13	0.14	< 0.02	0.37	0.81	0.95
MX-80 P	s5	0.24	5.22	0.15	< 0.02	0.30	4.82	1.18
MX-80 P	s5	0.20	4.92	0.14	< 0.02	0.19	4.53	1.18
MX-80 P	s5	0.23	4.64	0.12	< 0.02	0.33	4.25	1.18

Analyses performed with samples of 200 mesh size. Prepared at Äspö hard rock laboratory and-/or Bureau Veritas Commodities Canada Ltd. wH_2O_2-washing with H_2O_2, wHCl-washing with HCl, prepared with; extra organic carbon added (oc: 0.02, 0.1 and 1 %), extra inorganic carbon (ic: 0.1, 1 and 5 %), extra sulfide added (s: 0.1, 1 and 5 %).

4 Physical properties method development

4.1 Swelling pressure and hydraulic conductivity

Swelling pressure and hydraulic conductivity are important parameters for the design of the buffer and backfill, see Section 2.1. The technique to determine the swelling pressure and hydraulic conductivity have been developed by SKB in previous projects (Svensson et al. 2017) and is briefly described in this chapter. Furthermore, data from one of the eight investigated bentonites are described and interpreted in detail. The data from the rest of the investigated bentonites are presented in Appendix 1. A comparison between the different bentonites is made in Section 6.1.

4.1.1 Methodology

The tests are performed according to the following, see also Karnland et al. (2006) and Svensson et al. (2017):

1. The selected homogenous material is packed into the swelling pressure cell to a predetermined dry density. A photo of the used cells is shown in Figure 4-1. The specimen has a diameter of 35 mm and an approximate height of 5 mm.
2. The specimen is saturated with deionised water and the swelling pressure measured with an external load cell is recorded continuously (σ_s), see Figure 4-2. This is done over a time period of about one week. The swelling pressure is determined as the recorded load divided with the cross sectional area of the specimen ($A_c = D^2\pi/4$) and interpreted when the pressure is considered to be stable.
3. The hydraulic conductivity of the specimen is first determined with deionised water. The determination is made by applying a constant pore pressure gradient over the specimen while the amount of water per time unit (q) is measured continuously. The gradient (i) is defined as the applied pressure in meters of water column divided by the height of the sample. The evaluation is made according to Darcy's law, where the hydraulic conductivity (k_w) is determined as kw = q/(A x i) where A is the cross sectional area of the specimen. The measurement of the hydraulic conductivity continues for about one week and interpreted when the outflow is considered to be stable.
4. A 1 M $CaCl_2$ solution is pumped through the filters at the same pressure on both sides of the specimen during continuous measurement of the swelling pressure. The contact with the calcium chloride solution changes the counter-ions in the bentonite to calcium alone, and the results thus provide information on the swelling pressure and hydraulic conductivity at extremely unfavourable conditions both with respect to the type of counter-ion and high ionic strength. The process where the counter ions are changed to calcium in the specimen takes about 1 week.
5. The hydraulic conductivity of the sample is determined with the calcium chloride solution for about one week.
6. The specimen is taken out of the swelling pressure cell, and its bulk density (ρ) and water content (w) are determined. The bulk density is determined by weighing a sample both in air and submerged in paraffin oil with known density. The water content is determined by drying a sample in an oven at a temperature of 105 ºC for 24 hours. With the known density and water content the dry density (ρ_d) can be calculated, see Equation 4-3 below.

Altogether nine determinations of swelling pressure and hydraulic conductivity at different dry densities are made for each material. The described technique and data coming from the investigation is used for determining the swelling pressure and the hydraulic conductivity at extreme conditions. However, due to the chosen procedure the final determined dry density is misleading, since the salt ($CaCl_2$) in the water will be "added" to dry part of the sample and thereby affect the calculated dry density. Therefore, an additional determination of the swelling pressure is made with deionized water only. The preparation and determination are made according to item 1 and 2 above and after 1 week are the density and water content determined (item 6). These measurements of the swelling pressure are used to adjust the density of the initial determinations, see below.

The measurement accuracy for the determinations, both for swelling pressure and hydraulic conductivity, are estimate, see below.

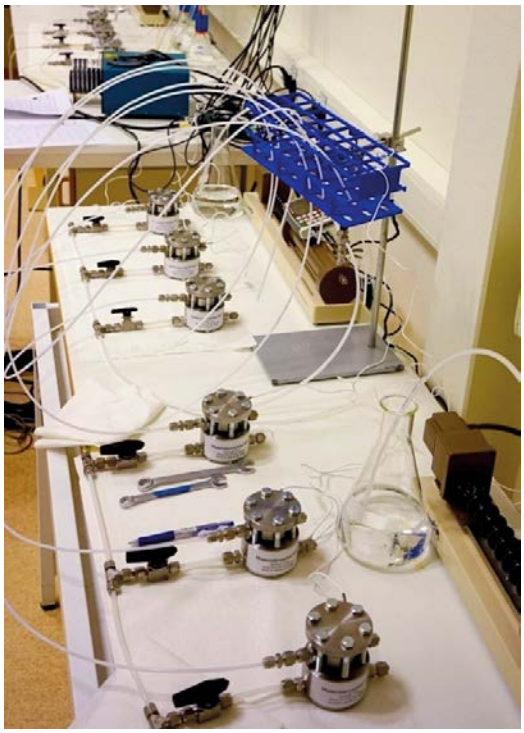

Figure 4-1. *The test cells for swelling pressure and hydraulic conductivity measurements.*

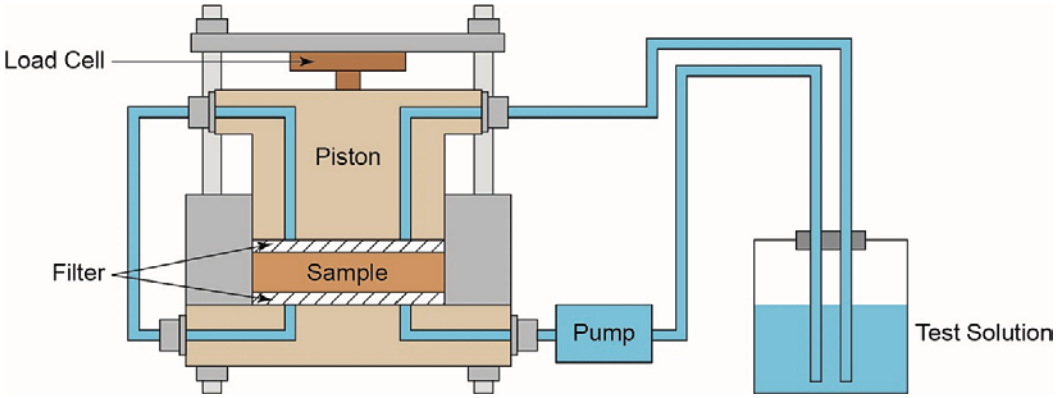

Figure 4-2. *Schematic drawing of a test cell for determining the swelling pressure.*

4.1.2 Analysis of data

The results from the measurements of swelling pressure and hydraulic conductivity made on a bentonite from Morocco presented in this section. In Table 4-1 are the initial data from the test summarised, test series 1. The density and water content are determined after the samples have had access to the strong salt solution, 1 M $CaCl_2$. The results of the swelling pressure measurements made on samples which only have had access to deionized water (mQ) are presented in Table 4-2, test series 2. The results from the measurement of swelling pressure and the hydraulic conductivity are plotted as function of the dry density of the specimen in Figure 4-3a. Following conclusions can be made from the plots:

- The swelling pressure is very much depending on the dry density of the bentonites. In Figure 4-3 are exponential functions adapted to the data sets.
- The data from the first data set (marked with green and red dots respectively in Figure 4-3a) indicates that the swelling pressure decreased as expected when the specimens got access to the strong salt solution.
- A comparison between the two sets of data where the specimens have had access to deionized water (marked with green and blue dots respectively in Figure 4-3a) shows that they are quite different. The reason for this is that, at the calculation of the dry density for the specimen made after the test the salt is affecting the determination of the water content in test series 1 and thus the dry density was overestimated for these specimens.
- The comparison of the hydraulic conductivity of the specimen with deionised water and with salty water (1 M $CaCl_2$) is shown in Figure 4-3b. The figure shows that for low dry densities the hydraulic conductivity is higher for the samples which had access to the salt solution: Furthermore, there is a tendency that for higher densities the opposite relationship applies i.e. the hydraulic conductivity is higher for the test made with deionised water.

Table 4-1. Results from tests made on bentonite Morocco 2017 both with deionized water and 1 M CaCl2 (test series 1).

				De-ionized water			1 M $CaCl_2$		
Test	ρ	w	ρ_d	σ_s	Gradient	k_w	σ_s	Gradient	k_w
No.	(kg/m^3)	(%)	(kg/m^3)	(kPa)	(m/m)	(m/s)	(kPa)	(m/m)	(m/s)
Morocco 2017 1	1895	33.2	1423	2446	5881	3.04E−13	1325	4901	3.96E−13
Morocco 2017 2	1960	31.3	1493	5659	6080	1.23E−13	3758	5066	1.05E−13
Morocco 2017 3	1982	28.7	1540	6567	6074	7.83E−14	4707	5061	7.78E−14
Morocco 2017 4	1880	35.2	1391	2287	13202	3.70E−13	1183	9430	5.63E−13
Morocco 2017 5	1997	26.0	1585	8639	14423	7.61E−14	6791	10302	5.47E−14
Morocco 2017 6	2034	25.6	1620	11238	14214	6.04E−14	9357	10153	4.45E−14
Morocco 2017 7	1895	33.4	1421	2656	9369	2.51E−13	1430	9369	3.66E−13
Morocco 2017 8	1989	27.2	1564	7755	10183	4.40E−14	6118	10183	5.94E−14
Morocco 2017 9	2000	24.5	1607	10776	10103	5.18E−14	8898	10103	4.42E−14

Table 4-2. Results from tests made on bentonite Morocco 2017 with deionized water (test series 2).

Test	ρ	w	ρ_d	σ_s
No.	(kg/m^3)	(%)	(kg/m^3)	(kPa)
Morocco 2017 mQ 1	1796	37.3	1308	2004
Morocco 2017 mQ 2	1921	29.2	1486	6732
Morocco 2017 mQ 3	1979	26.8	1561	10898
Morocco 2017 mQ 4	1793	36.9	1310	1864
Morocco 2017 mQ 5	1908	31.0	1457	4617
Morocco 2017 mQ 6	1941	29.3	1502	6908
Morocco 2017 mQ 7	1892	34.9	1402	4302
Morocco 2017 mQ 8	1984	29.1	1537	8918
Morocco 2017 mQ 9	1994	25.9	1584	12233

As stated above, there are large differences in the swelling pressure data from the tests made with deionized water, compare data set marked with green and blue dots respectively in Figure 4-3a, since the salt affects the determination of the dry density of the specimens. However, it is possible to adjust the density for the salt content in the pore water. This can theoretically be done if the density of the solid particles (ρ_s) and the salt concentration in the porous system are known. The density of the solid particles for the eight bentonites examined in this project has been determined. Although, the salt concentration of the salt solution used at the saturation is known it is not obvious that the salt concentration in the interlayer water in the saturated bentonite is the same. The salt concentration in the specimen is depending on the type of bentonite, the density of the specimen and the type of salt used in the test.

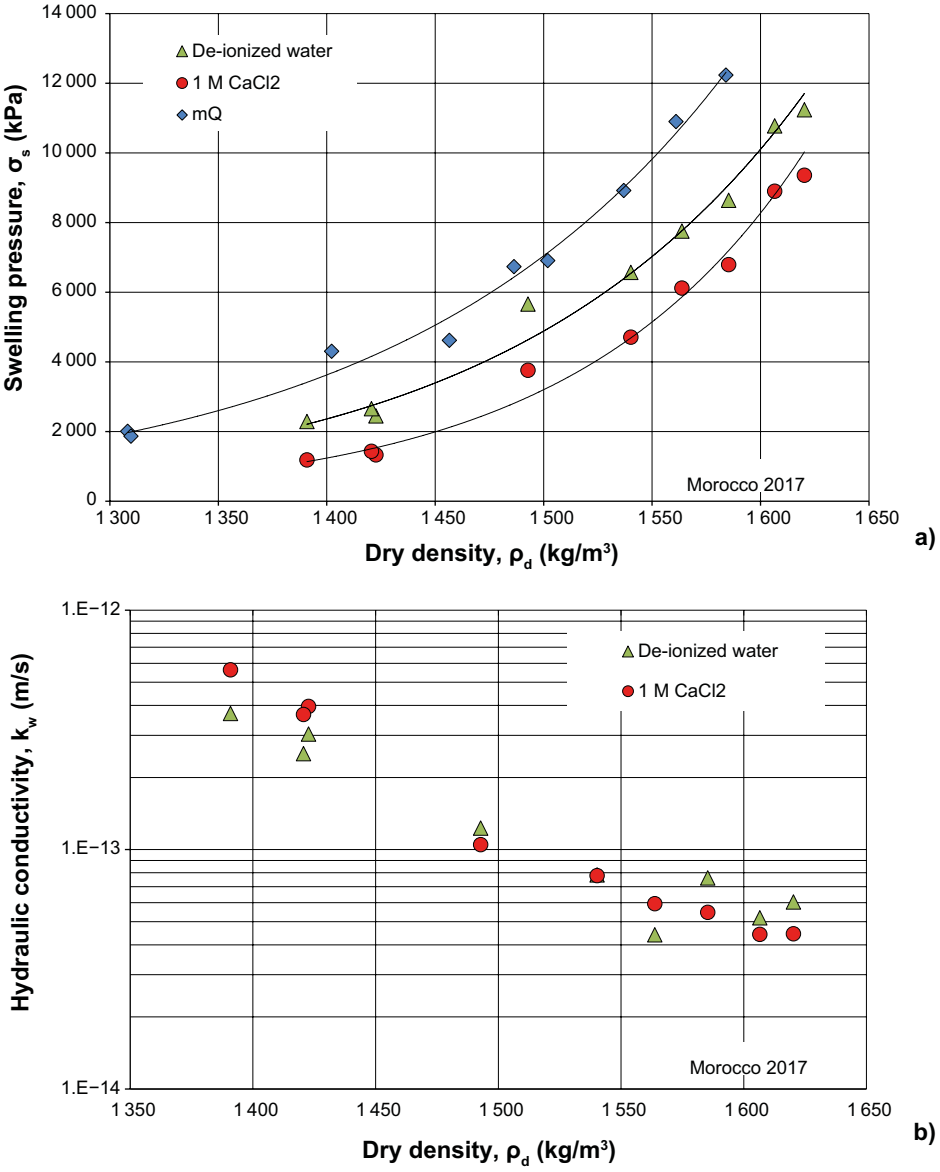

Figure 4-3. *Swelling pressure (a) and hydraulic conductivity (b) as function of dry density for the bentonite Morocco 2017.*

In this project, different salt concentration for the interlayer water of the specimen was assumed and corrected dry densities for series 1 were calculated. The salt concentration which best fitted the data was determined by comparing the corrected data from test series 1 with data from test series 2 in a plot of the swelling pressure. The results after corrections, for the bentonite from Morocco, are shown in Figure 4-4a. In this case it is assumed that the salt concentration within the porous system for the specimens was 1 M $CaCl_2$ i.e. the same salt concentration as for the water used at the saturation of the specimens. Corresponding adjustment of the dry density for hydraulic conductivity is shown in Figure 4-4b. Note that this correction must be made for each tested bentonite and thus the assumption of the salt concentration may varying between the materials, see also Appendix 1.

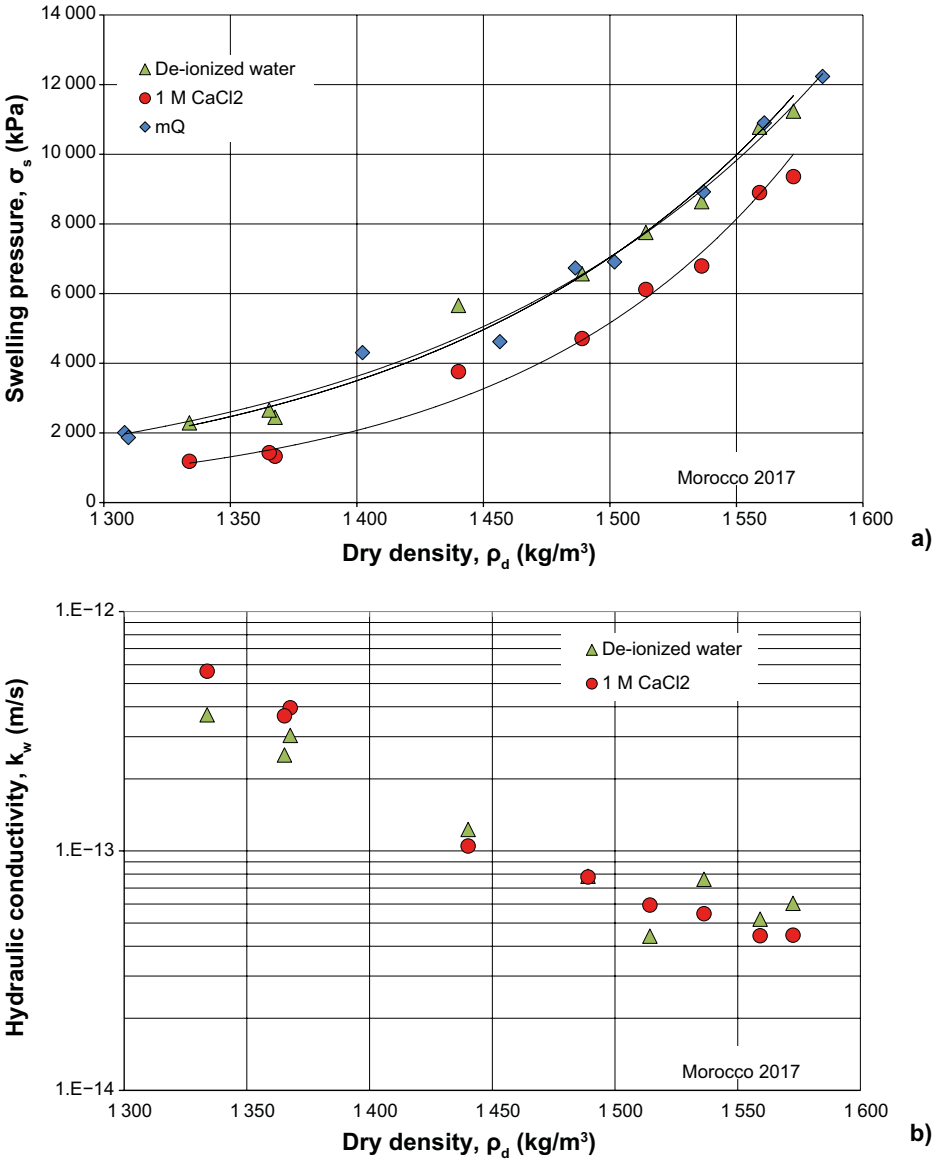

Figure 4-4. *Swelling pressure (a) and hydraulic conductivity (b) as function of dry density for the bentonite Morocco 2017 after adjusting for excess salt in the interlayer water assumed to be 1 M $CaCl_2$.*

4.1.3 Validation of the test method

Fast determination of swelling pressure

To investigate whether it is possible to determine the swelling pressure curve on samples which have had access to deionized water during only at maximum 24 hours a series of tests was done on MX-80 originated from Wyoming USA. The bentonite has a content of montmorillonite of about 90 % and a Cation Exchange Capacity of about 85 cmol/kg. At this investigation, in total 13 tests, the specimens had access to deionized water through filters at both bottom and top during continuous measurement of the swelling pressure (σ_s), see Figure 4-2. Specimens, with a thickness of about 5 mm, were placed in the oedometer. A vacuum pump was connected to the cells and the air inside tubes and filters was evacuated. At start the specimens got access to deionized water under pressure. An example of the measured swelling pressure is shown in Figure 4-5. The figure shows that an increase in the swelling pressure could be observed immediately after the samples had got access to water. During about 1 hour there was a drop in the swelling pressure following by an increase. The specimens reached their maximum swelling pressure after about 8 hours. The specimens had then access to water for another 10 hours. After this, the specimens were then taken out from the test cells and their water content (w) and bulk density (ρ) were determined according to standard procedures.

From the determined water content and dry density it is possible to calculate the degree of saturation (S_r), the void ratio (e) and the dry density (ρ_d) by the following equations:

$$S_r = \frac{w\rho\rho_s/\rho_w}{\rho_s(w+1)-\rho} \quad (4\text{-}1)$$

$$e = \frac{\rho_s-\rho}{\rho-\rho_w S_r} \quad (4\text{-}2)$$

$$\rho_d = \frac{\rho}{1+w} \quad (4\text{-}3)$$

where S_r describes how large part of the total pore volume which is filled with water. At this determination it is assumed that the solid particles of the bentonite is ρ_s = 2 780 kg/m^3 and that the density of the pore water is ρ_w = 1 000 kg/m^3. At a complete dry specimen is S_r = 0 and if all the voids are filled with water S_r = 1. The results from all 13 tests are shown in Table 4-3. A reference sample, which was saturated during 7 days, is also included in the table. The table shows that all the specimens had after the test a degree of saturation close to 1. The bulk density varied between 1 846 kg/m^3 and 1 987 kg/m^3 and the measured maximum swelling pressure varied between 2 149 kPa and 10 557 kPa.

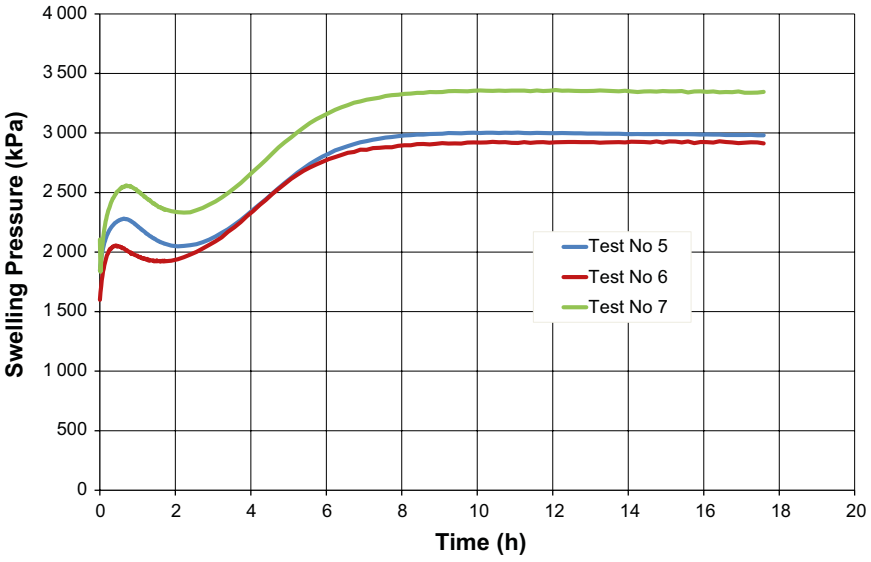

Figure 4-5. *Measured swelling pressure as function of time on samples of MX-80.*

Table 4-3. Evaluated bulk density (ρ), water content (w), degree of saturation (S_r), void ratio (e) and dry density (ρ_d) together with the maximum swelling pressure (σ_s) determined after 24 hours of saturation.

Test No	ρ (kg/m³)	w (-)	S_r (-)	e (-)	ρ_d (kg/m³)	σ_s (kPa)
Test 1	1 876	0.370	0.998	1.030	1 369	2 565
Test 2	1 873	0.350	0.969	1.004	1 387	3 187
Test 3	1 885	0.338	0.965	0.974	1 409	3 316
Test 4	1 846	0.371	0.968	1.065	1 346	2 149
Test 5	1 884	0.350	0.981	0.992	1 396	2 987
Test 6	1 874	0.350	0.970	1.003	1 388	2 922
Test 7	1 880	0.349	0.976	0.995	1 394	3 346
Test 8	1 885	0.359	0.994	1.004	1 387	3 130
Test 9	1 919	0.320	0.975	0.913	1 453	4 962
Test 10	1 904	0.339	0.987	0.956	1 421	3 910
Test 11	1 944	0.318	0.999	0.885	1 475	5 058
Test 12	1 987	0.270	0.966	0.777	1 564	10 557
Test 13	1 983	0.274	0.968	0.786	1 557	9 468
Ref*)	1 892	0.343	0.982	0.970	1 411	3 306

*) This sample was tested at the same time as the rest of the samples but saturated for more than 6 days.

The measured swelling pressure is plotted as function of the dry density of the specimens in Figure 4-6. Specimens which were saturated for a much longer time, > 14 days, are also plotted in the same figure. The data form these tests are shown in Table 4-4. The results indicate that the swelling pressure for specimens which were saturated during 24 h is in the same range as for the specimens saturated during more than 14 days. This is valid for the range in dry density between 1 250 kg/m³ and 1 650 kg/m³.

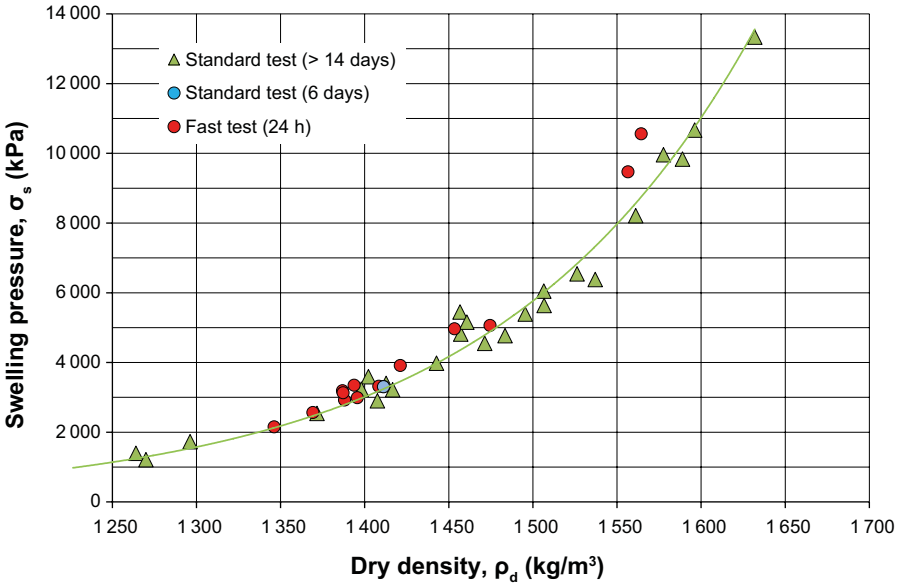

Figure 4-6. *Determined swelling pressure as function of the dry density of the specimens after about 24 h, 6 days and more than 14 days saturation respectively.*

The following conclusions can be drawn from the tests:

- Even at short time for saturation of the specimens, shorter than 24 h, they are close to fully saturated. For all of the specimens the calculated degree of saturation is between 0.966 and 0.999, see Table 4-3. However, there is a tendency that the degree of saturation decreases with increasing dry density of the specimens.
- Although, the specimens are saturated after about 24 hour it can´t be ruled out that the swelling pressure is not fully developed. However, the performed tests show that the maximum swelling pressure is reached after about 10 hours after start of the saturation, see Figure 4-5.When comparing the evaluated swelling pressure from these tests with results from tests where the specimens were saturated during 14 days the results are similar, see Figure 4-6.
- The used fast method can thus be used as a first check of a material at e.g. delivery control or as daily control of the bentonite at the facilities for producing buffer and backfill components (blocks and pellets).

Table 4-4. Evaluated bulk density (ρ), water content (w), degree of saturation (S_r), void ratio (e) and dry density (ρ_d) together with hydraulic conductivity (k_w) and maximum swelling pressure (σ_s) determined on samples with varying heights.

No	Height (mm)	ρ (kg/m^3)	w (-)	S_r (-)	e (-)	ρ_d (kg/m^3)	i (m/m)	k_w (m/s)	σ_s (kPa)
1	5	1805	0.428	0.992	1.199	1264	11030	2.82E−13	1395
2	5	1913	0.364	1.031	0.982	1402	11876	1.25E−13	3590
3	5	1929	0.324	0.992	0.908	1457	11448	1.2E−13	4815
4	5	1835	0.416	1.010	1.145	1296	12997	2.06E−13	1724
5	5	1904	0.348	0.999	0.968	1413	13670	1.27E−13	3398
6	5	1984	0.317	1.041	0.845	1506	14328	7.5E−14	6044
7	5	1879	0.370	1.001	1.027	1372	11728	1.51E−13	2537
8	5	1926	0.322	0.986	0.908	1457	12208	8.56E−14	5445
9	5	1953	0.337	1.036	0.903	1461	11762	9.95E−14	5156
10	10	1890	0.352	0.989	0.989	1398	9809	1.36E−13	3233
11	10	1944	0.310	0.987	0.874	1483	9813	7.99E−14	4768
12	10	2014	0.268	0.993	0.750	1589	10046	4.63E−14	9831
13	10	1786	0.456	1.001	1.266	1227	2517	5.16E−13	808
14	10	1796	0.449	1.004	1.244	1239	2439	4.1E−13	952
15	10	1818	0.431	1.009	1.189	1270	2406	3.94E−13	1211
16	10	1897	0.347	0.990	0.975	1408	5758	1.29E−13	2901
17	10	1965	0.287	0.973	0.821	1526	6059	7.98E−14	6543
18	10	2009	0.273	0.998	0.762	1578	6017	5.89E−14	9958
19	20	1904	0.344	0.993	0.962	1417	3027	1.16E−13	3216
20	20	1961	0.302	0.992	0.845	1507	3043	8.73E−14	5632
21	20	2033	0.246	0.970	0.704	1632	10128	3.49E−14	13333
22	20	1914	0.327	0.979	0.927	1443	8924	2.49E−13	3977
23	20	1949	0.303	0.982	0.859	1495	8980	2.01E−13	5389
24	20	1990	0.275	0.979	0.781	1561	8732	1.34E−13	8209
25	20	1938	0.317	0.990	0.889	1471	10113	1.17E−13	4548
26	20	1978	0.287	0.986	0.809	1537	10072	1.7E−13	6378
27	20	2011	0.260	0.975	0.742	1596	10237	7.61E−14	10666
28	20	1913	0.316	0.963	0.912	1454	9465	1.37E−13	4480
29	20	1972	0.283	0.972	0.809	1537	9647	1.13E−13	7158
30	20	1978	0.272	0.959	0.787	1555	9500	1.08E−13	8628

Influence of the sample height on the measurements

According to the standard for measuring swelling pressure the height of the specimen should be 5 mm. However, it can´t be ruled out that the dimensions and especial the height of the specimen are affecting the evaluated swelling pressure and hydraulic conductivity. For that reason, series of tests were made where the height of the samples was varied. Tests were made on MX-80 with heights 5, 10 and 20 mm respectively. The samples were prepared and saturated with de-ionized water for up to 30 days during continuous measurement of the swelling pressure in accordance with the standard. The hydraulic conductivity (k_w) was then measured with deionized water, in accordance with the standard procedure, by applying a pore pressure gradient (i) over the specimen. The specimens were then taken out from the test cells and their water content (w) and bulk density (ρ) were determined according to standard procedures. Finally the degree of saturation (S_r), the void ratio (e) and the dry density (ρ_d) were calculated with Equations 4-1 to 4-3. The results from all 30 tests are shown in Table 4-4. The table shows that all specimens were fully saturated, i.e. S_r is close to 1 although there is a small tendency that the degree of saturation was decreasing with increasing specimen height.

The measured swelling pressure for all test are plotted as a function of the dry density for the three different sample heights in Figure 4-7. Exponential curves are fitted to the data sets. The figure shows that the swelling pressure for the specimen height of 5 mm is about 400 kPa higher than for the rest of the tests i.e. for specimen heights 10 mm and 20 mm respectively. A possible explanation for this might be that the tests made with specimen height 5 mm are more homogeneous compared to the other although all of them are close to fully saturated. The inhomogeneity may have arisen both during compaction and at the water saturation of the specimens. Thereby it is not impossible that, after a longer time, also the larger specimens will be more homogenised and the swelling pressure might increase.

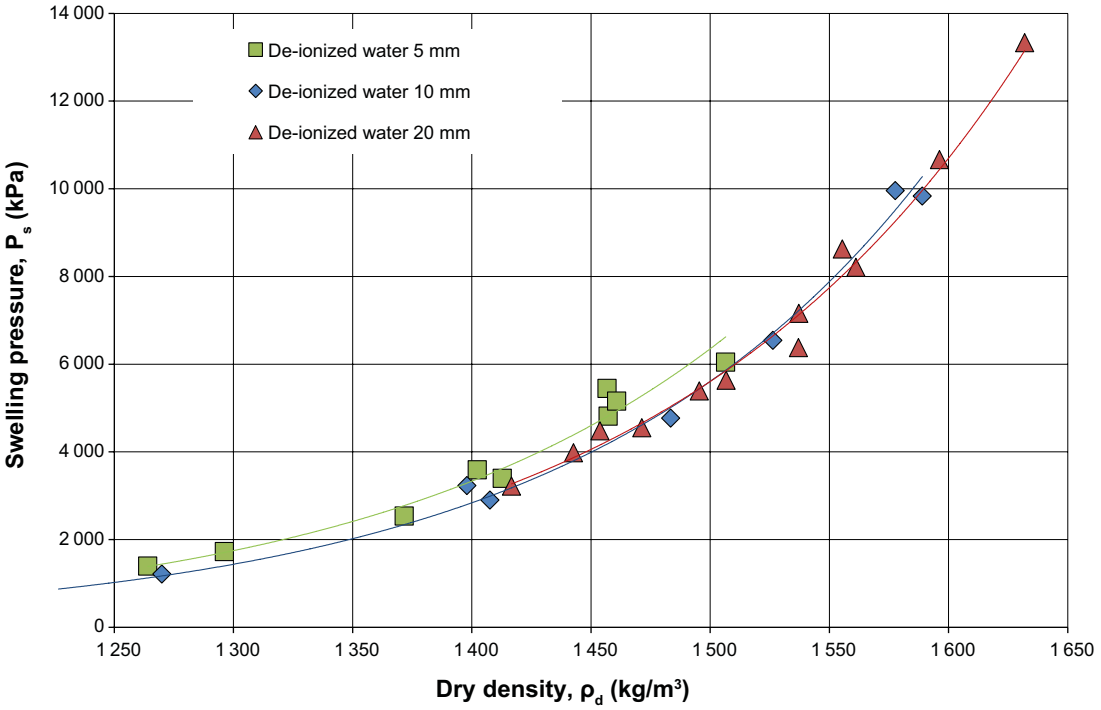

Figure 4-7. *Determined swelling pressure as function of the dry density for the specimens with three different heights 5, 10 and 20 mm respectively.*

Corresponding plot for the measured hydraulic conductivity is shown in Figure 4-8. The figure shows that the some data points from the tests with specimen height of 20 mm differ somewhat from the rest of the tests. The specimens with the height of 20 mm have in average about times 1.5–2 higher hydraulic conductivity compared to the rest of the specimens. An explanation for this might be that the smaller specimens are more homogeneous. Another possible explanation might be that there is a transition resistance between the specimen and the filters placed at the bottom and at the top. This possible transition resistance is present in all of the performed tests but affect more the evaluated hydraulic conductivity for the smaller specimens.

The assessment is that the measurement of swelling pressure according to the standard procedure i.e. with a height of 5 mm gives a relevant determination of the swelling pressure. When the hydraulic conductivity is determined on the same specimen there is a risk that the evaluated value is too low.

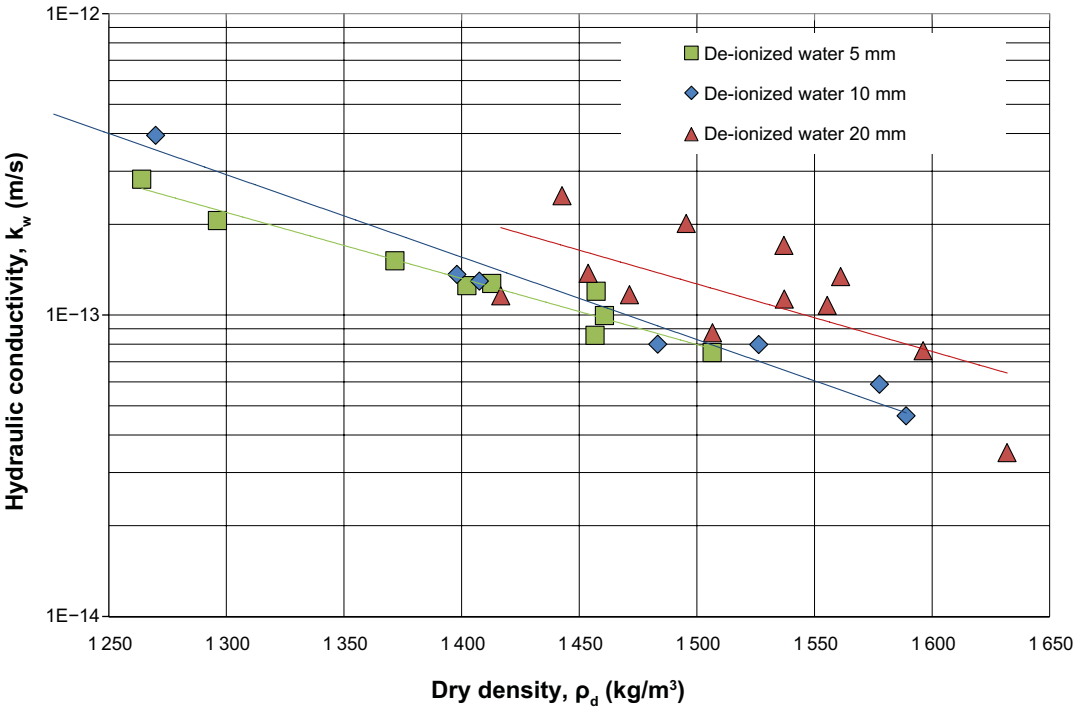

Figure 4-8. *Determined hydraulic conductivity as function of the dry density for the specimens with three different heights 5, 10 and 20 mm respectively.*

4.1.4 Accuracy in the determinations

The accuracy in the determination of swelling pressure and hydraulic conductivity is complex. Factors which might affect the accuracy are:

1. The accuracy in the measurement of water content and density of the specimen (see Section 4.4 and Section 4.6)
2. The accuracy of measuring the load (measured with the load cell placed on the top of the piston, see Figure 4-2).
3. The accuracy of measuring the volume of the water passing through the sample at the determination of the hydraulic conductivity.
4. The preparation and the condition under which the measurement of the swelling pressure and the hydraulic conductivity are made might also affect the determinations.
5. The bentonite is a geological material with a natural variation.

It is difficult to take into account these factors in a systematic way and therefor the suggestion is to use the following steps in order to estimate the accuracy in the measurements:

From the data shown in Figure 4-3 best fitted curves, in these cases exponential functions, are calculated and adapted with the use of the least square method. The residuals are calculated by subtracting the original data sets from the adapted curves, see Figure 4-9 and Figure 4-10. For this material there are no obvious trends in the residual plots. Since this is the case, it is possible to calculate the average and standard deviation of the residuals and thus use the standard deviation as an estimation of the accuracy in the determinations. The standard deviation and the mean value of the residuals for all of the investigated bentonites are shown in Table 4-5. See also Appendix 1.

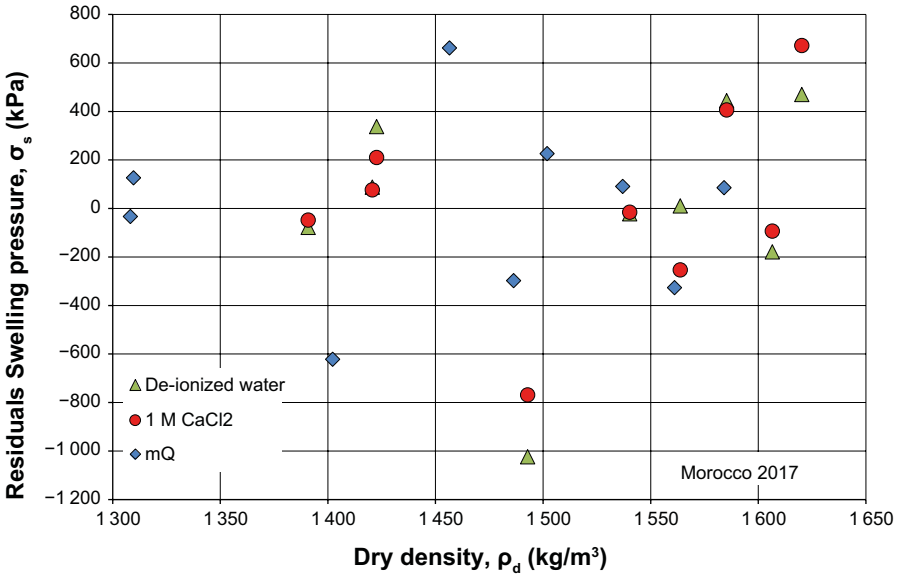

Figure 4-9. *The residual plot for the determined swelling pressure for the bentonite Morocco 2017.*

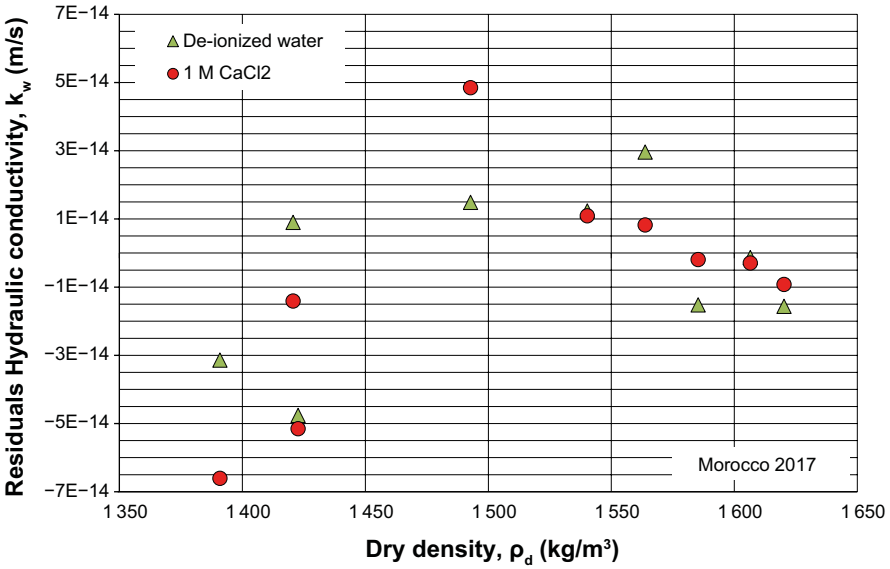

Figure 4-10. *The residual plots for the determined hydraulic conductivity for the bentonite Morocco 2017.*

Table 4-5. The average and standard deviation of the residuals from the determinations of swelling pressure and hydraulic conductivity on the investigated bentonites.

Test series	Number of tests	Swelling pressure		Hydraulic conductivity	
		Average (kPa)	Stdv (kPa)	Average (m/s)	Stdv (m/s)
Milos 2017 mQ	9	−2	652	-	-
Milos 2017 De-ionized water	9	3	892	−1.0E−11	3.6E−11
Milos 2017 1 M $CaCl_2$	9	68	1 137	−2.1E−12	6.4E−12
Morocco 2017 mQ	9	−10	371	-	-
Morocco 2017 De-ionized water	9	5	451	−5.1E−15	2.5E−14
Morocco 2017 1 M $CaCl_2$	9	21	408	−8.7E−15	3.4E−14
Bulgaria 2017 mQ	9	−7	620	-	-
Bulgaria 2017 De-ionized water	9	16	510	−2.6E−15	2.9E−14
Bulgaria 2017 1 M $CaCl_2$	9	36	495	−2.8E−15	2.7E−14
Turkey 2107 mQ	9	−12	396	-	-
Turkey 2017 De-ionized water	9	−20	350	−5.2E−16	2.1E−14
Turkey 2017 1 M $CaCl_2$	9	−31	232	−5.7E−16	7.4E−15
India 2018 mQ	9	−8	732	-	-
India 2018 De-ionized water	9	−26	576	−1.4E−16	1.0E−14
India 2018 1 M $CaCl_2$	9	−29	577	−5.8E−16	1.8E−14
BARA-KADE 2017 mQ	9	−2	320	-	-
BARA-KADE 2017 De-ionized water	9	14	260	−1.9E−15	2.0E−14
BARA-KADE 2017 1 M $CaCl_2$	9	18	100	−1.6E−14	7.2E−14
Bulgaria F 2017mQ	9	−15	199	-	-
Bulgaria F 2017 De-ionized water	9	−15	725	−1.4E−15	1.9E−14
Bulgaria F 2017 1 M $CaCl_2$	9	−16	741	−1.6E−15	1.8E−14
Sardinia 2017 mQ	9	1	254	-	-
Sardinia 2017 De-ionized water	9	83	826	−6.8E−15	2.8E−14
Sardinia 2017 1 M $CaCl_2$	9	133	1 025	−3.5E−14	1.2E−13

4.2 Unconfined compression strength

The unconfined compressive strength is an important parameter for the design of the buffer, see Section 2.1. The buffer around the canister will, besides minimising the risk for radio nuclides to be spread, also function as mechanical protection of the canister. Rock shear movements may occur when the stresses in the bedrock are released. Depending on the mechanical properties of the buffer, the rock shear movements may cause the insert in the canister to collapse or deform to such extent that the deformation of the copper shell will result in a breach and loss of the containment. The higher the strength of the buffer is the higher the stresses in the canister will be. The technique to determine the unconfined compressive strength has been described by SKB in previous projects (Svensson et al. 2017) and is briefly described in this chapter. Furthermore, data from one of the eight investigated bentonites are described and interpreted in detail. The data from the rest of the investigated bentonites are presented in Appendix 2. A comparison between the different bentonites is made in Section 6.2.

4.2.1 Methodology

The unconfined compressive strength is determined by the unconfined compression test as the deviator stress at failure. In this type of test a sample is compressed axially with a constant rate of strain with no radial confinement or external radial stress. The test is made on saturated specimen and can be regarded as a consolidated unconfined compression test.

The specimens used for the test are relatively small. The diameter is 20 mm and the height is 40 mm. The specimens are first compacted and then saturated in a separate device. The device used for the saturation is shown in Figure 4-11. The device consists of two end plates with filters and one central part with a height of 20 mm and with 10 holes in which the compacted specimens are placed. The specimens have then access to deionized water through the end plates for about 4 weeks. The height of the samples is set to 20 mm in order to minimize the time for saturation. The end plates are after saturation removed and the specimens are pressed out from central part. The actual test of the strength can then start. A schematic drawing of the test setup is shown in Figure 4-12. Note that in order to get a total sample height of 40 mm two samples are placed on top of each other. The test is made at a deformation rate of 0.8 % of the sample height per minute at continuously measurement of the applied load and deformation of the specimen. If no clear maximum in the stress can be determined the strength of the specimen is determined at a strain of 15 %.

The water content (w) and bulk density (ρ) for specimens are, after the tests, determined according to standard procedures. From the determined water content and dry density it is possible to calculate the degree of saturation (S_r), the void ratio (e) and the dry density (ρ_d) with Equations 4-1 to 4-3.

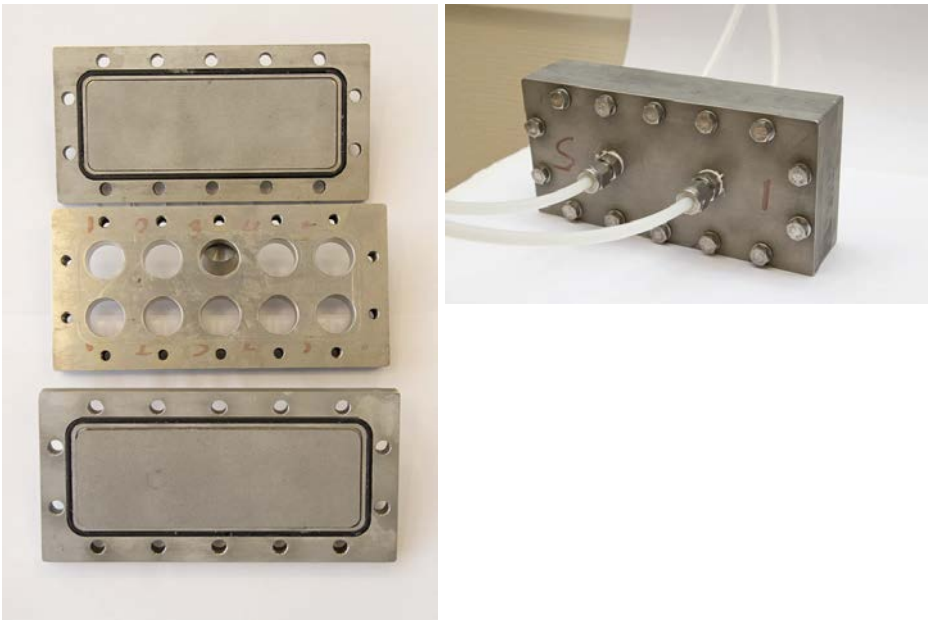

Figure 4-11. *The device used for saturating the specimens.*

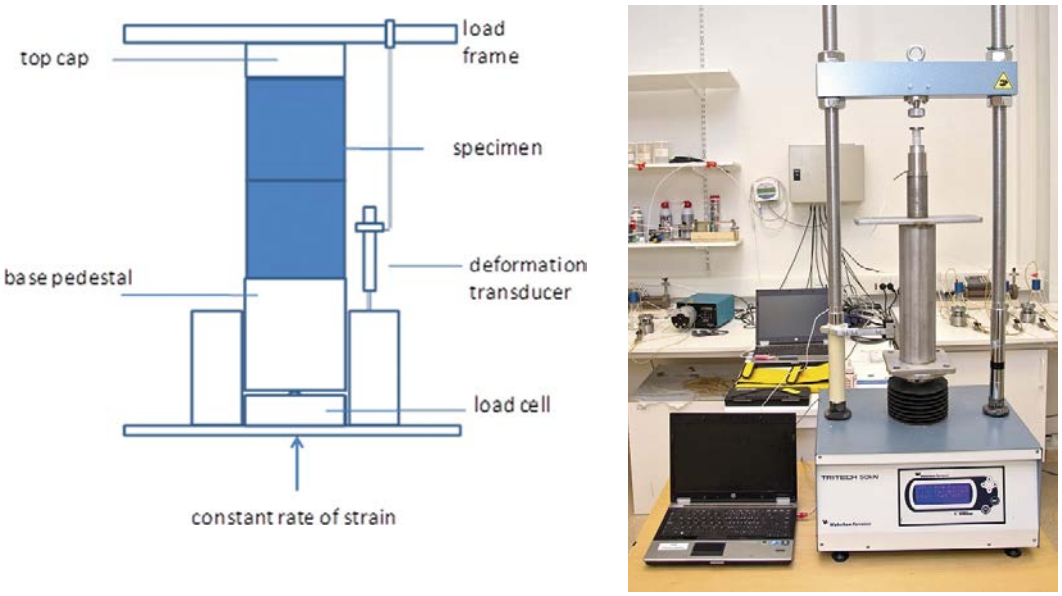

Figure 4-12. *Schematic drawing and a photo of the test setup (Dueck et al. 2010).*

4.2.2 Analysis of data

An example of data from the test is shown in Figure 4-13 where the applied vertical stress is plotted as function of the vertical strain of the specimens. The unconfined strength of the saturated specimens is determined as the maximum stress applied to the sample. This data is plotted together with the data from the determination of the dry density of the specimens, see Figure 4-14. From the data a best fitted curves, in these cases an exponential function, is calculated and adapted with the use of the least square method.

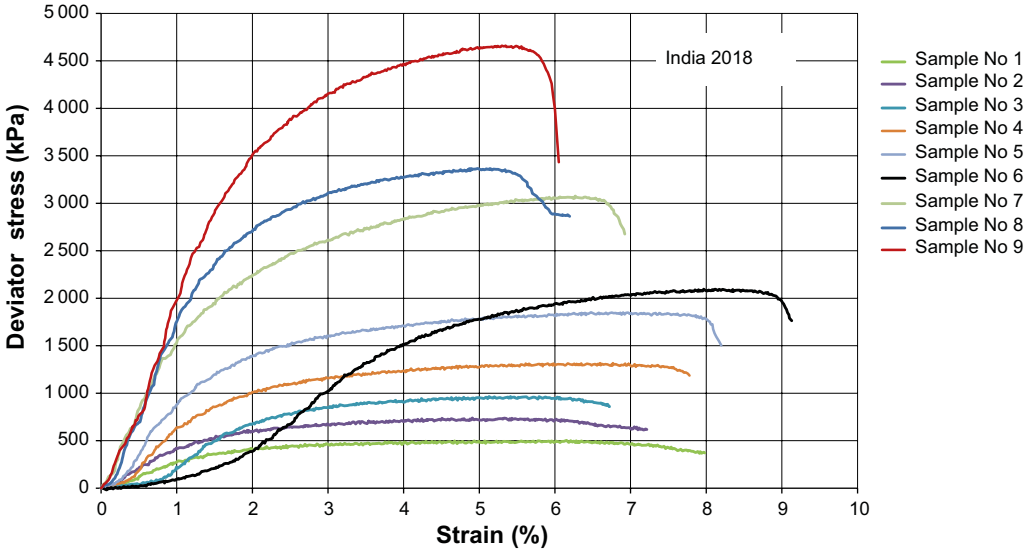

Figure 4-13. *Measured axial stress as function of strain on specimens of India 2018. The tests are made at different dry density of the specimens.*

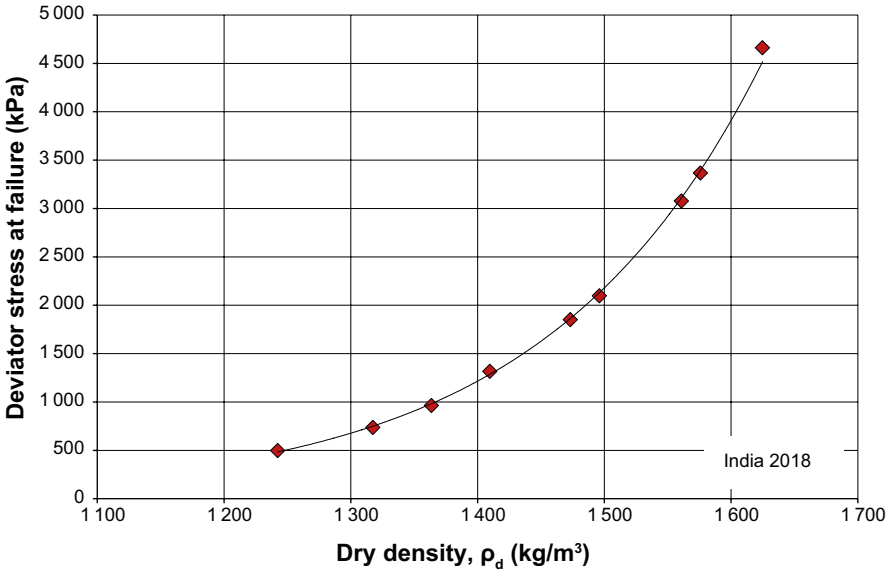

Figure 4-14. *Determined maximum strength as function of the dry density for the specimens for India 2018.*

4.2.3 Accuracy in the determinations

The accuracy in the determination of the unconfined compression strength is estimated in the same way as for the swelling pressure and the hydraulic conductivity, see Section 4.1. The determination is included the following steps:

From the data shown in Figure 4-14 a best fitted curve, in this case an exponential function, is calculated and adapted with the use of the least square method. By subtracting the original data set from the adapted curve the residuals are calculated, see Figure 4-15. For this material there is no obvious trend in the residual plot. Since this is the case, it is possible to calculate the average and standard deviation of the residuals and thus use the standard deviation as an estimation of the accuracy in the determination see Table 4-6. In this table are also the standard deviations and means of the residuals for the other investigated bentonites listed, see Appendix 2.

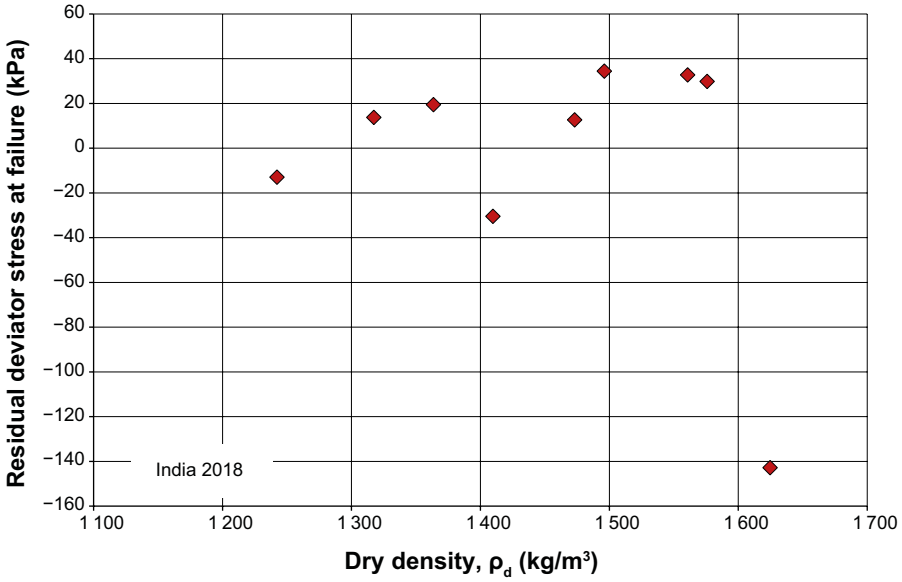

Figure 4-15. *The residual plot for the determined maximum strength for India 2018.*

Table 4-6. The average and standard deviation of the residuals from the determinations of the maximum strength on the 8 investigated bentonites.

Test series	Number	average (kPa)	Stdv (kPa)
India 2018	9	−5	56
BARA-KADE 2017	5	1	47
Bulgaria 2017	9	16	177
Morocco 2017	7	5	452
Milos 2017	5	3	128
Sardinia 2017	5	−1	50
Turkey 2017	5	1	16
MX-80 P 2014	10	−41	94
All Materials	45	2	183

4.3 Compaction properties

The compaction properties of a bentonite are important as input for the design of the buffer and the backfill blocks e.g. at the choice of water content and the dry density, but also at the production of them. The compaction properties are investigated with a laboratory test and the outcome of the test are primarily what dry density is possible to achieve and at what water content and compaction stress this can be made. The technique to determine the compaction properties of bentonites has been described by SKB in previous projects (Svensson et al. 2017) and is briefly described in this chapter. Furthermore, data from one of the six investigated bentonites are described and interpreted in detail. The data from the rest of the investigated bentonites are presented in Appendix R. A comparison between the different bentonites is made in Section 6.3.

4.3.1 Methodology

The presented laboratory test is based on tests made during several years of deliveries of bentonite to SKB for production of buffer and backfill blocks. The laboratory test also includes determinations of water content and bulk density of the compacted specimens. These determinations are made in accordance with standard procedures.

The water content of the specimens is varied between 10 % and 26 %. This interval in water content can possibly be changed depending on the initial water content of the bentonite and its ability to hold water. The mixing with water to the decided content is made in the laboratory in steps of 1 percentage steps. In total, approximately 1 kg of each mixture, with specified water content, is prepared. It is favourable if the mixed bentonite can be stored in a water tight container or a plastic bag for at least 48 hours before the actual compaction of the specimens to get a more homogeneous mixture.

A sample of about 20 g is taken from a mixture and placed in the mould, see Figure 4-16a. The sample is then compacted in a hydraulic press with a maximum load capacity of 20 tonnes, see Figure 4-16b. The diameter of the mould should be 35 mm. This procedure is repeated for each mixture 5 times were the compaction is made with the suggested compaction pressures of 25, 40, 60, 80 and 100 MPa respectively. The choice of compaction pressure might be varied due to type of bentonite but it is also depending on whether the bentonite will be used for the backfill or the buffer. The applied load in the press is normally specified in the unit tonnes or kN. The calculation of the compaction pressure from the measured load is made as follows:

$$\sigma_{comp} = \frac{Fx4}{\pi D^2} \quad (4\text{-}4)$$

where

σ_{comp} = compaction pressure (kPa)

F = applied load (kN)

D = mould diameter (m)

Figure 4-16. *Compaction of bentonite (a) the bentonite is filled into the mould, (b) a specimen is compacted with a press at a decided compaction pressure, (c) the compacted specimen is pressed out from the mould (Svensson et al. 2017).*

4.3.2 Analysis of data

After the compaction, the density and water content on the specimens are determined, compilations and analysis of the results are made. It is suggested that the dry density of the specimens are plotted as function of both the water content and the applied compaction pressure, see Figure 4-17. The data shown in the figure comes from compaction test made on a bentonite from Morocco. The figure shows that the dry density made at constant compaction pressure is decreasing at an increasing of the water content. There is a tendency that at the compaction pressure of 60 MPa and to some extent also at the compaction pressure 80 MPa the maximum dry density is reached at a water content of about 0.13, i.e. there is a maximum in the compaction curve. This type of maximum might be more pronounced for other types of bentonite. Furthermore, the figure shows that the dry density increase when the compaction pressure increases and the water content is kept constant.

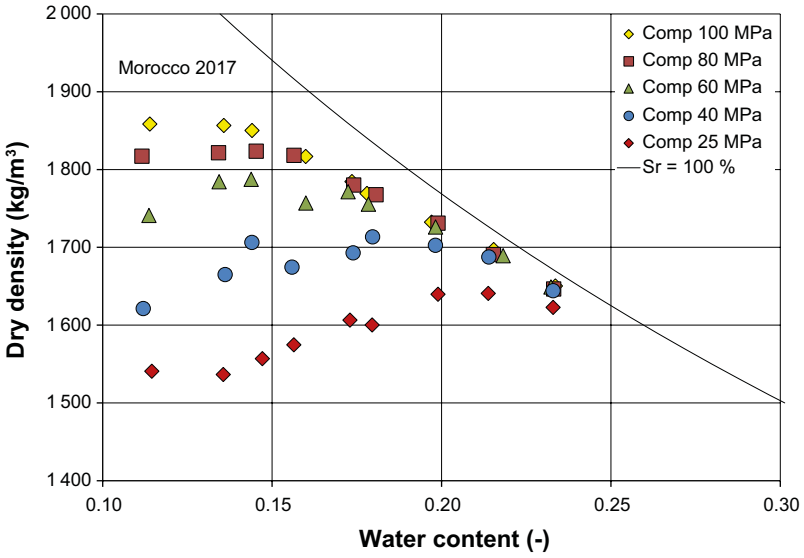

Figure 4-17. *Determined dry density as function of both water content and compaction pressure for the bentonite Morocco 2017.*

The results from the tests are used for optimising the water content and the compaction pressure at large scale production of buffer and backfill blocks. The most important requirement on the blocks is normally the achievable dry density. In addition to this there might also be requirements on the water content of the blocks in order to minimize the risk of damages during handling, storage and installation.

If, as an example for the bentonite Morocco 2017, the requirement on the dry density for the blocks is 1 700 kg/m^3 at a water content of 0.17 the blocks should be compacted with a compaction pressure of about 40 MPa.

4.3.3 Accuracy in the determination

The accuracy in the determination of compaction properties is complex. Factors which might affect the accuracy are:

- The accuracy in the measurement of the density and water content of the specimen.
- The accuracy in the measurement of the load measured with the load cell placed on the top of the piston at compaction.
- The bentonite is a geological material with a natural variation.

In order to estimate accuracy in this type of test a series of compaction tests were made on MX-80. In total 1 kg of the material was mixed to a water content of 17 %. The material was left in an air tight jar for at least 14 days in order to get the material homogenized. A total of 30 specimens were then compacted with the material at a compaction stress of 60 MPa. The compaction was made by three persons, 10 specimens each. The density and the water content were determined after the compaction and the dry density was calculated. The mean value and standard deviation of the determined parameters are shown in Table 4-7.

An estimate of the accuracy of the method can be obtained from the standard deviation of the determination of the dry density of the specimens, Stdv = 5.80 kg/m^3.

Table 4-7. The mean value and standard deviation of the water content, bulk density and dry density on 30 specimens of MX-80 compacted at compaction stress of 60 MPa.

	Mean value	Stdv
Water content	17.6 %	0.164 %
Bulk density	2 065 kg/m^3	6.92 kg/m^3
Dry density	1 756 kg/m^3	5.80 kg/m^3

4.4 Water content

4.4.1 Methodology and updates

Water in the bentonite is in the mineral montmorillonite, a layered silicate with hydrated interlayer ions. These ions are usually Na^+, Ca^{2+}, Mg^{2+} or K^+. Depending on the type of interlayer ions and ambient relative humidity, the bentonite will have more or less water in the structure in equilibrium with the environment. When the clay water varies with the particular ambient relative humidity, it is often important to relate the properties of the clay to its dry weight. After drying at 300 °C for 2 hours, the last water existing between the layers disappears (Brindley and Brown 1980).

Additional water is lost from the clay at higher temperatures (about 450–750 °C), but this water is not from hydrated interlayer ions. The water lost at these high temperatures is from dehydroxylation reactions of montmorillonite crystal structure (Newman 1987). It is important that the determination of water content is always done the same way, in order to obtain comparable results.

The practical procedure for determining the water content of the bentonite is to dry the bentonite in a ventilated oven at a temperature of 105 °C ± 5 °C for at least 24 hours. The mass loss of water is determined by a laboratory balance (a desiccator, as in the standard, is not used but the measurements

are done quickly, see Section 4.4.2 Estimation of measurement uncertainty, below for implication on the results). The mass ratio between the water and the dry material is referred to as geotechnical water content (w), while the mass ratio between the water and the moist material is referred to as general water content (wc). Both (w) and (wc) are expressed in weight percent.

The method has been updated according to the new version of the standard, Geotechnical ISO standard for soil, (ISO 17892-1:2014). The updated ISO method was, similar to earlier, not fully applicable but has been investigated and adapted to suit the laboratory. The practical procedure for the laboratory remains the same. The mass is kept, generally 25 g, with the possibility for variations. The standard stipulates at least 30 g of sample.

A new parameter for quality assurance has been introduced to the method, an extra control of the oven temperature.

4.4.2 Estimation of measurement uncertainty

The expanded uncertainty (U), has been estimated with a 95 % confidence interval. The uncertainty calculations were carried out in accordance with methodology for method measurement uncertainty estimation described by Magnusson et al. (2013) using the software application MUkit.

The expanded combined uncertainty was estimated in the following steps;

1. Quantifying within-laboratory reproducibility, $u(R_w)$, using data of
   – Samples of bentonite MX-80 were number of control samples n = 60 for each amount (2, 5 and 25 g) performed by three different persons at three different times. (Tables 4-8 to 4-10.)
2. Quantifying method and laboratory bias, u(bias), using data of
   – Samples of bentonite MX-80 were number of control samples n = 20 for each amount (2, 5 and 25 g) dried in a ventilated oven at a temperature of 105 °C ± 5 °C for 24 hours and 96 hours (reference). Standard uncertainty of certified concentration (here balance), $u(C_{ref})$ = 0.25 % (0.005 g). (Tables 4-11 to 4-13.)

When a plate of 20 samples is taken out of the oven the dry samples begin to take up water which affects the measured water content (every next sample exposed slightly longer to the RH in the room than the previous one), this affects the results of the larger 25 g samples much less than the 2 and 5 g samples.

3. Combining u(Rw) and u(bias) and calculating expanded uncertainty U using a coverage factor of 2 to achieve about 95 % confidence.

The expanded uncertainty U of the method was estimated to give an uncertainty for an amount of 25 g bentonite sample of 1 % and 5 % for an amount of 2 g and 5 g bentonite. Samples of 25 g are clearly preferred when possible, and the 1 % uncertainty is deemed acceptable, however, it is important to measure the weight of a sample quickly after removing it from the oven, especially when using smaller samples.

Table 4-8. Quantifying within-laboratory reproducibility, u(Rw). 2 g samples of bentonite MX-80 performed by different persons at three different times.

	Water content (wc) %	Water content (w) %
Mean value	8.948	9.828
Standard deviation	0.287	0.345
RSD%	3.20	3.51
n	60	60

Table 4-9. Quantifying within-laboratory reproducibility, u(Rw). 5 g samples of bentonite MX-80 performed by different persons at three different times.

	Water content (wc) %	Water content (w) %
Mean value	8.933	9.809
Standard deviation	0.160	0.194
RSD%	1.79	1.97
n	60	60

Table 4-10. Quantifying within-laboratory reproducibility, u(Rw). 25 g samples of bentonite MX-80 performed by different persons at three different times.

	Water content (wc) %	Water content (w) %
Mean value	8.946	9.825
Standard deviation	0.048	0.057
RSD%	0.53	0.48
n	40	40

Table 4-11. Quantifying method and laboratory bias, u(bias) 2 g.

Bentonite	wc (%) $x_{1(24\ h)}$	wc (%) $x_{2(96\ h)}$	sBias
Mean value n = 19	8.92	9.12	0.075

Table 4-12. Quantifying method and laboratory bias, u(bias) 5 g.

Bentonite	wc (%) $x_{1(24\ h)}$	wc (%) $x_{2(96\ h)}$	sBias
Mean value n = 20	9.84	10.02	0.046

Table 4-13. Quantifying method and laboratory bias, u(bias) 25 g.

Bentonite	wc (%) $x_{1(24\ h)}$	wc (%) $x_{2(96\ h)}$	sBias
Mean value n = 20	9.13	9.14	0.0046

4.5 Water content – microwave oven method

The aim was to evaluate the standard test method ASTM D4643-17 Standard Test Method for Determination of Water Content of Soil and Rock by Microwave Oven Heating and the possibility for a faster method to perform measurements of water content. The ASTM method was not fully applicable but an alternative method was tested and the method could be used in field to get a hint of the water content of the bentonite when no exactly values are needed.

4.5.1 Methodology and comparison with the oven method

An amount of 25 g bentonite MX-80 with three different water content levels (dry mass, w) were tested. The samples were placed in a paper form and dried for 5 minutes in a microwave oven with an effect of 800 W the weight were noticed before and after heating (Tables 4-14 to 4-16).

Comparing the results of the microwave method with the oven method it seems like the microwave method overestimates the water content to some degree, however, it can be used when quick indicative results are required.

Table 4-14. Quantifying reproducibility, u(R).

	Water content (wc) %	Water content (w) %
Mean value	9.9	11.0
Standard deviation	0.073	0.090
RSD%	0.74	0.82
n	15	15
Oven method as reference	9.3	10.2

Table 4-15. Quantifying reproducibility, u(R).

	Water content (wc) %	Water content (w) %
Mean value	14.9	17.6
Standard deviation	0.099	0.137
RSD%	0.66	0.78
n	14	14
Oven method as reference	14.4	16.8

Table 4-16. Quantifying reproducibility, u(R).

	Water content (wc) %	Water content (w) %
Mean value	16.8	20.2
Standard deviation	0.215	0.312
RSD%	1.28	1.54
n	15	15
Oven method as reference	16.2	19.3

4.6 Density

The bentonite buffer and backfill components in the repository are all in the compacted state. Many of the bentonite properties are functions of or have empirical correlations to the compaction density. Higher densities generally give for a specific bentonite: higher swelling pressure, lower plasticity and lower hydraulic conductivity. Density is denominated mainly in two ways: (1) the bulk density (the total density) and (2) the dry density (theoretical density after subtraction of the water content).

The method for performing analysis of density were described and reported earlier in SKB TR-16-14 some news is described here.

4.6.1 Methodology and updates

The method has been updated with a new version of the standard (ISO 17892-2:2014). The method have been investigated and adapted for laboratory operations of bentonite and the practical procedure are the same as earlier.

Some new parameters for quality assurance has been introduced to the method i.e. a temperature criteria of an interval of 15–25 °C for the test Milliq water when determining the density of the paraffin oil. Control samples of steel are now analysed once a week in Milliq and paraffin oil. Temperature control is performed of the Milliq and paraffin oil.

The analytical procedure is based on the standard method "immersion in fluid" and includes the determination of bulk density and dry density of a specimen of natural or compacted bentonite by measuring its mass in air and its apparent mass when suspended in fluid.

4.6.2 Estimation of measurement uncertainty

An estimation of the expanded combined uncertainty (*U*) close to 95 % confidence interval of the method has been carried out in accordance with methodology described by JCGM 100:2008, using the software application GUM Workbench – The tool for Expression of Uncertainty in Measurement Educational Version 1.3 and the User Manual.

Uncertainties and method equations were set up in the software and type values used for calculations. The expanded, combined uncertainty U, was estimated to 1 % for bentonite samples.

4.7 Thermal conductivity and specific heat

In order to avoid mineral transformation of the buffer, its temperature must not exceed 100 °C.

The thermal evolution of the repository depends on the thermal properties of the canister, rock and buffer, as well as on the energy output of the encapsulated spent nuclear fuel and on the canister spacing. For the buffer, the thermal evolution will depend on the thermal properties of the blocks and pellets and on the occurrence of air filled gaps between components (for example between the canister and buffer blocks). Additionally, the degree of saturation has a large impact on the thermal conductivity of the bentonite blocks. A saturated buffer has 2–3 times higher thermal conductivity than a dry buffer.

In order to analyse the temperature development in the repository, the thermal conductivity of the installed buffer must be known, as well as how it depends on its density and degree of saturation.

The expected density at saturation for the buffer is approximately 2 000 kg/m^3. However, between installation and full saturation, both higher and lower densities are expected and thus the method used for evaluating the thermal conductivity must be suitable for densities between 1 600–2 020 kg/m^3 at saturation.

A new method has been established in-house by SKB, the method and basic procedures are presented in the following section and further details including results from the selected bentonites are presented in Section 6.4.

4.7.1 Procedure and development

Methodology for determining the thermal conductivity (λ) and thermal diffusivity is described in (ISO 22007-1:2009, SS EN ISO 22007–1:2012), (SS-EN ISO Standard 22007-2:2015) and (ASTM D5334-14).

The method selected determines the thermal properties of bentonite clay with the TPS-method (Transient Plane Source), an absolute method. Thermal conductivity and thermal diffusivity are measured (isotropic) in parallel and from these two parameters, specific heat capacity per unit volume can be calculated assuming that the material is isotropic. Specific heat capacity (Cp) can also be measured separately with a specific sensor. This is needed for anisotropic measurement if no previous data for specific heat is available.

A Hot Disk TPS 2200 – Thermal Constants Analyser equipment with a thermal conductivity meter equipped with a double spiral heating sensor with isolation of kapton was purchased and has been used for measurements and testing of thermal conductivity, thermal diffusivity and specific heat capacity.

Specimens of buffer material are prepared to selected dry densities and water contents. Two samples halves are prepared with a weight of approximately 17 g, thickness around 10 mm and diameter of 35 mm.

The kapton sensor is placed inside the investigated buffer material i.e. in between the two sample halves. A constant electric current is led through the sensor which increases the temperature. The sensor works both as heat source and as a temperature sensor measurement device recording the increase in resistance as a function of time.

Different sensor sizes are available for measurement of different sample sizes.

The water content and density of the specimen is determined after the test, see Sections 4.4 and 4.6.

The physical properties of a sample may vary in different directions and a sample may be isotropic (equal properties in all directions) or anisotropic (different properties in different directions).

Measurements and calculations can be performed both isotropically and anisotropically.

In isotropic measurements, thermal conductivity and thermal diffusivity are measured (properties are assumed equally radial and axial). Thermal heat capacity per unit volume is calculated from these. In anisotropic measurements, the location of the sensor is more critical. Here, radial thermal diffusivity is measured and the axial thermal diffusivity can be calculated according to Equation 6-5 if the specific heat is known.

Measurement uncertainties have not been assessed at this stage and will be part of future studies.

4.8 Granular size distribution

Granule size distribution is mainly related to manufacturing issues. If the material is too coarse or too fine the quality of the blocks will be affected.

The method for performing granular size distribution measurements was described and reported earlier in SKB TR-16-14, and no updates have been done in the recent development stage.

5 Chemistry and mineralogy of selected bentonites

The chemistry and mineralogy were evaluated using the methods developed for quality control for bentonite buffer. The methods are optimised for an industrial scale application. Hence focus is not only on the result, but also on time spent, simplicity etc. At this stage, detailed understanding of the minor accessory minerals in the bentonites is less important. But when a specific bentonite has been selected for industrial application, detailed understanding and knowledge of the selected bentonite will be very useful to minimize the uncertainties of the quality control in a more optimal way. For detailed understanding also other complementary methods not included in the quality control proposed in this study will be utilised, such as infrared spectroscopy (FT IR), μ-raman spectroscopy, scanning electron microscopy (SEM), thermal gravimetric analysis (TGA/EGA), dissolution of poorly crystalline iron oxides using citrate-bicarbonate-dithionite (CBD), etc. Each to contribute to the total understanding of the bentonite, however, regarded to be outside of the scope of quality control, and hence also outside of the scope of this work. The listed mineralogy results from XRD are based on the mineral phases identified at the time of the quantification (using the Siroquant v 3 software), and the content could be different if other phases were included or if another software was used (for more info about the uncertainties and validation see Section 3.1). The methodology was done in accordance with Svensson et al. (2017). For carbon, sulfur and sulfide data, see Section 3.5.

5.1 Chemical homogeneity

The homogeneity of bentonite batches when it comes to the content is important, at least to some extent. The less homogenous the bentonite is the more it has to be blended and processed, or otherwise the properties of the produced bentonite blocks may change with time, unless the smectite content is monitored and the target density is adjusted to the smectite content to achieve constant properties.

Homogeneity could be tested by e.g. a high number of determinations of montmorillonite content and by testing the differences in physical properties. This is however very time consuming, and in this project we tried to evaluate the homogeneity using the chemical content determined by XRF. The standard deviation (SD) was plotted of each analysed element for four different batches (Figure 5-1). This SD was calculated from 20 samples taken from each batch. The chemical inhomogeneity was generally higher in the Indian bentonite and in the Bulgarian bentonite, compared to the Turkish and Moroccan bentonite. This is only a measure of the chemical content variation, and not directly comparable to the montmorillonite homogeneity.

Caution should be taken when interpreting this data. The absolute values of each element should also be taken into consideration, and the chemical data is in itself an indirect measure of what is really important. CEC and LECO (carbon and sulfur) would have been valuable complementary methods for the screening, and are recommended for the future.

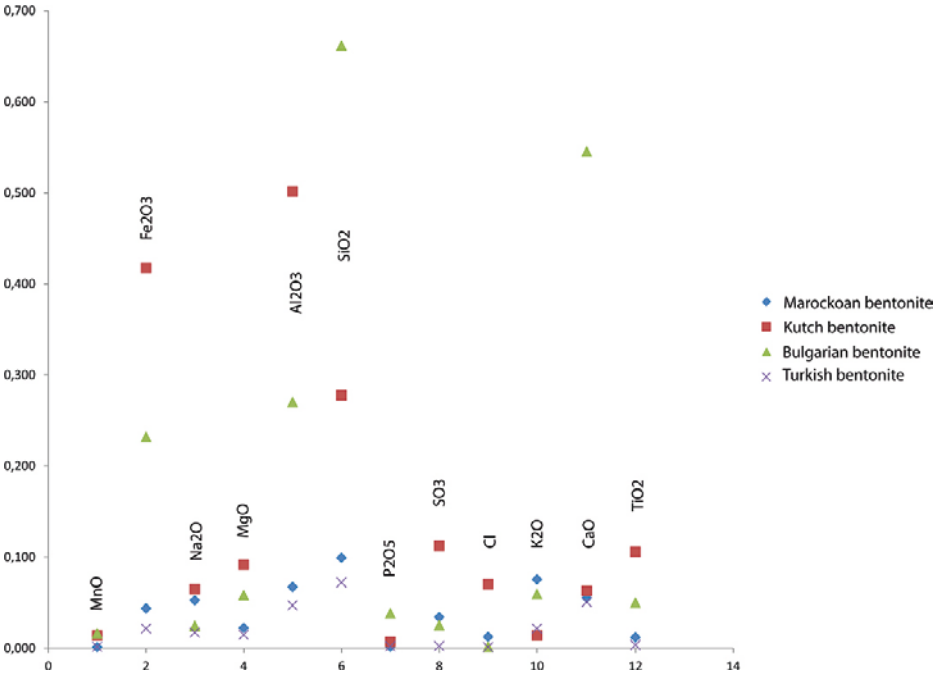

Figure 5-1. *Standard deviation (SD) of the chemical content determined by XRF for each of the analysed element for 20 samples from the four analysed batches of bentonite indicating somewhat higher or lower homogeneity.*

5.2 Milos bentonite

It is important to state that there are different qualities commercially available from Milos and this one, Milos 2017, is a low grade quality (intentional). High grade Milos materials products such as Deponit CAN are described in e.g. Svensson et al. 2011. The XRD pattern was rather complex (Figure 5-2) with plenty of reflections in the low angle region, mainly from clinoptilolite, mica/illite, kaolin and gypsum. The term low grade here is based on its low montmorillonite content of about 44 wt% based on XRD data (Table 5-1), or around 58 % based on CEC (Table 5-3).

CEC mean varied between 51.8 (CV% = 1.1) and 55.6 cmol(+)/kg (CV% = 0.6), and the clay fraction was 95.7 cmol(+)/kg (CV% = 0.2). The CEC values presented in Table 5-3 for composite and clay fraction were determined on the same occasion. The level of sulfur was high in this batch (2.5 wt% SO_3; Table 5-2).This is also seen in the XRD data as significant amounts of pyrite and gypsum (Table 5-1). The amount of total sodium was low (Table 5-2) and EC shows that it is a bentonite dominated by divalent cations Ca, Mg followed by Na and K. The sum(EC) was somewhat higher than CEC, most likely some of the gypsum went into solution upon the extraction.

Table 5-1. Mineralogy (XRD) of the Milos bentonite.

Phase	Average (wt%)	SD
Montmorillonite	43.6	1.0
Quartz	0.7	0.3
Calcite	2.8	1.2
Feldspar	10.2	1.1
Pyrite	1.0	0.3
Mica / illite	5.6	0.5
Gypsum	1.6	0.4
Tridymite	0.8	0.2
Clinoptilolite	6.1	1.6
Cristobalite	16.1	1.4
Kaolin	11.5	1.5

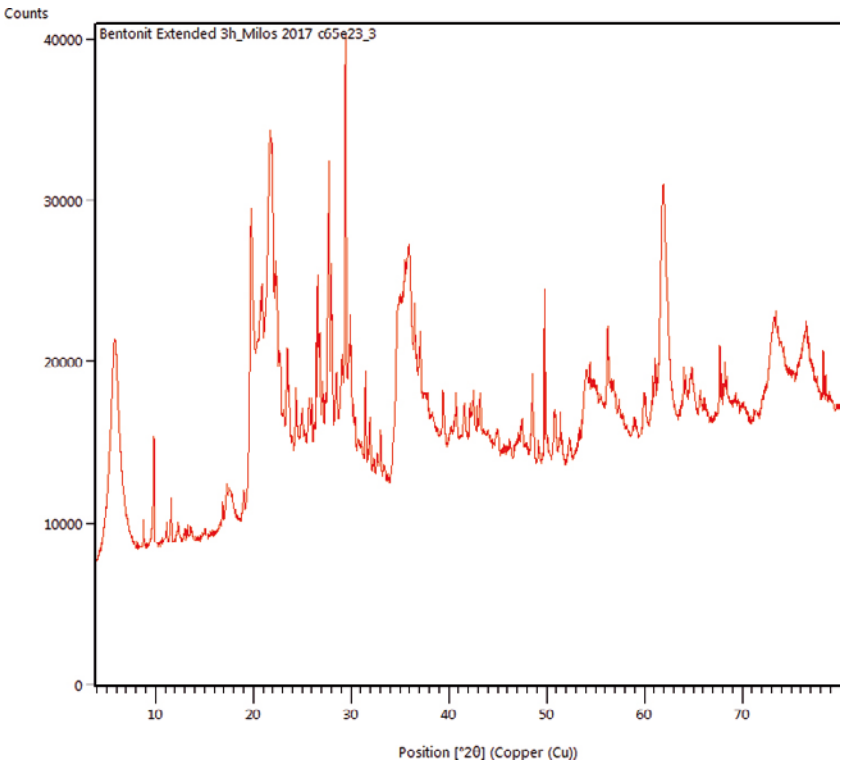

Figure 5-2. *XRD pattern of the investigated Milos bentonite.*

Table 5-2. Elemental composition (XRF; wt%) of Milos bentonite.

	MnO	Fe_2O_3	Na_2O	MgO	Al_2O_3	SiO_2	P_2O_5	SO_3	Cl	K_2O	CaO	TiO_2
Milos bentonite KBP1015 (n = 20)	0.03	3.04	0.36	2.56	18.35	67.90	0.01	2.50	0.03	1.29	3.39	0.56
SD	0.02	0.21	0.04	0.09	0.46	1.01	0.00	0.22	0.01	0.15	1.00	0.06

Table 5-3. CEC and EC of Milos bentonite (n = 2). CV% is given within parenthesis. CS is composite sample (bulk) and CF is clay fraction.

Bentonite	**CEC mean (cmol(+)/kg)**		Na^+_{mean}	Ca^{2+}_{mean}	Mg^{2+}_{mean}	K^+_{mean}	EC_{sum} (cmol(+)/kg)
	CS	**CF**					
Milos 2017	**55.6 (0.6)**	**95.7 (0.2)**	11.8	28.1	18.2	3.14	**61.2 (0.5)**
Date of analysis	2018-06-27	2018-06-27					2017-12-12

5.3 Moroccan bentonite

The low angle region of the XRD pattern (Figure 5-3) was dominated by the smectite 001 basal reflection, and only sporadically showed minor traces of mica/illite or gypsum. Several feldspars were present (Table 5-4). The montmorillonite content was high (around 85 wt% according to XRD) and had a correspondingly high CEC of 81 cmol(+)/kg (corresponding to approximately 77 wt% montmorillonite). EC data showed that the bentonite was mixed by Na^{+}, Ca^{2+} and Mg^{2+}, and the sum of the EC was very close to the CEC.

CEC of the Moroccan bentonite was analysed as duplicates on different occasions. For each occasion a CEC mean (n = 2) was calculated. CEC mean for composite sample varied between 80.6 (CV% = 0.9) and 84.1 cmol(+)/kg (CV% = 0.1), and the clay fraction was 104.3 cmol(+)/kg (n = 1).

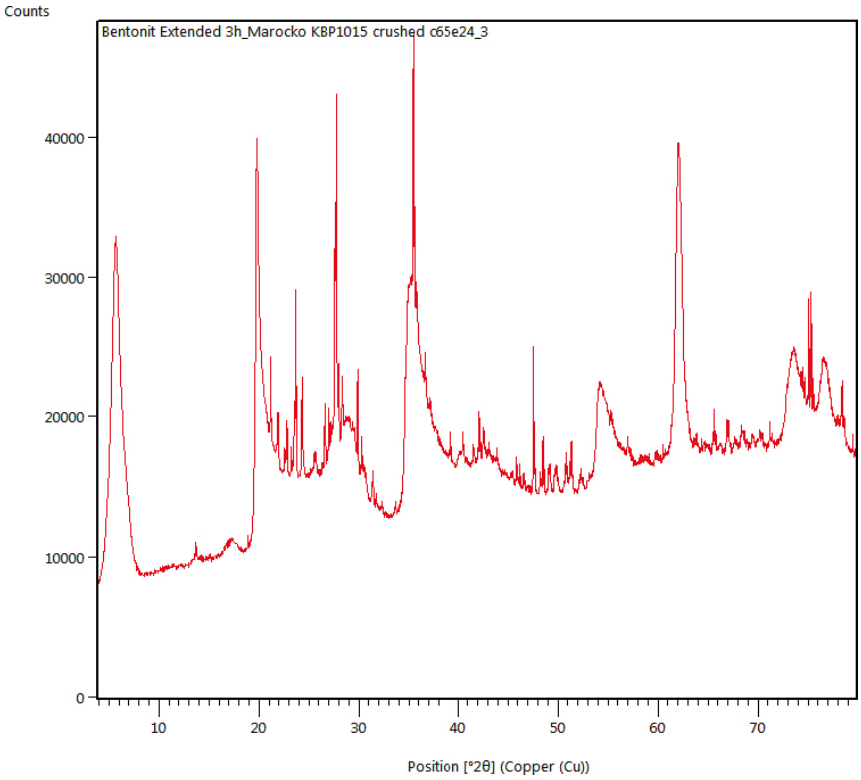

Figure 5-3. *XRD pattern of Moroccan bentonite.*

Table 5-4. Mineralogy (XRD) of Moroccan bentonite. Average of duplicates.

Phase	Average (wt%)	SD
Smectite	84.8	1.48
Calcite	1.0	0.00
Gypsum	0.15	0.21
Tridymite	0.40	0.28
Cristobalite	1.3	0.57
Mica/illite	1.7	2.33
Feldspar	11.7	1.25

Table 5-5. Elemental composition (XRF; wt%) of Moroccan bentonite.

	MnO	Fe_2O_3	Na_2O	MgO	Al_2O_3	SiO_2	P_2O_5	SO_3	Cl	K_2O	CaO	TiO_2
Marocko c65e25 (n = 4)	0.01	2.71	1.42	2.07	28.87	61.82	0.01	0.07	0.12	1.08	1.53	0.31
	0.00	0.02	0.03	0.01	0.07	0.05	0.00	0.00	0.00	0.02	0.03	0.00

Table 5-6. CEC and EC of Moroccan bentonite (n = 2). CV% is given within parenthesis. CS is composite sample (bulk) and CF is clay fraction. CEC value marked with a star (*) is based on one single measurement (n = 1).

Bentonite	CEC mean (cmol(+)/kg)		Na^+_{mean}	Ca^{2+}_{mean}	Mg^{2+}_{mean}	K^+_{mean}	EC_{sum} (cmol(+)/kg)
	CS	CF					
Morocco 2017	**80.6 (0.9)**	104.3*	33.05	20.1	27.7	1.49	**82.3 (1.5)**
Date of analysis	2018-09-06	2018-09-06					2017-12-12

5.4 Bulgarian bentonites

Three different batches of Bulgarian bentonite were compared. Qualitatively after equilibrating the clays to a high RH of approximately 80 % the XRD patterns looked very similar (Figure 5-4), and the clays are also rather similar regarding mineralogy and chemistry. The average montmorillonite contents determined using XRD were: 73.8 (20 kg batch), 82.6 (20 tonnes batch), and 79.2 wt% (F batch; Table 5-7), and the corresponding average CEC were 73.1 (20 kg), 79.4 (20 ton), and 76.2 cmol(+)/kg (F batch). CEC were determined using the standard method as well as an experimental quick method (Figure 5-5). Both varieties of the Cu-tri method (described in Section 3.3) showed exactly the same trend, however the quick method showed somewhat lower values, due to the shorter exchange time and lack of ultrasonic treatment. Both CEC series showed very strong linear relation to the montmorillonite content as determined by XRD (Figure 5-6).

Table 5-7. Mineralogy (XRD) of Bulgarian bentonite batches. Presented as wt% (SD; n = 3).

Phase	Bulgaria 20 kg	SD	Bulgaria 20 ton	SD	Bulgaria F	SD
Montmorillonite	73.8	1.7	82.6	0.5	79.2	1.7
Calcite	5.7	1.9	4.0	0.3	6.3	1.5
Gypsum	0.3	0.2	0.5	0.1	0.4	0.1
Tridymite	1.4	0.1	0.2	0.1	1.4	0.1
Cristobalite	8.5	0.3	6.4	0.2	6.4	0.5
Mica/illite	8.2	0.2	6.3	0.3	5.3	0.2
Feldspar	2.1	0.1	0.0	0.0	1.1	0.3

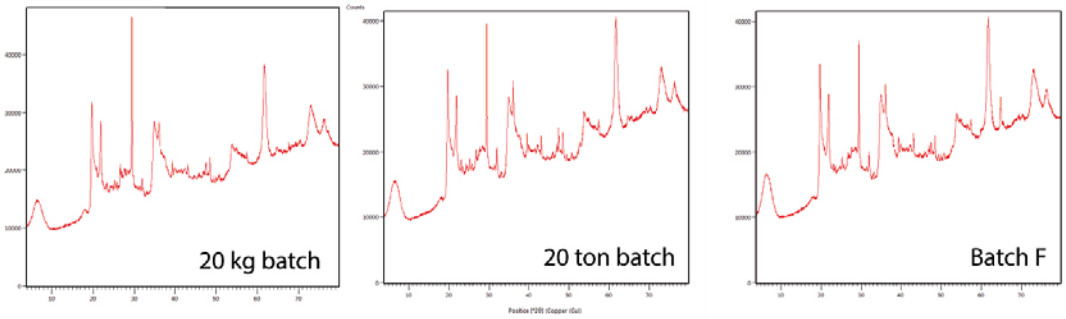

Figure 5-4. *XRD patterns of Bulgarian bentonite batches.*

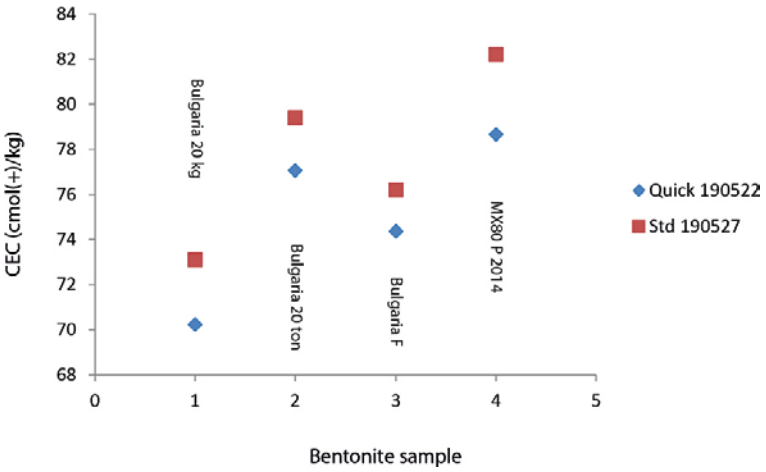

Figure 5-5. *CEC of Bulgarian bentonite batches (average values from triplicates) using the standard measurement (Std) compared to an alternative somewhat quicker method (Quick), both using the Cu-tri complex.*

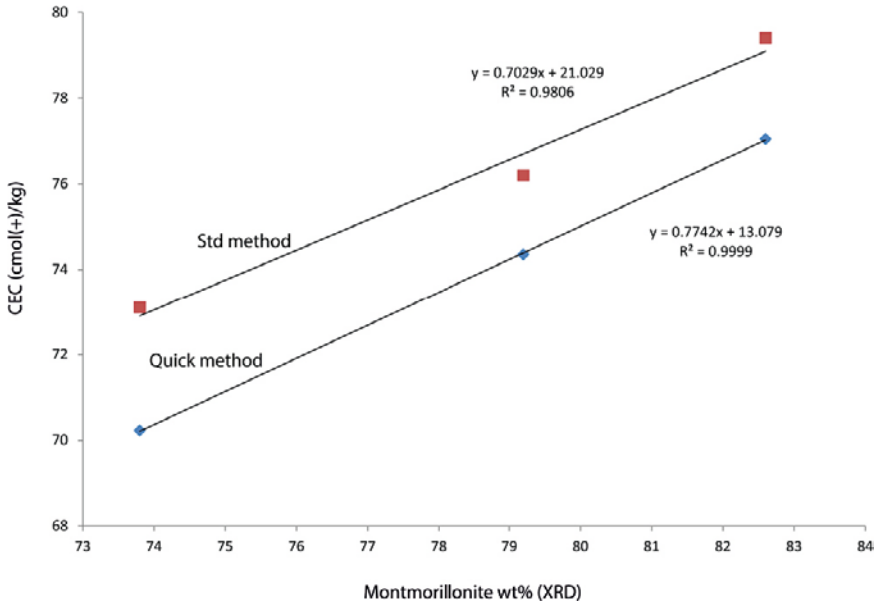

Figure 5-6. *CEC of Bulgarian bentonite as a function of the montmorillonite content as determined by XRD.*

Some earlier CEC measurements were made of the Bulgarian bentonite batches on different occasions using duplicate samples not listed in any of the tables. Due to the high repeatability of the method, and somewhat lower reproducibility it was important to analyse all batches at the same occasion (Table 5-8). In the early measurements (n = 2) the 20 kg batch varied between 71.0 (CV% = 2.2) and 75.2 cmol(+)/kg (CV% = 1.8), and the clay fraction varied between 85.3 (CV% = 0.1) and 87.2 cmol(+)/kg (CV% = 0.6). The 20 tonnes batch varied between 76.8 (CV% = 0.3) and 78.6 cmol(+)/kg (CV% = 0.3), for this batch no clay fraction was analysed. The Bulgaria F batch varied between 73.3 (CV% = 3.3) and 81.3 cmol(+)/kg (CV% = 0.2), and the clay fraction was 89.9 cmol (+)/kg (CV = 1.8 %).

Table 5-8. CEC and EC of Bulgarian bentonite batches. CV% is given within parenthesis. CS is composite sample (bulk), and CF is clay fraction. CEC/CS; n = 3, CEC/CF; n = 2 EC; n = 2.

Bentonite	CEC mean (cmol(+)/kg)		Na^{+}_{mean}	Ca^{2+}_{mean}	Mg^{2+}_{mean}	K^{+}_{mean}	EC_{sum} (cmol(+)/kg)
	CS	CF					
Bulgaria 20 kg (2017)	**73.1 (1.1)**	85.3	19.7	49.9	7.8	4.4	**81.8 (0.3)**
Bulgaria 20 tonnes (2018)	**79.4 (0.4)**	-	-	-	-	-	-
Bulgaria F (2017)	**76.2 (0.6)**	89.9	24.6	47.3	7.6	4.0	**83.5 (0.2)**
Date of analysis	2019-05-27	2019-05-27					2017-12-12

Based on the equation from the standard measurement (Figure 5-6; linear regression) the CEC of 100 % montmorillonite can be calculated to 91.3, while 85.3 (20 kg) and 89.9 (F batch) were observed for the clay fraction. The clay fractions are never totally pure montmorillonite and sometimes problems with dispersion arise because of the very compact and dense nature of dried clay fractions, hence the observed CEC was somewhat lower than the calculated theoretical value. Based on chemistry (Table 5-9) the MgO content as well as the (Mg+Al)/(Si+K) ratio (that is often proportional to the montmorillonite content) is highest in the F batch (0.317), and lower in 20 kg (0.308) and 20 tonnes (0.309). Hence, at first sight the chemistry indicated higher montmorillonite content for the F batch, however, this is a very indirect and insecure procedure that assumes that most of the Mg and Al is in the montmorillonite. The higher MgO content in the F-batch is not originating from the interlayer cations, as EC(MgO) is even somewhat higher in the 20 kg batch compared to the F batch (Table 5-8). Most likely a Mg-rich mineral is present in the bentonite. Sometimes calcite is Mg-rich and when plotting the MgO content as a function of the calcite content in the batches a linear relation was found (Figure 5-7).

Table 5-9. Chemical composition (XRF; wt%) of Bulgarian bentonite batches.

Bentonite	Na_2O	MgO	Al_2O_3	SiO_2	P_2O_5	SO_3	Cl	K_2O	CaO	TiO_2	MnO	Fe_2O_3	(Mg+Al)/(Si+K)
Bulgaria 20 kg c65e21 (n = 4)	0.481	3.581	16.974	64.877	0.182	0.038	0.005	1.838	4.548	1.113	0.061	6.301	**0.308**
Bulgaria F c65e6a (n = 4)	0.651	3.629	17.189	64.222	0.176	0.064	0.003	1.502	5.016	1.123	0.083	6.344	**0.317**
Bulgaria 20 ton #1	0.557	3.494	16.946	64.561	0.156	0.041	0.002	1.593	4.621	1.188	0.068	6.775	**0.309**
Bulgaria 20 ton #2	0.567	3.479	16.937	64.699	0.169	0.054	0.003	1.574	4.626	1.171	0.067	6.655	**0.308**
Bulgaria 20 ton #3	0.562	3.484	16.895	64.653	0.171	0.042	0.002	1.575	4.698	1.174	0.067	6.679	**0.308**
c65ec9, c65edf, c65ef5 (n = 6)													

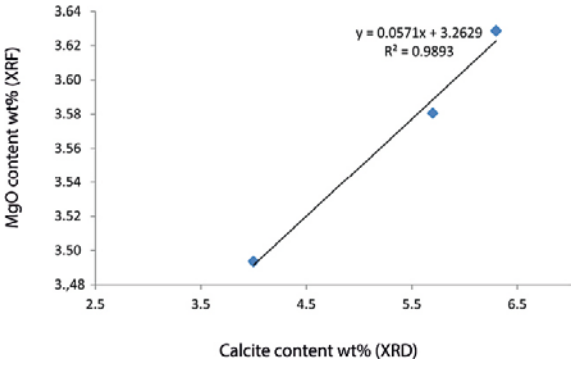

Figure 5-7. *MgO content as a function of calcite content in Bulgarian bentonite.*

As most of the accessory minerals are rich in Ca (calcite), Si (cristobalite), K (mice/illite, feldspar) and Fe (possibly and unidentified Fe-oxide) the $1/(CaO+Fe_2O_3+SiO_2+K_2O)$ ratio was tested against the montmorillonite content (Figure 5-8). This turned out not to work. All of the elements are also occurring in the montmorillonite, however the accessory minerals are expected to be higher in them. The problem is that Ca is present both as an interlayer cation and as calcite, and when present as calcite all elements in the XRF are overestimated because carbon in carbonates is not detected. Carbonate data was not available for all three batches but in two of them, and the detected CO_2 was rather proportional to the calcite content determined from XRD (Figure 5-9). Hence, instead the $1/(CaO+Fe_2O_3+SiO_2+K_2O)$ ratio was replaced by $1/(calcite+Fe_2O_3+SiO_2+K_2O)$ ratio (Figure 5-8) and this turned out to be fairly proportional to the montmorillonite content. One has to remember K is present as a montmorillonite interlayer cation (Table 5-8) and Fe and Si are also present in the montmorillonite, hence this estimation is only very approximate, however should agree trend wise with XRD and CEC. In the future, when carbon data as well as sulfur data is available an index such as $1/(CO_2+SO_2+Fe_2O_3+SiO_2+K_2O)$ probably can be used for this bentonite as an independent check of the XRD and CEC data trends. With more information about the location of other elements the index can evolve with time and potentially become more and more useful.

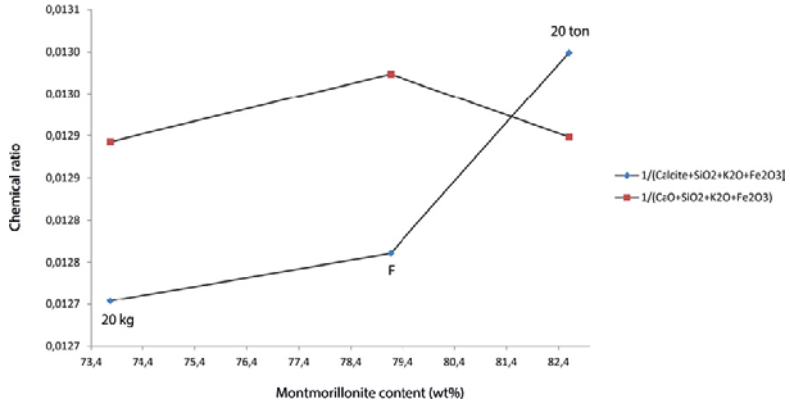

Figure 5-8. *Two different chemical ratios as a function of the montmorillonite content for the Bulgarian bentonites.*

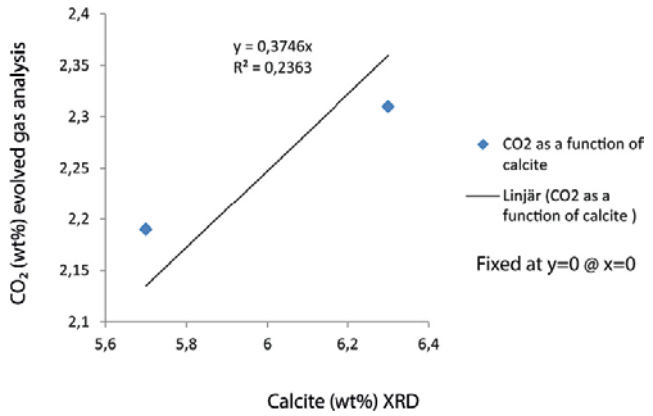

Figure 5-9. *Evolved CO_2 as a function of the calcite content for the Bulgarian bentonites.*

5.5 Turkish bentonites

Three different Turkish bentonites were analysed (arrived in small scale jars), Pertek (68.1), Guvendik-Korukopru (G-K; 74.8) and Yolustu (79.5 wt% montmorillonite; Table 5-10).

The G-K type was selected for a big delivery (200 kg batch; Figure 5-10). The 200 kg G-K batch was estimated to have 72.4 wt% montmorillonite using XRD (Table 5-11), and 79.8 % montmorillonite using the CEC ratio of the composite sample and the clay fraction (Table 5-13). The sum(EC) was 93.3 and significantly higher than the CEC of 68.6 cmol(+)/kg (Table 5-13). This was attributed to the presence of clinoptilolite (Table 5-11) that is exchanging with ammonium ions but not the Cu-tri complex.

CEC of the Turkish bentonite 200 kg G-K batch was analysed as duplicates on different occasions. For each occasion a CEC mean (n = 2) was calculated. Due to limited sustainability, copper-tri solution was prepared for each occasion. There was some difficulty in dispersing the bentonite completely in water before adding the copper-tri solution, see Section 3-3. CEC mean for composite sample varied between 68.6 cmol(+)/kg (CV% = 0.5) and 74.5 cmol(+)/kg (CV% = 0.5), and the clay fraction was 86.0 cmol(+)/kg (CV% = 1.3). The CEC values presented for composite and clay fraction are determined on same occasion.

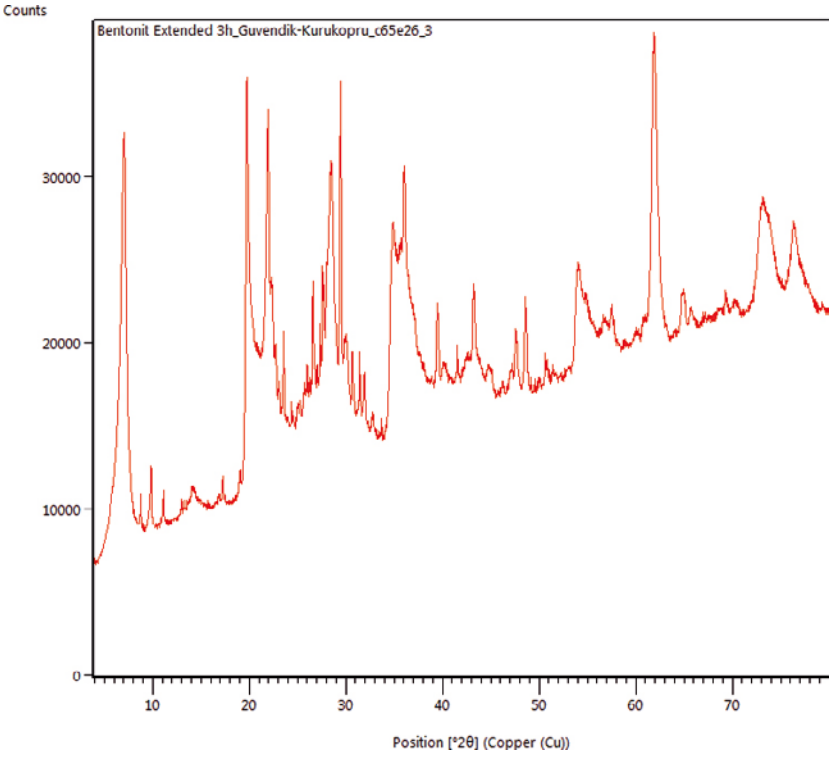

Figure 5-10. *XRD pattern of Turkish bentonite Guvendik-Kurukopru 200 kg batch.*

Table 5-10. Overview of Turkish bentonites small batches (jars). Wt%.

Parameter	Pertek	Guvendik-Korukopru	Yolustu
CEC mean (n = 2)	**68.1**	**74.8**	**79.5**
(Mg+Al)/(Si+K) mean	**16.6**	**17.3**	**23.0**
Montmorillonite	**73**	**77.3**	**78.3**
Quartz	0	0.3	0
Cristobalite	2.9	3.6	3.8
Calcite	4.3	3.6	3.3
Clinoptilolite	14.4	10.7	8.5
Mica/illite	5.3	4.5	6.2

Table 5-11. Mineralogy (XRD) Turkish bentonite 200 kg G-K batch. Average of triplicate. Wt%.

Parameter	Average	SD	U_r
Montmorillonite	72.43	1.39	1.84
Quartz	0.17		
Cristobalite	3.77		
Calcite	4.33		
Clinoptilolite	12.23		
Mica/illite	7.03		

Table 5-12. Elemental composition of Turkish bentonites (wt%).

Bentonite	MnO	Fe_2O_3	Na_2O	MgO	Al_2O_3	SiO_2	P_2O_5	SO_3	Cl	K_2O	CaO	TiO_2
G-K	0.10	4.76	2.05	1.98	19.23	66.62	0.02	0.06	0.01	1.23	3.52	0.41
SD (n = 6)	0.001	0.035	0.025	0.022	0.075	0.187	0.004	0.006	0.002	0.011	0.120	0.003
Yolustu	0.09	4.53	2.01	2.12	19.52	66.76	0.03	0.03	0.01	0.94	3.56	0.41
SD (n = 3)	0.001	0.037	0.005	0.004	0.007	0.045	0.002	0.004	0.002	0.002	0.041	0.006
Partek	0.11	4.58	2.21	1.89	19.44	66.30	0.04	0.04	0.00	1.29	3.69	0.42
SD (n = 3)	0.002	0.021	0.008	0.011	0.045	0.027	0.002	0.003	0.002	0.006	0.053	0.004
G-K 200 kg	0.11	4.79	2.14	2.04	19.31	66.12	0.03	0.04	0.01	1.35	3.64	0.43
SD (n = 20)	0.002	0.022	0.017	0.015	0.047	0.072	0.002	0.002	0.001	0.022	0.051	0.003

Table 5-13. CEC and EC of Turkish 200 kg G-K bentonite (n = 2). CV% is given within parenthesis. CS is composite sample (bulk) and CF is clay fraction.

Bentonite	CEC mean (cmol(+)/kg)		Na^+_{mean}	Ca^{2+}_{mean}	Mg^{2+}_{mean}	K^+_{mean}	EC_{sum} (cmol(+)/kg)
	CS	CF					
Turkey 2017	**68.6 (0.5)**	**86.0 (1.3)**	71.5	13.7	2.76	5.29	**93.3 (0.9)**
Date of analysis	2018-09-06	2018-09-06					2017-12-12

5.6 Wyoming bentonite (Bara-Kade)

The XRD pattern looked rather similar to a typical MX-80 bentonite (Figure 5-11) and the montmorillonite content was determined by XRD to 85.3 wt% (Table 5-14), which is a typical value for a Wyoming bentonite comparable to MX-80. XRF data in Figure 5-15.

CEC of BARA-KADE bentonite was analysed as duplicates on different occasions. For each occasion a CEC mean (n = 2) was calculated. Due to limited sustainability, copper-tri solution was prepared for each occasion. All bentonite samples were easily dispersed in water before adding the copper-tri solution. CEC mean for composite sample varied between 84.0 cmol(+)/kg (CV% = 0.6) and 89.9 cmol(+)/kg (CV% = 0.6). Clay fraction was not prepared and analysed. The CEC and EC data are summarised in Table 5-16.

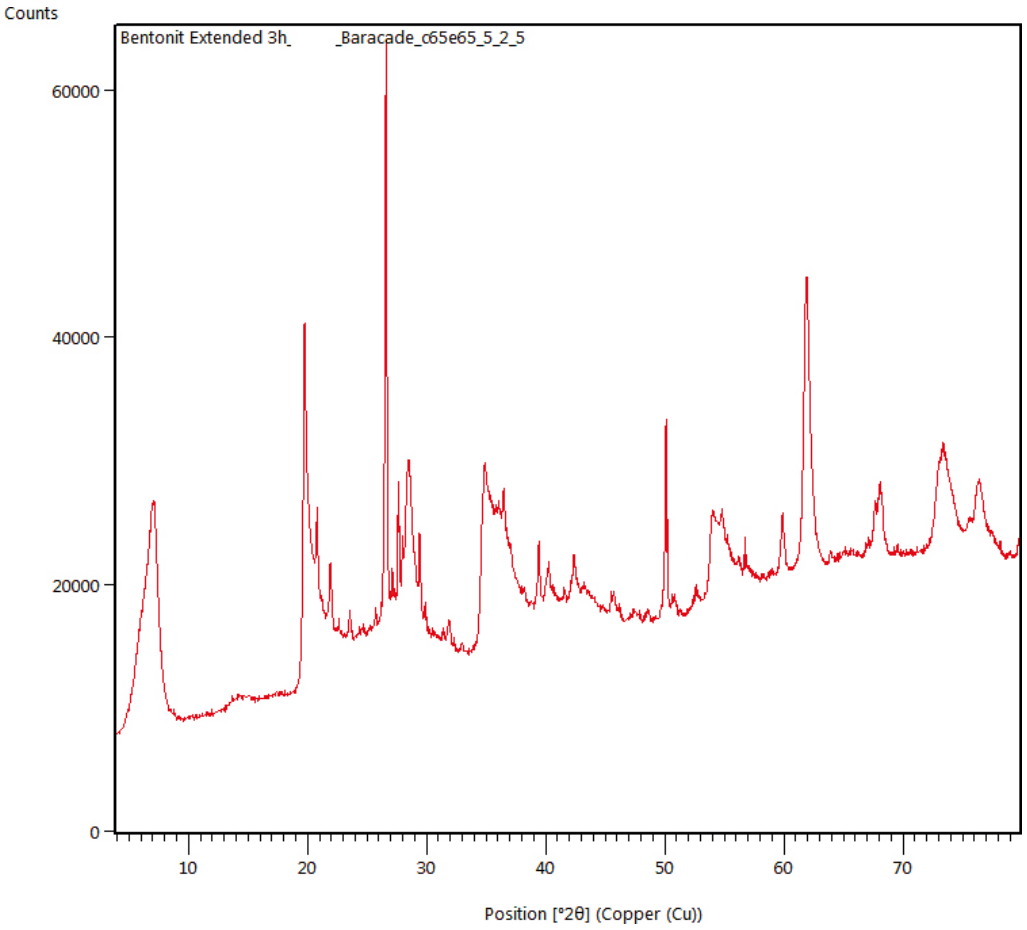

Figure 5-11. *XRD pattern of Bara Kade bentonite.*

Table 5-14. Mineralogy (XRD) Bara-Kade bentonite. Average of triplicate. Wt%.

Phase	Average	SD
Montmorillonite	85.3	1.5
Quartz	6.1	0.36
Calcite	0.3	0.26
Cristobalite	1.2	0.06
Feldspar	0.6	0.4
Pyrite	0.2	0
Mica / illite	4.97	0.74
Gypsum	1.33	0.21

Table 5-15. Bara Kade Elemental composition (XRF; wt%).

	MnO	Fe_2O_3	Na_2O	MgO	Al_2O_3	SiO_2	P_2O_5	SO_3	Cl	K_2O	CaO	TiO_2
Baracade c65e65 (n = 4)	0.04	5.00	1.71	2.49	21.63	66.44	0.00	0.37	0.00	0.61	1.52	0.18
	0.00	0.02	0.03	0.01	0.02	0.08	0.00	0.02	0.00	0.00	0.06	0.00

Table 5-16. CEC and EC of BARA-KADE bentonite (n = 2). CV% is given within parenthesis. CS is composite sample (bulk). Clay fraction (CF) was not prepared and analysed.

Bentonite	CEC mean (cmol(+)/kg) CS	CF	Na^+_{mean}	Ca^{2+}_{mean}	Mg^{2+}_{mean}	K^+_{mean}	EC_{sum} (cmol(+)/kg)
BARA-KADE 2017	**84.0 (0.6)**	-	55.15	25.8	5.25	1.53	**87.7 (0.3)**
Date of analysis	2018-05-07						2017-12-12

5.7 Sardinian bentonite

The montmorillonite content was determined by XRD to 85.2 wt% (Table 5-17), and the XRD pattern looked rather clean with few other phases present except from montmorillonite (Figure 5-12). XRF data in Figure 5-18.

CEC of Sardinian bentonite was analysed as duplicates on different occasions. For each occasion a CEC mean (n = 2) was calculated. Due to limited sustainability, copper-tri solution was prepared for each occasion. There was some difficulty in dispersing the bentonite completely in water before adding the copper-tri solution, see Section 3-3. CEC mean for composite sample varied between 108.0 cmol(+)/kg (CV% = 1.6) and 111.8 cmol(+)/kg (CV% = 0.7). Clay fraction was not prepared and analysed. The CEC and EC data are summarised in Table 5-19.

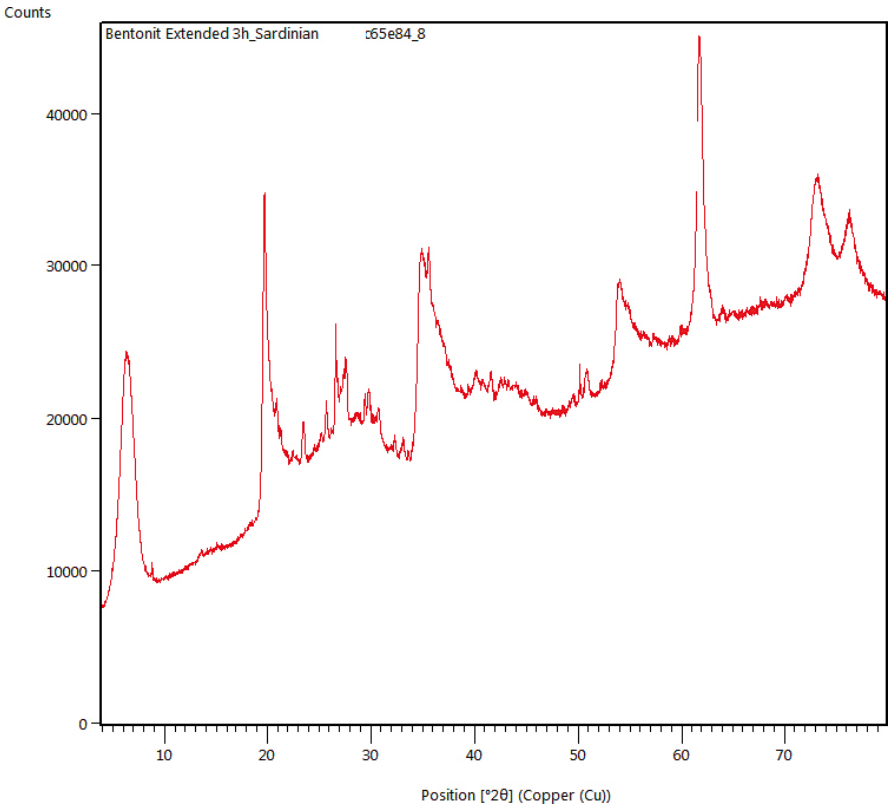

Figure 5-12. *XRD pattern of Sardinian bentonite.*

Table 5-17. Mineralogy (XRD) Sardinian bentonite. Average of triplicate. Wt%.

Phase	Average (n = 3)	SD
Montmorillonite	85.20	0.14
Quartz	0.90	0.28
Cristobalite	0.25	0.07
Calcite	0.20	0.00
Hematite	0.65	0.07
Feldspar	4.75	0.21
Mica/illite	8.00	0.42

Table 5-18. XRF data (wt%).

	MnO	Fe_2O_3	Na_2O	MgO	Al_2O_3	SiO_2	P_2O_5	SO_3	Cl	K_2O	CaO	TiO_2
Sardinien c65e84 (n = 4)	0.09	7.37	1.12	5.57	18.93	62.66	0.05	0.04	0.05	1.58	1.80	0.75
	0.01	0.03	0.02	0.02	0.01	0.03	0.00	0.00	0.00	0.01	0.01	0.00

Table 5-19. CEC and EC of Sardinian bentonite (n = 2). CV% is given within parenthesis. CS is composite sample (bulk). Clay fraction (CF) was not prepared and analysed.

Bentonite	CEC mean (cmol(+)/kg) CS	CF	Na^+_{mean}	Ca^{2+}_{mean}	Mg^{2+}_{mean}	K^+_{mean}	EC_{sum} (cmol(+)/kg)
Sardinia 2017	**108.0 (1.6)**	-	38.25	32.85	49.9	1.74	**122.7 (2.1)**
Date of analysis	2018-05-07						2018-06-28

5.8 Indian bentonite

The Indian bentonite showed a very complex XRD pattern (Figure 5-13) with many minerals present (Table 5-20). The combination of high Fe_2O_3 content and a Cu X-ray anode gave rise to a noisy background due to fluorescence. The smectite content was estimated to 77 wt% using XRD, however the presence of several clay minerals and poorly crystalline Fe-minerals made the fitting less straight forward compared to the less complex bentonites, and hence the uncertainty is higher. Determination of the smectite content with the CEC method indicates 89 wt%, however, the clay fraction is also holding kaolin as well as other phases, and in this case seems to have overestimated the smectite content. XRF data in Figure 5-21.

CEC of Indian bentonite was analysed as duplicates on different occasions. For each occasion a CEC mean (n = 2) was calculated. Due to limited sustainability, copper-tri solution was prepared for each occasion. All bentonite samples were easily dispersed in water before adding the copper-tri solution. CEC mean for composite sample varied between 79.8 cmol(+)/kg (CV% = 0.05) and 80.2 cmol(+)/kg (CV% = 0.5). CEC for clay fraction was analysed on one occasion and CEC mean was calculated to 89.4 cmol(+)/kg (CV% = 0.5). The CEC and EC data are summarised in Table 5-22. The CEC values presented for composite and clay fraction are determined on same occasion.

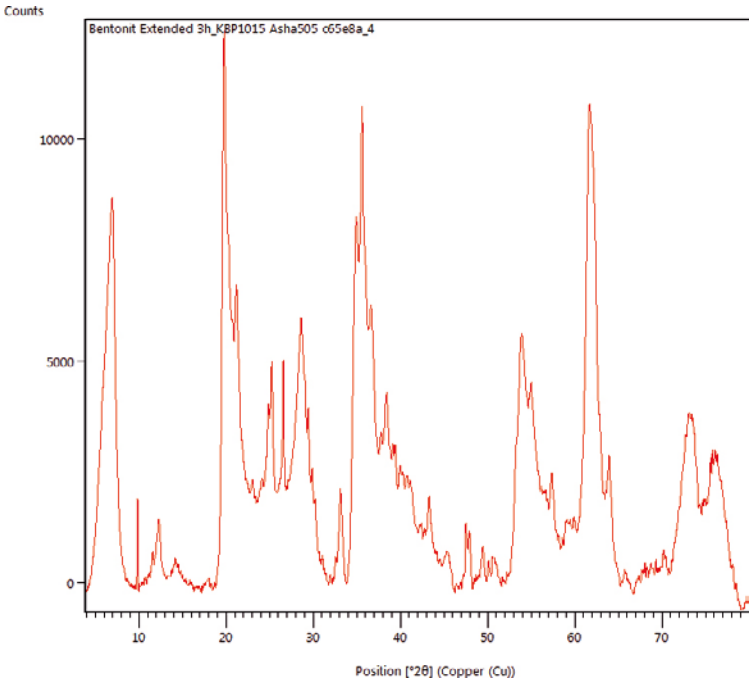

Figure 5-13. *XRD pattern of Indian bentonite.*

Table 5-20. Mineralogy (XRD) Indian bentonite. Average of triplicate. Wt%.

Indian bentonite c65e8a		
Phase	**Average wt%**	**SD**
Quartz	0.65	0.21
Calcite	0.30	0.00
Maghemite	3.10	0.28
Anatase	2.45	0.07
Goethite	3.95	0.07
Smectite	77.20	0.71
Feldspar	1.00	0.00
Kaolin	6.80	0.00
Gypsum	1.43	0.49
Clinoptilolite	1.03	1.62
Cristobalite	2.53	1.93

Table 5-21. XRF data (wt%).

	MnO	**Fe_2O_3**	**Na_2O**	**MgO**	**Al_2O_3**	**SiO_2**	**P_2O_5**	**SO_3**	**Cl**	**K_2O**	**CaO**	**TiO_2**
Asha 505 c65e89 (n = 6)	0.11	21.13	1.58	1.89	21.17	48.55	0.02	0.63	0.68	0.13	1.26	2.40
SD	0.01	0.10	0.02	0.03	0.06	0.11	0.00	0.02	0.05	0.00	0.03	0.03

Table 5-22. CEC and EC of Indian bentonite (n = 2). CV% is given within parenthesis. CS is composite sample (bulk) and CF is clay fraction.

Bentonite	**CEC mean (cmol(+)/kg)**		**Na^+_{mean}**	**Ca^{2+}_{mean}**	**Mg^{2+}_{mean}**	**K^+_{mean}**	**EC_{sum} (cmol(+)/kg)**
	CS	**CF**					
India 2018	**79.8 (0.05)**	**89.4 (0.05)**	55.4	18.9	17.3	0.55	**92.1 (5.1)**
Date of analysis	2018-09-18	2018-09-18					2018-06-28

6 Physical properties of selected bentonites

Important parameters at judging the behaviour of a bentonite are, swelling pressure, hydraulic conductivity, unconfined compression strength, compaction properties and thermal properties. The methods used for determine these parameters are described in Chapter 4 and summarised in this chapter where also the investigated bentonites are compared with each other. Furthermore, the parameters grain density, granule size distribution and water content are summarised. These parameters are not essential for the behaviour of the bentonite but are used for additional description of the materials. Finally are the retention properties and shrinkage/expantion for some of the investigated bentonites described. At this stage are these methods considered to be complementary methods. The assessment is that the method for determining the retention properties of bentonites will in the future be a complementary method for measuring the swelling properties of a bentonite. However, this requires further testing and development of the method.

6.1 Swelling pressure and hydraulic conductivity

The swelling pressure and the hydraulic conductivity have been investigated for in total 8 deliveries of bentonites. For one of the bentonites, Bulgaria 2017, two different deliveries were investigated. The investigated bentonites are listed in the labels in Figure 6-1. The investigations are made as described in Section 4.1 and include the following steps:

- Preparation of the specimen to a specific dry density.
- Saturation of the specimen with deionized water during continuous measurement of the swelling pressure for about 7 days.
- Measurement of the hydraulic conductivity by applying a pore pressure gradient over the specimens for about 7 days.
- The specimens get access to a 1 M $CaCl_2$ solution for another 7 days during continuous measurement of the swelling pressure.
- Measurement of the hydraulic conductivity with 1 M $CaCl_2$ solution by applying a pore pressure gradient over the specimens for about 7 days.
- Determine the bulk density and the water content on the specimen.

Since the measurements of the water content and the bulk density are made on the specimens after they have had access to 1 M $CaCl_2$ solution, the evaluated dry density will be incorrect. By making another set of test where the specimens have access to deionized water and only the swelling pressure is determined it is possible to adjust the curves for the salt concentration in the pore system. This is made by assuming a salt content in the specimens and then recalculating their dry densities, see Section 4.1. The data from all of the 8 investigated bentonite clays are provided in Appendix 1 and a summary of the determined swelling pressures and hydraulic conductivities, before adjustment of the densities, is provided in Table 6-2.

In Figure 6-1 and Figure 6-2 the corrected data from the measurement of the swelling pressure for the 8 investigated bentonites are summarized. Figure 6-1 involves the swelling pressure measurements made with deionized water while corresponding data for the measurements made with 1 M $CaCl_2$-solution is shown in Figure 6-2.

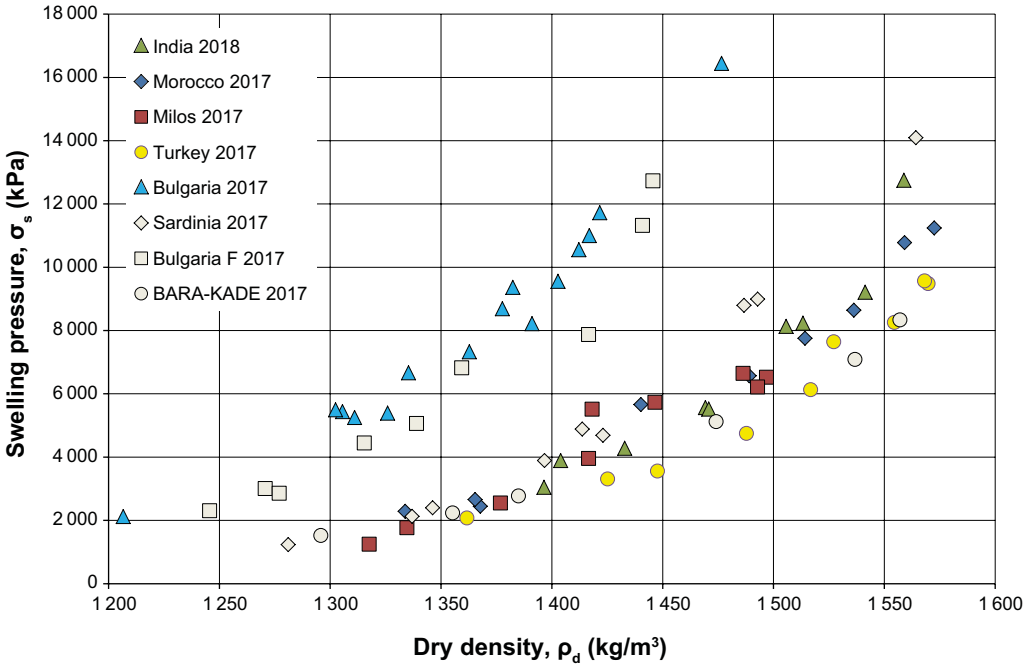

Figure 6-1. *Determined swelling pressure,* ***measured with deionized water****, as function of dry density for the 8 investigated bentonites. Note that the dry densities are corrected.*

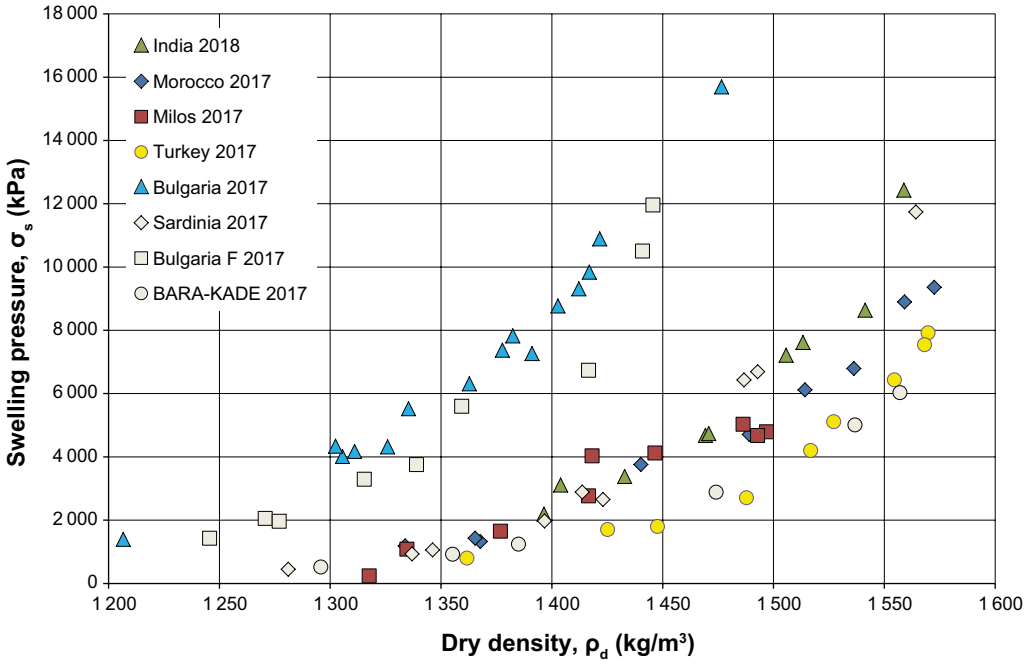

Figure 6-2. *Determined swelling pressure,* ***measured with 1 M $CaCl_2$-solution****, as function of dry density for the 8 investigated bentonites. Note that corrected values for dry densities are used.*

The requirement concerning the swelling pressure for a buffer material is that the swelling pressure should not exceed 10 MPa and not be lower than 3 MPa. This should be valid for the whole life time of the repository. The data for the investigated bentonites can be used to determine the interval within which the density should be in order to fulfil these requirements. The lower limit is evaluated from the measurement made with 1 M $CaCl_2$ solution while the upper limit is evaluated from the measurements made with de-ionized water. The determined intervals for the investigated bentonites are shown in Table 6-1.

Table 6-1. The dry density for 8 investigated bentonite in order to fulfil the requirements on swelling pressure.

Mtrl	Dry density at swelling pressure 3 MPa (1 M $CaCl_2$) (kg/m^3)	Dry density at swelling pressure 10 MPa (deionized water) (kg/m^3)
India 2018	1 420	1 540
Morocco 2017	1 440	1 550
Milos 2017	1 440	1 530
Turkey 2017	1 485	1 580
Bulgaria 2017	1 280	1 400
Sardinia 2017	1 430	1 510
Bulgaria F 2017	1 315	1 425
BARA-KADE 2017	1 480	1 585

Corresponding plots for the determinations of the hydraulic conductivity are shown in Figure 6-3 and Figure 6-4. The requirement on the hydraulic conductivity for a buffer material is that it must not exceed 1E−12 m/s. When comparing the minimum acceptable density in order to fulfil the requirement for the swelling pressure, see Table 6-1, with the data in Figure 6-3 and Figure 6-4 is it clear that the requirement on the maximum hydraulic conductivity is fulfilled for these densities and for all investigated bentonites except for the Milos bentonite.

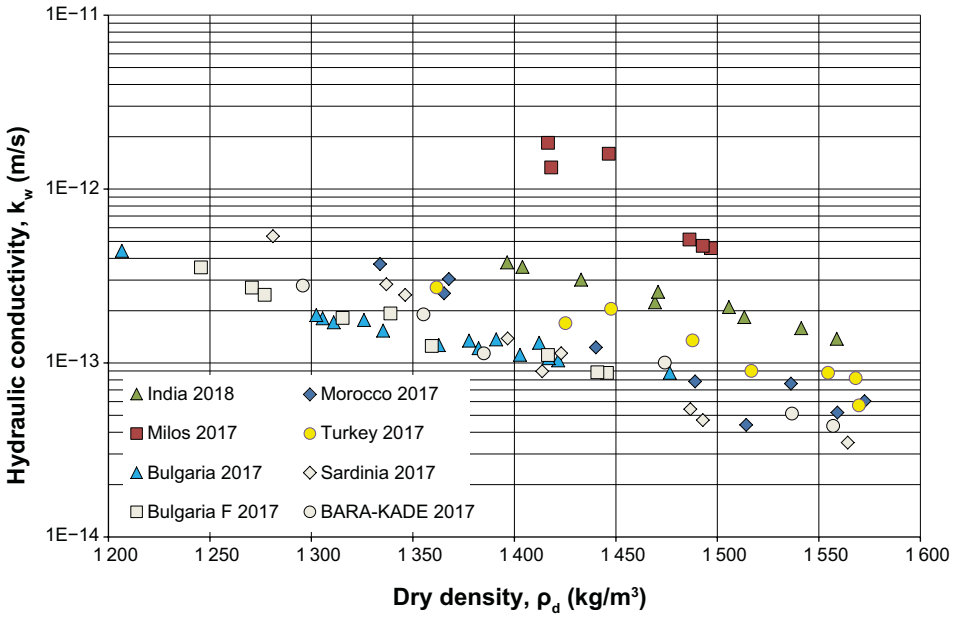

Figure 6-3. *Determined hydraulic conductivity,* ***measured with deionized water****, as function of dry density for the 8 investigated bentonites. Note that corrected values for dry densities are used.*

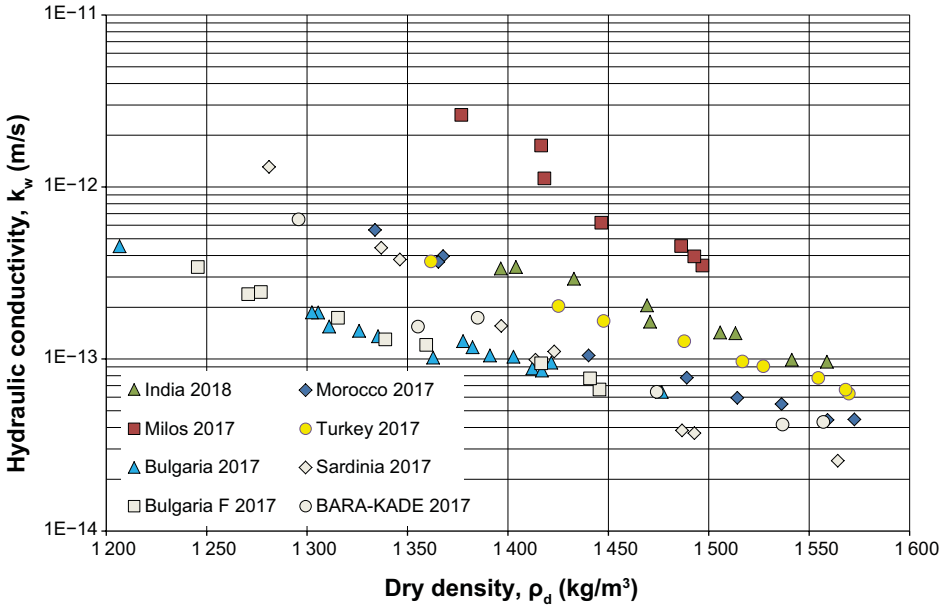

Figure 6-4. *Determined hydraulic conductivity,* ***measured with 1 M $CaCl_2$-solution****, as function of dry density for the 8 investigated bentonites. Note that corrected values for dry densities are used.*

Table 6-2. Summary of swelling pressure (SP) and hydraulic conductivity (HC), for detailed data see Appendix 1. DI is deionised water.

Turkey 2017									
Dry density (kg/m^3)	1362	1448	1488	1425	1555	1570	1517	1527	1568
SP DI (kPa)	2072	3553	4748	3308	8253	9480	6125	7643	9564
SP 1 M $CaCl^2$ (kPa)	797	1796	2705	1701	6428	7917	4199	5109	7540
HC DI (m/s)	2.71E−13	2.05E−13	1.35E−13	1.69E−13	8.78E−14	5.70E−14	8.99E−14	-	8.17E−14
HK 1 M $CaCl^2$ (m/s)	3.69E−13	1.66E−13	1.27E−13	2.03E−13	7.76E−14	6.28E−14	9.66E−14	9.06E−14	6.63E−14
Bulgaria 2017 (more data available)									
Dry density (kg/m^3)	1306	1391	1412	1363	1403	1422	1207	1311	1477
SP DI (kPa)	5437	8218	10552	7328	9553	11724	2121	5250	16443
SP 1 M $CaCl^2$ (kPa)	4014	7265	9310	6309	8768	10886	1394	4172	15694
HC DI (m/s)	1.81E−13	1.37E−13	1.30E−13	1.27E−13	1.11E−13	1.04E−13	4.41E−13	1.71E−13	8.77E−14
HK 1 M $CaCl^2$ (m/s)	1.86E−13	1.05E−13	8.81E−14	1.02E−13	1.03E−13	9.52E−14	4.52E−13	1.54E−13	6.44E−14
Bulgaria F 2017									
Dry density (kg/m^3)	1246	1271	1339	1315	1359	1446	1277	1417	1441
SP DI (kPa)	2300	3003	5057	4442	6816	12726	2855	7872	11318
SP 1 M $CaCl^2$ (kPa)	1426	2053	3754	3287	5597	11958	1959	6731	10500
HC DI (m/s)	3.54E−13	2.71E−13	1.92E−13	1.81E−13	1.25E−13	8.77E−14	2.46E−13	1.11E−13	8.82E−14
HK 1 M $CaCl^2$ (m/s)	3.42E−13	2.38E−13	1.30E−13	1.74E−13	1.21E−13	6.63E−14	2.45E−13	9.42E−14	7.70E−14
India 2018									
Dry density (kg/m^3)	1396	1469	1513	1404	1506	1559	1433	1471	1541
SP DI (kPa)	3046	5564	8231	3890	8129	12748	4280	5518	9210
SP 1 M $CaCl^2$ (kPa)	2192	4674	7617	3107	7210	12431	3380	4734	8633
HC DI (m/s)	3.78E−13	2.23E−13	1.84E−13	3.57E−13	2.10E−13	1.38E−13	3.01E−13	2.56E−13	1.59E−13
HK 1 M $CaCl^2$ (m/s)	3.36E−13	2.05E−13	1.41E−13	3.43E−13	1.43E−13	9.63E−14	2.93E−13	1.65E−13	9.90E−14
BARA-KADE 2017									
Dry density (kg/m^3)	1293	1352	1471	1383	1534	1555			
SP DI (kPa)	1518	2232	5118	2767	7085	8333			
SP 1 M $CaCl^2$ (kPa)	514	921	2879	1240	5004	6028			
HC DI (m/s)	2.78E−13	1.90E−13	1.00E−13	1.14E−13	5.11E−14	4.34E−14			
HK 1 M $CaCl^2$ (m/s)	6.48E−13	1.54E−13	6.43E−14	1.74E−13	4.15E−14	4.30E−14			

Table 6-2. Continued.

Morocco 2017									
Dry density (kg/m^3)	1368	1440	1489	1334	1536	1573	1365	1514	1559
SP DI (kPa)	2446	5659	6567	2287	8639	11238	2656	7755	10776
SP 1 M $CaCl^2$ (kPa)	1325	3758	4707	1183	6791	9357	1430	6118	8898
HC DI (m/s)	3.04E−13	1.23E−13	7.83E−14	3.70E−13	7.61E−14	6.04E−14	2.51E−13	4.40E−14	5.18E−14
HK 1 M $CaCl^2$ (m/s)	3.96E−13	1.05E−13	7.78E−14	5.63E−13	5.47E−14	4.45E−14	3.66E−13	5.94E−14	4.42E−14
Milos 2017									
Dry density (kg/m^3)	1318	1377	1447	1335	1417	1497	1418	1493	1486
SP DI (kPa)	1243	2543	5727	1763	3954	6523	5509	6212	6641
SP 1 M $CaCl^2$ (kPa)	234	1646	4121	1081	2765	4787	4029	4672	5029
HC DI (m/s)	1.62E−10	1.69E−11	1.59E−12	1.32E−11	1.66E−12	4.57E−13	1.33E−12	4.71E−13	5.12E−13
HK 1 M $CaCl^2$ (m/s)	4.19E−11	2.62E−12	6.19E−13	1.89E−11	1.74E−12	3.49E−13	1.12E−12	3.94E−13	4.53E−13
Sardinia 2017									
Dry density (kg/m^3)	1281	1423	1564	1337	1346	1397	1414	1493	1487
SP DI (kPa)	1232	4689	14094	2125	2396	3888	4885	8992	8795
SP 1 M $CaCl^2$ (kPa)	446	2649	11740	932	1060	1972	2888	6692	6430
HC DI (m/s)	5.36E−13	1.14E−13	3.49E−14	2.83E−13	2.46E−13	1.38E−13	8.96E−14	4.69E−14	5.43E−14
HK 1 M $CaCl^2$ (m/s)	1.31E−12	1.11E−13	2.56E−14	4.43E−13	3.79E−13	1.56E−13	9.89E−14	3.71E−14	3.84E−14

6.2 Unconfined compression strength

The unconfined compression strength has been investigated for the bentonites shown Table 6-3. The investigations are done as described in Section 4.2 and includes the following steps:

- Preparation of the specimen to a specific dry density.
- Saturation of the specimen with deionized water for about 4 weeks.
- The strength of the specimens is determined in a hydraulic press.
- The water content and the bulk density of the specimens are determined.
- An exponential curve is fitted to the individual determinations of the strength.
- The density required to exceed the strength of 4 000 kPa is determined from the fitted curve (interpolation or extrapolation)

Data from measurements of the unconfined compression strengths on 8 investigated bentonites are summarized in Figure 6-5, see also Appendix 2. The figure shows that the compression strengths for the 8 bentonites are similar except for Bulgaria 2017 which has a much higher strength compare to the others. The requirement on the unconfined compression strength is that it at saturated conditions must not exceed 4 000 kPa which imply restrictions on the maximum acceptable dry density for the buffer material. In Table 6-3 are the calculated dry densities for the investigated bentonites listed at an unconfined compression strength of 4 000 kPa. These values should be compared with the densities for the investigated bentonites to reach a maximum swelling pressure of 10 000 kPa, see Section 6.1 Table 6-1. At this comparison it is obvious that the densities of saturated specimens to reach a strength of 4 000 kPa is higher compare to the density to reach the maximum swelling pressure and thus it is the swelling pressure which is governing the maximum acceptable density of the buffer. This is valid for all of the investigated bentonites.

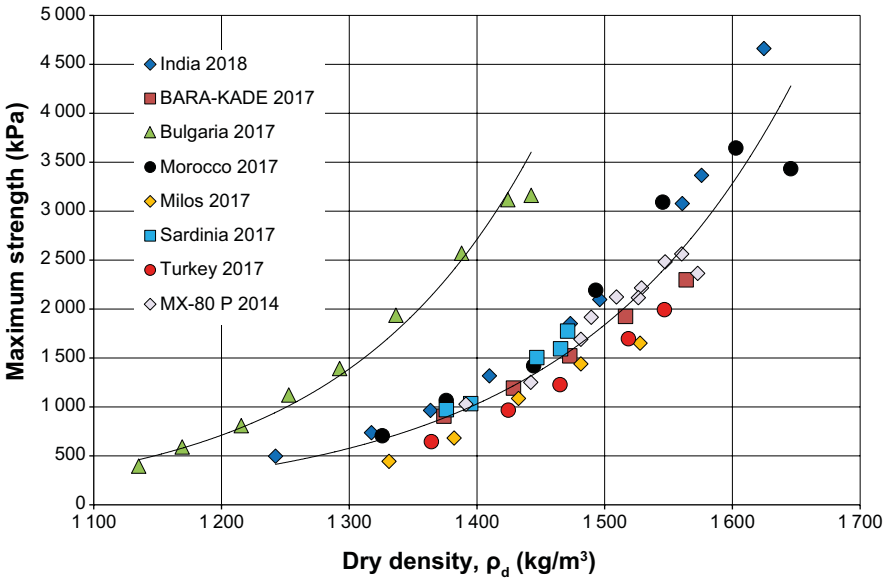

Figure 6-5. *The maximum strength as function of dry density for the eight investigated bentonites.*

Table 6-3. The required dry density for the 8 investigated bentonite to exceed the strength of 4 000 kPa.

Test series	Dry density (kg/m^3)
India 2018	1 605
BARA-KADE 2017	1 670
Bulgaria 2017	1 460
Morocco 2017	1 630
Milos 2017	1 640
Sardinia 2017	1 605
Turkey 2017	1 660
MX-80 P 2014*)	1 645
All Materials	1 635

*) This bentonite is also investigated in Svensson et al. (2017).

6.3 Compaction properties

There are no requirements on the compaction properties for the buffer materials similar to those for the swelling pressure, hydraulic conductivity and strength. However, the compaction properties are important as input for the design of the buffer components. The compaction properties are varying between the bentonites and therefore it is important to evaluate the compaction properties as described in Section 4.3. In Figure 6-6 are the evaluated dry densities of specimens for 6 different bentonites compacted with 60 MPa plotted as function of the water content. The figure is indicating that the evaluated dry density is very much depending on the type of bentonite but also on the water content.

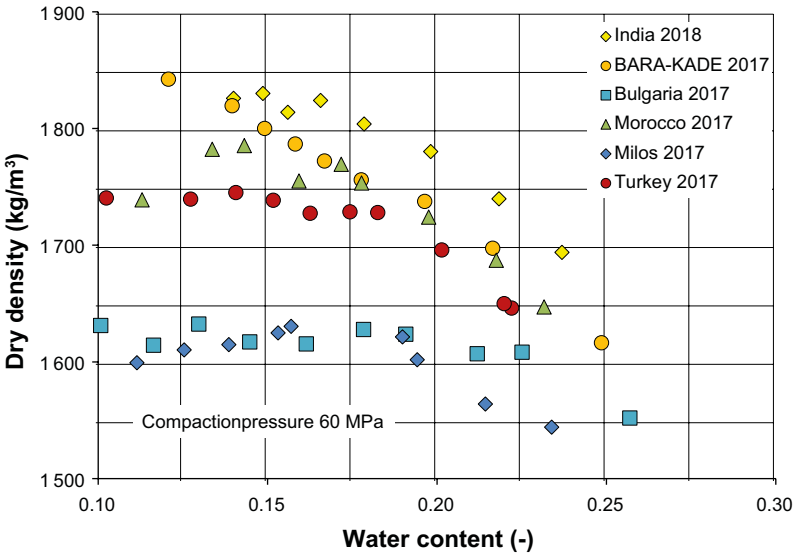

Figure 6-6. *Dry density as function of water content after compaction of 6 bentonites. The compactions of all specimens are made with 60 MPa.*

6.4 Thermal properties

6.4.1 Specific heat

Sample preparation

The specific heat per weight unit is not expected to be a function of dry density. Therefore only the water content is varied and one compaction pressure, in this case 60 MPa, is used. The target water content (w) for these measurements are 10 %, 12 %, 14 %, 15 %, 16 %, 17 %, 18 %, 20 %, 22 %, and 24 %. However, the water content was measured in the samples as well and this value is used for the evaluation.

Specific heat measurements

The specific heat, also denoted C_p, is measured in a special sensor, shown in Figure 6-7. The material sample to be tested is placed in this sensor. The sample is then heated and the temperature response with time is measured. If the mass of the sample is known then the specific heat can be calculated. The specific heat of air is very low and can therefore be neglected. If the specific heat of the air is neglected then the amounts of air filled pores in the sample should not affect the specific heat. This would also imply that the specific heat per weight unit is not affected by the dry density of the sample.

The result of the measurements is shown in Figure 6-8. The result shows that the specific heat has a clear dependence of water content. All of the bentonite types tested has similar values on the specific heat although some differences seem to exist. Even though there is some scatter in the results it seems like some of the bentonite types have slightly higher values of specific heat compared to other.

For the case of modelling this have a small effect as the specific heat only affects the heat transport calculations in short timespans. However, as the specific heat is also used to calculate the anisotropy of the thermal conductivity this might be a source of uncertainty.

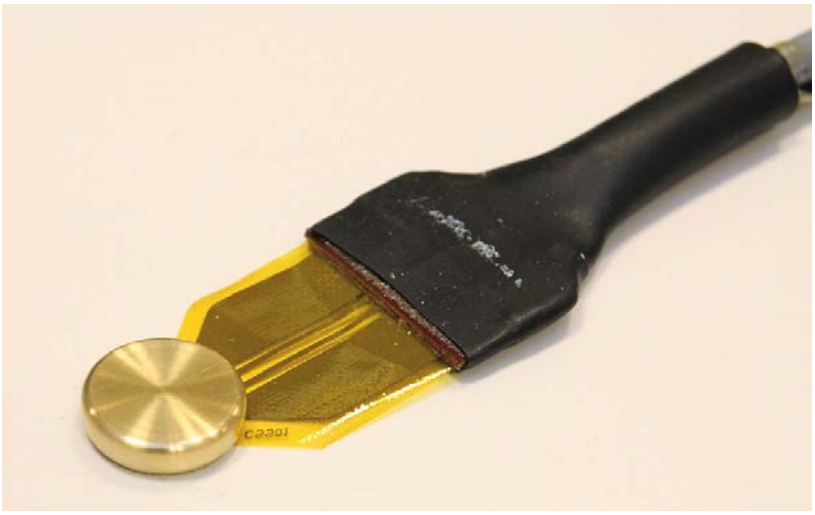

Figure 6-7. *Picture of the sensor used for specific heat measurement.*

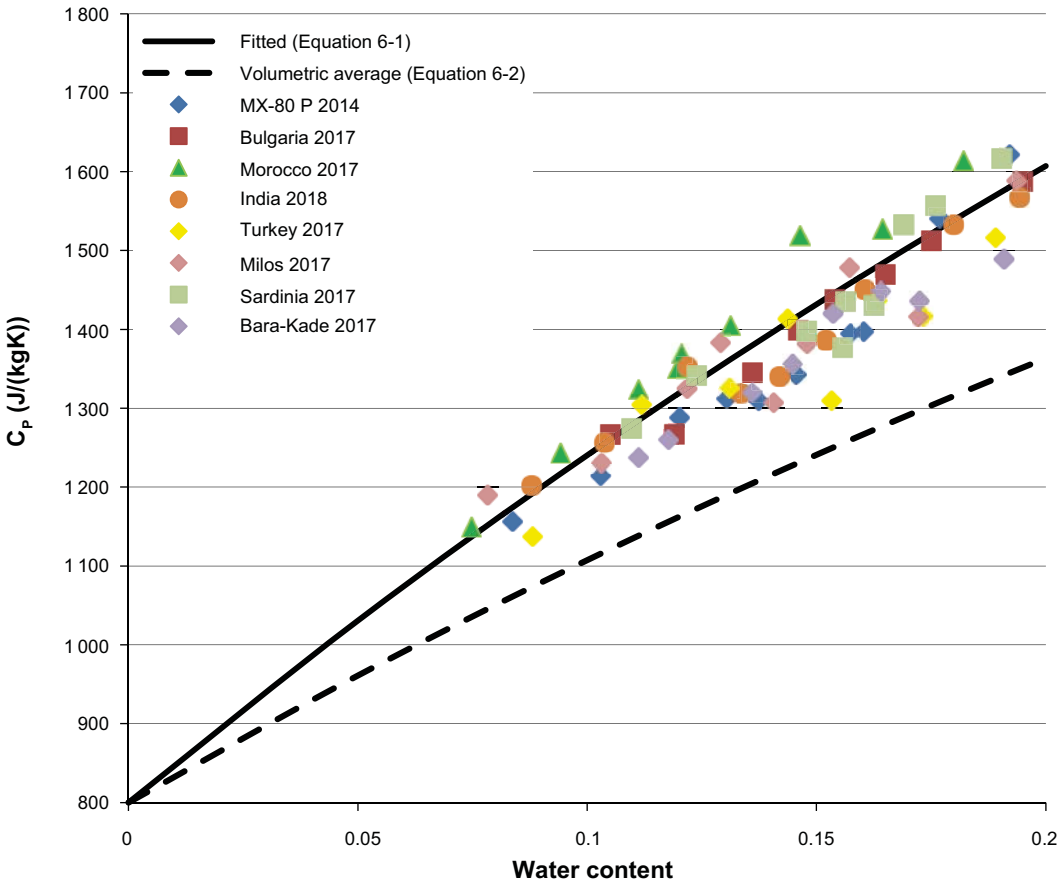

Figure 6-8. *Measured specific heat of different materials.*

In order to find a suitable expression for the specific heat that can be used in modelling one can start with the assumption that the specific heat for the bentonite should be the volumetric average of the two materials, clay and water. Since the specific heat of water is approximately 4 180 J/kg/K at 20 °C and the specific heat of bentonite is approximately 800 J/kg/K (Skauge et al. 1983) the total specific heat capacity, C_p, could be described by Equation 6-1.

$$C_p = \frac{800+4180w}{1+w} \qquad (6\text{-}1)$$

Where w is the water content defined as the mass of water divided by the dry mass. This equation is shown in Figure 6-8. The result shows that the Equation 6-1 underestimates the specific heat. Therefore a modified equation, Equation 6-2, is suggested:

$$C_p = \frac{800+k_1 4180w}{1+w} \qquad (6\text{-}2)$$

Where k_1 is a fitting constant. With a value of 1.35 the equation seems to be a good fit to be used for modelling which seems to work well for all of the bentonites, see Figure 6-8. However, the k_1 is also fitted for each individual material to be used in the determination of anisotropic properties in the thermal conductivity. The result from this fitting is found in Table 6-4.

Table 6-4. Constant k1 fitted to experimental data for individual materials

Material	k_1
Bara-Kade 2017	1.25
Sardinia 2017	1.34
Milos 2017	1.31
MX-80 P 2014	1.26
Morocco 2017	1.45
Bulgaria 2017	1.32
Turkey 2017	1.22
India 2018	1.31

6.4.2 Thermal conductivity

Sample preparation

The thermal conductivity of a soil is expected to be dependent on the water content and the dry density of the sample. Therefore the samples were compacted with these two parameters varied. The test matrix used in this work was the same as have been used for the compaction tests, see Section 6.3. This means that each material is mixed to 10 different water contents and each of these is used for compaction with 5 different compaction pressures. The 10 water contents were the compacted with 5 different compaction pressures. This means that thermal conductivity was measured on 50 samples, all with different water content and density, on each material. The sample preparation started with adjusting the water content. The bentonite material to be tested were mixed to a predefined water content and then the bentonite was left in air tight vessels to make sure that the water content was homogeneous over the sample. The samples were then compacted in a mould with a diameter of 35 mm with 5 different compaction pressures, 25 MPa, 40 MPa, 60 MPa, 80 MPa and 100 MPa. The resulting sample and mould are shown in Figure 6-9. More detail about the method can be found in Section 4.7.

Figure 6-9. *The mould and a bentonite sample after compaction.*

Thermal conductivity measurement

In a porous material the normalized cross section area can be described by the expression in Equation 6-3.

$$A = 1 - \frac{V_a}{V_T} \tag{6-3}$$

Where V_a is the volume of air and V_T is the total volume. This can be described by Equation 6-4 for a bentonite with a certain density as:

$$A = 1 - \varphi(1 - S_r) = \frac{\rho_d}{\rho_s} + w\frac{\rho_d}{\rho_w} \tag{6-4}$$

Where ϕ is the porosity, S_r is the saturation ρ_d is the dry density, ρ_s is the particle density and ρ_w is the density of water. It is assumed that the thermal conductivity, λ, should be proportional to the normalized cross section area. If a constant thermal conductivity is assumed for the clay phase then the test results should be a straight line when plotted against the cross section area. From Figure 6-11 to Figure 6-18 it can be seen that the values fit quite well to a straight line within the measured interval.

By fitting the thermal conductivity values to a straight line the thermal conductivity at full saturation was calculated for the different materials. The density seems to play a minor role on the maximum thermal conductivity at full saturation. These values are shown in Table 6-5. As can be seen from the table the differences in thermal conductivity are not very large for the measured bentonite types. This is also illustrated by Figure 6-10 were thermal conductivity for all materials are shown in one graph.

Table 6-5. Saturated thermal conductivity for different materials.

Material	Saturated thermal conductivity (W/mK)
Bulgaria 2017	1.30
MX-80 P 2014	1.32
Morocco 2017	1.21
India 2018	1.21
Turkey 2017	1.19
Milos 2017	1.34
Sardinia 2017	1.28
Bara Kade 2017	1.28

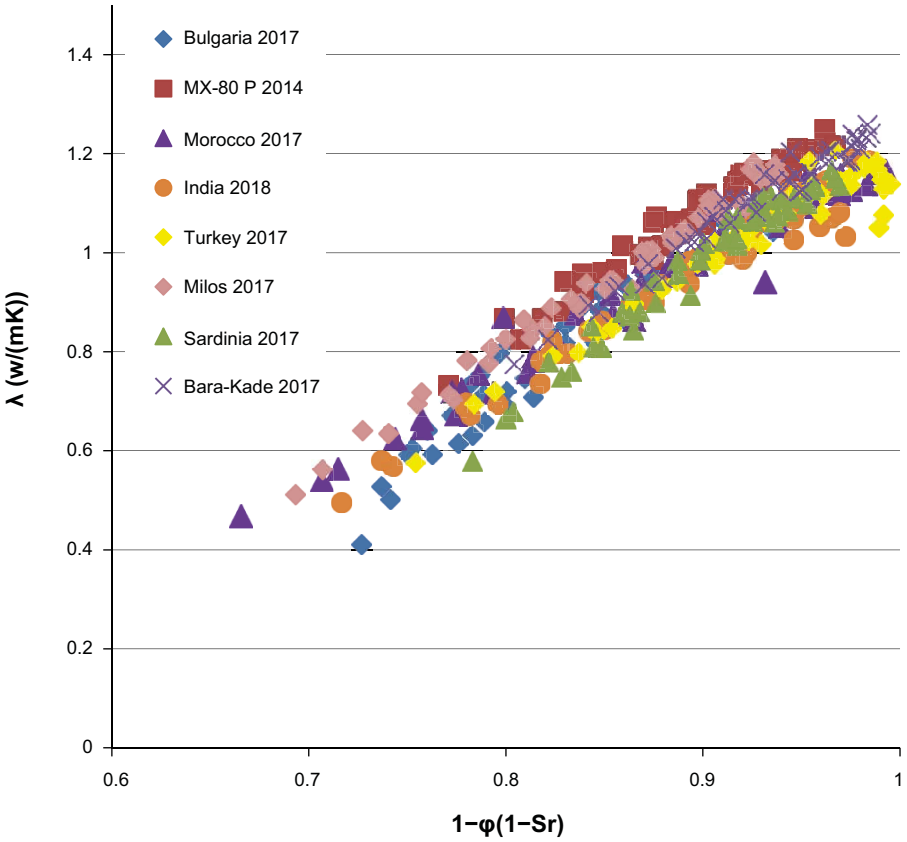

Figure 6-10. *Comparison of thermal conductivity between different bentonite types.*

Anisotropy in the thermal conductivity

The method used measures the geometric mean value of the thermal conductivity in radial and axial direction. If the specific heat is known the thermal conductivity in the different directions can be calculated according to Equation 6-5 and Equation 6-6. The measurements shown in Figure 6-11 to Figure 6-18 suggests that anisotropy is quite large. The thermal conductivity in the compaction direction is approximately 30–50 % lower than the thermal conductivity perpendicular to the compaction direction.

$$C_p = \frac{\lambda_{axial}}{\kappa_{axial}} = \frac{\lambda_{radial}}{\kappa_{radial}} = \frac{\lambda_{radial}}{\kappa_{bulk}} \tag{6-5}$$

$$\lambda_{bulk}^2 = \lambda_{axial}\lambda_{radial} \tag{6-6}$$

Where λ is the thermal conductivity and κ is the thermal diffusivity.

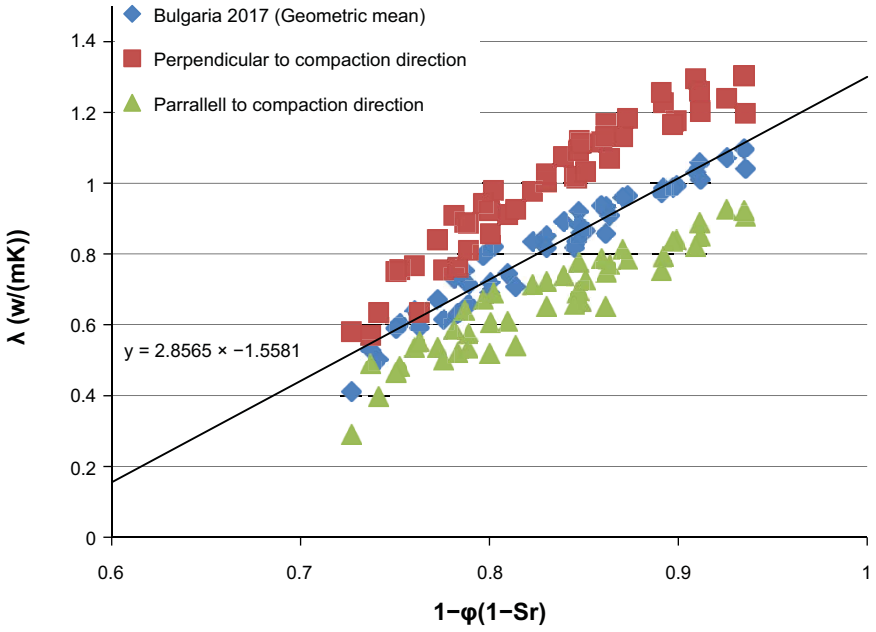

Figure 6-11. *Thermal conductivity measurements for Bulgaria 2017.*

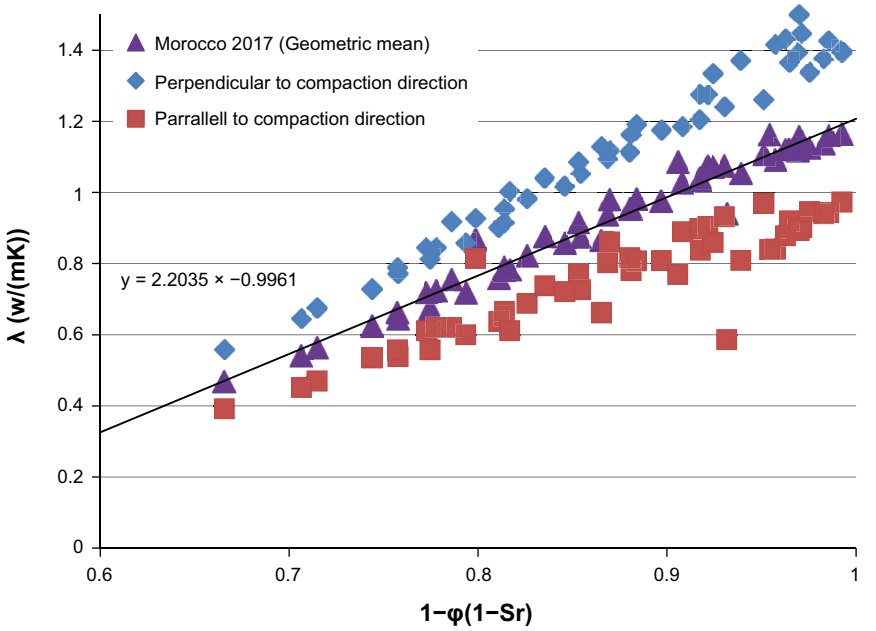

Figure 6-12. *Thermal conductivity measurements for Morocco 2017.*

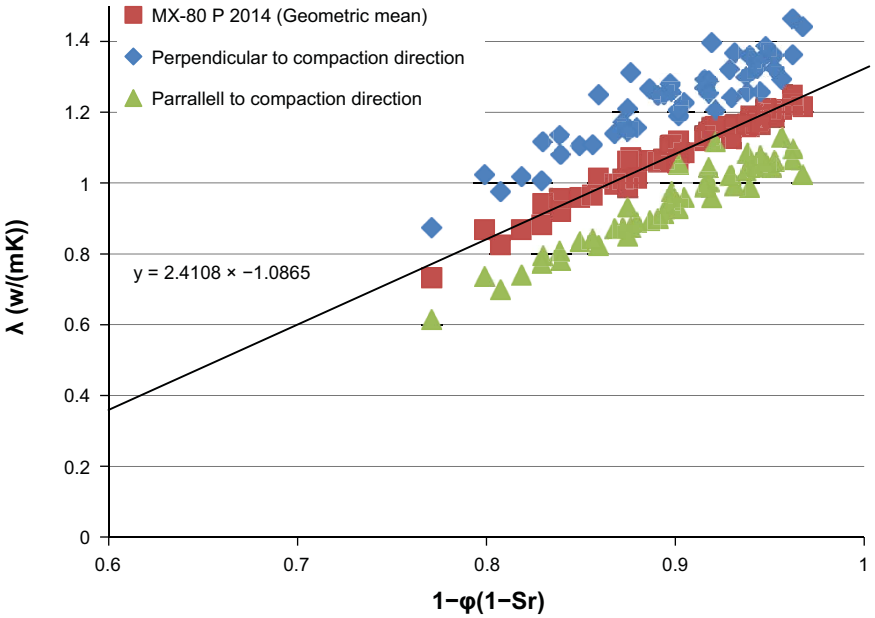

Figure 6-13. *Thermal conductivity measurements for MX-80 P 2014.*

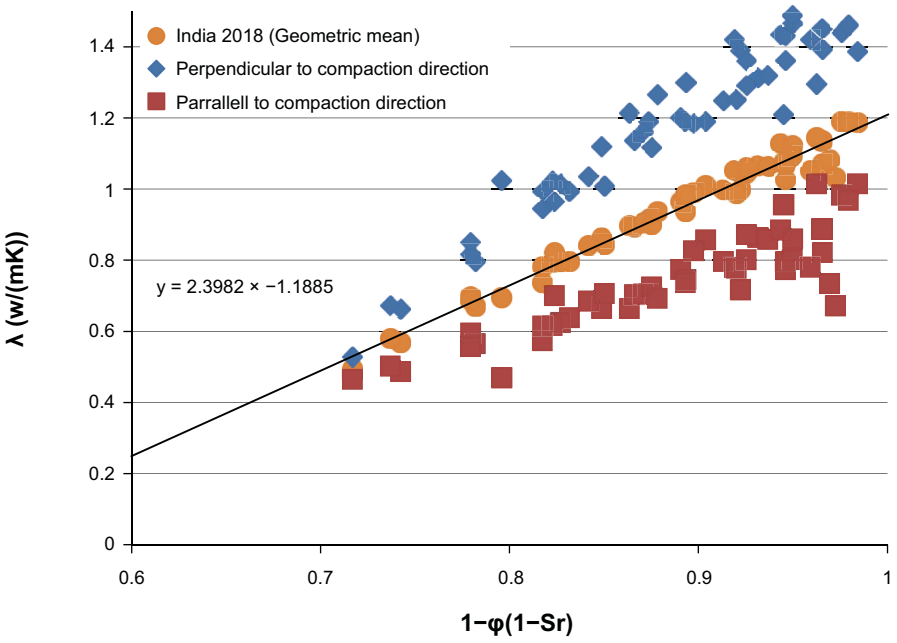

Figure 6-14. *Thermal conductivity measurements for India 2018.*

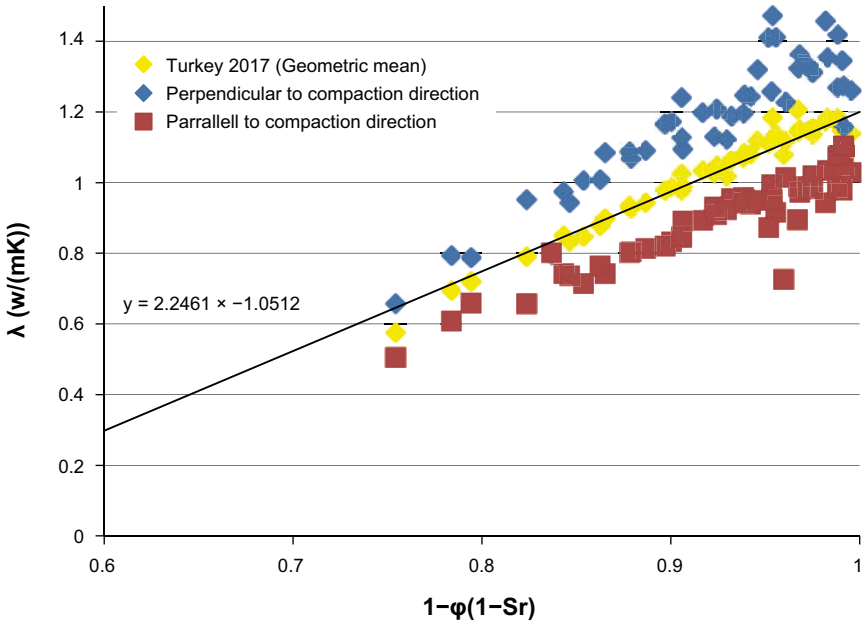

Figure 6-15. *Thermal conductivity measurements for Turkey 2017.*

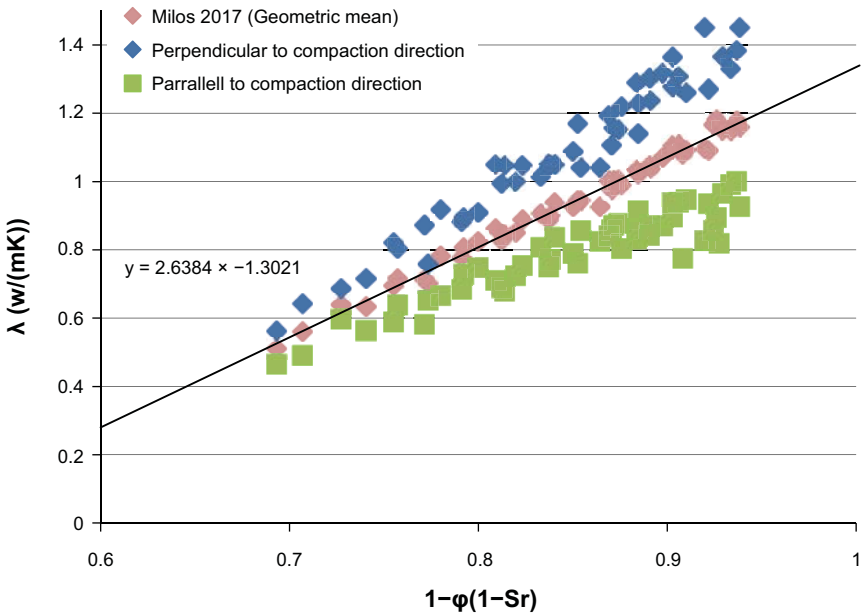

Figure 6-16. *Thermal conductivity measurements for Milos 2017.*

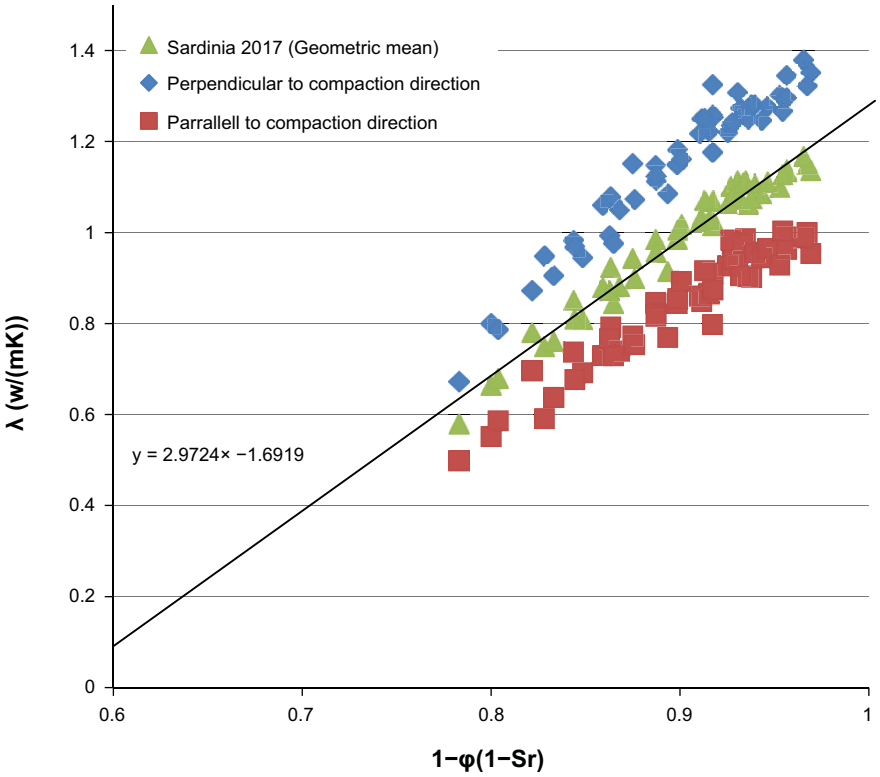

Figure 6-17. *Thermal conductivity measurements for Sardinia 2017.*

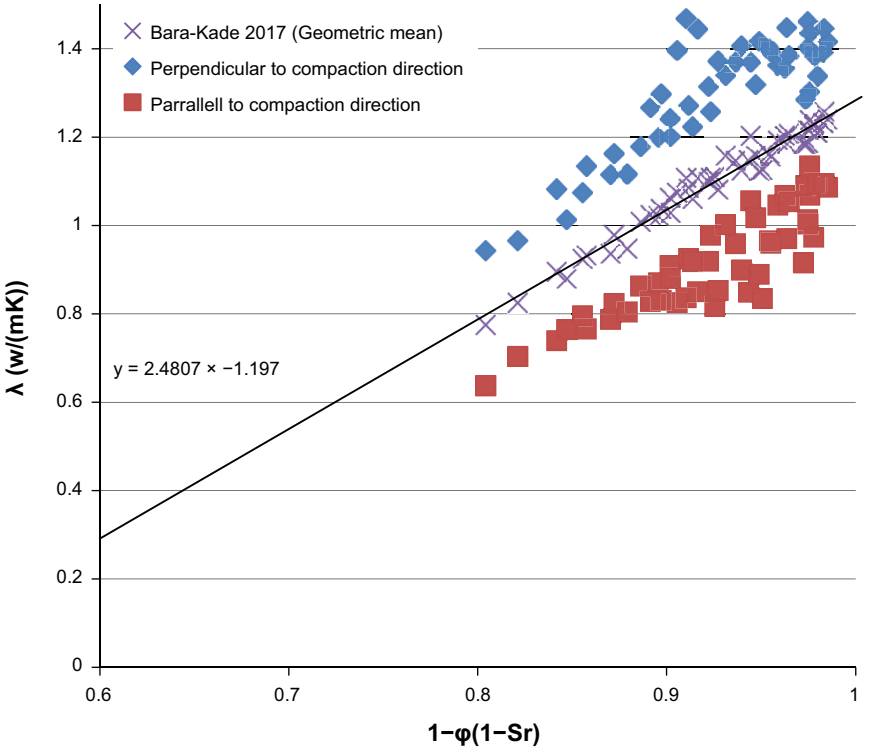

Figure 6-18. *Thermal conductivity measurements for Bara-Kade 2017.*

6.5 Retention properties

General

The retention properties are important and describe the water uptake in an unsaturated bentonite before full swelling pressure has been reached which are needed for example in THM modelling. Since the measurement with the method used is quite time consuming it was decided to measure the retention properties on only two of the materials, Bulgaria 2017 and Morocco 2017. The retention properties can be compiled in a retention curve which describes the relation between the water content and the water potential for the material. This retention curve also normally exhibits a hysteresis effect and the curve differs depending on if the material is being hydrated or dehydrated.

Methodology

One method used to determine the retention curve is the jar method. With this method a sample (approximately 10 g) of bentonite is placed in a basket hanging from the jar lid. In the bottom of the jar a salt solution is placed to control the relative humidity in the jar, See Figure 6-19. Salt solutions which generate relative humidity of 11 %, 33 %, 58 % 75 %, 84 %, 93 % and 97 % were prepared. The bentonite, which has been prepared to an initial water content is placed in the jar and the weight is determined regularly. When the weight change with time is smaller than a certain value the sample is considered to be close enough to equilibrium and the test is stopped. Three initial water contents are chosen to capture the hysteresis effect. The initial water contents of the used materials are shown in Table 6-6.

Table 6-6. Initial water contents used for determination of the retention curve.

Material	Initial water content 1	Initial water content 2	Initial water content 3
Bulgaria 2017	2 %	20 %	63 %
Morocco 2017	2 %	18 %	62 %

Since the jar method is not suitable at very high relative humidity, above approximately 98 %, the measurements have been complemented with additional psychrometer measurements. In this case the bentonite samples are mixed to an specified water content and the water potential is measured. The measurement is done when equilibrium has been reached in the air surrounding the bentonite and the sensor.

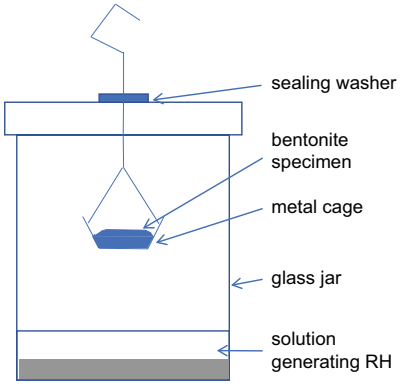

Figure 6-19. *Sketch of the test setup for the jar method. Figure taken from Johannesson et al. (2008).*

Result

The result from the jar method measurements are shown in Table 6-7 and the psychrometer measurements are shown in Table 6-8. The results are also plotted in Figures 6-20 and 6-21. The results show that the Moroccan bentonite has a smaller hysteresis effect then the Bulgarian, the psychrometer results fits well with the measurements done with the jar method.

Table 6-7. Results from the jar method. Water content (%) at equilibrium at different relative humidity.

Material	**Initial Water content (%)**	***RH*(%)**	**LiCl *RH*(%)**	**$MgCl_2$ *RH*(%)**	**NaBr *RH*(%)**	**NaCl *RH*(%)**	**KCl *RH*(%)**	**NaCl 2 m *RH*(%)**	**K_2SO_4 *RH*(%)**
		0	11	33	58	75	84	93	97
Bulgaria 2017 2 %	2.4	1.8	4.6	8.2	12.6	17.6	20.9	27.9	34.5
Bulgaria 2017 20 %	20.6	0.9	5.4	11.1	18.1	21.5	24.8	30.1	37.3
Bulgaria 2017 63 %	63.0	1.2	5.0	11.3	18.1	23.6	27.5	32.4	37.8
Morocco 2017 2 %	2.3	1.2	4.2	8.5	13.1	17.0	19.5	22.9	27.1
Morocco 2017 18 %	17.6	1.3	5.5	10.8	15.7	18.4	20.6	24.1	28.5
Morocco 2017 62 %	62.3	0.7	5.8	10.4	15.2	18.9	21.2	25.7	33.4

Table 6-8. Results from the psychrometer measurements.

Material	Water content *w*	Relative humidity *RH*
	%	%
Bulgaria 2017	38.2	96.7
Bulgaria 2017	37.7	96.3
Bulgaria 2017	40.4	97.8
Bulgaria 2017	42.9	98.2
Bulgaria 2017	47.0	98.8
Bulgaria 2017	53.1	99.3
Morocco 2017	29.2	96.3
Morocco 2017	28.8	96.1
Morocco 2017	35.4	98.6
Morocco 2017	34.4	98.4
Morocco 2017	42.3	99.3
Morocco 2017	41.5	99.2
Morocco 2017	45.2	99.4
Morocco 2017	44.9	99.4

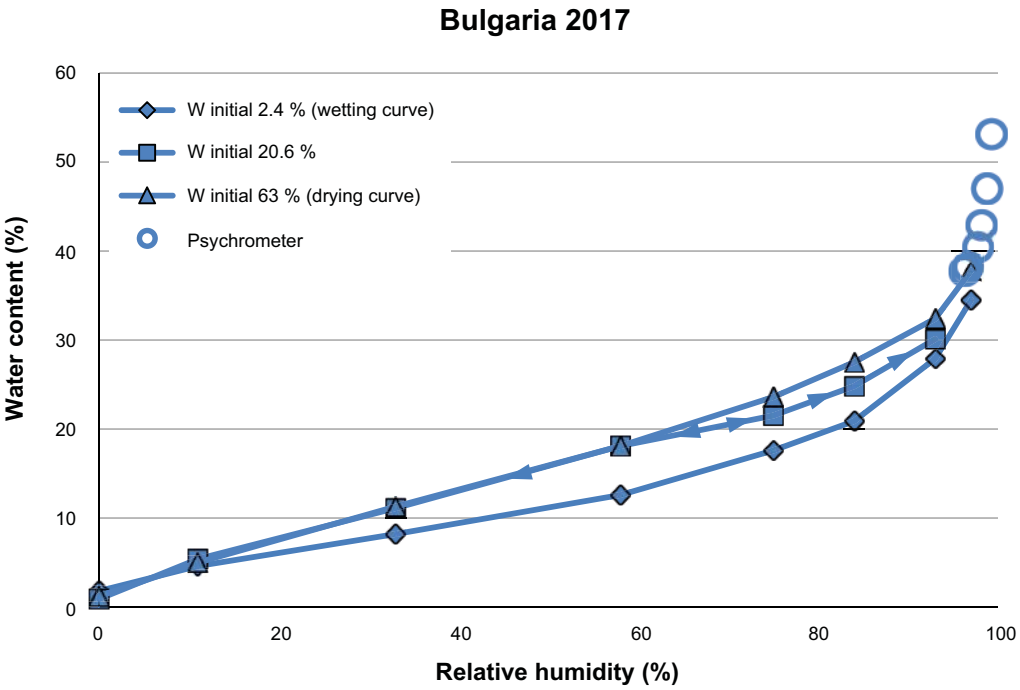

Figure 6-20. *Retention curve for Bulgaria 2017.*

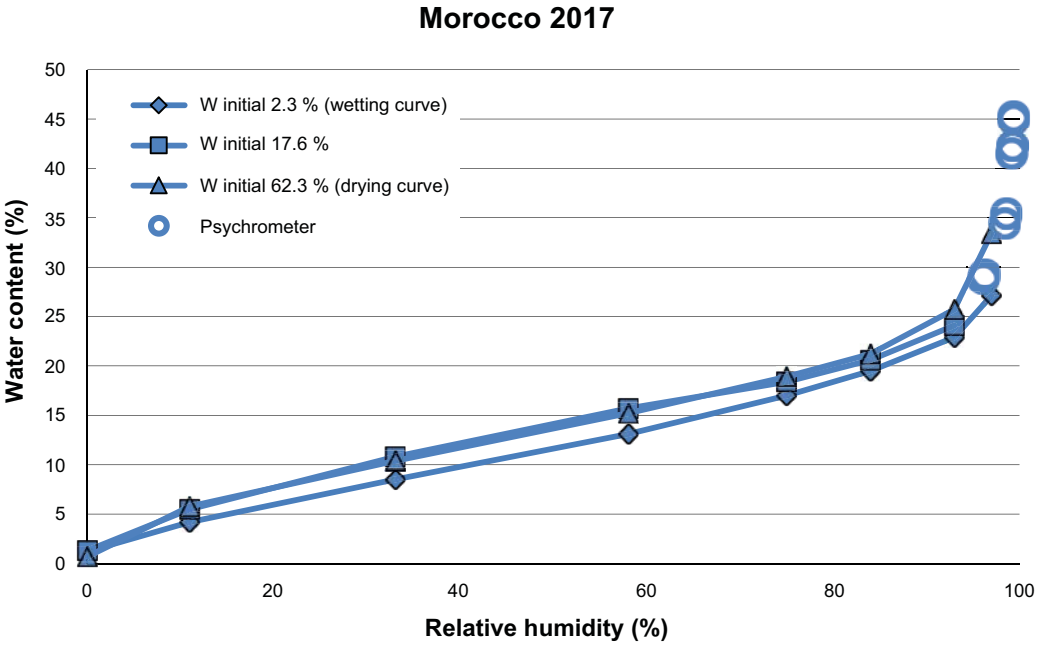

Figure 6-21. *Retention curve for Morocco 2017.*

6.6 Grain density

The grain density is the density of the solid phase of the clay and is used for a number of calculation for example to calculate parameters such as porosity and saturation. Therefore the grain density of the materials in this report was determined. The method used is to determine the density in volumetric flasks, see Figure 6-22. The method is described in detail in Karnland et al. (2006). The results are shown in Table 6-9.

Table 6-9. Results from the grain density determinations.

Material	Number of determinations	Grain density kg/m^3	std deviation kg/m^3
India 2018	7	2931	19
Bara-Kade 2017	3	2770	6
Bulgaria F 2017	3	2758	5
Bulgaria 2017	4	2757	7
Morocco 2017	6	2737	16
Milos 2017	4	2606	13
Sardinia 2017	4	2812	10
Turkey 2017	6	2605	83
Bara-Kade 2017	4	2769	6
MX-80 2012	8	2783	21

Figure 6-22. *Volumetric flasks were the grain density is being determined.*

6.7 Shrinkage/expansion curve

6.7.1 Methodology

To measure the shrinkage/expansion curve of the material, small samples with a height of approximately 10 mm and a diameter of approximately 35 mm was compacted. The samples had different initial water content and were compacted with two different compaction pressures. Details about the compaction pressure and the initial water content for the different samples are shown in Table 6-10. The samples were then placed in a climate chamber with a controlled relative humidity. The samples were weighed regularly and the height and diameter of the samples were measured. When equilibrium had been reached the relative humidity in the climate chamber was changed and the process was repeated. Since the water content was known from the beginning the water content was calculated from the weight loss or gain and the density was calculated from the dimensional measurements and weight. When no or small changes in weight are registered the bentonite was considered to be close enough to equilibrium with the relative humidity in the surrounding air. The relative humidity in the climate chamber was then changed either to a higher relative humidity to get the swelling curve or to a lower relative humidity to get a shrinkage curve. Altogether 3 series of tests were made, where series 1 and 2 were allowed to shrink (decreasing relative humidity) and series 3 was allowed to swell (increasing relative humidity). Similar test has earlier been done (Eriksson 2018) for MX-80 material.

Table 6-10. Samples used in this study to determine the shrinkage/swelling curve.

Sample	Initial water content	Compaction pressure	Material
1	14 %	30 MPa	Bulgaria 2017
2	17.5 %	30 MPa	Bulgaria 2017
3	21 %	30 MPa	Bulgaria 2017
4	25 %	30 MPa	Bulgaria 2017
5	30 %	30 MPa	Bulgaria 2017
6	14 %	60 MPa	Bulgaria 2017
7	17.5 %	60 MPa	Bulgaria 2017
8	21 %	60 MPa	Bulgaria 2017
9	25 %	60 MPa	Bulgaria 2017
10	30 %	60 MPa	Bulgaria 2017

6.7.2 Results

To evaluate the result the height and the diameter are normalized with a height and a diameter so that the dimension is one at zero water content. The result is summarized in Figure 6-23 and Figure 6-24. Even though the samples have different densities it seems like the expansion/shrinkage can be described as a function of water content. The shrinkage curve and the swelling curve do not seem to be equal which suggests that there is some hysteresis effect. It can also be noted that the material swelling and shrinkage is anisotropic. The height dimension which is in the compaction direction expands and shrinks more with water content than the diameter which is perpendicular to the compaction direction.

In Figure 6-25 and Figure 6-26 results from MX-80 (Eriksson 2018) is presented for comparison. The MX-80 material seems to behave in the same way as the Bulgarian material. However the MX-80 material seems the shrink slightly faster with water content than the Bulgarian material.

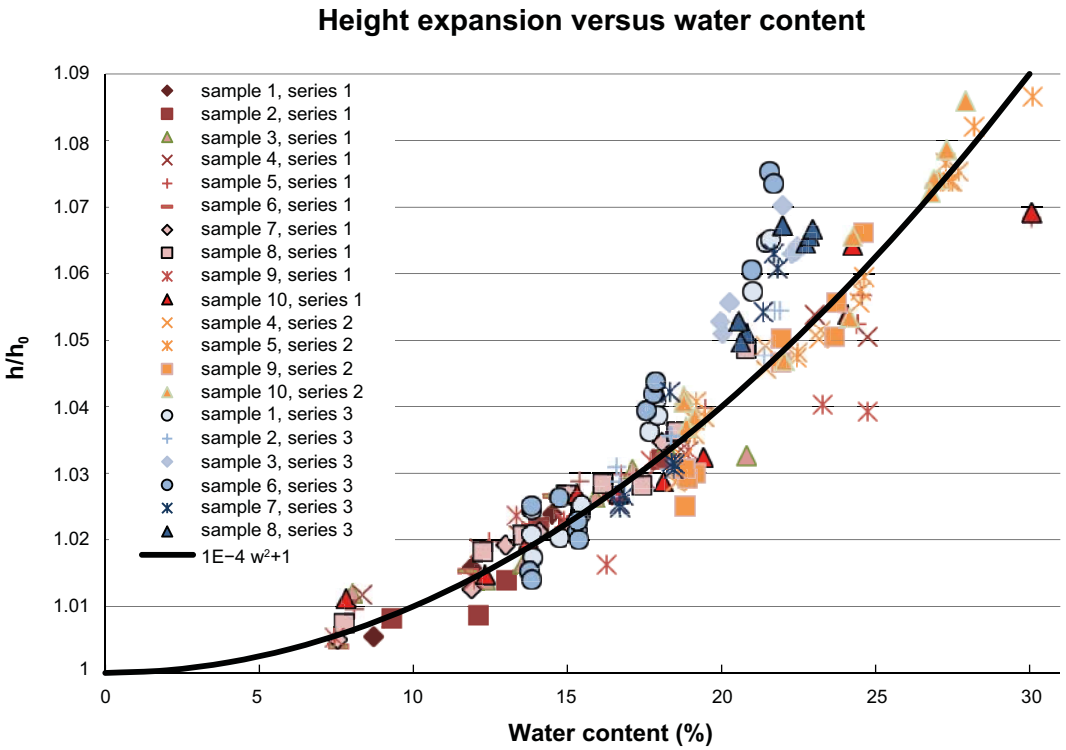

Figure 6-23. *Normalized expansion (series 3) and shrinkage (series 1 and series 2) in the compaction direction.*

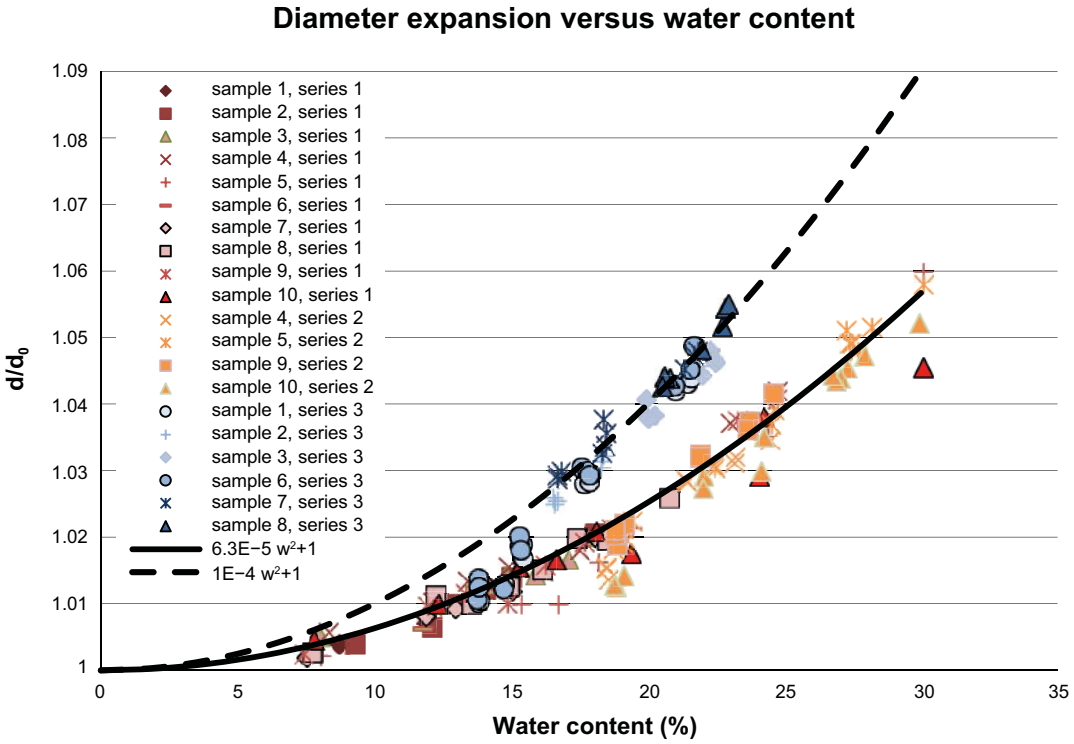

Figure 6-24. *Normalized expansion (series 3) and shrinkage (series 1 and series 2) perpendicular to the compaction direction. The dashed line represents the shrinkage in the compaction direction and is added for comparison.*

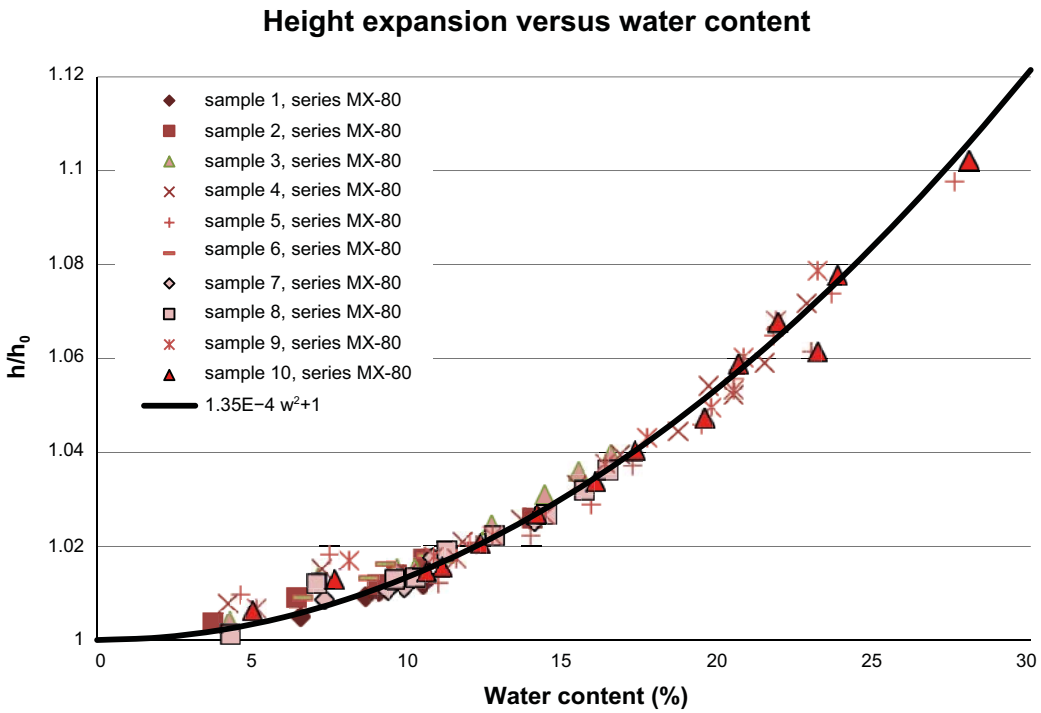

Figure 6-25. *Normalized shrinkage in the compaction direction for MX-80. Data is taken from Eriksson (2018).*

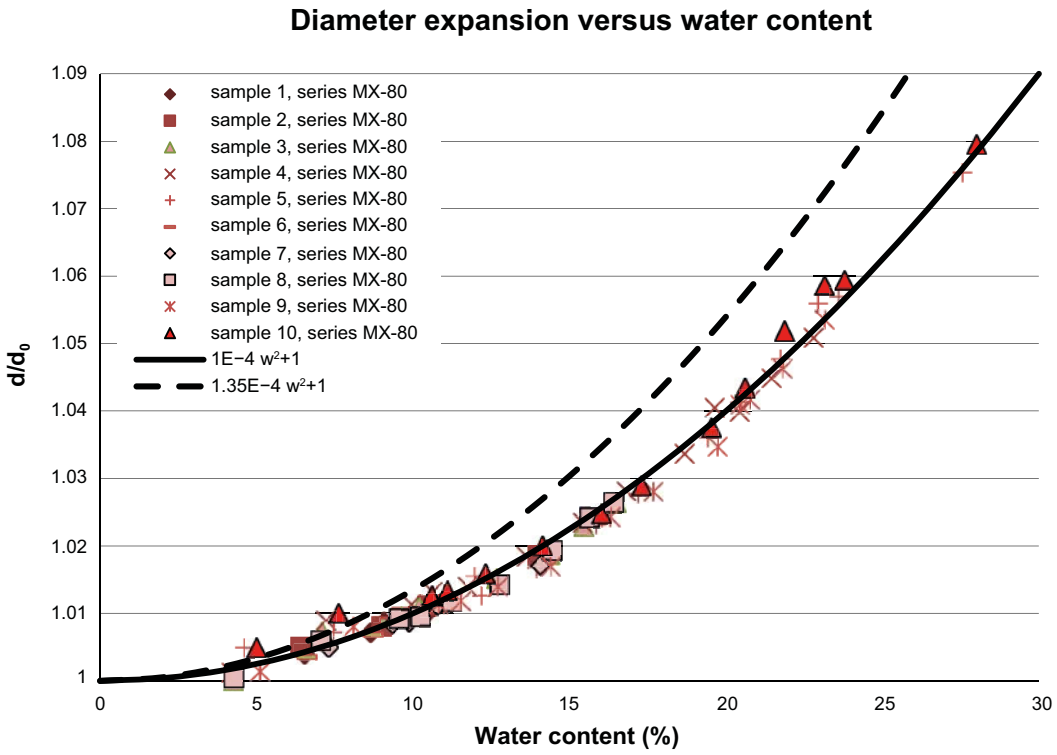

Figure 6-26. *Normalized shrinkage perpendicular to the compaction direction for MX-80. Data is taken from Eriksson (2018). The dashed line represents the shrinkage in the compaction direction and is added for comparison.*

6.8 Granule size distribution

The granule size distribution of all materials has been measured since the granule size affects the properties of the material e.g. at compaction. The measurements were done according to the methodology described in Svensson et al. (2017) with the sieve sizes 20 mm, 6.3 mm, 2 mm, 0.71 mm, 0.25 mm and 0.063 mm.

Some of the used materials in this work were very fine powders and had a 100 % passing on the finest sieve and thus, the granule size distribution of these materials are not shown here and these materials are India 2018, Turkey 2016 and Turkey 2017. The results are shown in Figure 6-27.

6.9 Water content

The geotechnical (water/dry mass) and general (water/total mass) water contents of the tested materials are presented in Table 6-11.

Table 6-11. Geotechnical and general water content of the tested materials.

Material	Geotechnical water content (w)	General water content (wc)
Milos 2017	17.9	15.1
Morocco 2017	17.7	15.0
Bulgaria 2017	20.1	16.7
Bulgaria 2018	19.6	16.4
Bulgaria F 2017	18.8	15.9
Turkey 2017	9.3	8.5
India 2018	14.4	12.6
BaraCade F	11.4	10.2
Sardinia 2017	19.4	16.3

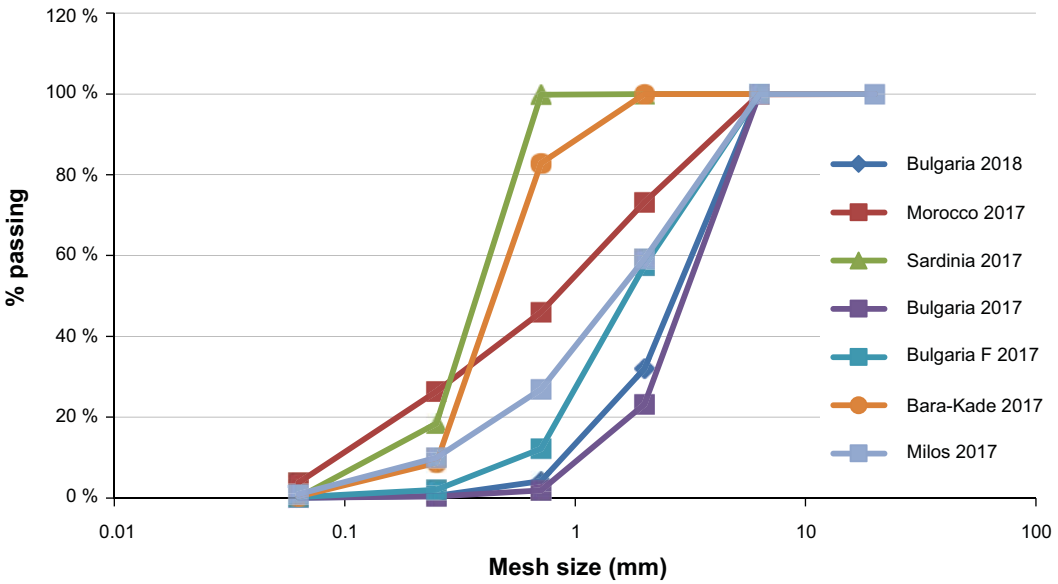

Figure 6-27. *Granule size distribution for the materials in this investigation.*

7 Discussion and conclusions

Development and testing of methods suitable for quality control of bentonite as KBS-3 buffer/backfill was performed. A number of different bentonite batches were also analysed, and some relations between bentonite content and properties were studied, e.g. the impact from montmorillonite content on the swelling pressure and the hydraulic conductivity. The overall impression from the testing of the methods was that the included methods were relevant, their performance was suitable for the application, and seems to cover what is needed. However, further development and optimisations are expected in the future. All included bentonites seems to be potential candidates for use as buffer and/or backfill, with the exception of the included Milos bentonite that intentionally was lower in montmorillonite. Other qualities higher in montmorillonite from Milos would also be useful candidate materials.

The swelling pressure and hydraulic conductivity of MX-80 was studied as a function of the montmorillonite content. The result showed that a decrease of 5 % by weight lowered the swelling pressure and increased the hydraulic conductivity. Hence, the quality control of the bentonite is from this observation recommended to be able to detect relative differences in montmorillonite content somewhere in the range of 3–5 wt%.

XRD showed repeatability for MX-80 bentonite of approximately ± 2.0 % by analysing triplicate samples. However, more complex bentonites (several clay minerals) are expected to show higher scattering. Exact identification of all mineral phases present in the bentonites was not possible, and the Rietveld refinement fittings used for quantification were not perfect, however, the quantified amount of montmorillonite and major phases was reasonable when compared to CEC and XRF, and relative changes in montmorillonite content in the above recommended range seems reasonable to detect. Some scattering in the data from larger single grains present in the sample indicated that the sample treatment may need to be further improved in the future.

XRF showed somewhat different repeatability for each element. Determinations of chemical indexes or ratios were tested as indirect measures of the montmorillonite content in a bentonite, this seems possible, however requires knowledge about the chemical composition of the accessory minerals, hence the same ratio is not usable in all types of bentonites.

The CEC method showed good repeatability but with a lower reproducibility. Hence, it is recommended to analyse all samples that are to be compared at once and to average triplicate samples in order to quantify small relative changes. Overall XRD and CEC seems to fulfil the needed performance for monitoring the montmorillonite content of the bentonite clay (at least when averaging triplicate samples). There are several possibilities for artefacts or man made errors in the XRD and the CEC method, however, by combining XRD, CEC, XRF and evolved gas analysis it is possible to minimise this risk. These methods are the basis for quality control regarding the material content, and other techniques come in as a complement when needed (e.g. EC).

EC typically showed somewhat larger sum than the CEC, this is common because of the minor dissolution of e.g. gypsum. In some cases EC was much larger than CEC, this was attributed to the presence of clinoptilolite, a zeolite that can exchange with ammonium ions used in EC, but that cannot exchange with the Cu-tri complex. Presence of clinoptilolite is expected to lead to an over estimation of the montmorillonite content if the supplier is using methylene blue or ammonium ions to quantify the CEC instead of Cu-tri. The EC method works generally very well for SKB's purpose and need no further refinement.

The quantification of organic carbon, carbonate, sulfide and sulfate was tested by additions to the bentonite or by removal by pre-treatments. The Milos material was relatively high in sulfide and total sulfur, while the others all were low. All tested bentonites were low in organic carbon. The effect from pre-treatments and additions was also evaluated. Removal of carbonate with acid worked well, the organic carbon was not removed by hydrogen peroxide (however the result may be an effect of the method uncertainty at low organic carbon levels), addition of organic carbon was captured at the highest addition, addition of sulfide was captured at low and high levels, and additions of carbonate lead to an over estimation of the carbonate content.

The material physical properties were also studied, and they are also important quality control parameters. The swelling pressure and the hydraulic conductivity measurements involved measurements with both de-ionized water and with a 1 M $CaCl_2$-solution. The measured swelling pressure and hydraulic conductivity were depending on the dry density of the specimen and the type of bentonite. At the determinations was also the standard deviation of the method calculated, which reflects the accuracy in the measurements and also this varied between the bentonites. Most bentonites showed similar results, however, the Bulgarian bentonite was significantly different from the others, showing higher swelling pressures at comparable densities. With DI water the bentonite generally gives its maximum swelling pressure, and the DI determination is used to ensure that the bentonite do not swell too much, while the 1 M $CaCl_2$ is used in order to ensure that the bentonite give rise to a high enough swelling pressure at high salinity. The use of DI and 1 M $CaCl_2$ will cover all possible evolution of the ground water chemistry with respect to bentonite properties, since they are bounding on salinity and calcium content.

Based on XRD and CEC some differences in montmorillonite content were found in the Bulgarian bentonite batches, indicating that the Bulgaria F was somewhat higher compared to Bulgarian 20 kg (79.2 versus 73.4 wt%). But the swelling pressure was actually somewhat higher in the 20 kg batch than in the F batch (Figure 7-1), and possibly the hydraulic conductivity of the 20 kg batch was somewhat lower than the F-batch. No complete dataset is yet available for the third batch (20 tonnes), when this data is available this can be further evaluated. The observation that the 20 kg batch with a lower montmorillonite showed a higher swelling pressure than the F batch with higher montmorillonite content was unexpected. There are however at least the following possibilities for this observation: (i) the observed difference is within the uncertainty of the method, (ii) the "salt correction" of the individual data sets introduced a systematic error, (iii) one or several water soluble phases were removed during the measurement to different degree in the batches, hence increasing the montmorillonite content somewhat, (iv) the determination of the montmorillonite content was incorrect, and (v) the Bulgarian bentonites are vastly different compared the other bentonites when it comes to swelling pressure. The reason for this is currently unknown. Hence there is a yet unknown parameter affecting the swelling pressure. This parameter could be different also within a deposit, between different batches etc. This could be the reason for the observed difference. Hence it is important to never rationalise the quality control too much, and to continue to improve the understanding of the relation between the content and the properties, as well as the methods themselves. A summary of CEC and EC results of all batches is seen in Table 7-1.

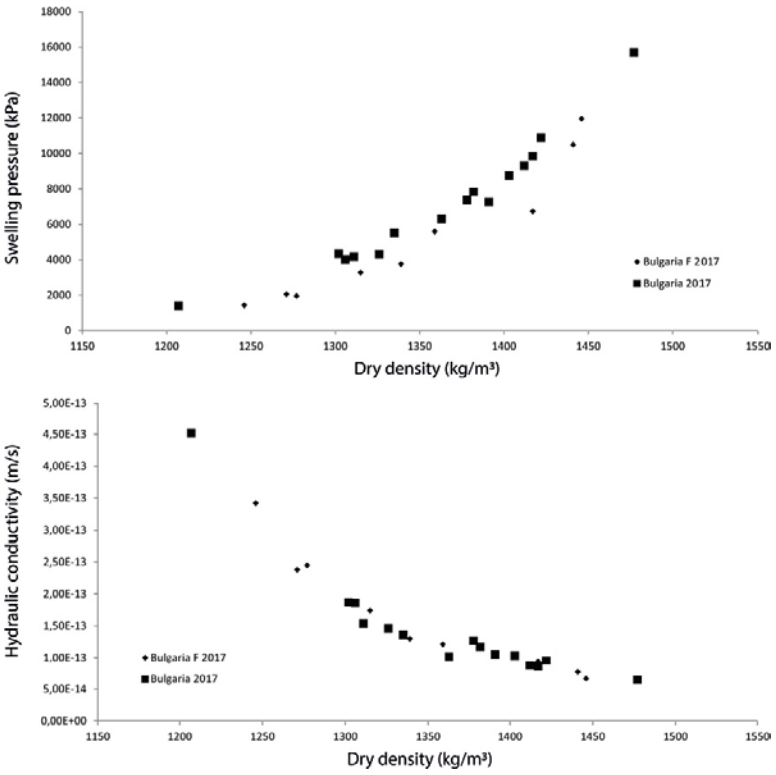

Figure 7-1. *Swelling pressure and hydraulic conductivity of two Bulgarian bentonite batches with 1 M $CaCl_2$ solution.*

Table 7-1. Summary of CEC and EC for the studied bentonite batches. CS = composite sample (bulk), CF = clay fraction, and * indicates single measurement (n = 1).

Bentonite	Delivery (kg)	Sample id	CEC mean (cmol(+)/kg)		Na^{+}_{mean}	Ca^{2+}_{mean}	Mg^{2+}_{mean}	K^{+}_{mean}	EC_{sum} (cmol(+)/kg)
			CS	CF					
Milos 2017	20	c65e23 (CS) c65e66 (CF)	55.6	95.7	11.8	28.1	18.2	3.1	61.2
Morocco 2017	20	c65e25 (CS) c65e6b (CF)	80.6	104.3*	33.1	20.1	27.7	1.5	82.3
Bulgaria 2017	20	c65e21 (CS) c65e68 (CF)	73.1	85.3	19.7	49.9	7.8	4.4	81.8
Bulgaria 2018	20 000	c65ec9 (CS)	79.4	-	-	-	-	-	-
Bulgaria F 2017	200	c65e6a (CS) c65f3b (CF)	76.2	89.9	24.6	47.3	7.6	4.0	83.5
Turkey 2017	200	c65e26 (CS) c65e6d (CF)	68.6	86.0	71.5	13.7	2.8	5.3	93.3
India 2018	20 000	c65e89 (CS)	79.8	89.4	55.5	19.7	17.3	0.6	92.1
BARA-KADE 2017	200	c65e65 (CS)	83.6	-	55.2	25.9	5.3	1.5	87.7
Sardinia 2018	200	c65e84 (CS)	108.0	-	38.3	32.6	49.9	1.7	122.7

The swelling pressure and the hydraulic conductivity measurements were made, according to a standard method developed in previous projects, on the above listed bentonites and involve measurements with both de-ionized water and with a 1 M $CaCl_2$-solution. The measured swelling pressure and hydraulic conductivity were depending on the dry density of the specimen and the type of bentonite. In Figure 7-2 and Figure 7-3 are for the salt content corrected data for the measurement of the swelling pressure for the 8 investigated bentonites summarised. The made correction is described in Section 4.1. Figure 7-2 involves the swelling pressure measurements made with deionized water while corresponding data for the measurements made with 1 M $CaCl_2$-solution is shown in Figure 7-3.

The standard deviation of the method was also calculated, which reflects the accuracy in the measurements. The standard deviations were also varying between the investigated bentonites.

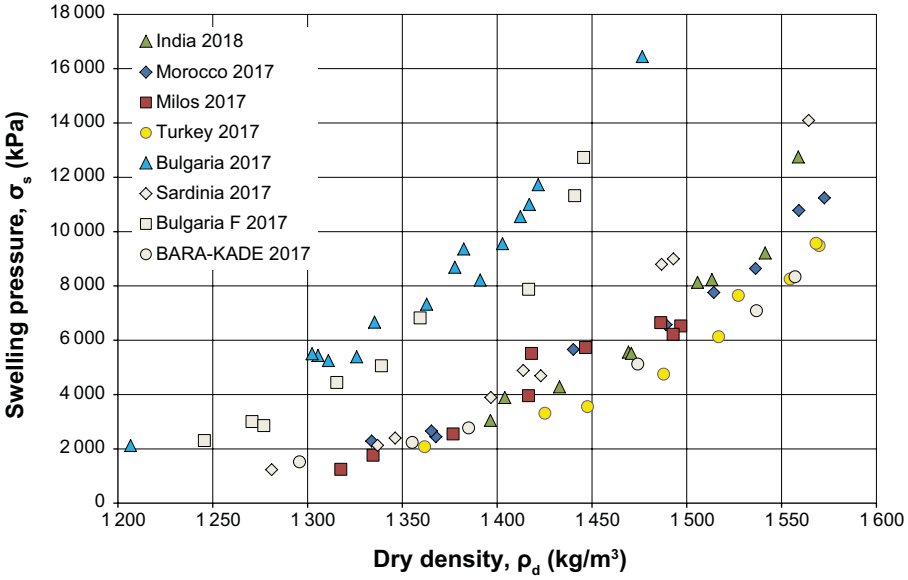

Figure 7-2. *Determined swelling pressure, measured with deionized water, as function of dry density for the 8 investigated bentonites. Note that the dry densities are corrected (see Section 4.1).*

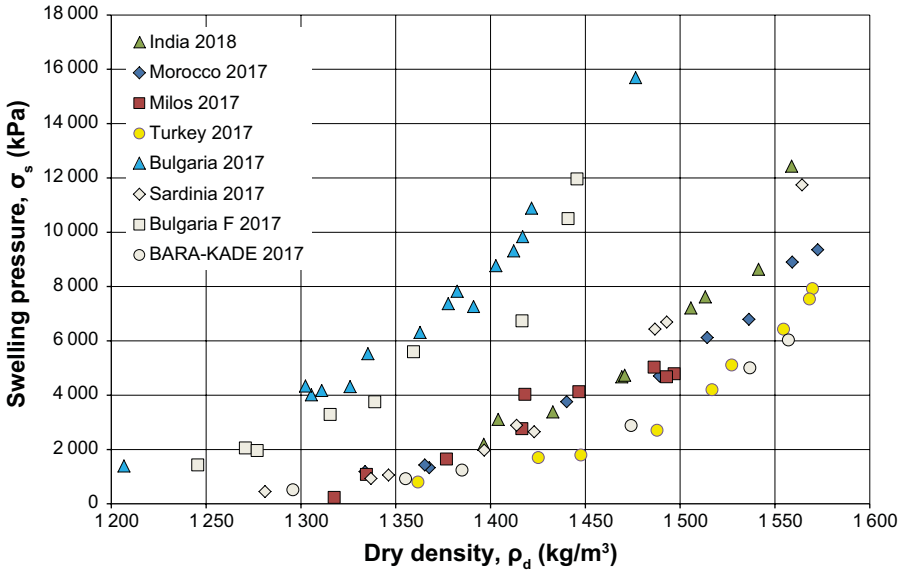

Figure 7-3. *Determined swelling pressure,* ***measured with 1 M CaCl2-solution****, as function of dry density for the 8 investigated bentonites. Note that the dry densities are corrected (see Section 4.1).*

An important parameter at the design of the buffer is the unconfined compressive strength. This was determined with a so called unconfined compression test. The compressive strength was measured on total eight bentonites and was very much depending on the dry density of the saturated specimens. The variation between the different bentonites was small except for one bentonite, Bulgaria, which had a much higher strength compared to rest of the investigated bentonites, see Figure 7-4. The standard deviation of the measurement was also calculated, which reflects the accuracy in the measurements. The standard deviation varied between the investigated bentonites and was highest for the bentonite Morocco and lowest for the bentonite Turkey.

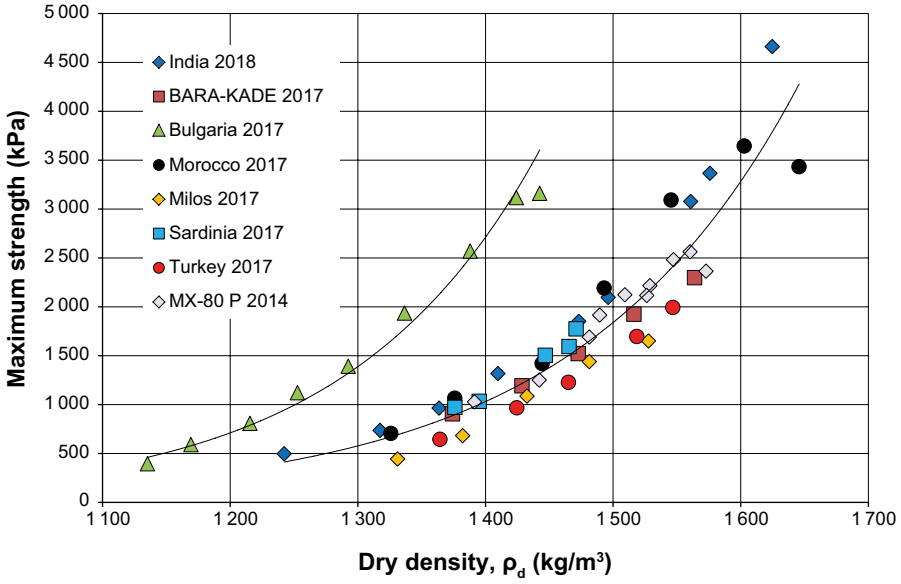

Figure 7-4. *The maximum strength as function of dry density for the eight investigated bentonites.*

The strength is mainly dependent on the density but an alternative way to plot the strength data is shown in Figure 7-5. In this case the strength is plotted as function of the swelling pressures of the materials where the swelling pressure is estimated from the measured density of the specimens together with calculated relationship between the density and swelling pressure for the investigated bentonites presented in Appendix 1. The figure is indicating that there is a relationship between the swelling pressure and the strength which is rather independent of bentonite type. However, it should be noted, that the relationship might not be unique but might change with e.g. stress/moisture paths (hysteresis) and chemical equilibrium since these factors will influence differently on the strength and on the swelling pressure.

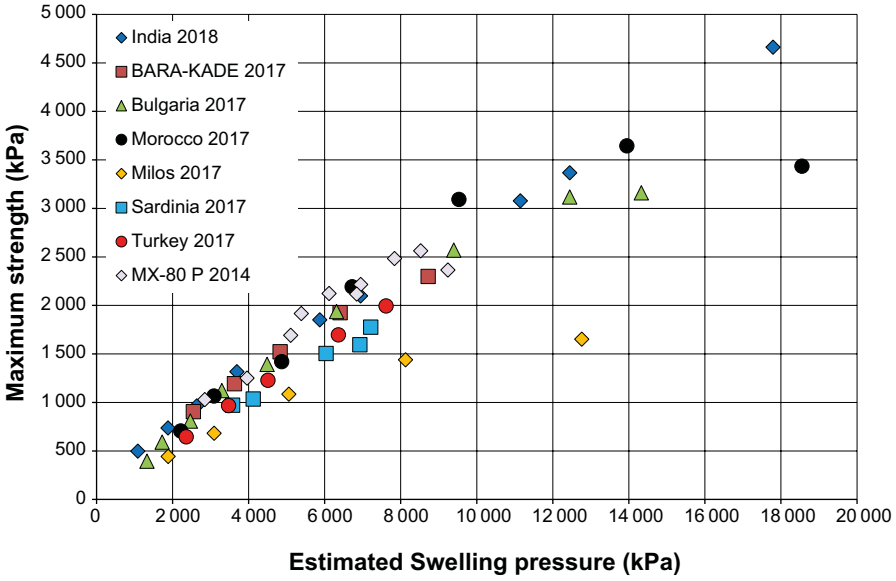

Figure 7-5. *The maximum strength as function of the estimated swelling pressure for the eight investigated bentonites.*

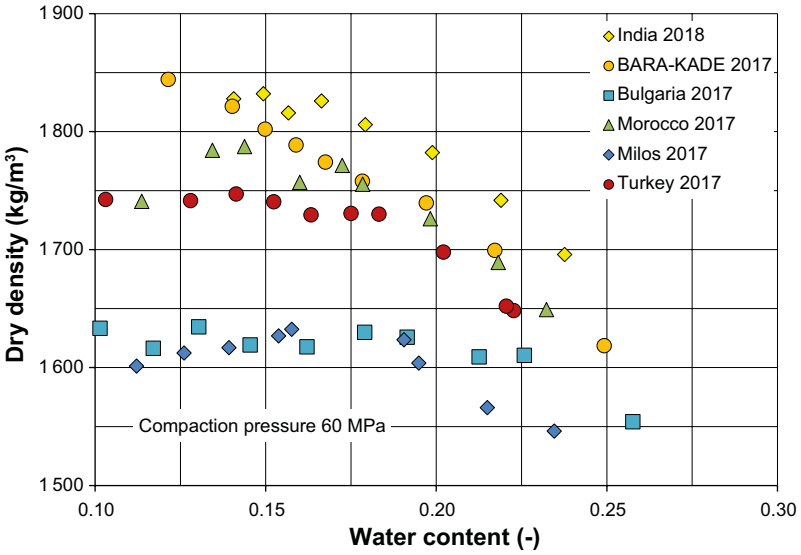

Figure 7-6. *Dry density as function of water content after compaction of 7 bentonites. The compactions of all specimens are made with 60 MPa.*

The compaction properties of a bentonite are important as input for the design of the buffer and the backfill blocks but also at the production of them. The compaction properties were investigated with a laboratory test and the outcome of the test were, what dry density was possible to achieve and at what water content and compaction stress this could be made. The compaction properties varied between the bentonites, see Figure 7-6 where the results of compaction of seven bentonites at a compaction of 60 MPa at different water content are compared. An estimation of the accuracy of the determination was also made by repeating the compaction 30 times at the same conditions i.e. the same bentonite type, water content and compaction pressure.

The grain density is used for a number of calculations, for example to calculate parameters such as porosity and saturation. The India 2007 material stands out with a higher grain density at 2 931 kg/m^3 probably due to high iron content. Milos 2017 and Turkey 2017 are on the lower side, with around 2 605 kg/m3 while the others have a grain density between 2 737 kg/m^3 and 2 812 kg/m^3.

A method to measure thermal conductivity with a transient plan sensor has been developed. The results from the measurements are in accordance with measurements done earlier with other methods. The materials thermal conductivity does not differ much from each other. All the tested materials have a saturated thermal conductivity in the range 1.19–1.34 W/mK.

References

SKB's (Svensk Kärnbränslehantering AB) publications can be found at www.skb.com/publications. SKBdoc documents will be submitted upon request to document@skb.se.

Ammann L, Bergaya F, Lagaly G, 2005. Determination of the cation exchange capacity of clays with copper complexes revisited. Clay Minerals 40, 441–453.

ASTM D4643-17. Standard test method for determination of water content of soil and rock by microwave oven heating. West Conshohocken, PA: ASTM International.

ASTM D5334-14. Standard test method for determination of thermal conductivity of soil and soft rock by thermal needle probe procedure. West Conshohocken, PA: ASTM International.

Belyayeva N I, 1967. Rapid method for the simultaneous determination of the exchange capacity and content of the exchange capacity and content of exchangeable cations in solonetzic soils. Soviet Soil Science 1409–1413.

Brindley G W, Brown G, 1980. Crystal structures of clay minerals and their x-ray identification. London: Mineralogical Society. (Mineralogical Society Monograph 5)

Dueck A, Börgesson L, Johannesson L-E, 2010. Stress-strain relation of bentonite at undrained shear. Laboratory tests to investigate the influence of material composition and test technique. SKB TR-10-32, Svensk Kärnbränslehantering AB.

Eriksson P, 2018. Investigation of alternatives to the buffer protection. SKB P-16-07, Svensk Kärnbränslehantering AB.

ISO 17892-1:2014. Geotechnical investigation and testing – Laboratory testing of soil – Part 1: Determination of water content. Geneva: International Organization for Standardization.

ISO 17892-1:2014. Geotechnical ISO standard for soil, Geotechnical investigation and testing – Laboratory testing of soil – Part 2: Determination of bulk density. Geneva: International Organization for Standardization.

ISO 22007-1:2009. Plastics – Determination of thermal conductivity and thermal diffusivity – Part 1: General principles. Geneva: International Organization for Standardization.

ISO 22007-2:2015. Plastics – Determination of thermal conductivity and thermal diffusivity – Part 2: Transient plane heat source (hot disc) method. Geneva: International Organization for Standardization.

Jackson M L, 1975. Soil chemical analysis: advanced course. 2nd ed. Madison, WI: University of Wisconsin.

JCGM 100:2008. GUM 1995 with minor corrections. Evaluation of measurement data – Guide to the expression of uncertainty in measurement.

Johannesson L-E, Sandén T, Dueck A, 2008. Deep repository – engineered barrier system. Wetting and homogenization in backfill materials. Laboratory tests for evaluating modeling parameters. SKB R-08-136, Svensk Kärnbränslehantering AB.

Karnland O, 2010. Chemical and mineralogical characterization of the bentonite buffer for the acceptance control procedure in a KBS-3 repository. SKB TR-10-60, Svensk Kärnbränslehantering AB.

Karnland O, Olsson S, Nilsson U, 2006. Mineralogy and sealing properties of various bentonites and smectite-rich clay materials. SKB TR-06-30, Svensk Kärnbränslehantering AB.

Magnusson B, Näykki T, Hovind H, Krysell M, 2013. Handbok för beräkning av mätosäkerhet vid miljölaboratorier. Nordtest Technical Report 537.

Meier L P, Kahr G, 1999. Determination of the cation exchange capacity (CEC) of clay minerals using the complexes of copper(II) ion with triethylenetetramine and tetraethylenepentamine. Clays and Clay Minerals 47, 386–388.

Newman A C D (ed), 1987. Chemistry of clays and clay minerals. Harlow: Longman. (Mineralogical Society Monograph 6)

Posiva SKB, 2017. Safety functions, performance targets and technical design requirements for a KBS-3V repository. Conclusions and recommendations from a joint SKB and Posiva working group. Posiva SKB Report 01, Posiva Oy, Svensk Kärnbränslehantering AB.

Sena C, Grandia F, Arcos D, Molinero J, Duro L, 2008. Complementary modelling of radionuclide retention in the near-surface system at Forsmark. Development of a reactive transport model using Forsmark 1.2 data. SKB R-08-107, Svensk Kärnbränslehantering AB.

Skauge A, Fuller N, Loren H, 1983. Specific heats of clay minerals: sodium and calcium kolinites, sodium and calcium montmorillonite, illite and attapulgite. Thermochimica Acta 61, 139–145.

Svensson D, Hansen S, 2010. Freezing and thawing of montmorillonite – a time resolved synchrotron X-ray study. Applied Clay Science 49, 127–134.

Svensson D, Dueck A, Nilsson U, Olsson S, Sandén T, Lydmark S, Jägerwall S, Pedersen K, Hansen S, 2011. Alternative buffer material. Status of the ongoing laboratory investigation of reference materials and test package 1. SKB TR-11-06, Svensk Kärnbränslehantering AB.

Svensson D, Lundgren C, Johannesson, L-E, Norrfors, K, 2017. Developing strategies for acquisition and control of bentonite for a high level radioactive waste repository. SKB TR-16-14, Svensk Kärnbränslehantering AB.

Svensson P D, 2015. The bentonite barrier: swelling properties, redox chemistry and mineral evolution. PhD thesis. Lund University.

Appendix A

Swelling pressure/hydraulic conductivity

Milos 2017

Table A-1. Results from tests made on bentonite Milos 2017 both with deionized water and 1 M $CaCl_2$.

				De-ionized water			1 M $CaCl_2$		
Test No.	ρ (kg/m³)	w (-)	ρ_d (kg/m³)	σ_s (kPa)	Gradient (m/m)	k_w (m/s)	σ_s (kPa)	Gradient (m/m)	k_w (m/s)
Milos 2017 1	1838	0.340	1372	1243	317	1.62E−10	234	317	4.19E−11
Milos 2017 2	1858	0.300	1429	2543	313	1.69E−11	1646	313	2.62E−12
Milos 2017 3	1909	0.276	1496	5727	299	1.59E−12	4121	299	6.19E−13
Milos 2017 4	1840	0.325	1389	1763	1458	1.32E−11	1081	1166	1.89E−11
Milos 2017 5	1883	0.283	1467	3954	1436	1.66E−12	2765	1149	1.74E−12
Milos 2017 6	1953	0.265	1544	6523	1460	4.57E−13	4787	1168	3.49E−13
Milos 2017 7	1880	0.280	1469	5509	6331	1.33E−12	4029	5427	1.12E−12
Milos 2017 8	1932	0.255	1540	6212	6463	4.71E−13	4672	5540	3.94E−13
Milos 2017 9	1930	0.258	1534	6641	6246	5.12E−13	5029	5353	4.53E−13

Table A-2. Results from tests made on bentonite Milos 2017 with deionized water.

Test No.	ρ (kg/m³)	w (-)	ρ_d (kg/m³)	σ_s (kPa)
Milos 2017 1 mQ	1758	0.374	1280	1044
Milos 2017 2 mQ	1859	0.339	1389	3343
Milos 2017 3 mQ	1867	0.276	1463	5470
Milos 2017 4 mQ	1839	0.354	1358	2681
Milos 2017 5 mQ	1856	0.306	1421	4667
Milos 2017 6 mQ	1867	0.285	1453	5758
Milos 2017 7 mQ	1821	0.308	1393	3252
Milos 2017 8 mQ	1822	0.289	1414	5010
Milos 2017 9 mQ	1855	0.277	1453	6992

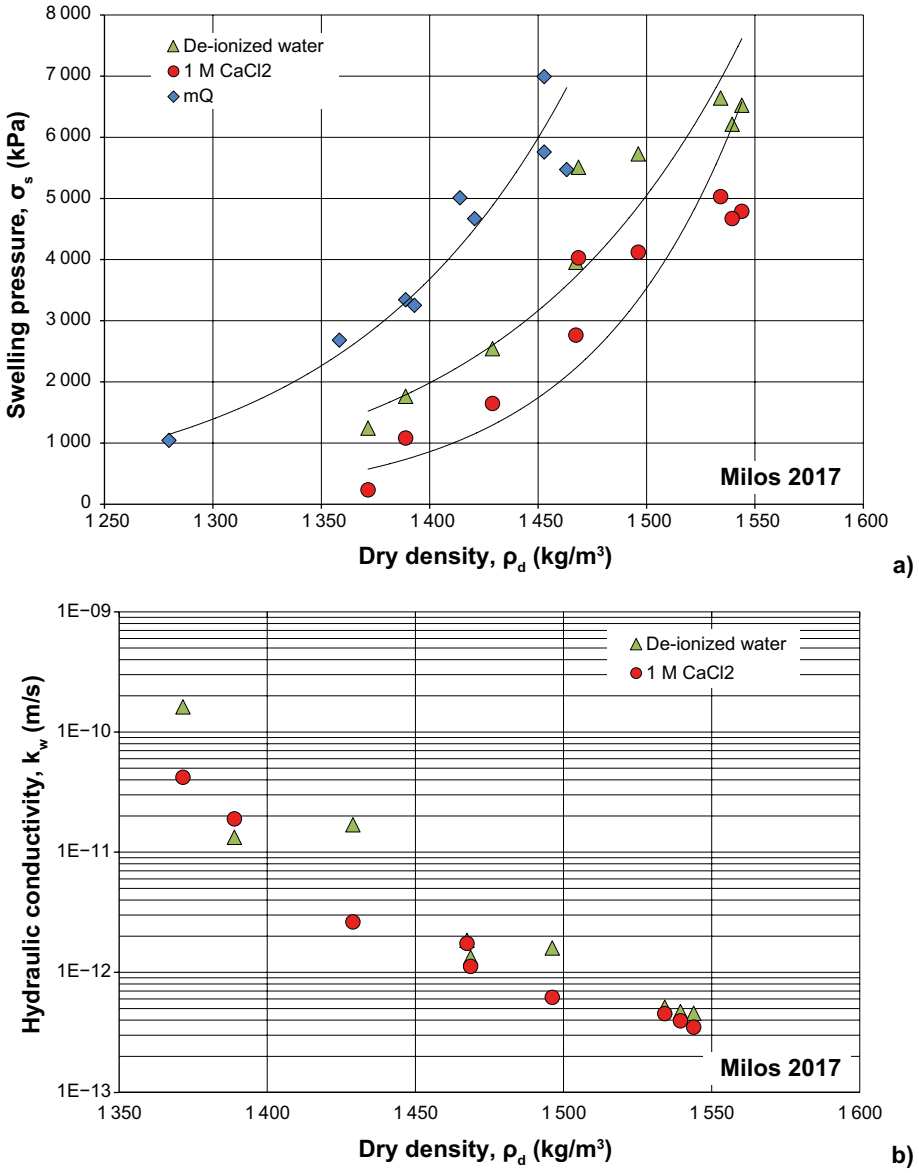

Figure A-1. Swelling pressure (a) and hydraulic conductivity (b) as function of dry density for bentonite Milos 2017.

Table A-3. Corrected densities and water content together with measured swelling pressure and hydraulic conductivity for Milos 2017. The corrected parameters are calculated with the assumption that the salinity in the interlayer water is 1 M $CaCl_2$ and ρ_s = 2 608 kg/m³.

	Corrected parameters			De-ionized water			1 M $CaCl_2$		
Test No.	ρ (kg/m³)	w (-)	ρ_d (kg/m³)	σ_s (kPa)	Gradient (m/m)	k_w (m/s)	σ_s (kPa)	Gradient (m/m)	k_w (m/s)
Milos 2017 1	1 812	0.375	1 318	1 243	317	1.62E−10	234	317	4.19E−11
Milos 2017 2	1 849	0.343	1 377	2 543	313	1.69E−11	1 646	313	2.62E−12
Milos 2017 3	1 892	0.308	1 447	5 727	299	1.59E−12	4 121	299	6.19E−13
Milos 2017 4	1 823	0.366	1 335	1 763	1 458	1.32E−11	1 081	1 166	1.89E−11
Milos 2017 5	1 873	0.322	1 417	3 954	1 436	1.66E−12	2 765	1 149	1.74E−12
Milos 2017 6	1 923	0.284	1 497	6 523	1 460	4.57E−13	4 787	1 168	3.49E−13
Milos 2017 7	1 874	0.321	1 418	5 509	6 331	1.33E−12	4 029	5 427	1.12E−12
Milos 2017 8	1 920	0.286	1 493	6 212	6 463	4.71E−13	4 672	5 540	3.94E−13
Milos 2017 9	1 916	0.289	1 486	6 641	6 246	5.12E−13	5 029	5 353	4.53E−13

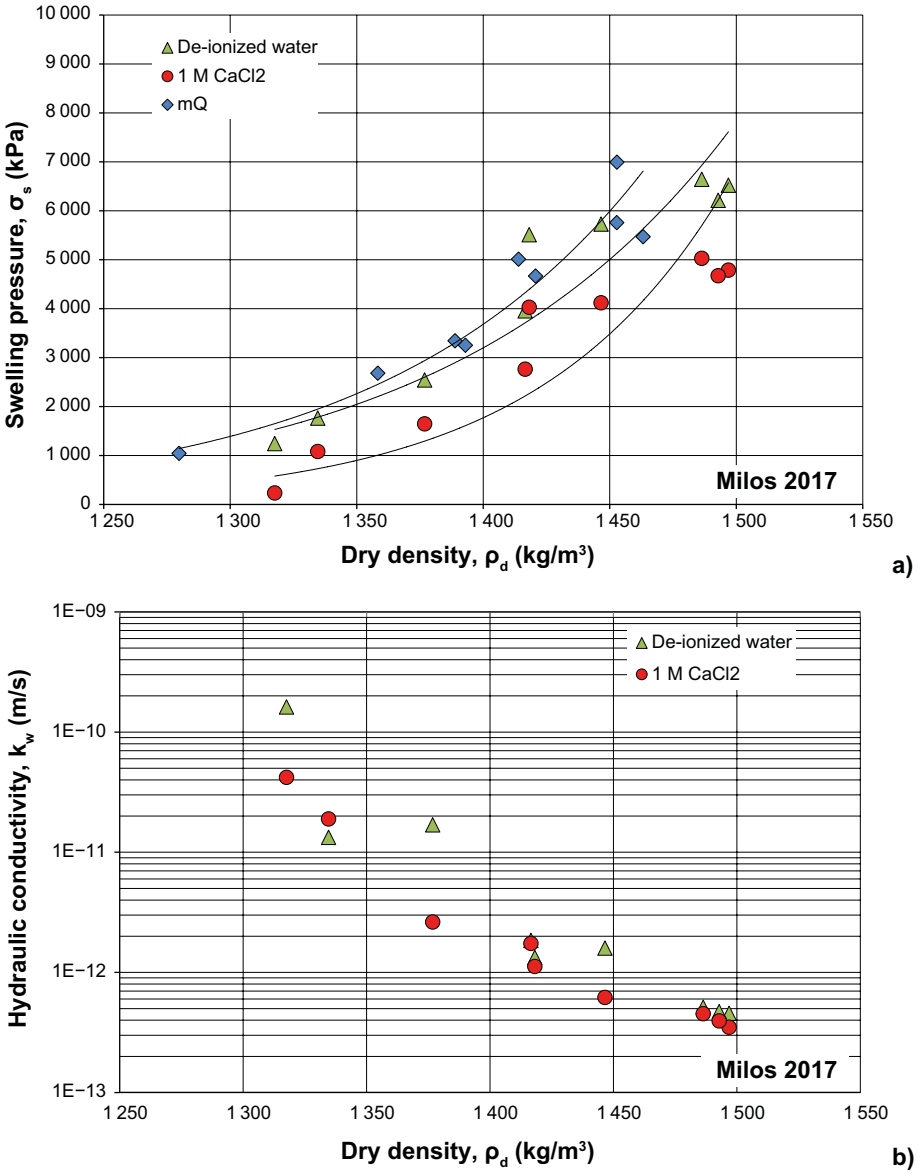

Figure A-2. *Swelling pressure (a) and hydraulic conductivity (b) as function of dry density for bentonite Milos 2017 after adjusting for excess salt in the interlayer water assumed to be 1 M $CaCl_2$.*

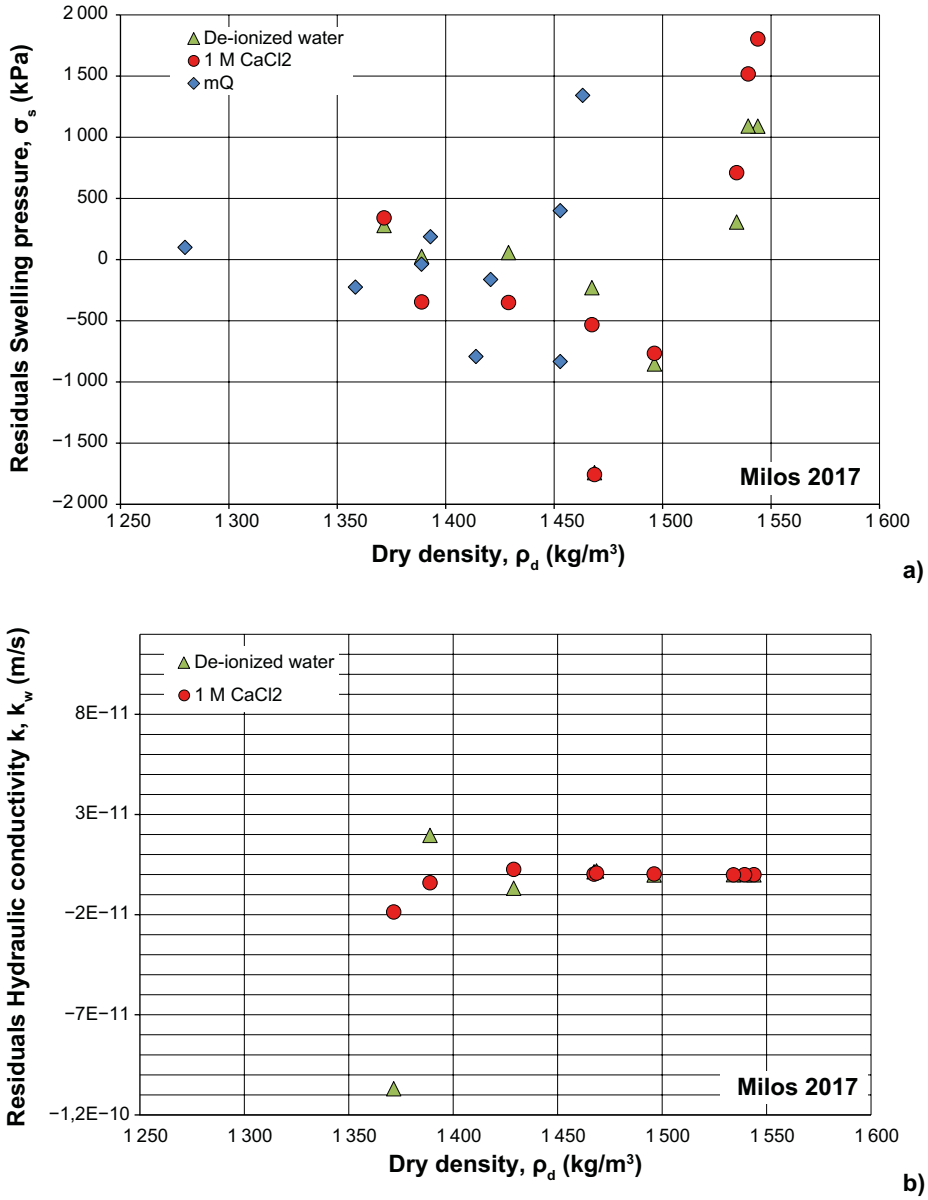

Figure A-3. The residual plot for determined swelling pressure (a) and hydraulic conductivity (b) for bentonite Milos 2017.

Table A-4. Mean and standard deviation for the residuals shown in Figure A-3.

Test series	Number of tests	Swelling pressure Average (kPa)	Swelling pressure Stdv (kPa)	Hydraulic cond. Average (m/s)	Hydraulic cond. Stdv (m/s)
Milos 2017 mQ	9	−2	652	-	-
Milos 2017 De-ionized water	9	3	892	−1.0E−11	3.6E−11
Milos 2017 1 M $CaCl_2$	9	68	1 137	−2.1E−12	6.4E−12

Appendix B

Swelling pressure/hydraulic conductivity

Morocco 2017

Table B-1. Results from tests made on bentonite Morocco 2017 both with deionized water and 1 M$CaCl_2$.

Test No.	ρ (kg/m^3)	w (-)	ρ_d (kg/m^3)	De-ionized water σ_s (kPa)	Gradient (m/m)	k_w (m/s)	1 M $CaCl_2$ σ_s (kPa)	Gradient (m/m)	k_w (m/s)
Morocco 2017 1	1895	0.332	1423	2446	5881	3.04E−13	1325	4901	3.96E−13
Morocco 2017 2	1960	0.313	1493	5659	6080	1.23E−13	3758	5066	1.05E−13
Morocco 2017 3	1982	0.287	1540	6567	6074	7.83E−14	4707	5061	7.78E−14
Morocco 2017 4	1880	0.352	1391	2287	13202	3.70E−13	1183	9430	5.63E−13
Morocco 2017 5	1997	0.260	1585	8639	14423	7.61E−14	6791	10302	5.47E−14
Morocco 2017 6	2034	0.256	1620	11238	14214	6.04E−14	9357	10153	4.45E−14
Morocco 2017 7	1895	0.334	1421	2656	9369	2.51E−13	1430	9369	3.66E−13
Morocco 2017 8	1989	0.272	1564	7755	10183	4.40E−14	6118	10183	5.94E−14
Morocco 2017 9	2000	0.245	1607	10776	10103	5.18E−14	8898	10103	4.42E−14

Table B-2. Results from tests made on bentonite Morocco 2017 with deionized water.

Test No.	ρ (kg/m^3)	w (-)	ρ_d (kg/m^3)	σ_s (kPa)
Morocco mQ 1	1796	0.373	1308	2004
Morocco mQ 2	1921	0.292	1486	6732
Morocco mQ 3	1979	0.268	1561	10898
Morocco mQ 4	1793	0.369	1310	1864
Morocco mQ 5	1908	0.310	1457	4617
Morocco mQ 6	1941	0.293	1502	6908
Marocco mQ 7	1892	0.349	1402	4302
Marocco mQ 8	1984	0.291	1537	8918
Morocco mQ 9	1994	0.259	1584	12233

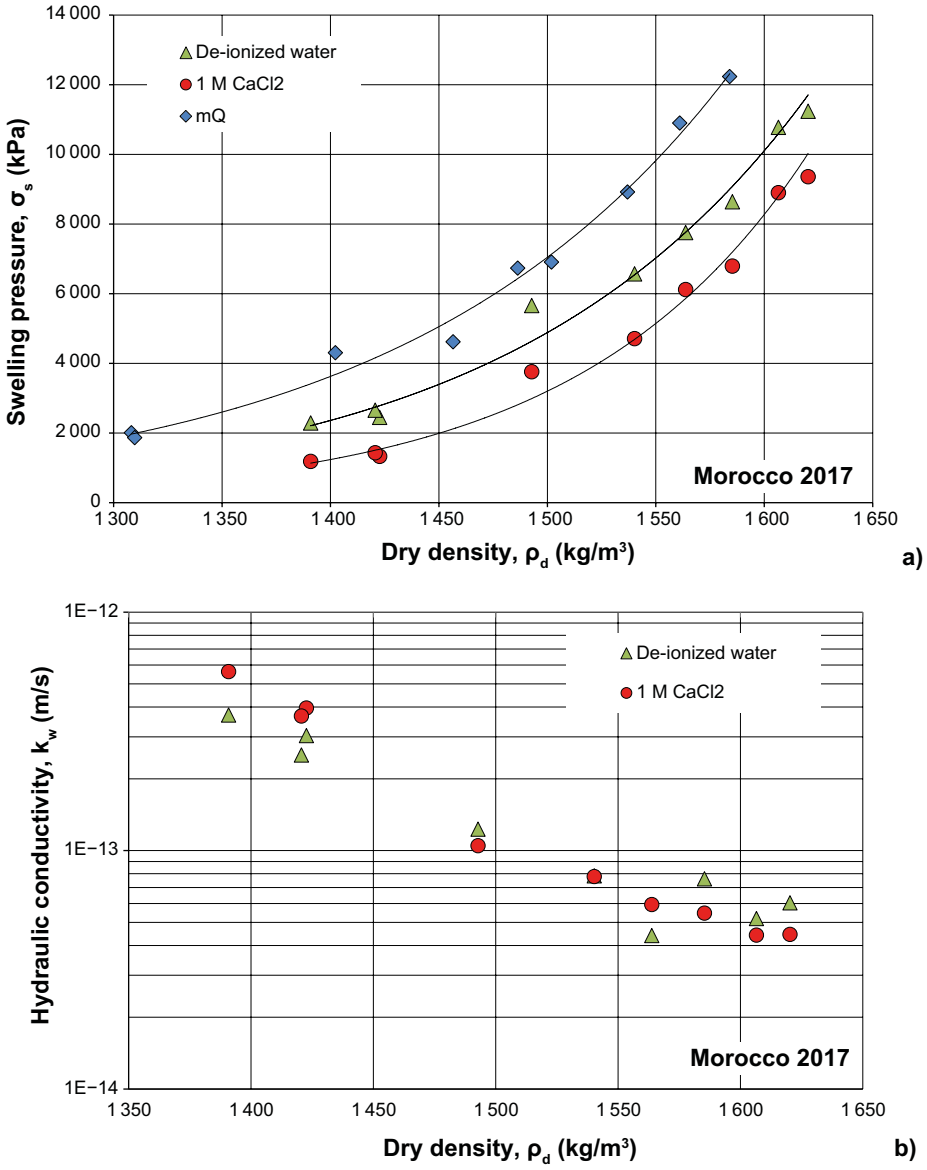

Figure B-1. Swelling pressure (a) and hydraulic conductivity (b) as function of dry density for bentonite Morocco 2017.

Table B-3. Corrected densities and water content together with measured swelling pressure and hydraulic conductivity for Morocco 2017. The corrected parameters are calculated with the assumption that the salinity in the interlayer water is 1 M $CaCl_2$ and ρ_s = 2 737 kg/m³.

	Corrected parameters			De-ionized water			1 M $CaCl_2$		
Test No.	ρ (kg/m³)	w (-)	ρ_d (kg/m³)	σ_s (kPa)	Gradient (m/m)	k_w (m/s)	σ_s (kPa)	Gradient (m/m)	k_w (m/s)
Morocco 2017 1	1 868	0.366	1 368	2 446	5 881	3.04E−13	1 325	4 901	3.96E−13
Morocco 2017 2	1 914	0.329	1 440	5 659	6 080	1.23E−13	3 758	5 066	1.05E−13
Morocco 2017 3	1 945	0.306	1 489	6 567	6 074	7.83E−14	4 707	5 061	7.78E−14
Morocco 2017 4	1 847	0.384	1 334	2 287	13 202	3.70E−13	1 183	9 430	5.63E−13
Morocco 2017 5	1 975	0.286	1 536	8 639	14 423	7.61E−14	6 791	10 302	5.47E−14
Morocco 2017 6	1 998	0.271	1 573	11 238	14 214	6.04E−14	9 357	10 153	4.45E−14
Morocco 2017 7	1 867	0.367	1 365	2 656	9 369	2.51E−13	1 430	9 369	3.66E−13
Morocco 2017 8	1 961	0.295	1 514	7 755	10 183	4.40E−14	6 118	10 183	5.94E−14
Morocco 2017 9	1 990	0.276	1 559	10 776	10 103	5.18E−14	8 898	10 103	4.42E−14

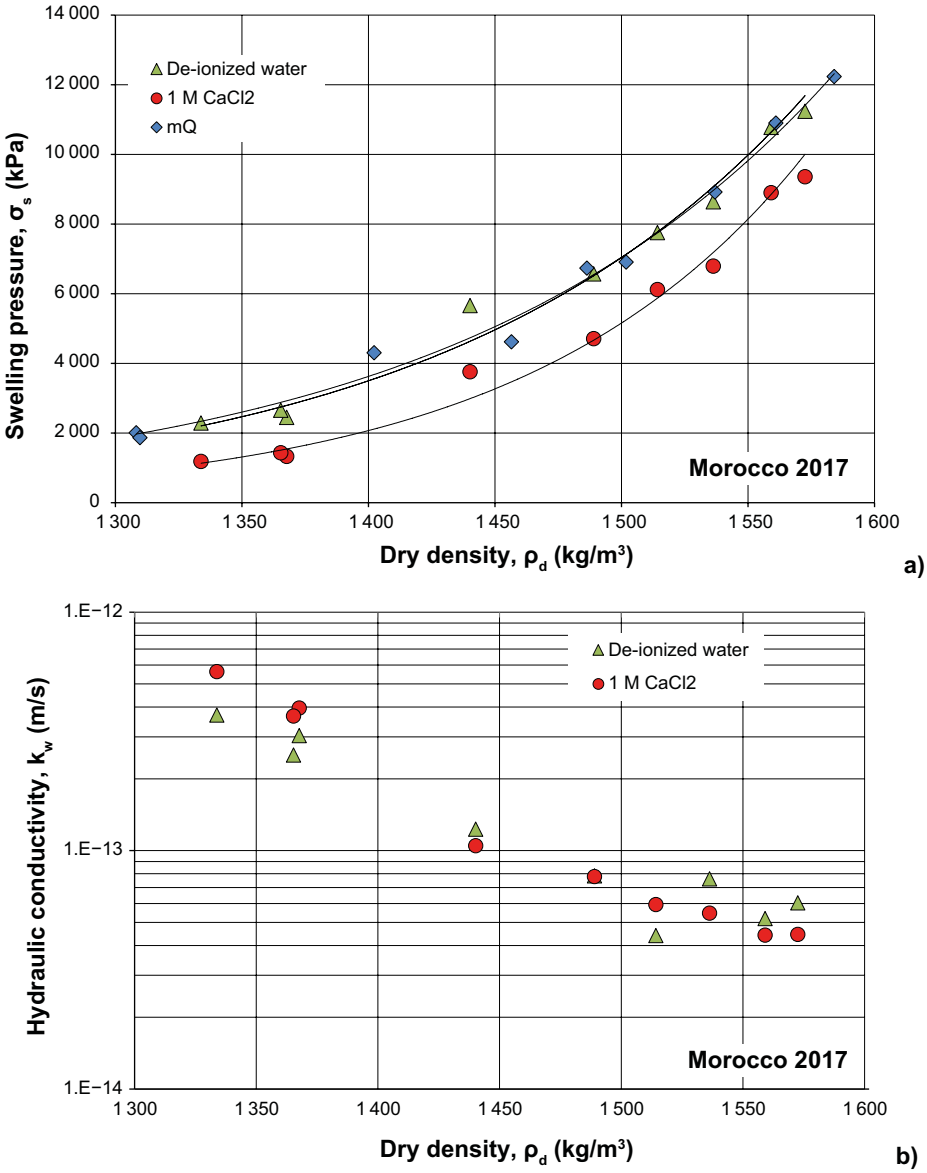

Figure B-2. *Swelling pressure (a) and hydraulic conductivity (b) as function of dry density for bentonite Morocco 2017 after adjusting for excess salt in the interlayer water assumed to be 1 M $CaCl_2$.*

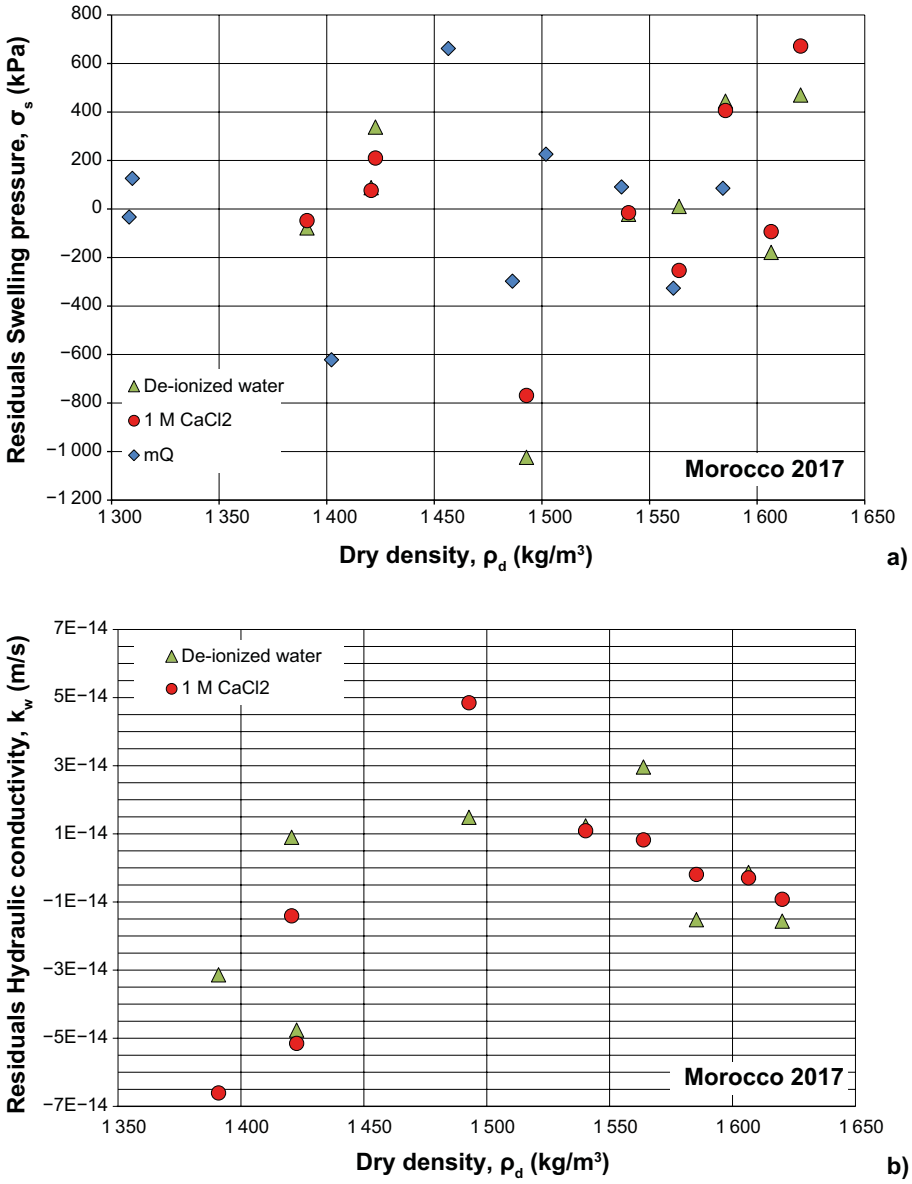

Figure B-3. *The residual plot for determined swelling pressure (a) and hydraulic conductivity (b) for bentonite Morocco 2017.*

Table B-4. Mean and standard deviation for the residuals shown in Figure B-3.

Test series	Number of tests	Swelling pressure Average (kPa)	Swelling pressure Stdv (kPa)	Hydraulic cond. Average (m/s)	Hydraulic cond. Stdv (m/s)
Morocco 2017 mQ	9	−10	371	-	-
Morocco 2017 De-ionized water	9	5	451	−5.1E−15	2.5E−14
Morocco 2017 1 M $CaCl_2$	9	21	408	−8.7E−15	3.4E−14

Appendix C

Swelling pressure/hydraulic conductivity

Bulgaria 2017

Table C-1. Results from tests made on bentonite Bulgaria 2017 both with deionized water and 1 M $CaCl_2$.

Test No.	ρ (kg/m³)	w (-)	ρ_d (kg/m³)	De-ionized water σ_s (kPa)	De-ionized water Gradient (m/m)	De-ionized water k_w (m/s)	1 M $CaCl_2$ σ_s (kPa)	1 M $CaCl_2$ Gradient (m/m)	1 M $CaCl_2$ k_w (m/s)
Bulgaria 2017 1	1881	0.359	1384	5390	10058	1.77E−13	4314	7041	1.46E−13
Bulgaria 2017 2	1920	0.327	1446	8218	10255	1.37E−13	7265	7179	1.05E−13
Bulgaria 2017 3	1944	0.325	1466	10552	10023	1.30E−13	9310	7016	8.81E−14
Bulgaria 2017 4	1906	0.342	1419	7328	15352	1.27E−13	6309	10235	1.02E−13
Bulgaria 2017 5	1935	0.328	1457	9553	15298	1.11E−13	8768	10199	1.03E−13
Bulgaria 2017 6	1945	0.319	1475	11724	14521	1.04E−13	10886	9681	9.52E−14
Bulgaria 2017 7	1824	0.437	1269	2121	5889	4.41E−13	1394	4908	4.52E−13
Bulgaria 2017 8	1868	0.365	1369	5250	6257	1.71E−13	4172	5214	1.54E−13
Bulgaria 2017 9	1881	0.379	1364	5437	6104	1.81E−13	4014	5087	1.86E−13
Bulgaria 2017 10	1876	0.378	1361	5497	23455	1.89E−13	4336	13135	1.87E−13
Bulgaria 2017 11	1913	0.335	1433	8689	24802	1.34E−13	7371	13889	1.27E−13
Bulgaria 2017 12	1914	0.332	1438	9361	24363	1.22E−13	7824	13644	1.17E−13
Bulgaria 2017 13	1893	0.359	1393	6665	24492	1.53E−13	5524	15675	1.36E−13
Bulgaria 2017 14	1932	0.314	1471	11000	24144	1.06E−13	9835	15452	8.57E−14
Bulgaria 2017 15	1960	0.283	1528	16443	23684	8.77E−14	15694	15158	6.44E−14

Table C-2. Results from tests made on bentonite Bulgaria 2017 with deionized water.

Test No.	ρ (kg/m³)	w (-)	ρ_d (kg/m³)	σ_s (kPa)
Bulgaria 2017 mQ 1	1784	0.453	1228	2592
Bulgaria 2017 mQ 2	1824	0.408	1295	4704
Bulgaria 2017 mQ 3	1878	0.342	1399	10490
Bulgaria 2017 mQ 4	1816	0.430	1270	3680
Bulgaria 2017 mQ 5	1840	0.380	1333	7200
Bulgaria 2017 mQ 6	1919	0.336	1436	14130
Bulgaria 2017 mQ 7	1845	0.394	1323	5690
Bulgaria 2017 mQ 8	1876	0.365	1375	8106
Bulgaria 2017 mQ 9	1887	0.346	1402	9224

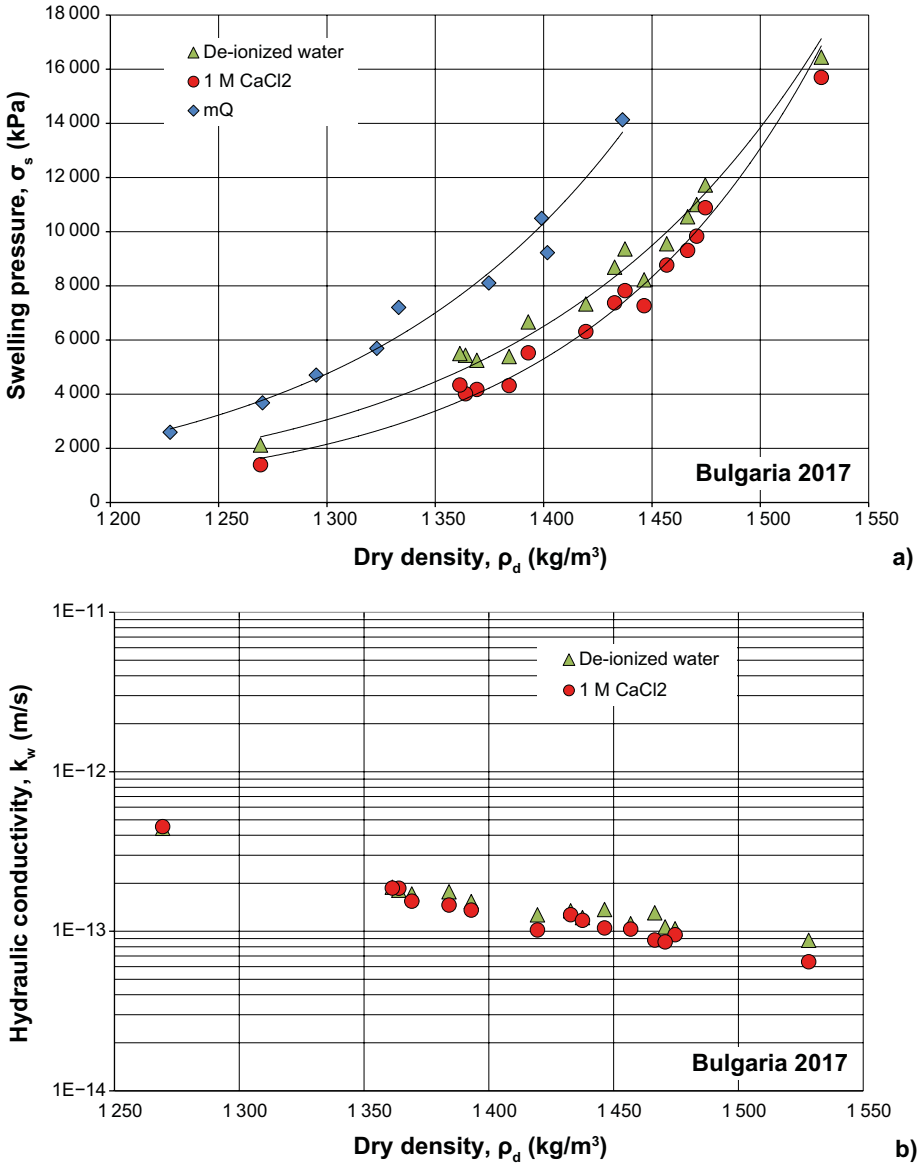

Figure C-1. *Swelling pressure (a) and hydraulic conductivity (b) as function of dry density for bentonite Bulgaria 2017.*

Table C-3. Corrected densities and water content together with measured swelling pressure and hydraulic conductivity for Bulgaria 2017. The corrected parameters are calculated with the assumption that the salinity in the interlayer water is 1 M $CaCl_2$ and ρ_s = 2 757 kg/m^3.

	Corrected parameters			De-ionized water			1 M $CaCl_2$		
Test No.	ρ (kg/m^3)	w (-)	ρ_d (kg/m^3)	σ_s (kPa)	Gradient (m/m)	k_w (m/s)	σ_s (kPa)	Gradient (m/m)	k_w (m/s)
Bulgaria 2017 1	1 845	0.391	1 326	5 390	10 058	1.77E−13	4 314	7 041	1.46E−13
Bulgaria 2017 2	1 887	0.356	1 391	8 218	10 255	1.37E−13	7 265	7 179	1.05E−13
Bulgaria 2017 3	1 900	0.345	1 412	10 552	10 023	1.30E−13	9 310	7 016	8.81E−14
Bulgaria 2017 4	1 869	0.371	1 363	7 328	15 352	1.27E−13	6 309	10 235	1.02E−13
Bulgaria 2017 5	1 894	0.350	1 403	9 553	15 298	1.11E−13	8 768	10 199	1.03E−13
Bulgaria 2017 6	1 906	0.341	1 422	11 724	14 521	1.04E−13	10 886	9 681	9.52E−14
Bulgaria 2017 7	1 769	0.466	1 207	2 121	5 889	4.41E−13	1 394	4 908	4.52E−13
Bulgaria 2017 8	1 836	0.400	1 311	5 250	6 257	1.71E−13	4 172	5 214	1.54E−13
Bulgaria 2017 9	1 832	0.403	1 306	5 437	6 104	1.81E−13	4 014	5 087	1.86E−13
Bulgaria 2017 10	1 830	0.405	1 302	5 497	23 455	1.89E−13	4 336	13 135	1.87E−13
Bulgaria 2017 11	1 878	0.363	1 378	8 689	24 802	1.34E−13	7 371	13 889	1.27E−13
Bulgaria 2017 12	1 881	0.361	1 382	9 361	24 363	1.22E−13	7 824	13 644	1.17E−13
Bulgaria 2017 13	1 851	0.386	1 335	6 665	24 492	1.53E−13	5 524	15 675	1.36E−13
Bulgaria 2017 14	1 903	0.343	1 417	11 000	24 144	1.06E−13	9 835	15 452	8.57E−14
Bulgaria 2017 15	1 941	0.315	1 477	16 443	23 684	8.77E−14	15 694	15 158	6.44E−14

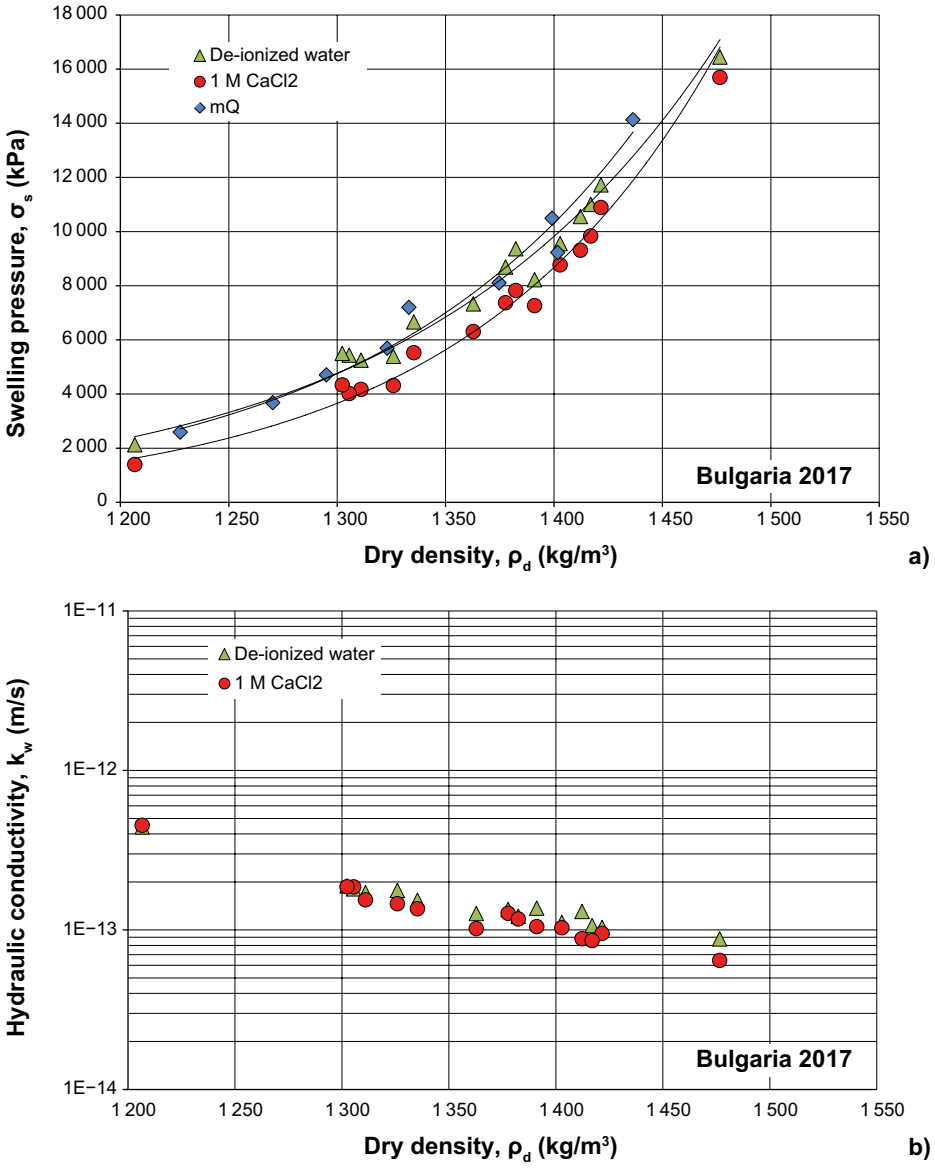

Figure C-2. *Swelling pressure (a) and hydraulic conductivity (b) as function of dry density for bentonite Bulgaria 2017 after adjusting for excess salt in the interlayer water assumed to be 1 M $CaCl_2$.*

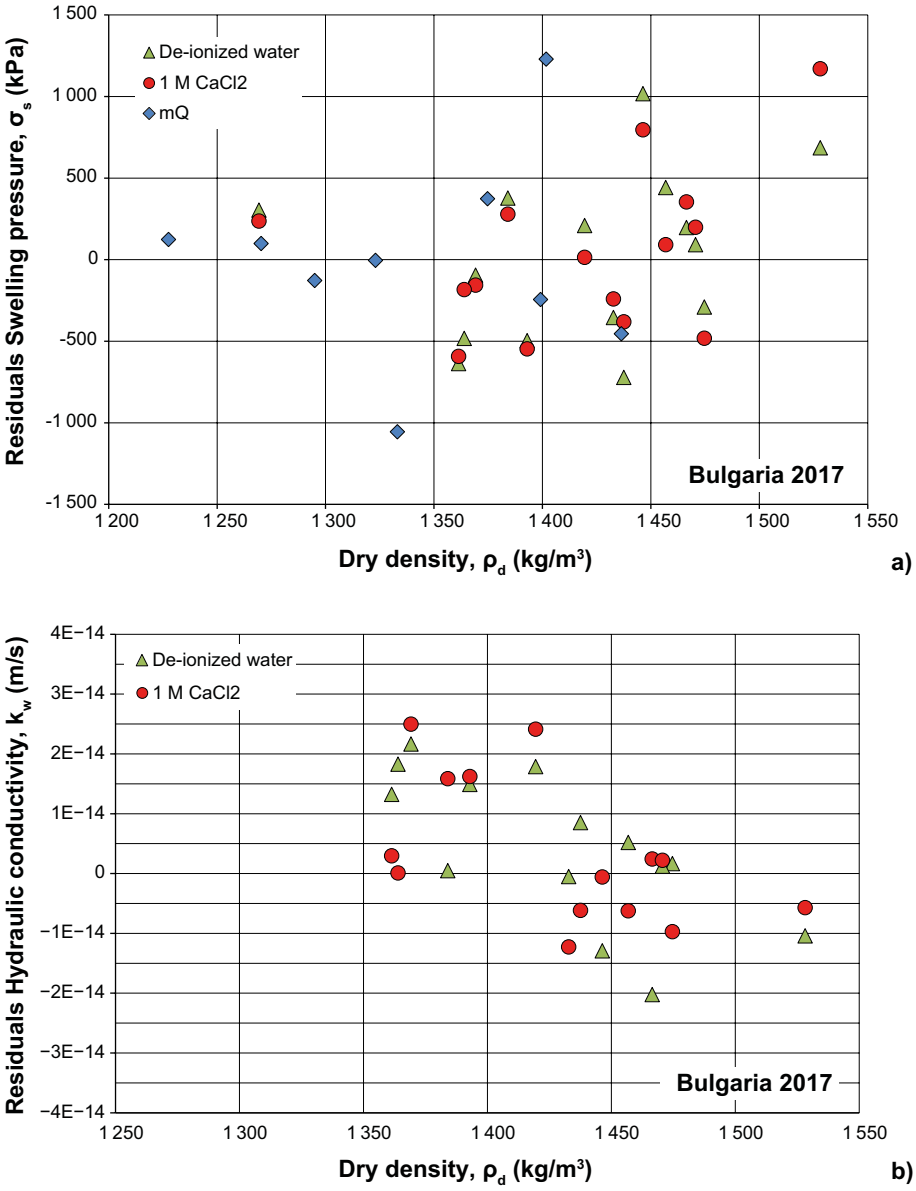

Figure C-3. The residual plot for determined swelling pressure (a) and hydraulic conductivity (b) for bentonite Bulgaria 2017.

Table C-4. Mean and standard deviation for the residuals shown in Figure C-3.

Test series	Number of tests	Swelling pressure Average (kPa)	Swelling pressure Stdv (kPa)	Hydraulic cond. Average (m/s)	Hydraulic cond. Stdv (m/s)
Bulgaria 2017 mQ	9	−7	620	-	-
Bulgaria 2017 De-ionized water	9	16	510	−2.6E−15	2.9E−14
Bulgaria 2017 1 M $CaCl_2$	9	36	495	−2.8E−15	2.7E−14

Appendix D

Swelling pressure/hydraulic conductivity

Turkey 2017

Table D-1. Results from tests made on bentonite from Turkey 2017 both with deionized water and 1 M $CaCl_2$.

Test No.	ρ (kg/m³)	w (-)	ρ_d (kg/m³)	De-ionized water σ_s (kPa)	Gradient (m/m)	k_w (m/s)	1 M $CaCl_2$ σ_s (kPa)	Gradient (m/m)	k_w (m/s)
Turkey 2017 1	1882	0.340	1405	2072	6770	2.71E−13	797	3869	3.69E−13
Turkey 2017 2	1927	0.295	1488	3553	6968	2.05E−13	1796	3982	1.66E−13
Turkey 2017 3	1946	0.274	1527	4748	7168	1.35E−13	2705	4096	1.27E−13
Turkey 2017 4	1928	0.315	1466	3308	10834	1.69E−13	1701	7879	2.03E−13
Turkey 2017 5	1992	0.252	1591	8253	11141	8.78E−14	6428	8102	7.76E−14
Turkey 2017 6	2019	0.257	1606	9480	10892	5.70E−14	7917	7921	6.28E−14
Turkey 2017 7	1971	0.268	1555	6125	16132	8.99E−14	4199	10083	9.66E−14
Turkey 2017 8	1999	0.277	1565	7643	2020	-	5109	10098	9.06E−14
Turkey 2017 9	1996	0.245	1604	9564	16584	8.17E−14	7540	10365	6.63E−14

Table D-2. Results from tests made on bentonite from Turkey 2017 with deionized water.

Test No.	ρ (kg/m³)	w (-)	ρ_d (kg/m³)	σ_s (kPa)
Turkey 2017 mQ 1	1859	0.345	1382	2714
Turkey 2017 mQ 2	1961	0.286	1525	6772
Turkey 2017 mQ 3	1984	0.302	1524	7255
Turkey 2017 mQ 4	1882	0.340	1404	2933
Turkey 2017 mQ 5	1938	0.331	1456	4330
Turkey 2017 mQ 6	1957	0.281	1528	5896
Turkey 2017 mQ 7	1957	0.299	1507	5759
Turkey 2017 mQ 8	1938	0.267	1529	6910
Turkey 2017 mQ 9	1983	0.269	1562	8566

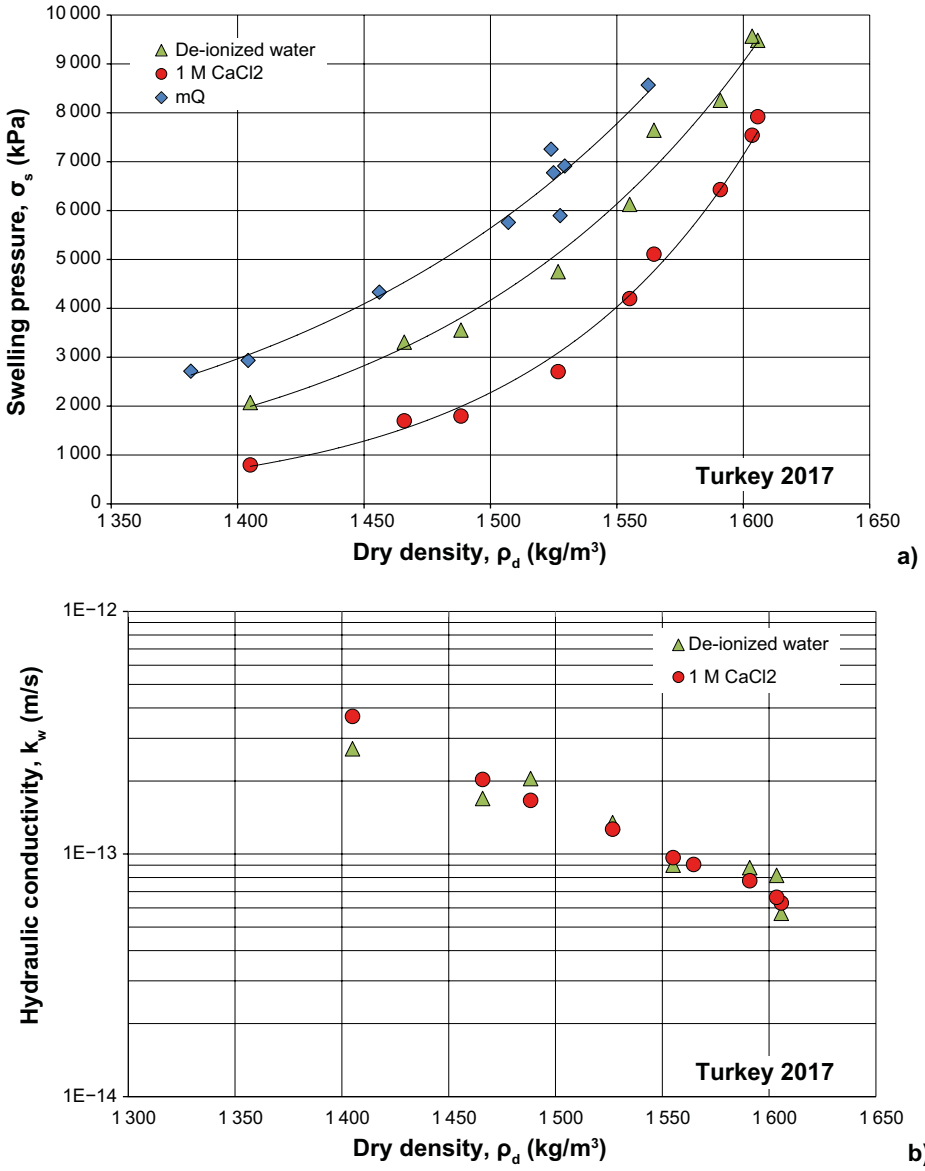

Figure D-1. *Swelling pressure (a) and hydraulic conductivity (b) as function of dry density for bentonite from Turkey 2017.*

Table D-3. Corrected densities and water content together with measured swelling pressure and hydraulic conductivity for Turkey 2017. The corrected parameters are calculated with the assumption that the salinity in the interlayer water is 0.8 M $CaCl_2$ and ρ_s = 2 648 kg/m³.

	Corrected parameters			De-ionized water			1 M $CaCl_2$		
Test No.	ρ (kg/m³)	w (-)	ρ_d (kg/m³)	σ_s (kPa)	Gradient (m/m)	k_w (m/s)	σ_s (kPa)	Gradient (m/m)	k_w (m/s)
Turkey 2017 1	1 848	0.357	1 362	2 072	6 770	2.71E−13	797	3 869	3.69E−13
Turkey 2017 2	1 901	0.313	1 448	3 553	6 968	2.05E−13	1 796	3 982	1.66E−13
Turkey 2017 3	1 926	0.294	1 488	4 748	7 168	1.35E−13	2 705	4 096	1.27E−13
Turkey 2017 4	1 887	0.324	1 425	3 308	10 834	1.69E−13	1 701	7 879	2.03E−13
Turkey 2017 5	1 968	0.266	1 555	8 253	11 141	8.78E−14	6 428	8 102	7.76E−14
Turkey 2017 6	1 977	0.259	1 570	9 480	10 892	5.70E−14	7 917	7 921	6.28E−14
Turkey 2017 7	1 944	0.282	1 517	6 125	16 132	8.99E−14	4 199	10 083	9.66E−14
Turkey 2017 8	1 951	0.277	1 527	7 643	2 020	-	5 109	10 098	9.06E−14
Turkey 2017 9	1 976	0.260	1 568	9 564	16 584	8.17E−14	7 540	10 365	6.63E−14

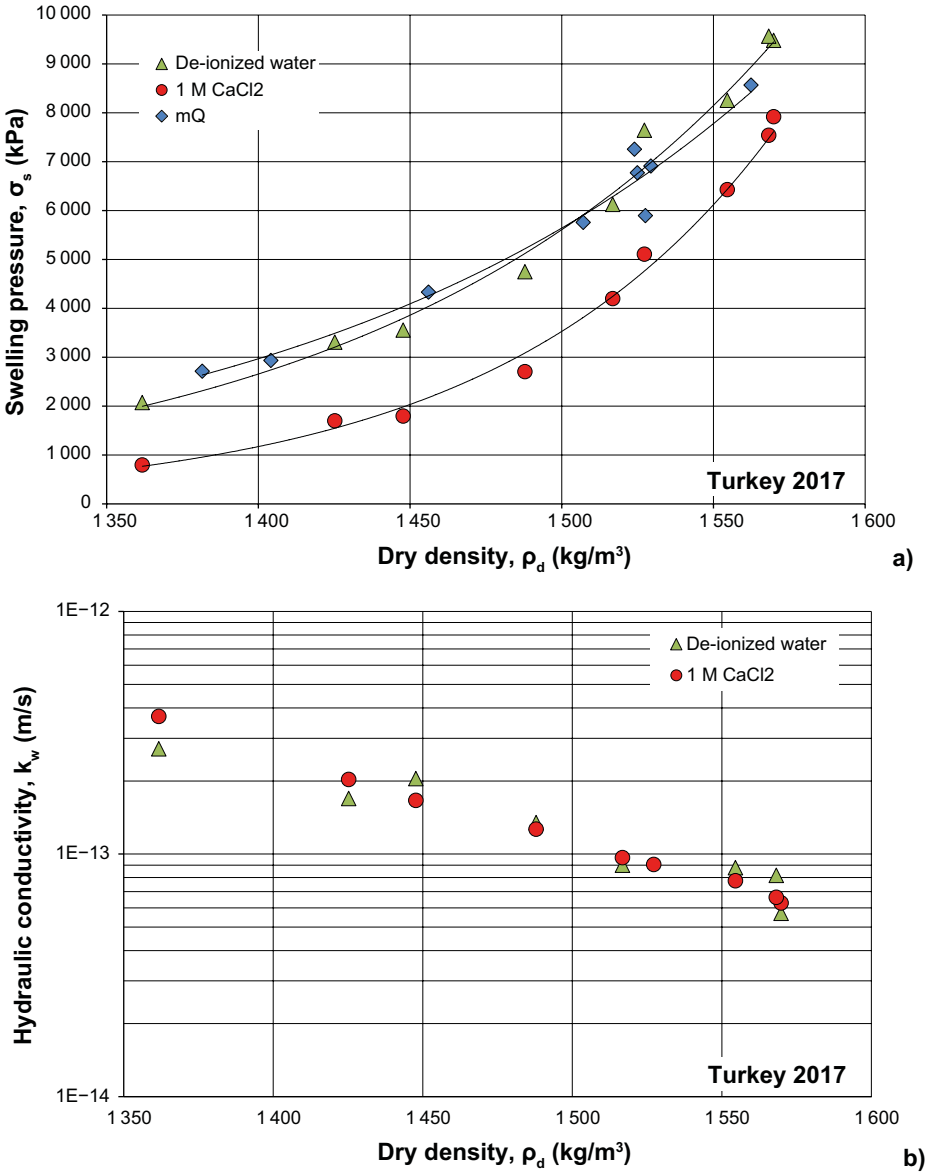

Figure D-2. *Swelling pressure (a) and hydraulic conductivity (b) as function of dry density for bentonite from Turkey 2017 after adjusting for excess salt in the interlayer water assumed to be 0.8 M $CaCl_2$.*

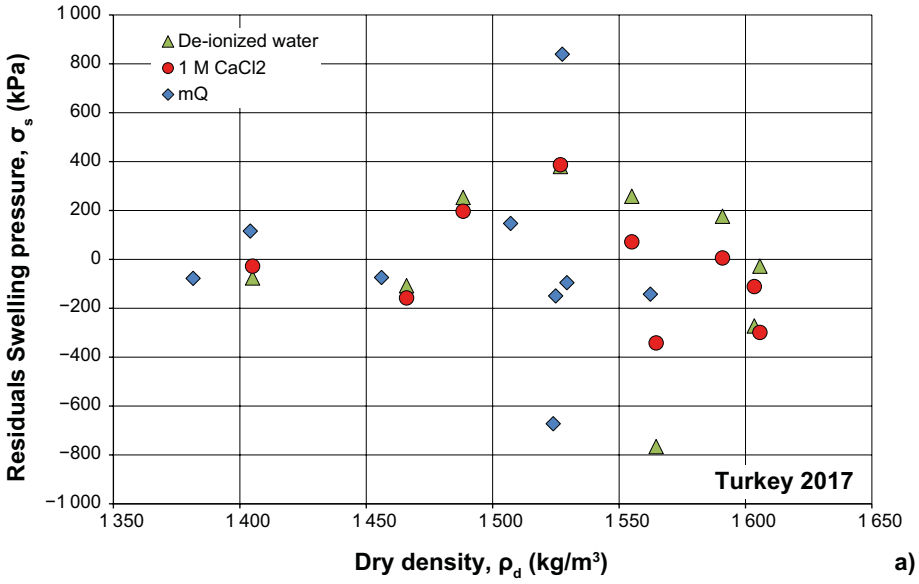

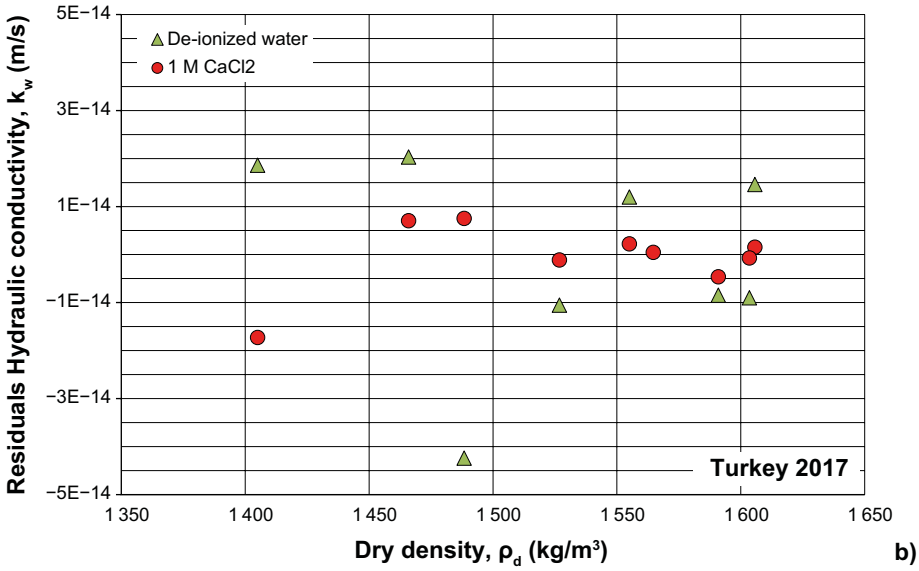

Figure D-3. *The residual plot for determined swelling pressure (a) and hydraulic conductivity (b) for bentonite from Turkey 2017.*

Table D-4. Mean and standard deviation for the residuals shown in Figure D-3.

Test series	Number of tests	Swelling pressure Average (kPa)	Swelling pressure Stdv (kPa)	Hydraulic cond. Average (m/s)	Hydraulic cond. Stdv (m/s)
Turkey 2017 mQ	9	−12	396	-	-
Turkey 2017 De-ionized water	9	−20	350	−5.2E−16	2.1E−14
Turkey 2017 1 M $CaCl_2$	9	−31	232	−5.7E−16	7.4E−15

Appendix E

Swelling pressure/hydraulic conductivity

India 2018

Table E-1. Results from tests made on bentonite India 2018 both with deionized water and 1 M $CaCl_2$.

Test No.	ρ (kg/m³)	w (-)	ρ_d (kg/m³)	De-ionized water σ_s (kPa)	Gradient (m/m)	k_w (m/s)	1 M $CaCl_2$ σ_s (kPa)	Gradient (m/m)	k_w (m/s)
India 2018 1	1956	0.345	1455	3046	9892	3.78E−13	2192	4946	3.36E−13
India 2018 2	1985	0.302	1525	5564	9892	2.23E−13	4674	4908	2.05E−13
India 2018 3	2023	0.291	1567	8231	9892	1.84E−13	7617	4901	1.41E−13
India 2018 4	1933	0.322	1462	3890	13438	3.57E−13	3107	9599	3.43E−13
India 2018 5	2000	0.283	1560	8129	13957	2.10E−13	7210	9969	1.43E−13
India 2018 6	2060	0.279	1611	12748	13742	1.38E−13	12431	9816	9.63E−14
India 2018 7	1968	0.320	1490	4280	9816	3.01E−13	3380	7853	2.93E−13
India 2018 8	2003	0.313	1526	5518	9806	2.56E−13	4734	7845	1.65E−13
India 2018 9	2042	0.281	1594	9210	10204	1.59E−13	8633	8163	9.90E−14

Table E-2. Results from tests made on bentonite India 2018 with deionized water.

Test No.	ρ (kg/m³)	w (-)	ρ_d (kg/m³)	σ_s (kPa)
India 2018 1 mQ	1897	0.401	1354	2283
India 2018 2 mQ	1962	0.339	1465	5474
India 2018 3 mQ	2015	0.314	1533	8173
India 2018 4 mQ	1927	0.344	1434	4490
India 2018 5 mQ	1987	0.329	1496	8003
India 2018 6 mQ	2020	0.301	1554	11498
India 2018 7 mQ	1944	0.360	1429	4579
India 2018 8 mQ	2045	0.323	1545	8846
India 2018 9 mQ	2024	0.283	1577	12528

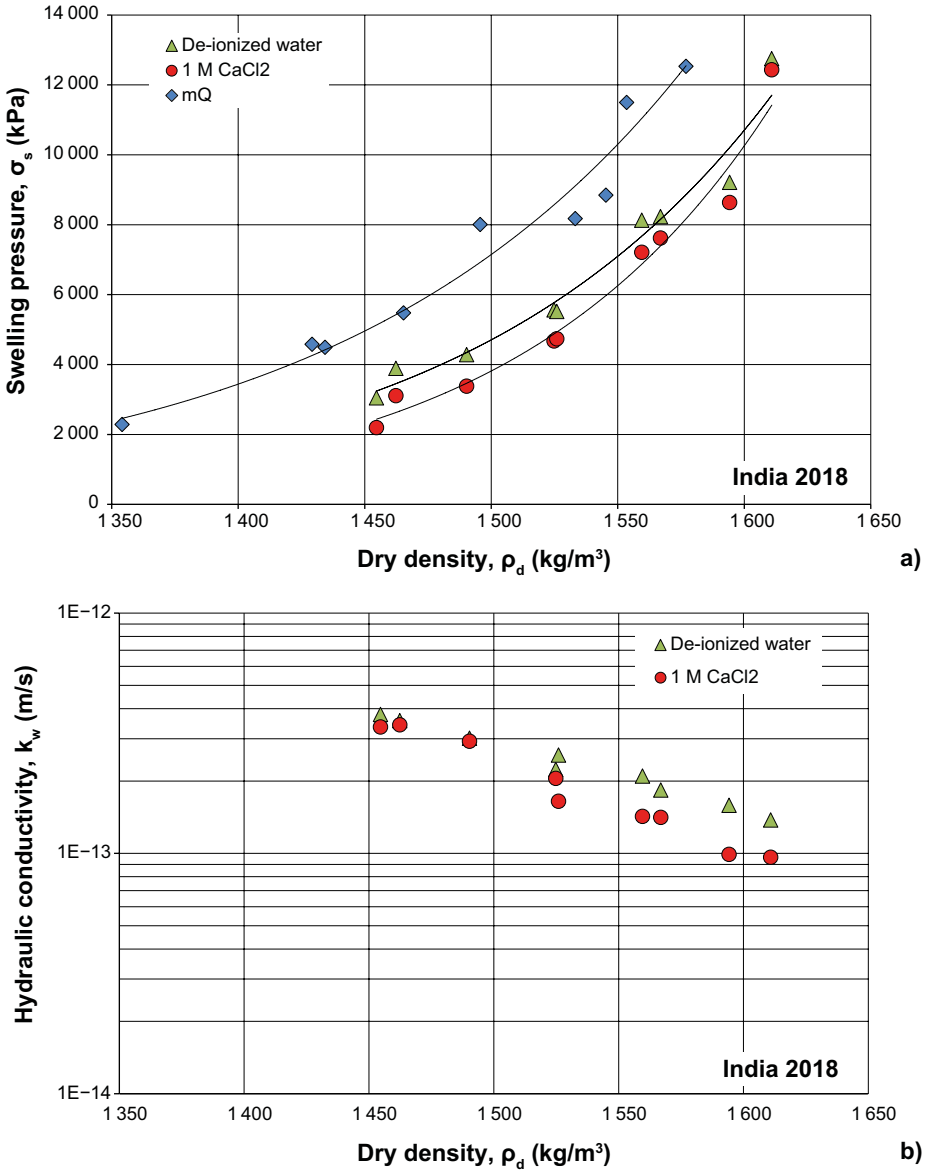

Figure E-1. Swelling pressure (a) and hydraulic conductivity (b) as function of dry density for bentonite India 2018.

Table E-3. Corrected densities and water content together with measured swelling pressure and hydraulic conductivity for India 2018. The corrected parameters are calculated with the assumption that the salinity in the interlayer water is 1 M $CaCl_2$ and ρ_s = 2 931 kg/m³.

	Corrected parameters			De-ionized water			1 M $CaCl_2$		
Test No.	ρ (kg/m³)	w (-)	ρ_d (kg/m³)	σ_s (kPa)	Gradient (m/m)	k_w (m/s)	σ_s (kPa)	Gradient (m/m)	k_w (m/s)
India 2018 1	1 920	0.375	1 396	3 046	9 892	3.78E−13	2 192	4 946	3.36E−13
India 2018 2	1 968	0.339	1 469	5 564	9 892	2.23E−13	4 674	4 908	2.05E−13
India 2018 3	1 997	0.320	1 513	8 231	9 892	1.84E−13	7 617	4 901	1.41E−13
India 2018 4	1 925	0.371	1 404	3 890	13 438	3.57E−13	3 107	9 599	3.43E−13
India 2018 5	1 992	0.323	1 506	8 129	13 957	2.10E−13	7 210	9 969	1.43E−13
India 2018 6	2 027	0.300	1 559	12 748	13 742	1.38E−13	12 431	9 816	9.63E−14
India 2018 7	1 944	0.357	1 433	4 280	9 816	3.01E−13	3 380	7 853	2.93E−13
India 2018 8	1 969	0.339	1 471	5 518	9 806	2.56E−13	4 734	7 845	1.65E−13
India 2018 9	2 016	0.308	1 541	9 210	10 204	1.59E−13	8 633	8 163	9.90E−14

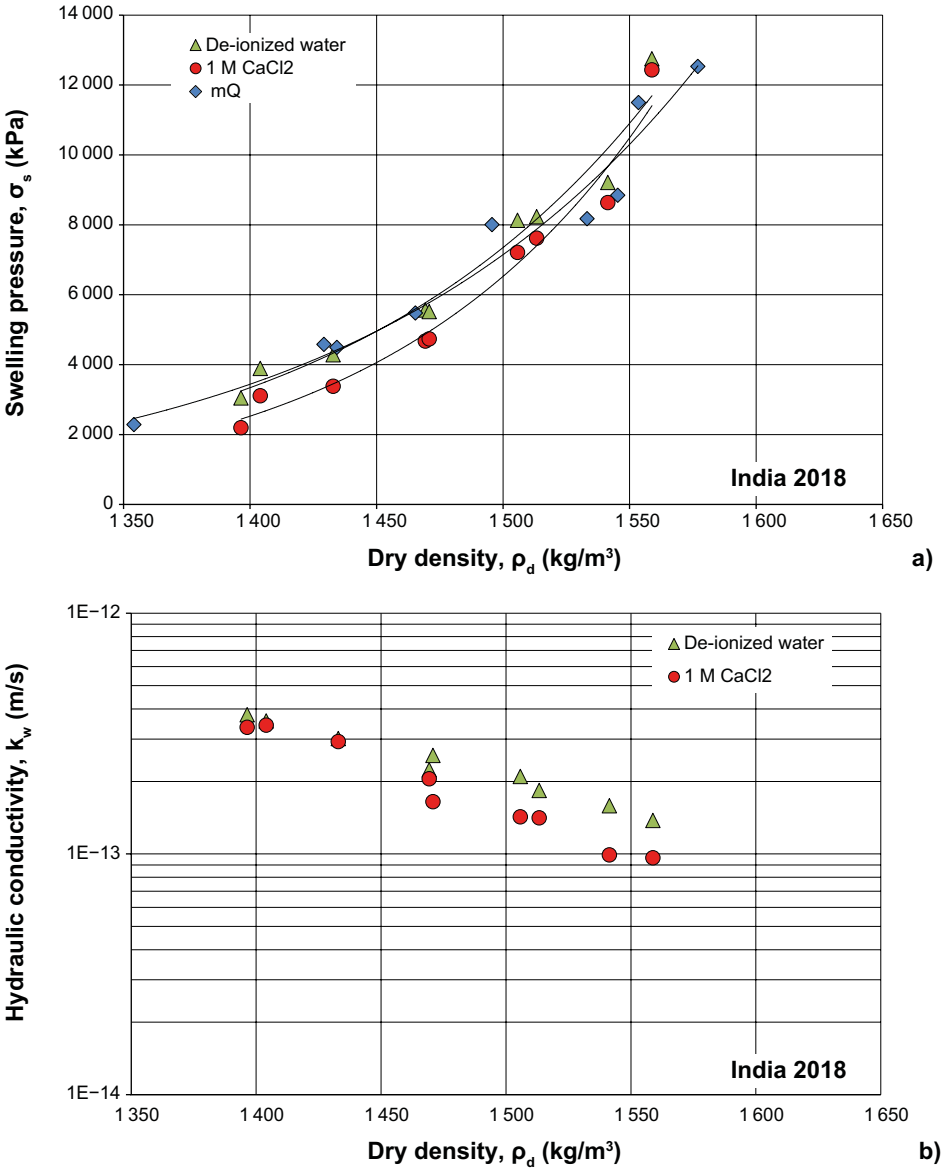

Figure E-2. *Swelling pressure (a) and hydraulic conductivity (b) as function of dry density for bentonite India 2018 after adjusting for excess salt in the interlayer water assumed to be 1 M $CaCl_2$.*

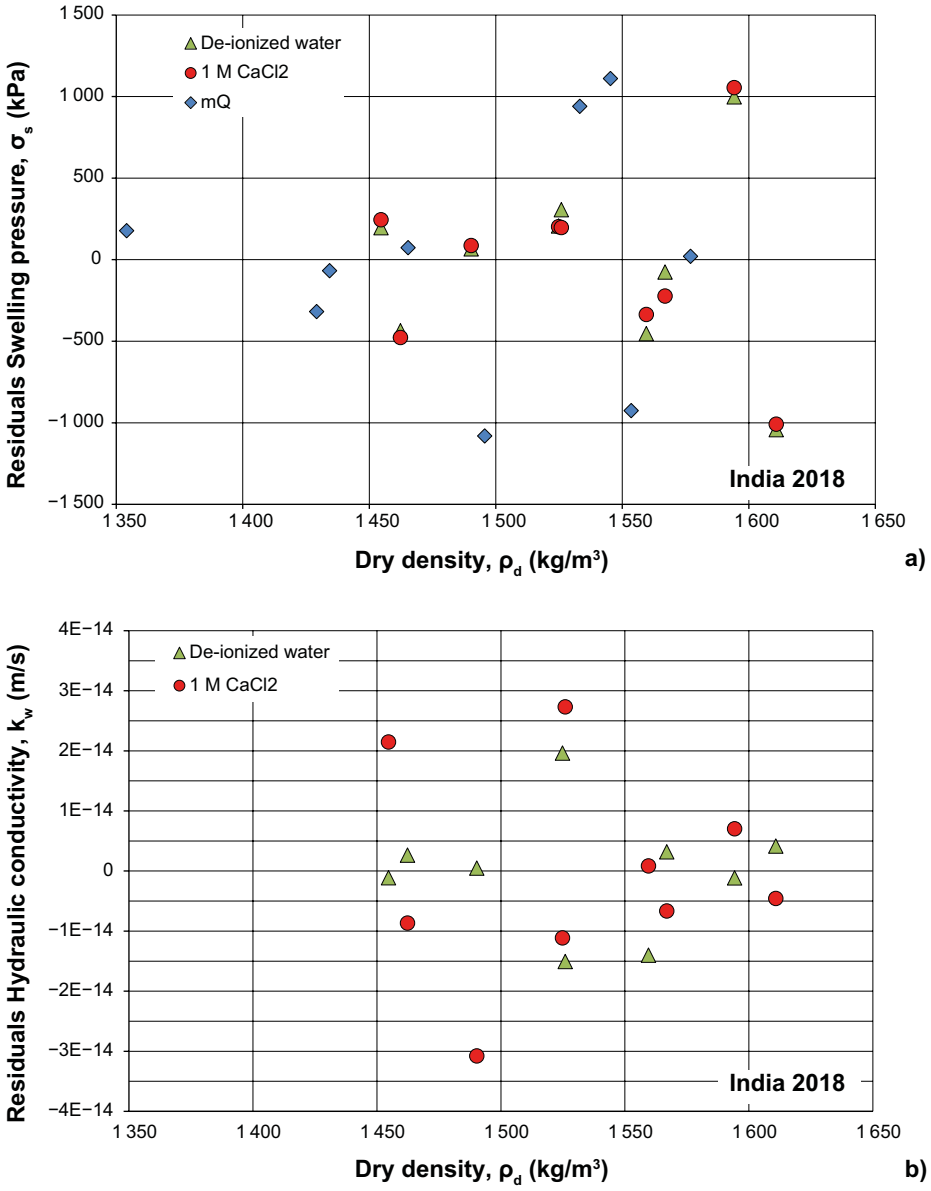

Figure E-3. *The residual plot for determined swelling pressure (a) and hydraulic conductivity (b) for bentonite India 2018.*

Table E-4. Mean and standard deviation for the residuals shown in Figure E-3.

Test series	Number of tests	Swelling pressure Average (kPa)	Stdv (kPa)	Hydraulic cond. Average (m/s)	Stdv (m/s)
India 2018 mQ	9	−7	732	-	-
India 2018 De-ionized water	9	−26	576	1.4E−16	1.0E−14
India 2018 1 M $CaCl_2$	9	−29	577	−5.8E−16	1.8E−14

Appendix F

Swelling pressure/hydraulic conductivity

PM BARA-KADE 2017

Table F-1. Results from tests made on bentonite BARA-KADE 2017 both with deionized water and 1 M $CaCl_2$.

Test No.	ρ (kg/m³)	w (-)	ρ_d (kg/m³)	De-ionized water σ_s (kPa)	Gradient (m/m)	k_w (m/s)	1 M $CaCl_2$ σ_s (kPa)	Gradient (m/m)	k_w (m/s)
BARA-KADE 2017 1	1832	0.367	1340	1518	9271	2.78E−13	514	4172	6.48E−13
BARA-KADE 2017 2	1885	0.348	1398	2232	9487	1.90E−13	921	4269	1.54E−13
BARA-KADE 2017 3	1968	0.301	1513	5118	9926	1.00E−13	2879	9926	6.43E−14
BARA-KADE 2017 4	1909	0.338	1427	2767	17061	1.14E−13	1240	8530	1.74E−13
BARA-KADE 2017 5	1993	0.266	1574	7085	17971	5.11E−14	5004	8986	4.15E−14
BARA-KADE 2017 6	2008	0.260	1594	8333	17814	4.34E−14	6028	8907	4.30E−14

Table F-2. Results from tests made on bentonite BARA-KADE 2017 with deionized water.

Test No.	ρ (kg/m³)	w (-)	ρ_d (kg/m³)	σ_s (kPa)
BARA-KADE 2017 1 mQ	1907	0.326	1439	3740
BARA-KADE 2017 2 mQ	1937	0.304	1485	5603
BARA-KADE 2017 3 mQ	1980	0.293	1531	6798
BARA-KADE 2017 4 mQ	1857	0.364	1361	2274
BARA-KADE 2017 5 mQ	1913	0.333	1436	3719
BARA-KADE 2017 6 mQ	1981	0.298	1526	6256
BARA-KADE 2017 7 mQ	1913	0.318	1451	4548
BARA-KADE 2017 8 mQ	1944	0.293	1504	6248
BARA-KADE 2017 9 mQ	2005	0.274	1574	9415

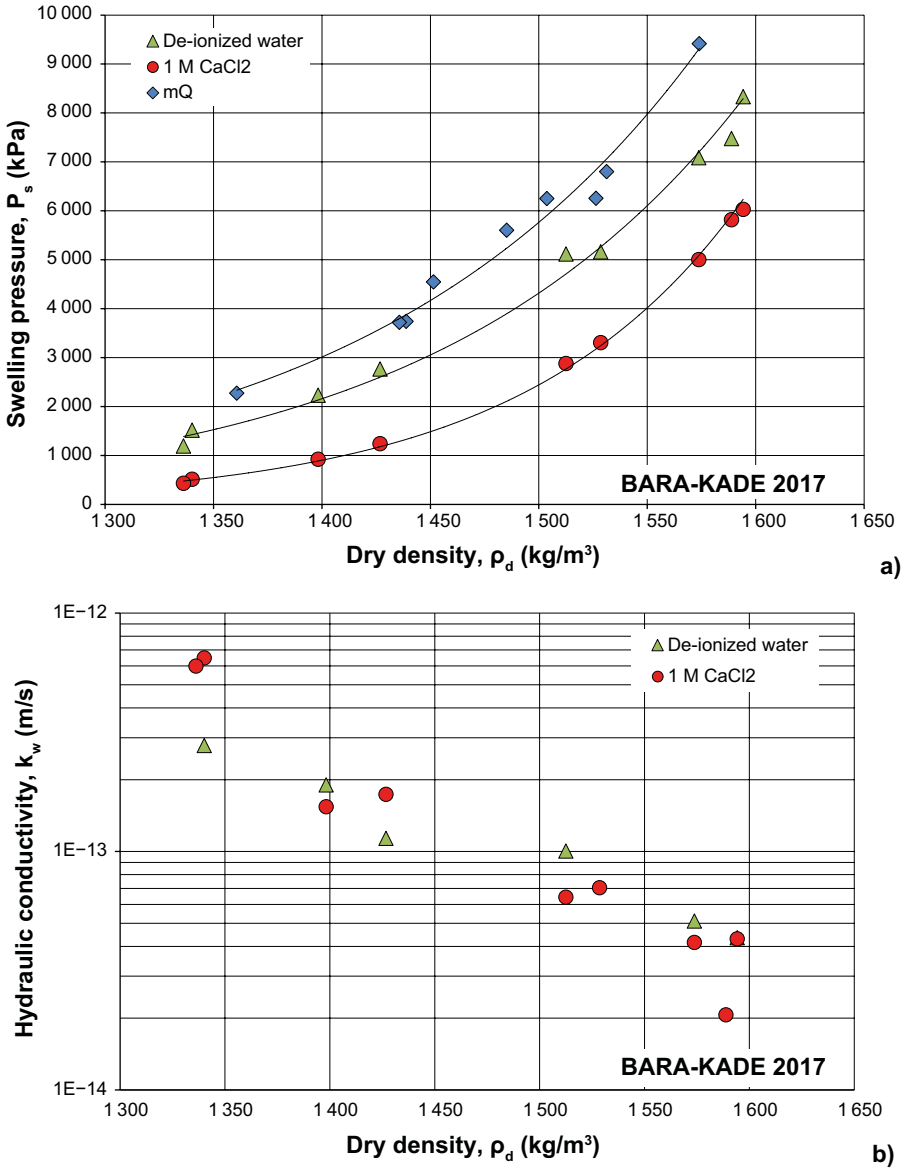

Figure F-1. *Swelling pressure (a) and hydraulic conductivity (b) as function of dry density for bentonite BARA-KADE 2017.*

Table F-3. Corrected densities and water content together with measured swelling pressure and hydraulic conductivity for BARA-KADE 2017. The corrected parameters are calculated with the assumption that the salinity in the interlayer water is 0.8 M $CaCl_2$ and ρ_s = 2 770 kg/m³.

	Corrected parameters			De-ionized water			1 M $CaCl_2$		
Test No.	ρ (kg/m³)	w (-)	ρ_d (kg/m³)	σ_s (kPa)	Gradient (m/m)	k_w (m/s)	σ_s (kPa)	Gradient (m/m)	k_w (m/s)
BARA-KADE 2017 1	1 826	0.413	1 293	1 518	9 271	2.78E−13	514	4 172	6.48E−13
BARA-KADE 2017 2	1 864	0.379	1 352	2 232	9 487	1.90E−13	921	4 269	1.54E−13
BARA-KADE 2017 3	1 940	0.319	1 471	5 118	9 926	1.00E−13	2 879	9 926	6.43E−14
BARA-KADE 2017 4	1 884	0.362	1 383	2 767	17 061	1.14E−13	1 240	8 530	1.74E−13
BARA-KADE 2017 5	1 981	0.291	1 534	7 085	17 971	5.11E−14	5 004	8 986	4.15E−14
BARA-KADE 2017 6	1 994	0.282	1 555	8 333	17 814	4.34E−14	6 028	8 907	4.30E−14

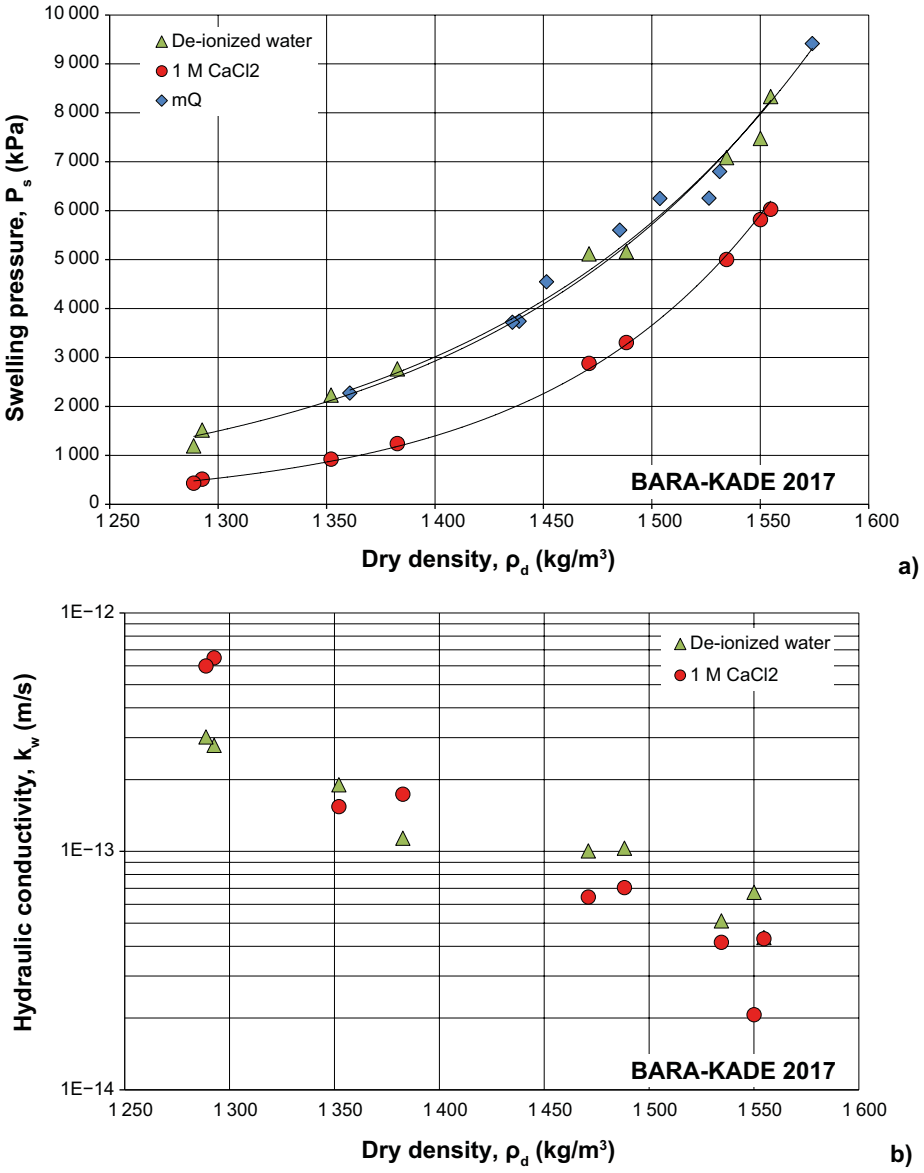

Figure F-2. *Swelling pressure (a) and hydraulic conductivity (b) as function of dry density for bentonite BARA-KADE 2017 after adjusting for excess salt in the interlayer water assumed to be 0.8 M $CaCl_2$.*

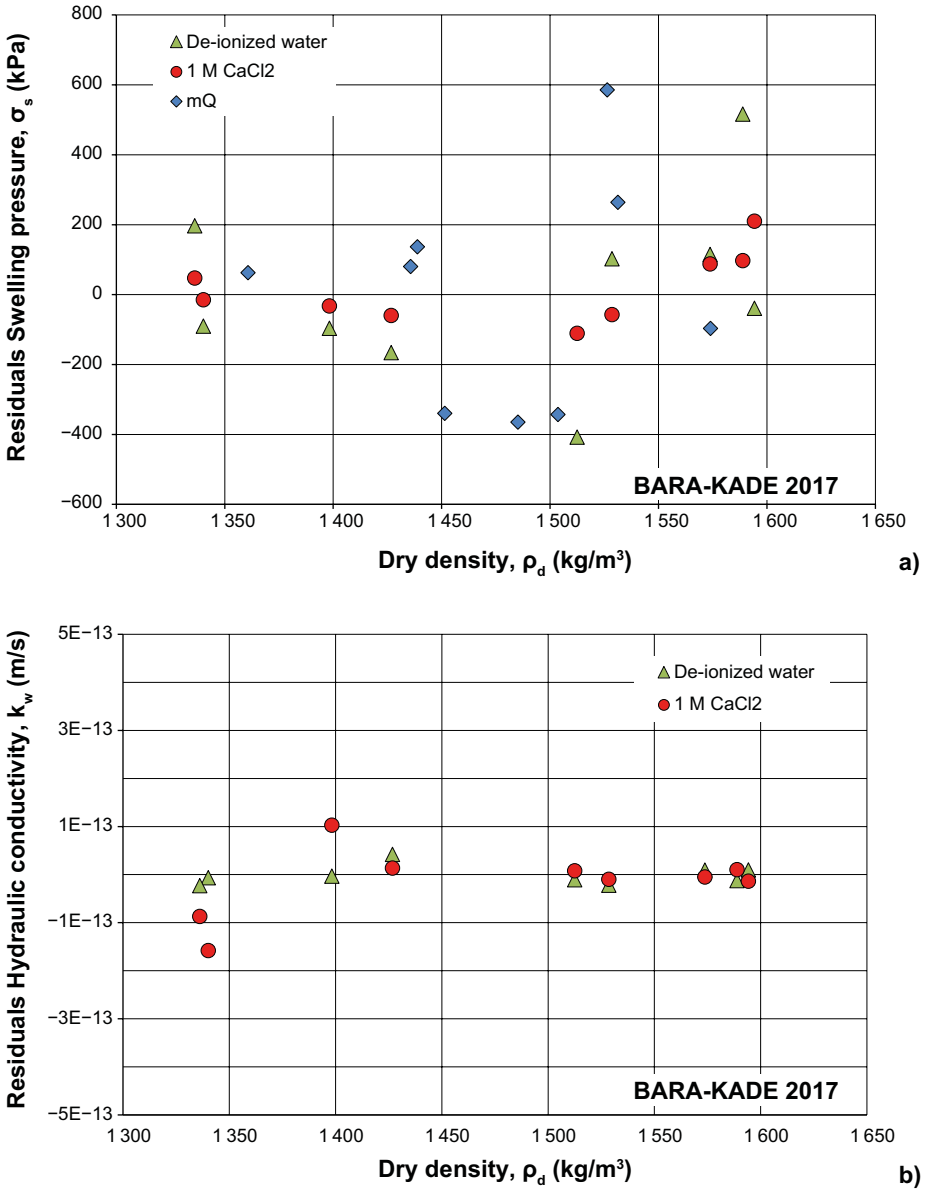

Figure F-3. *The residual plot for determined swelling pressure (a) and hydraulic conductivity (b) for bentonite BARA-KADE 2017.*

Table F-4. Mean and standard deviation for the residuals shown in Figure F-3.

Test series	Number of tests	Swelling pressure Average (kPa)	Stdv (kPa)	Hydraulic cond. Average (m/s)	Stdv (m/s)
BARA-KADE 2017 mQ	9	−2	320	-	-
BARA-KADE 2017 De-ionized water	9	14	260	−1.9E−15	2.0E−14
BARA-KADE 2017 1 M $CaCl_2$	9	18	100	−1.6E−14	7.2E−14

Appendix G

Swelling pressure/hydraulic conductivity

Bulgaria F 2017

Table G-1. Results from tests made on bentonite Bulgaria F 2017 both with deionized water and 1 M $CaCl_2$.

Test No.	ρ (kg/m³)	w (-)	ρ_d (kg/m³)	De-ionzed water σ_s (kPa)	Gradient (m/m)	k_w (m/s)	1 M $CaCl_2$ σ_s (kPa)	Gradient (m/m)	k_w (m/s)
Bulgaria F 2017 1	1836	0.432	1282	2300	6700	3.54E−13	1426	3829	3.42E−13
Bulgaria F 2017 2	1823	0.395	1307	3003	6580	2.71E−13	2053	3760	2.38E−13
Bulgaria F 2017 3	1875	0.366	1373	5057	6732	1.92E−13	3754	3847	1.30E−13
Bulgaria F 2017 4	1870	0.385	1350	4442	14432	1.81E−13	3287	8659	1.74E−13
Bulgaria F 2017 5	1885	0.353	1393	6816	14781	1.25E−13	5597	8868	1.21E−13
Bulgaria F 2017 6	1946	0.318	1477	12726	14738	8.77E−14	11958	8843	6.63E−14
Bulgaria F 2017 7	1828	0.392	1313	2855	12191	2.46E−13	1959	5627	2.45E−13
Bulgaria F 2017 8	1922	0.326	1449	7872	12853	1.11E−13	6731	5932	9.42E−14
Bulgaria F 2017 9	1934	0.313	1473	11318	13050	8.82E−14	10500	6023	7.70E−14

Table G-2. Results from tests made on bentonite Bulgaria F 2017 with deionized water.

Test Nr.	ρ (kg/m³)	w (-)	ρ_d (kg/m³)	σs (kPa)
Bulgaria F 2017 mQ 1	1814	0.422	1276	2950
Bulgaria F 2017 mQ 2	1811	0.392	1301	3894
Bulgaria F 2017 mQ 3	1847	0.375	1343	5080
Bulgaria F 2017 mQ 4	1848	0.383	1336	5144
Bulgaria F 2017 mQ 5	1890	0.357	1393	7656
Bulgaria F 2017 mQ 6	1914	0.342	1427	9546
Bulgaria F 2017 mQ 7	1853	0.388	1336	4985
Bulgaria F 2017 mQ 8	1904	0.345	1416	9285
Bulgaria F 2017 mQ 9	1893	0.324	1429	10250

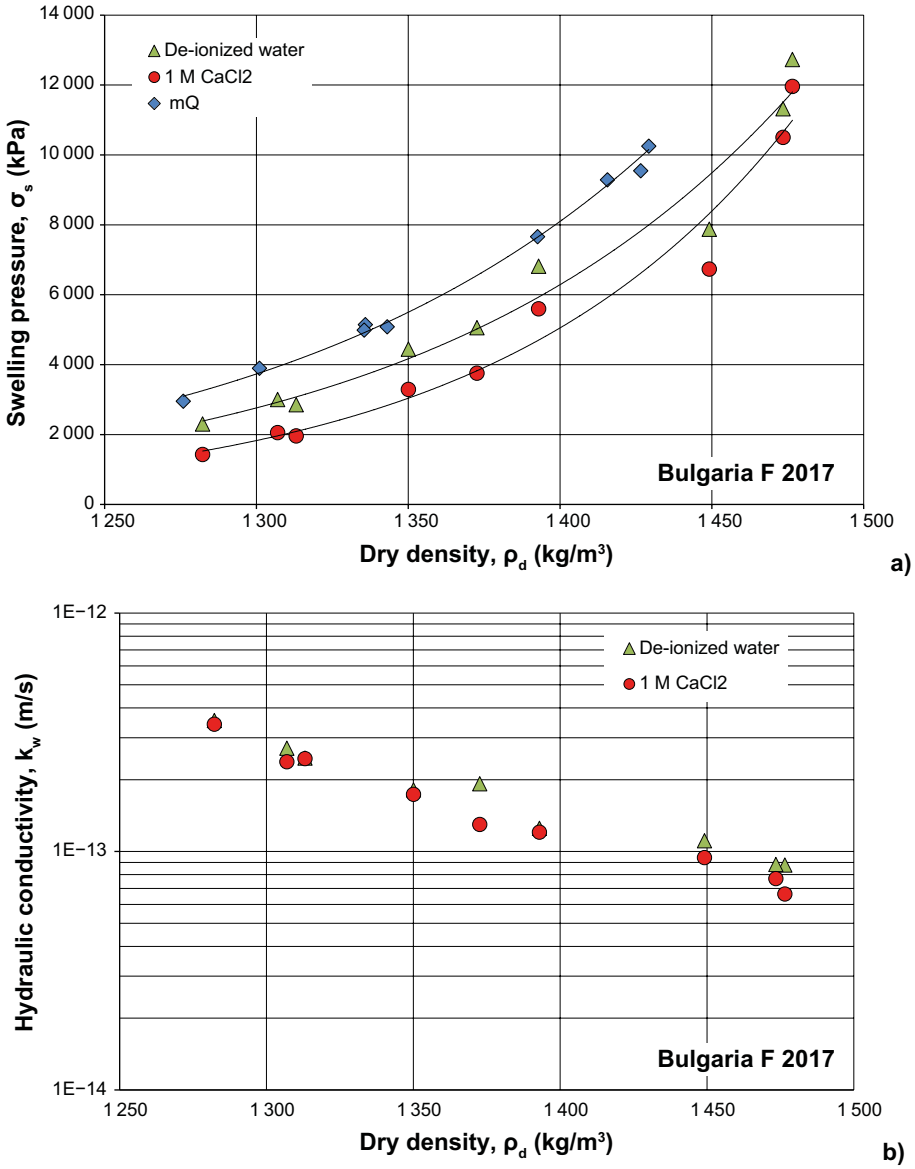

Figure G-1. *Swelling pressure (a) and hydraulic conductivity (b) as function of dry density for bentonite Bulgaria F 2017.*

Table G-3. Corrected densities and water content together with measured swelling pressure and hydraulic conductivity for Bulgaria F 2017. The corrected parameters are calculated with the assumption that the salinity in the interlayer water is 0.6 M $CaCl_2$ and ρ_s = 2 758 kg/m³.

	Corrected parameters			De-ionzed water			1 M $CaCl_2$		
Test No.	ρ (kg/m³)	w (-)	ρ_d (kg/m³)	σ_s (kPa)	Gradient (m/m)	k_w (m/s)	σ_s (kPa)	Gradient (m/m)	k_w (m/s)
Bulgaria F 2017 1	1 794	0.440	1 246	2 300	6 700	3.54E−13	1 426	3 829	3.42E−13
Bulgaria F 2017 2	1 810	0.424	1 271	3 003	6 580	2.71E−13	2 053	3 760	2.38E−13
Bulgaria F 2017 3	1 854	0.384	1 339	5 057	6 732	1.92E−13	3 754	3 847	1.30E−13
Bulgaria F 2017 4	1 839	0.398	1 315	4 442	14 432	1.81E−13	3 287	8 659	1.74E−13
Bulgaria F 2017 5	1 867	0.373	1 359	6 816	14 781	1.25E−13	5 597	8 868	1.21E−13
Bulgaria F 2017 6	1 922	0.329	1 446	12 726	14 738	8.77E−14	11 958	8 843	6.63E−14
Bulgaria F 2017 7	1 814	0.420	1 277	2 855	12 191	2.46E−13	1 959	5 627	2.45E−13
Bulgaria F 2017 8	1 903	0.343	1 417	7 872	12 853	1.11E−13	6 731	5 932	9.42E−14
Bulgaria F 2017 9	1 919	0.331	1 441	11 318	13 050	8.82E−14	10 500	6 023	7.70E−14

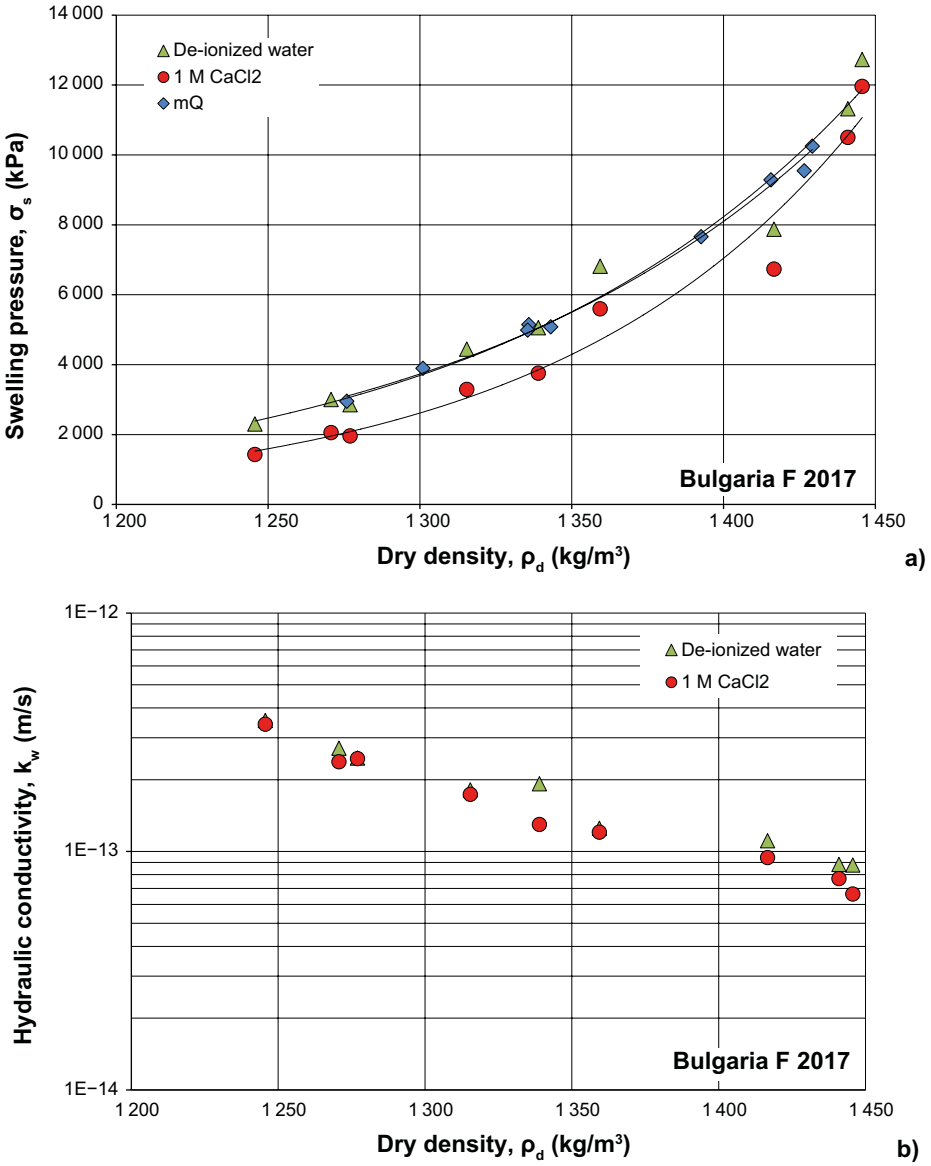

Figure G-2. *Swelling pressure (a) and hydraulic conductivity (b) as function of dry density for bentonite Bulgaria F 2017 after adjusting for excess salt in the interlayer water assumed to be 0.6 M $CaCl_2$.*

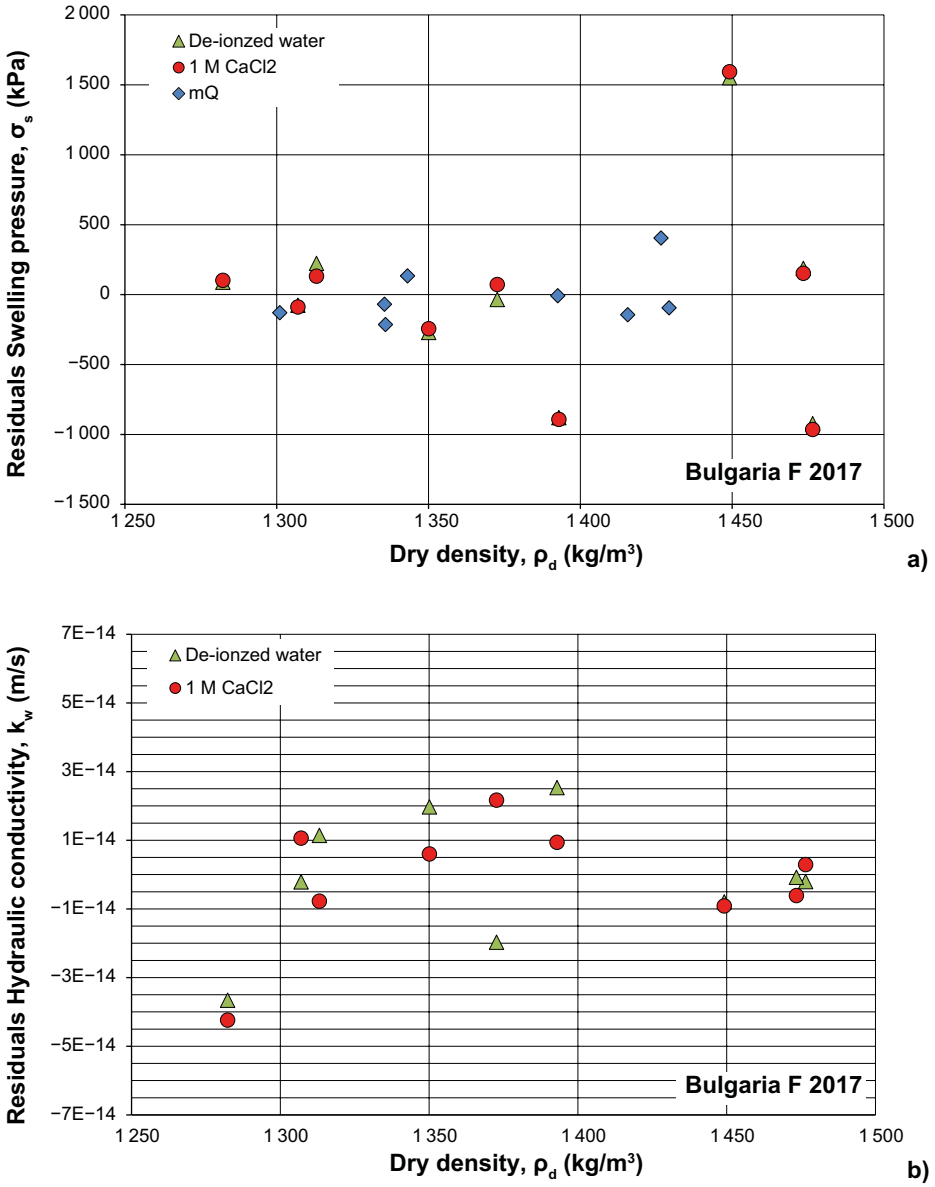

Figure G-3. *The residual plot for determined swelling pressure (a) and hydraulic conductivity (b) for bentonite Bulgaria F 2017.*

Table G-4. Mean and standard deviation for the residuals shown in Figure G-3.

Test series	Number of tests	Swelling pressure Average (kPa)	Swelling pressure Stdv (kPa)	Hydraulic cond. Average (m/s)	Hydraulic cond. Stdv (m/s)
Bulgaria F 2017 mQ	9	−15	199	-	-
Bulgaria F 2017 De-ionized water	9	−15	725	−1.4E−15	1.9E−14
Bulgaria F 2017 1 M $CaCl_2$	9	−16	741	−1.6E−15	1.8E−14

Appendix H

Swelling pressure/hydraulic conductivity

Sardinia 2017

Table H-1. Results from tests made on bentonite Sardinia 2017 both with deionized water and 1 M $CaCl_2$.

Test No.	ρ (kg/m³)	w (-)	ρ_d (kg/m³)	De-ionized water σ_s (kPa)	Gradient (m/m)	k_w (m/s)	1 M $CaCl_2$ σ_s (kPa)	Gradient (m/m)	k_w (m/s)
Sardinia 2017 1	1856	0.403	1323	1232	9305	5.36E−13	446	4032	1.31E−12
Sardinia 2017 2	1936	0.326	1461	4689	9230	1.14E−13	2649	10255	1.11E−13
Sardinia 2017 3	2027	0.268	1599	14094	9211	3.49E−14	11740	10235	2.56E−14
Sardinia 2017 4	1886	0.369	1378	2125	13676	2.83E−13	932	4884	4.43E−13
Sardinia 2017 5	1888	0.361	1387	2396	14095	2.46E−13	1060	5034	3.79E−13
Sardinia 2017 6	1928	0.342	1436	3888	13611	1.38E−13	1972	4861	1.56E−13
Sardinia 2017 7	1942	0.337	1452	4885	15423	8.96E−14	2888	10603	9.89E−14
Sardinia 2017 8	1991	0.302	1529	8992	15728	4.69E−14	6692	10813	3.71E−14
Sardinia 2017 9	1967	0.291	1523	8795	15690	5.43E−14	6430	10787	3.84E−14

Table H-2. Results from tests made on bentonite Sardinia 2017 with deionized water.

Test Nr.	ρ (kg/m³)	w (-)	ρ_d (kg/m³)	σ_s (kPa)
Sardinia 2017 1 mQ	1867	0.375	1357	2988
Sardinia 2017 2 mQ	1931	0.332	1449	5860
Sardinia 2017 3 mQ	1982	0.283	1545	12246
Sardinia 2017 4 mQ	1861	0.352	1376	3651
Sardinia 2017 5 mQ	1921	0.343	1431	5188
Sardinia 2017 6 mQ	1905	0.300	1465	6779
Sardinia 2017 7 mQ	1895	0.341	1413	4856
Sardinia 2017 8 mQ	1914	0.329	1440	6298
Sardinia 2017 9 mQ	1953	0.310	1491	8487

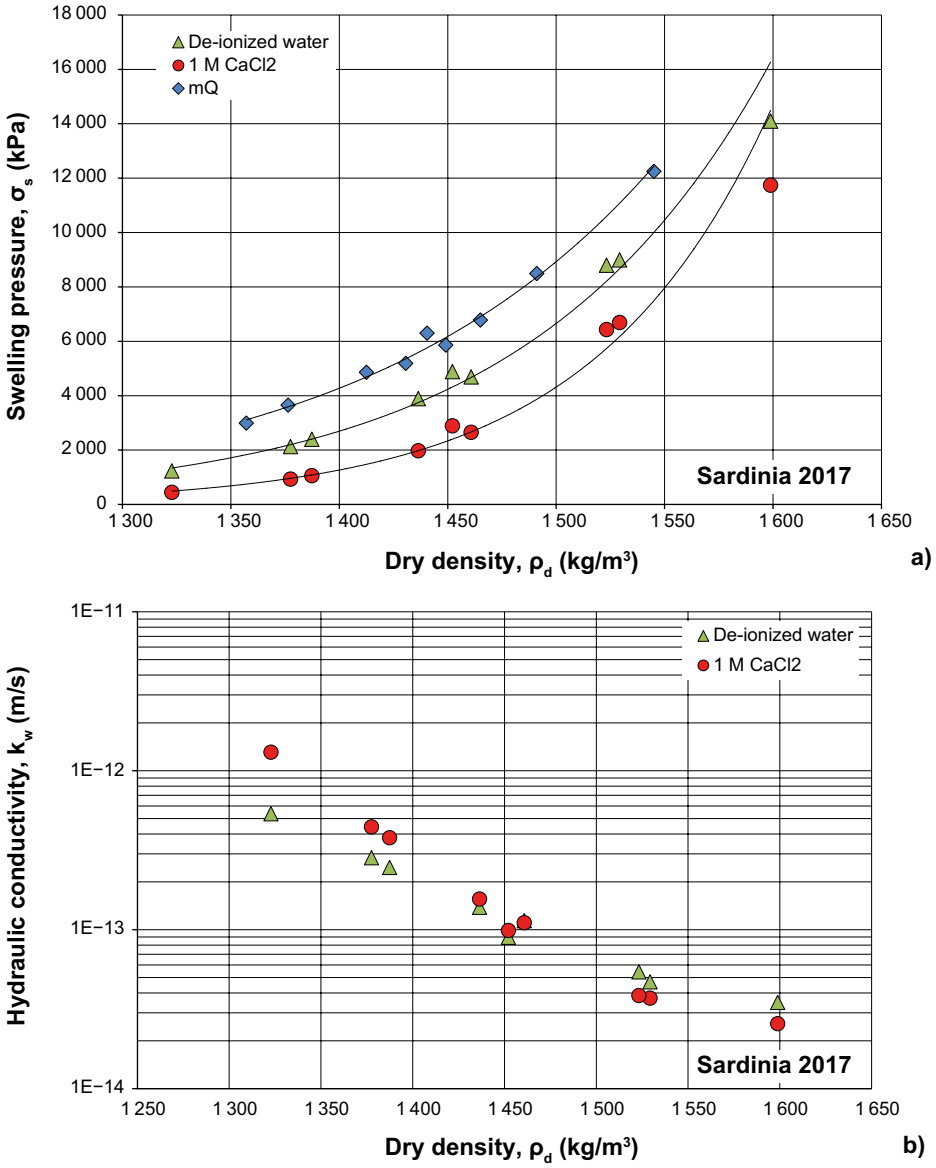

Figure H-1. *Swelling pressure (a) and hydraulic conductivity (b) as function of dry density for bentonite Sardinia 2017.*

Table H-3. Corrected densities and water content together with measured swelling pressure and hydraulic conductivity for Sardinia 2017. The corrected parameters are calculated with the assumption that the salinity in the interlayer water is 0.7 M $CaCl_2$ and ρ_s = 2 812 kg/m³.

	Corrected parameters			De-ionized water			1 M $CaCl_2$		
Test No.	ρ (kg/m³)	w (-)	ρ_d (kg/m³)	σ_s (kPa)	Gradient (m/m)	k_w (m/s)	σ_s (kPa)	Gradient (m/m)	k_w (m/s)
Sardinia 2017 1	1 826	0.425	1 281	1 232	9 305	5.36E−13	446	4 032	1.31E−12
Sardinia 2017 2	1 917	0.347	1 423	4 689	9 230	1.14E−13	2 649	10 255	1.11E−13
Sardinia 2017 3	2 008	0.284	1 564	14 094	9 211	3.49E−14	11 740	10 235	2.56E−14
Sardinia 2017 4	1 862	0.392	1 337	2 125	13 676	2.83E−13	932	4 884	4.43E−13
Sardinia 2017 5	1 868	0.387	1 346	2 396	14 095	2.46E−13	1 060	5 034	3.79E−13
Sardinia 2017 6	1 900	0.360	1 397	3 888	13 611	1.38E−13	1 972	4 861	1.56E−13
Sardinia 2017 7	1 911	0.352	1 414	4 885	15 423	8.96E−14	2 888	10 603	9.89E−14
Sardinia 2017 8	1 962	0.314	1 493	8 992	15 728	4.69E−14	6 692	10 813	3.71E−14
Sardinia 2017 9	1 958	0.317	1 487	8 795	15 690	5.43E−14	6 430	10 787	3.84E−14

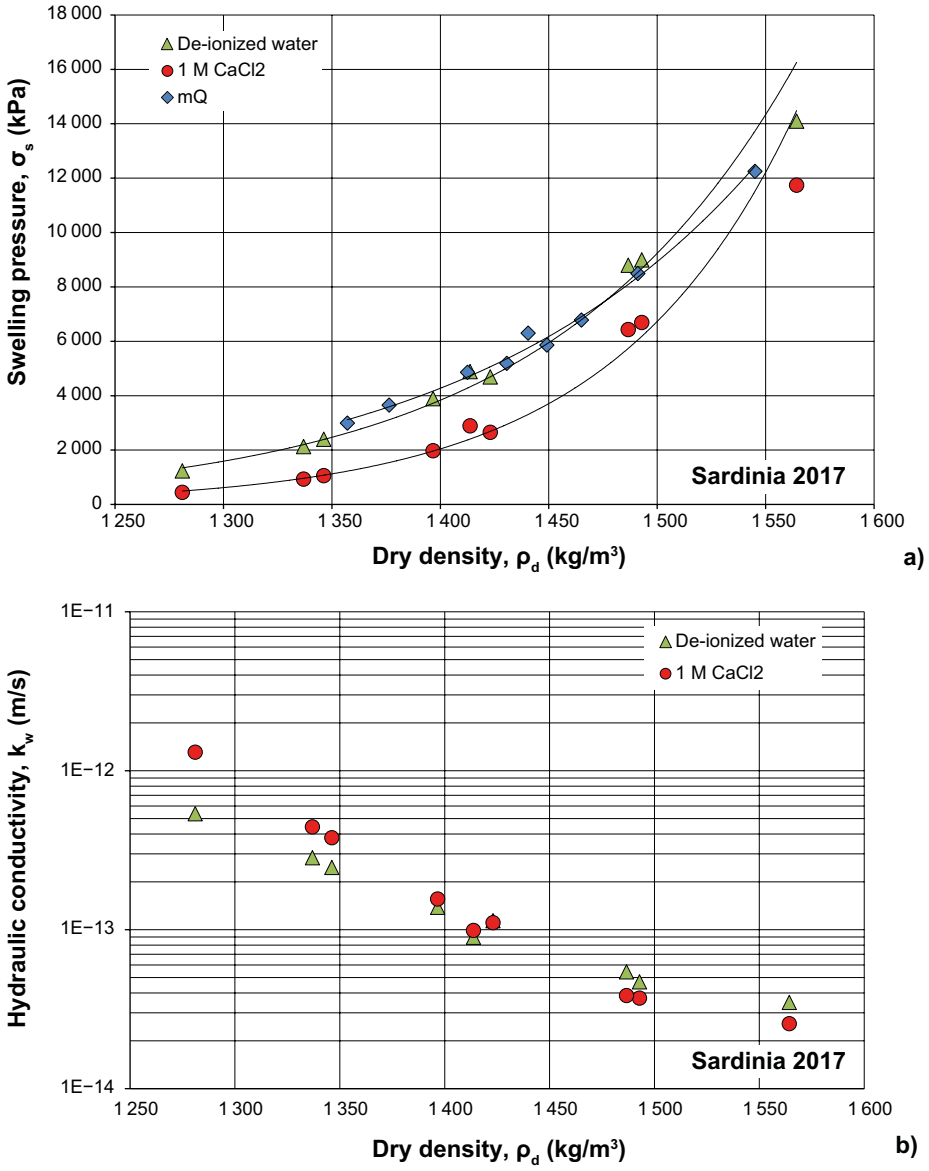

Figure H-2. *Swelling pressure (a) and hydraulic conductivity (b) as function of dry density for bentonite Sardinia 2017 after adjusting for excess salt in the interlayer water assumed to be 0.7 M $CaCl_2$.*

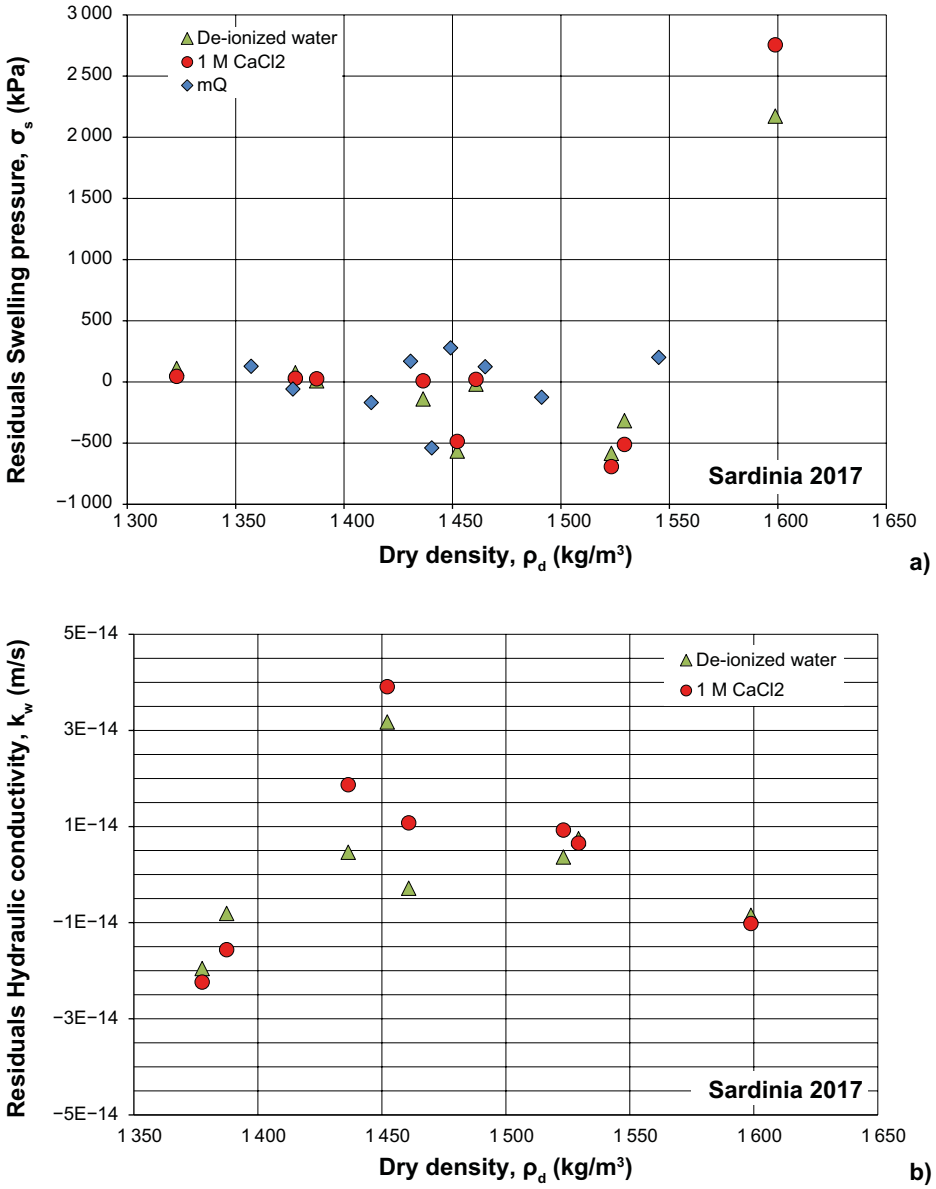

Figure H-3. *The residual plot for determined swelling pressure (a) and hydraulic conductivity (b) for bentonite Sardinia 2017.*

Table H-4. Mean and standard deviation for the residuals shown in Figure H-3.

Test series	Number of tests	Swelling pressure Average (kPa)	Swelling pressure Stdv (kPa)	Hydraulic cond. Average (m/s)	Hydraulic cond. Stdv (m/s)
Sardinia 2017 mQ	9	1	254	-	-
Sardinia 2017 De-ionized water	9	83	826	−6.8E−15	2.8E−14
Sardinia 2017 1 M $CaCl_2$	9	133	1 025	−3.5E−14	1.2E−14

Appendix J

Unconfined compression test

India 2018

Table J-1. Evaluated bulk density (ρ), water content (w), degree of saturation (S_r), void ratio (e) and dry density (ρ_d) together with the vertical stress (q_f) and strain (ε_f) at failure for the bentonite India 2018. Note that the degree of saturation and the void ratio are calculated at the assumption of the density on the solid particles is set to ρ_s = 2 931 kg/m^3.

Test No	ρ (kg/m^3)	w (%)	S_r (-)	e (-)	ρ_d (kg/m^3)	q_f (kPa)	ε_f (%)
India 2018 1	1 798	44.7	0.965	1.359	1 242	497	6.3
India 2018 2	1 864	41.5	0.993	1.225	1 317	736	5.4
India 2018 3	1 897	39.1	0.997	1.149	1 364	963	5.8
India 2018 4	1 919	36.1	0.982	1.079	1 410	1 317	6.8
India 2018 5	1 966	33.5	0.992	0.990	1 473	1 851	6.9
India 2018 6	1 978	32.2	0.984	0.959	1 496	2 096	8.1
India 2018 7	2 024	29.7	0.991	0.878	1 561	3 077	6.3
India 2018 8	2 036	29.2	0.995	0.860	1 576	3 366	5.0
India 2018 9	2 063	27.0	0.984	0.804	1 625	4 661	5.3

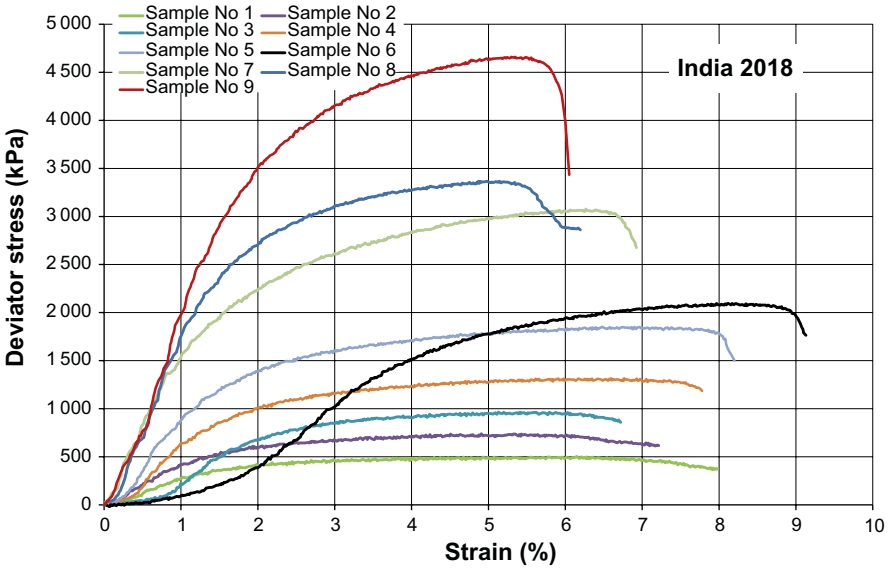

Figure J-1. *Measured axial stress as function of strain on specimens of India 2018. The tests are made at different dry density of the specimens.*

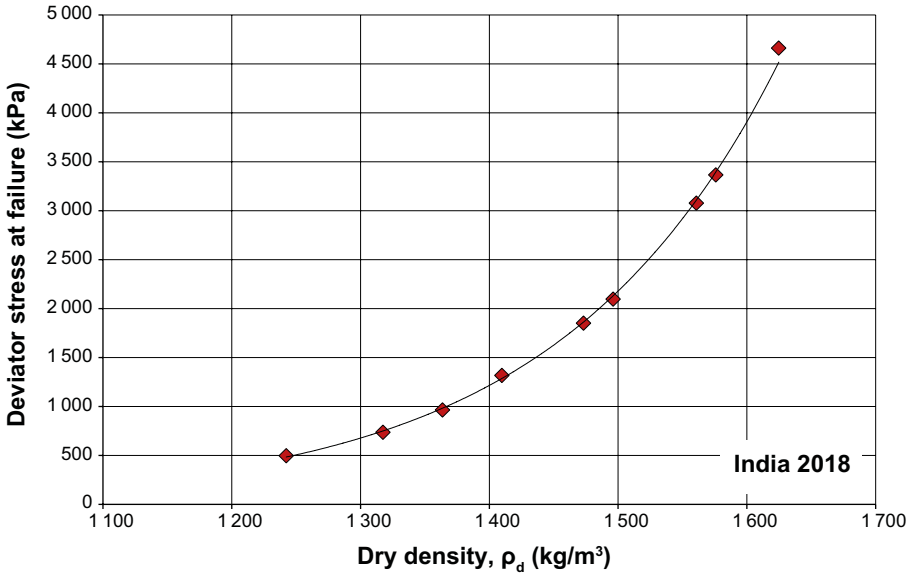

Figure J-2. Determined maximum strength as function of the dry density for the specimens of bentonite India 2018.

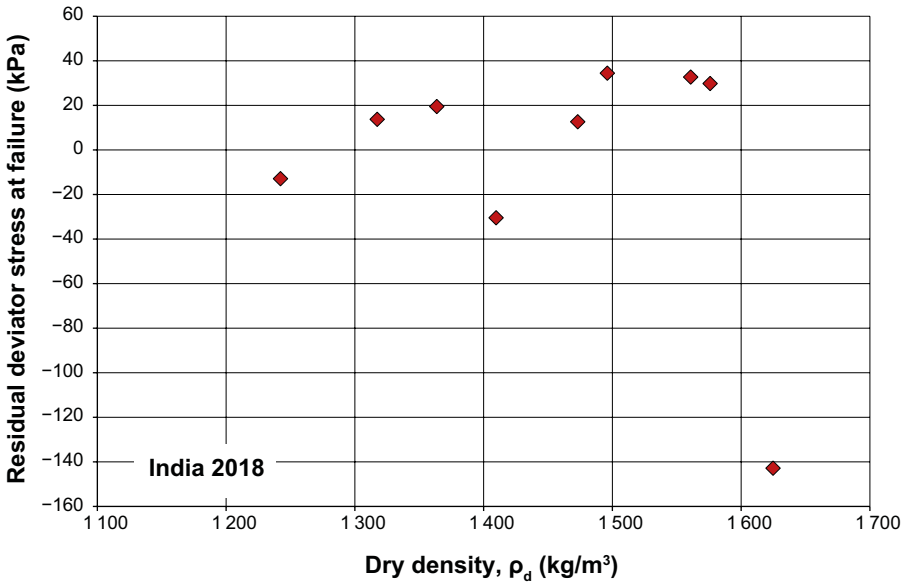

Figure J-3. The residual plot for the determined maximum strength of India 2018.

Table J-3. Mean and standard deviation for the residuals shown in Figure J-3.

Test series	Number of tests	Average (kPa)	Stdv (kPa)
India 2018	7	−5	56

Appendix K

Unconfined compression test

BARA-KADE 2017

Table K-1. Evaluated bulk density (ρ), water content (w), degree of saturation (Sr), void ratio (e) and dry density (ρd) together with the vertical stress (q_f) and strain (ε_f) at failure for the bentonite BARA-KADE 2017. Note that the degree of saturation and the the void ratio are calculated at the assumption of the density on the solid particles is set to ρ_s = 2 770 kg/m^3.

Test No	ρ (kg/m^3)	w (%)	S_r (-)	e (-)	ρ_d (kg/m^3)	q_f (kPa)	ε_f (%)
BARA-KADE 2017 1	1 851	34.7	0.947	1.016	1 374	905	6.2
BARA-KADE 2017 2	1 896	32.7	0.965	0.939	1 429	1 192	6.0
BARA-KADE 2017 3	1 918	30.3	0.952	0.881	1 473	1 521	5.9
BARA-KADE 2017 4	1 950	28.6	0.959	0.827	1 516	1 924	5.8
BARA-KADE 2017 5	1 982	26.8	0.961	0.771	1 564	2 298	6.3

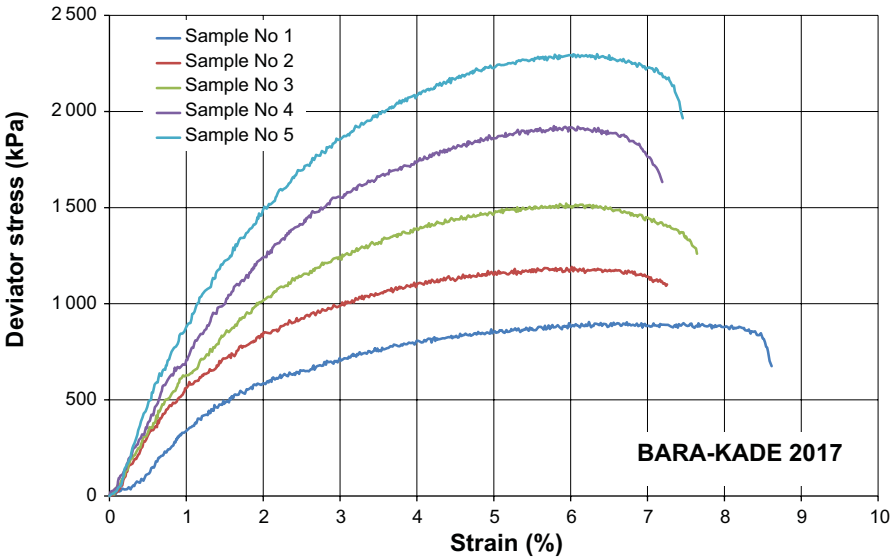

Figure K-1. *Measured axial stress as function of strain on specimens of Bara-Kade 2017. The tests are made at different dry density of the specimens.*

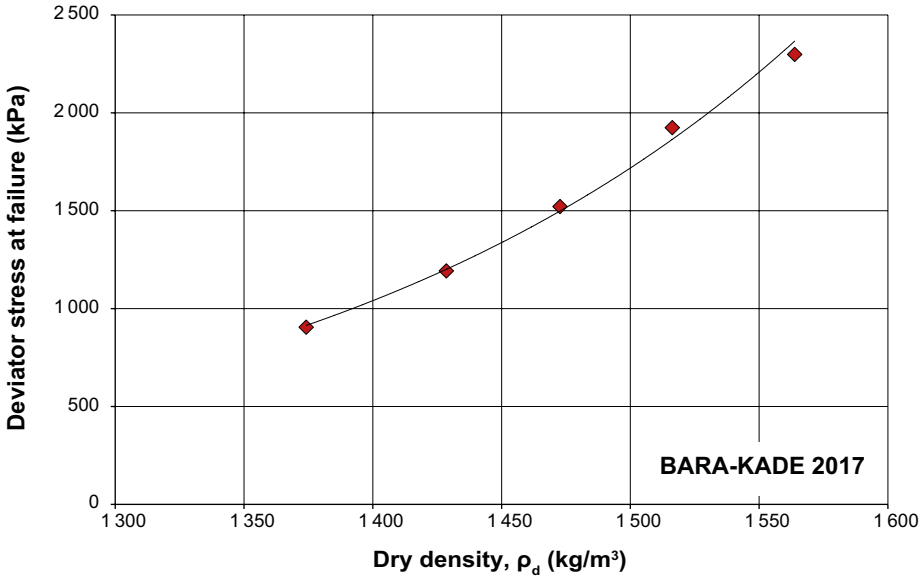

Figure K-2. Determined maximum strength as function of the dry density for the specimens of bentonite Bara-Kade 2017.

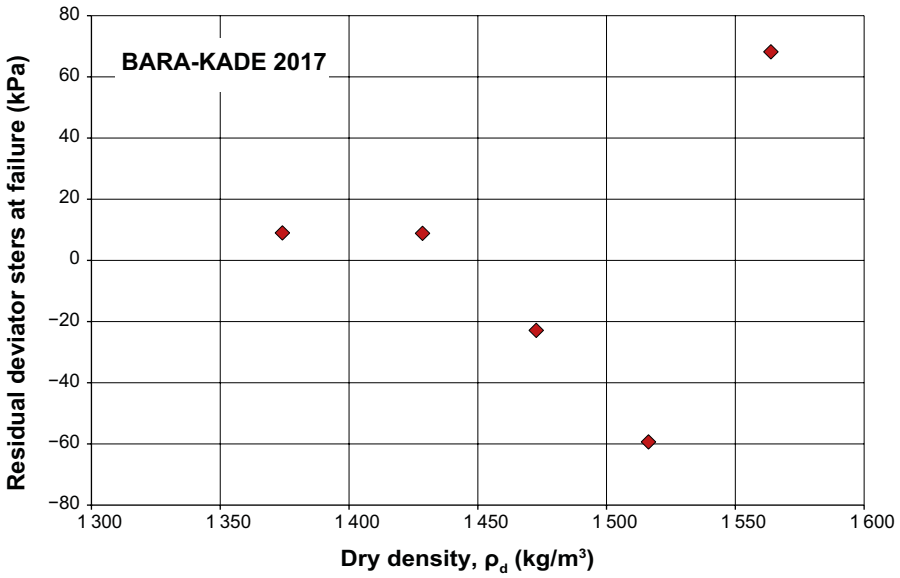

Figure K-3. The residual plot for the determined maximum strength of Bara-Kade 2017.

Table K-3. Mean and standard deviation for the residuals shown in Figure K-3.

Test series	Number of tests	Average (kPa)	Stdv (kPa)
Bara-Kade 2017	5	1	47

Appendix L

Unconfined compression test

Bulgaria 2017

Table L-1. Evaluated bulk density (ρ), water content (w), degree of saturation (Sr), void ratio (e) and dry density (ρd) together with the vertical stress (q_f) and strain (ε_f) at failure for the bentonite Bulgaria 2017. Note that the degree of saturation and the the void ratio are calculated at the assumption of the density on the solid particles is set to ρ_s = 2 757 kg/m^3.

Test No	ρ (kg/m^3)	w (%)	S_r (-)	e (-)	ρ_d (kg/m^3)	q_f (kPa)	ε_f (%)
Bulgaria 2017 1	1 689	0.488	0.941	1.429	1 135	394	3.3
Bulgaria 2017 2	1 716	0.467	0.949	1.358	1 169	591	4.0
Bulgaria 2017 3	1 758	0.447	0.971	1.268	1 215	808	4.2
Bulgaria 2017 4	1 773	0.416	0.954	1.201	1 253	1 122	4.8
Bulgaria 2017 5	1 808	0.399	0.970	1.133	1 293	1 391	4.5
Bulgaria 2017 6	1 833	0.371	0.963	1.063	1 337	1 936	3.8
Bulgaria 2017 7	1 869	0.347	0.970	0.986	1 388	2 570	3.6
Bulgaria 2017 8	1 886	0.324	0.954	0.936	1 424	3 117	3.9
Bulgaria 2017 9	1 898	0.316	0.955	0.911	1 442	3 161	2.8

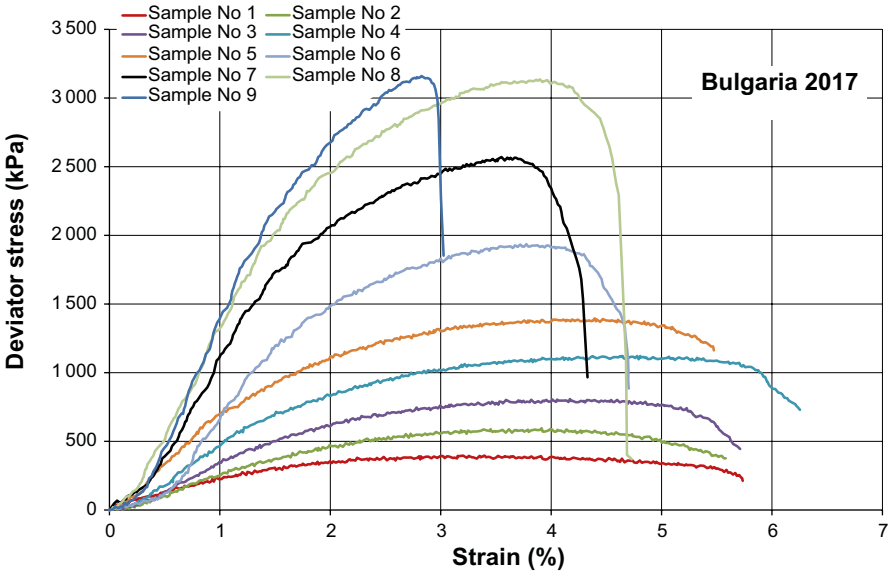

Figure L-1. *Measured axial stress as function of strain on specimens of Bulgaria 2017. The tests are made at different dry density of the specimens.*

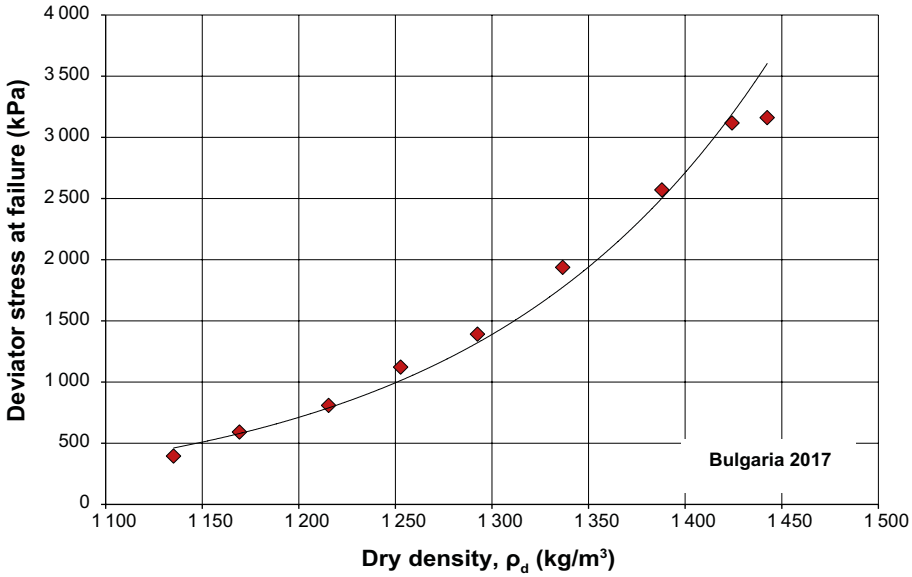

Figure L-2. *Determined maximum strength as function of the dry density for the specimens of bentonite Bulgaria 2017.*

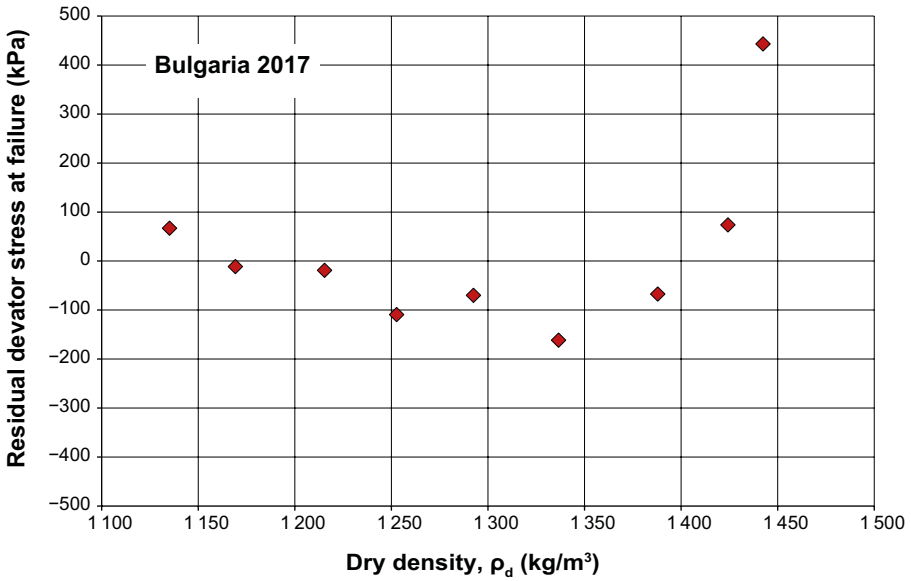

Figure L-3. *The residual plot for the determined maximum strength of Bulgaria 2017.*

Table L-3. Mean and standard deviation for the residuals shown in Figure L-3.

Test series	Number of tests	Average (kPa)	Stdv (kPa)
Bulgaria 2017	9	16	177

Appendix M

Unconfined compression test

Morocco 2017

Table M-1. Evaluated bulk density (ρ), water content (w), degree of saturation (Sr), void ratio (e) and dry density (ρd) together with the vertical stress (q_f) and strain (ε_f) at failure for the bentonite Morocco 2017. Note that the degree of saturation and the the void ratio are calculated at the assumption of the density on the solid particles is set to ρ_s = 2 737 kg/m^3.

Test No	ρ (kg/m^3)	w (%)	S_r (-)	e (-)	ρ_d (kg/m^3)	q_f (kPa)	ε_f (%)
Morocco 2017 1	1 769	33.4	0.860	1.064	1 326	705	4.1
Morocco 2017 2	1 817	32.1	0.888	0.989	1 376	1 066	4.4
Morocco 2017 3	1 882	30.3	0.927	0.895	1 444	1 419	4.0
Morocco 2017 4	1 911	28.0	0.920	0.833	1 493	2 192	5.4
Morocco 2017 5	1 964	27.1	0.961	0.771	1 545	3 091	6.2
Morocco 2017 6	1 999	24.7	0.957	0.708	1 603	3 644	5.0
Morocco 2017 7	2 030	23.3	0.964	0.663	1 646	3 434	2.7

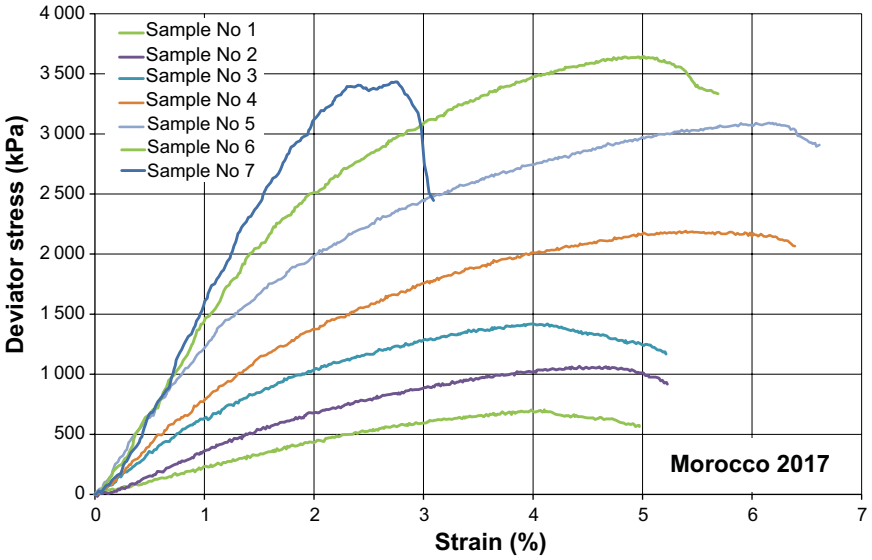

Figure M-1. *Measured axial stress as function of strain on specimens of Morocco 2017. The tests are made at different dry density of the specimens.*

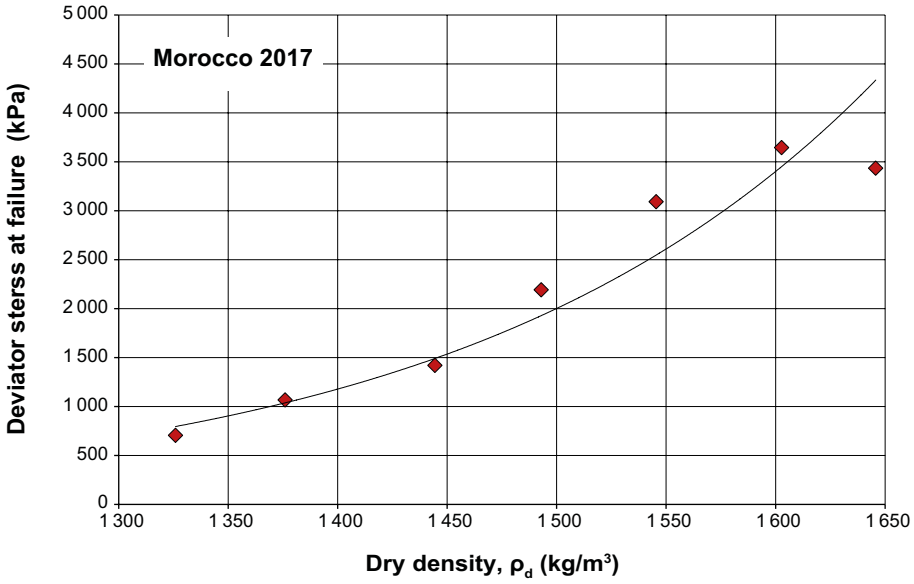

Figure M-2. *Determined maximum strength as function of the dry density for the specimens of bentonite Morocco 2017.*

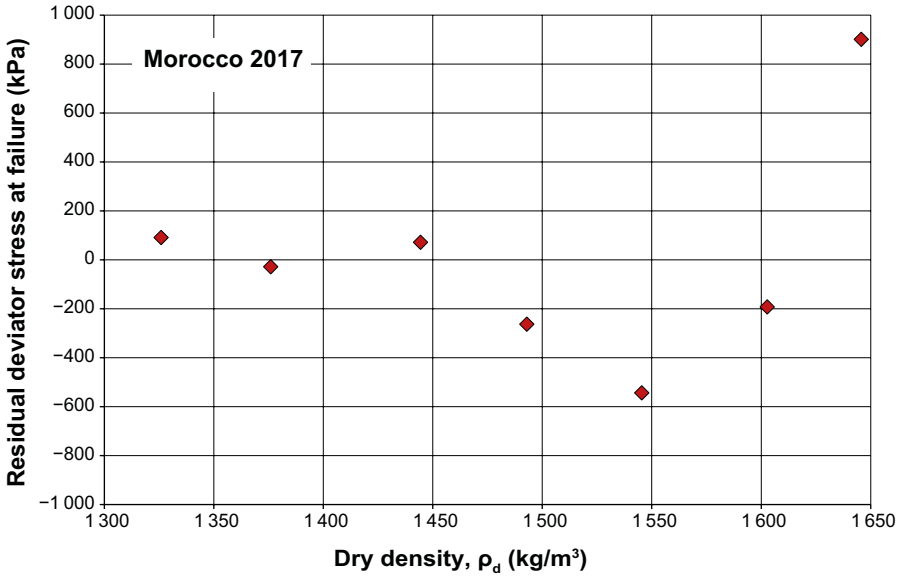

Figure M-3. *The residual plot for the determined maximum strength of Morocco 2017.*

Table M-3. Mean and standard deviation for the residuals shown in Figure M-3.

Test series	Number of tests	Average (kPa)	Stdv (kPa)
Morocco 2017	7	5	452

Appendix N

Unconfined compression test

Milos 2017

Table N-1. Evaluated bulk density (ρ), water content (w), degree of saturation (Sr), void ratio (e) and dry density (ρ_d) together with the vertical stress (q_f) and strain (ε_f) at failure for the bentonite Milos 2017. Note that the degree of saturation and the the void ratio are calculated at the assumption of the density on the solid particles is set to ρ_s = 2 606 kg/m^3.

Test No	ρ (kg/m^3)	w (%)	S_r (-)	e (-)	ρ_d (kg/m^3)	q_f (kPa)	ε_f (%)
Milos 2017 1	1 759	32.1	0.874	0.958	1 331	443	4.4
Milos 2017 2	1 787	29.3	0.862	0.885	1 382	682	4.2
Milos 2017 3	1 826	27.4	0.873	0.819	1 433	1 085	4.1
Milos 2017 4	1 859	25.5	0.875	0.759	1 481	1 439	3.4
Milos 2017 5	1 891	23.8	0.878	0.706	1 528	1 651	3.1

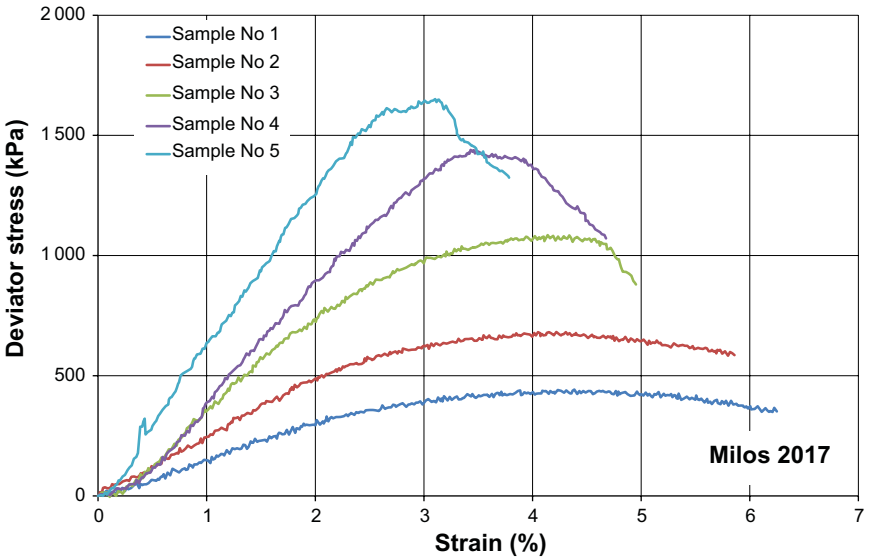

Figure N-1. Measured axial stress as function of strain on specimens of Milos 2017. The tests are made at different dry density of the specimens.

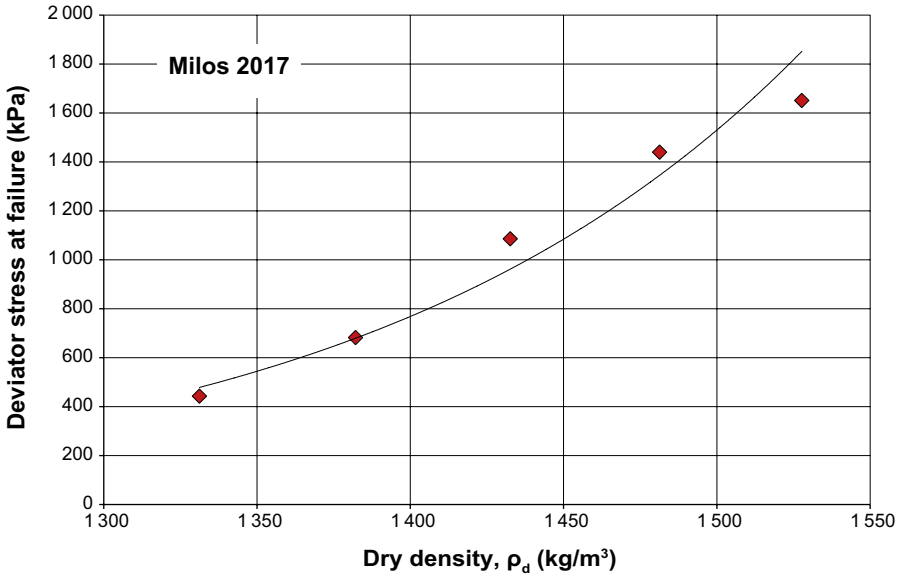

Figure N-2. *Determined maximum strength as function of the dry density for the specimens of bentonite Milos 2017.*

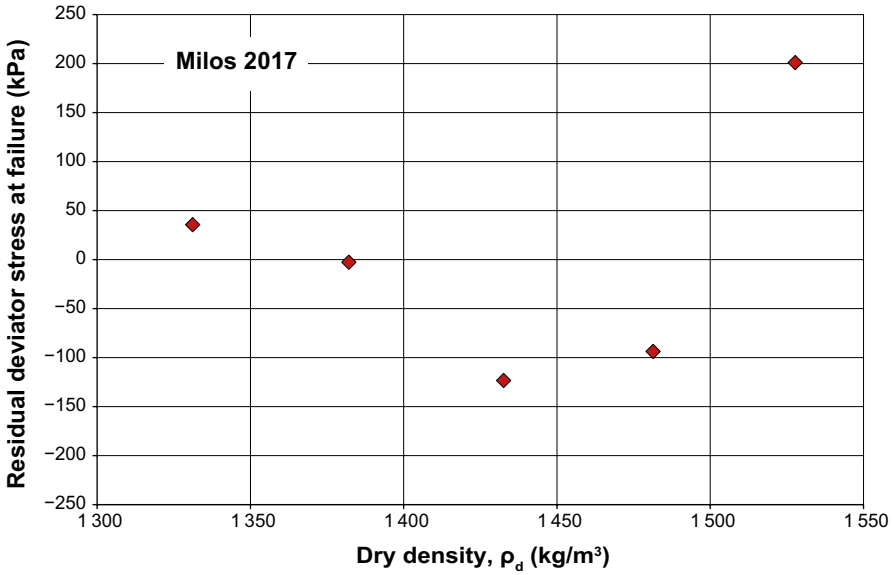

Figure N-3. *The residual plot for the determined maximum strength of Milos 2017.*

Table N-3. Mean and standard deviation for the residuals shown in Figure N-3.

Test series	Number of tests	Average (kPa)	Stdv (kPa)
Milos 2017	5	3	128

Appendix O

Unconfined compression test

Sardinia 2017

Table O-1. Evaluated bulk density (ρ), water content (w), degree of saturation (S_r), void ratio (e) and dry density (ρ_d) together with the vertical stress (q_f) and strain (ε_f) at failure for the bentonite Sardinia 2017. Note that the degree of saturation and the the void ratio are calculated at the assumption of the density on the solid particles is set to ρ_s = 2 812 kg/m^3.

Test No	ρ (kg/m^3)	w (%)	S_r (-)	e (-)	ρ_d (kg/m^3)	q_f (kPa)	ε_f (%)
Sardinia 2017 1	1 858	35.1	0.945	1.044	1 376	972	5.9
Sardinia 2017 2	1 863	33.6	0.929	1.016	1 395	1 034	4.4
Sardinia 2017 3	1 907	31.8	0.948	0.943	1 447	1 504	5.3
Sardinia 2017 4	1 913	30.5	0.935	0.919	1 466	1 594	5.2
Sardinia 2017 5	1 926	31.0	0.955	0.912	1 471	1 775	5.6

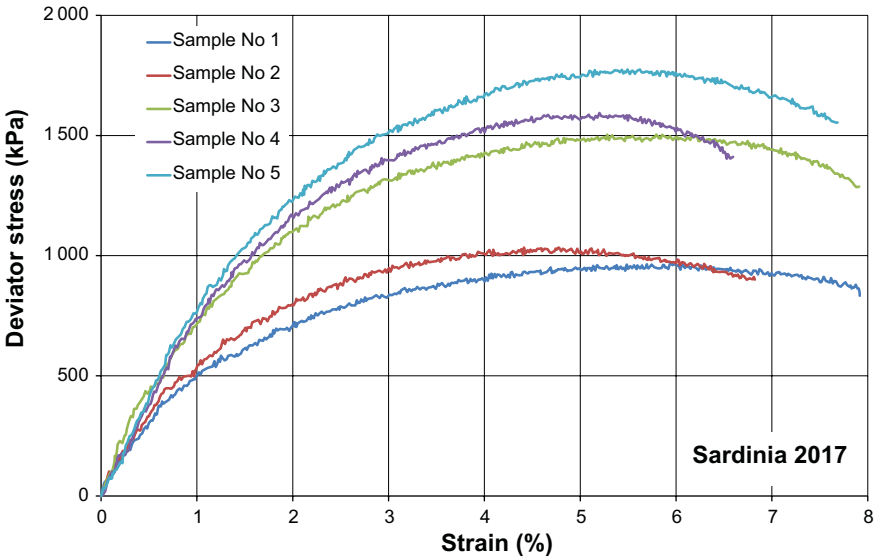

Figure O-1. *Measured axial stress as function of strain on specimens of Sardinia 2017. The tests are made at different dry density of the specimens.*

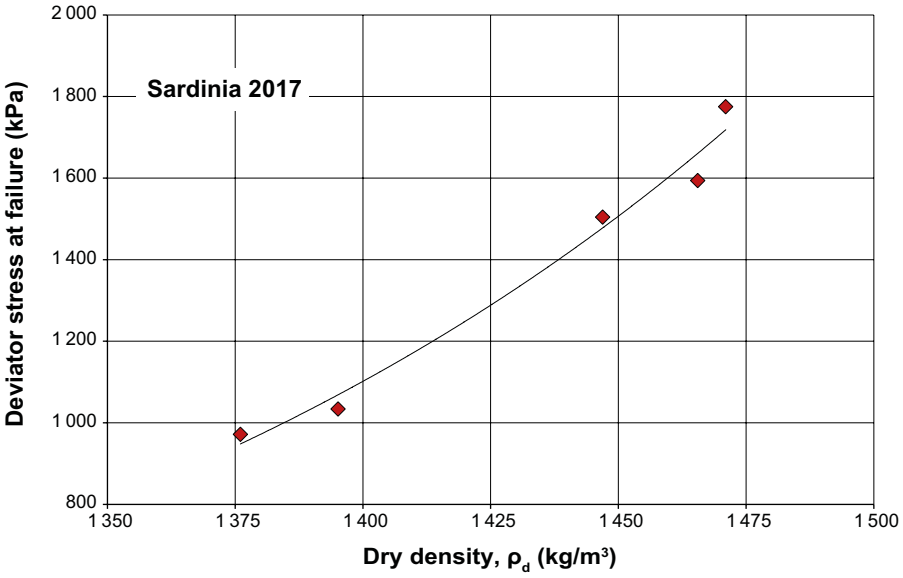

Figure O-2. *Determined maximum strength as function of the dry density for the specimens of bentonite Sardinia 2017.*

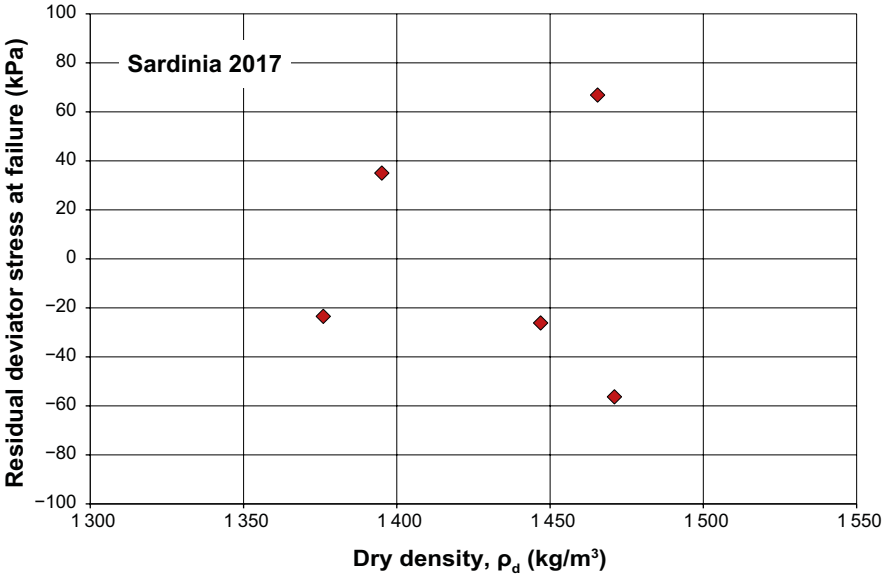

Figure O-3. *The residual plot for the determined maximum strength of Sardinia 2017.*

Table O-3. Mean and standard deviation for the residuals shown in Figure O-3.

Test series	Number of tests	Average (kPa)	Stdv (kPa)
Sardinia 2017	5	−1	50

Appendix P

Unconfined compression test

Turkey 2017

Table P-1. Evaluated bulk density (ρ), water content (w), degree of saturation (S_r), void ratio (e) and dry density (ρ_d) together with the vertical stress (q_f) and strain (ε_f) at failure for the bentonite Turkey 2017. Note that the degree of saturation and the the void ratio are calculated at the assumption of the density on the solid particles is set to ρ_s = 2 605 kg/m^3.

Test No	ρ (kg/m^3)	w (%)	S_r (-)	e (-)	ρ_d (kg/m^3)	q_f (kPa)	ε_f (%)
Turkey 2017 1	1 839	34.8	0.997	0.909	1 364	644	6.7
Turkey 2017 2	1 889	32.6	1.026	0.829	1 425	967	8.6
Turkey 2017 3	1 911	30.4	1.019	0.778	1 465	1 227	6.9
Turkey 2017 4	1 951	28.4	1.036	0.715	1 519	1 696	9.8
Turkey 2017 5	1 965	27.1	1.031	0.684	1 547	1 994	7.2

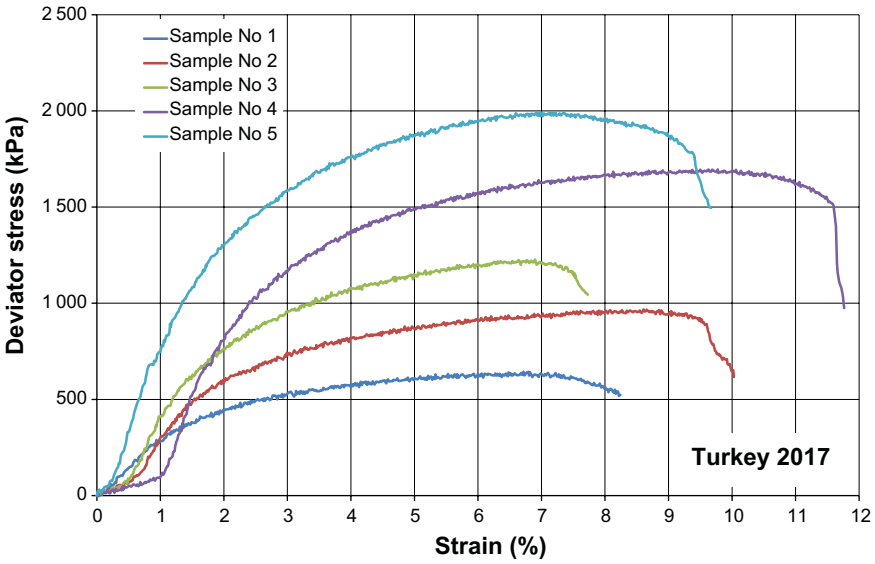

Figure P-1. *Measured axial stress as function of strain on specimens of Turkey 2017. The tests are made at different dry density of the specimens.*

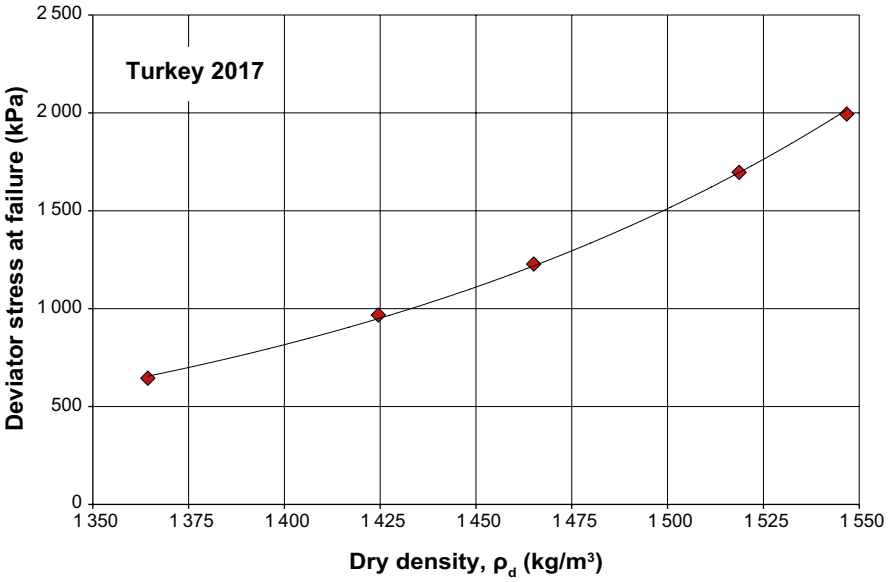

Figure P-2. Determined maximum strength as function of the dry density for the specimens of bentonite Turkey 2017.

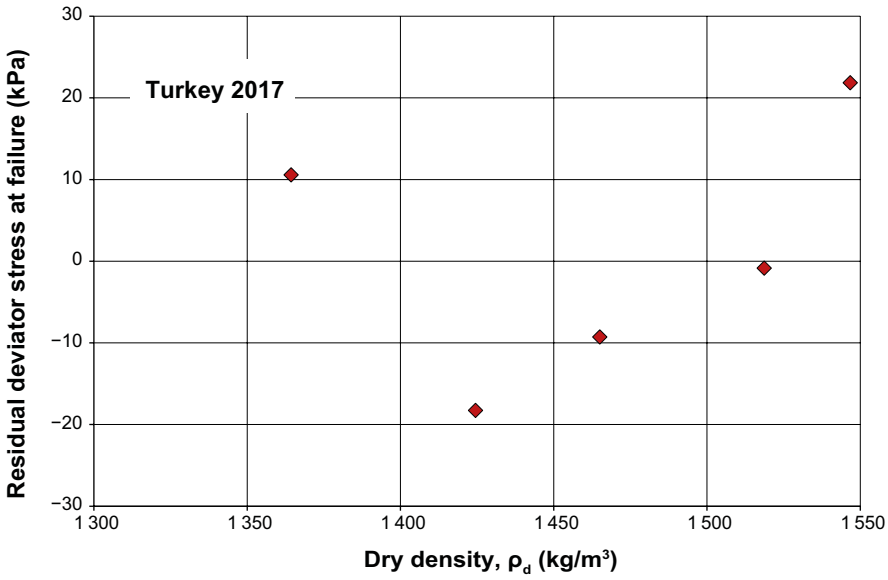

Figure P-3. The residual plot for the determined maximum strength of India 2018.

Table P-3. Mean and standard deviation for the residuals shown in Figure P-3.

Test series	Number of tests	Average (kPa)	Stdv (kPa)
Turkey 2017	5	1	16

Appendix Q

Unconfined compression test

MX-80 P 2014

Table Q-1. Evaluated bulk density (ρ), water content (w), degree of saturation (S_r), void ratio (e) and dry density (ρ_d) together with the vertical stress (q_f) and strain (ε_f) at failure for the bentonite MX-80 P 2014. Note that the degree of saturation and the the void ratio are calculated at the assumption of the density on the solid particles is set to ρ_s = 2 780 kg/m^3.

Test No	ρ (kg/m^3)	w (%)	S_r (-)	e (-)	ρ_d (kg/m^3)	q_f (kPa)	ε_f (%)
MX-80 P2014 1	1 942	0.303	0.974	0.866	1 490	1 915	7.6
MX-80 P 2014 2	1 959	0.298	0.983	0.842	1 509	2 122	6.8
MX-80 P 2014 3	1 971	0.289	0.982	0.818	1 529	2 216	6.2
MX-80 P 2014 4	1 978	0.278	0.972	0.797	1 547	2 482	6.7
MX-80 P 2014 5	1 990	0.275	0.979	0.782	1 560	2 563	6.5
MX-80 P 2014 6	1 859	0.336	0.937	0.998	1 391	1 028	7.5
MX-80 P 2014 7	1 904	0.320	0.959	0.928	1 442	1 250	6.8
MX-80 P 2014 8	1 928	0.302	0.956	0.877	1 481	1 691	6.4
MX-80 P 2014 9	1 954	0.280	0.949	0.821	1 526	2 116	6.2
MX-80 P 2014 10	1 987	0.263	0.953	0.768	1 573	2 365	5.2

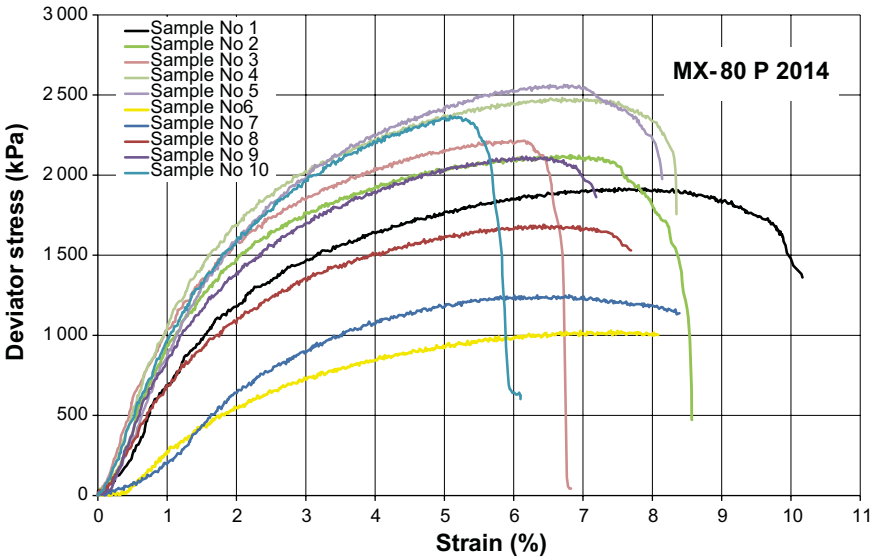

Figure Q-1. *Measured axial stress as function of strain on specimens of MX-80 P 2014. The tests are made at different dry density of the specimens.*

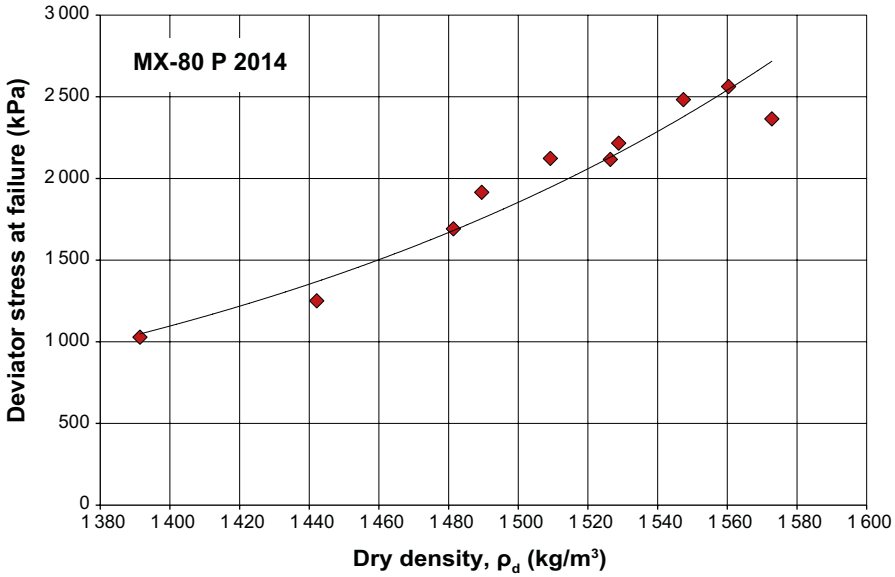

Figure Q-2. *Determined maximum strength as function of the dry density for the specimens of bentonite MX-80 P 2014.*

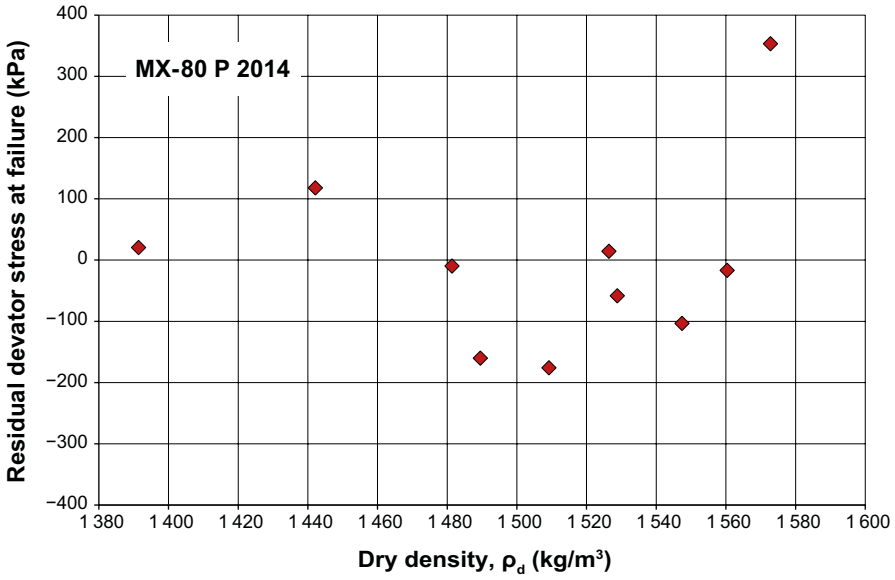

Figure Q-3. *The residual plot for the determined maximum strength of MX-80 P 2014.*

Table Q-3. Mean and standard deviation for the residuals shown in Figure Q-3.

Test series	Number of tests	Average (kPa)	Stdv (kPa)
MX-80 P 2014	10	−41	94

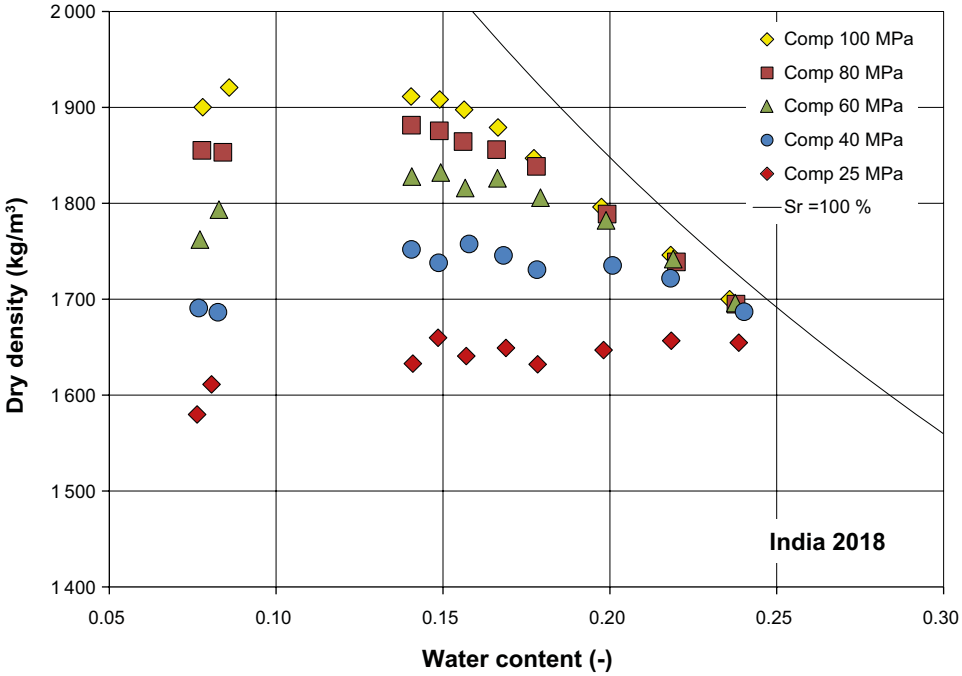

Figure R-1. *Determined dry density as function of both water content and compaction pressure for the bentonite India 2018.*

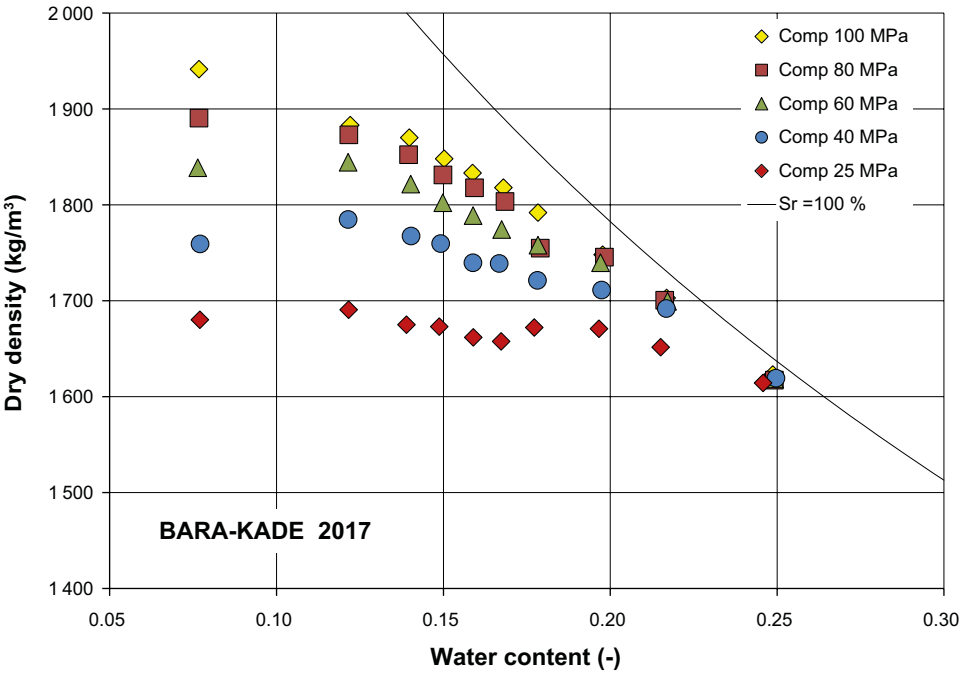

Figure R-2. *Determined dry density as function of both water content and compaction pressure for the bentonite Bara-Kade 2017.*

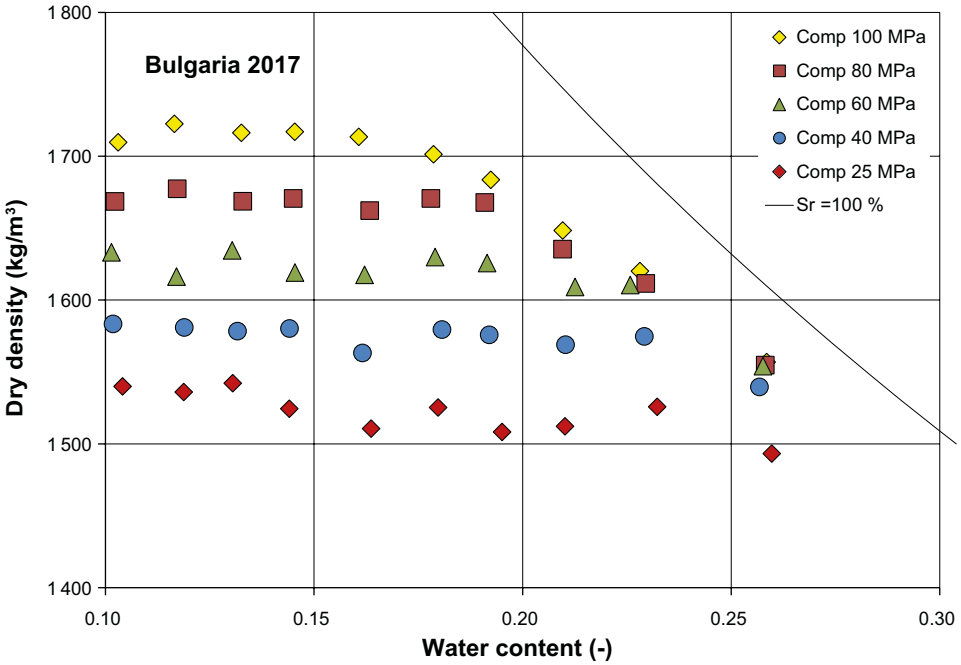

Figure R-3. *Determined dry density as function of both water content and compaction pressure for the bentonite Bulgaria 2017.*

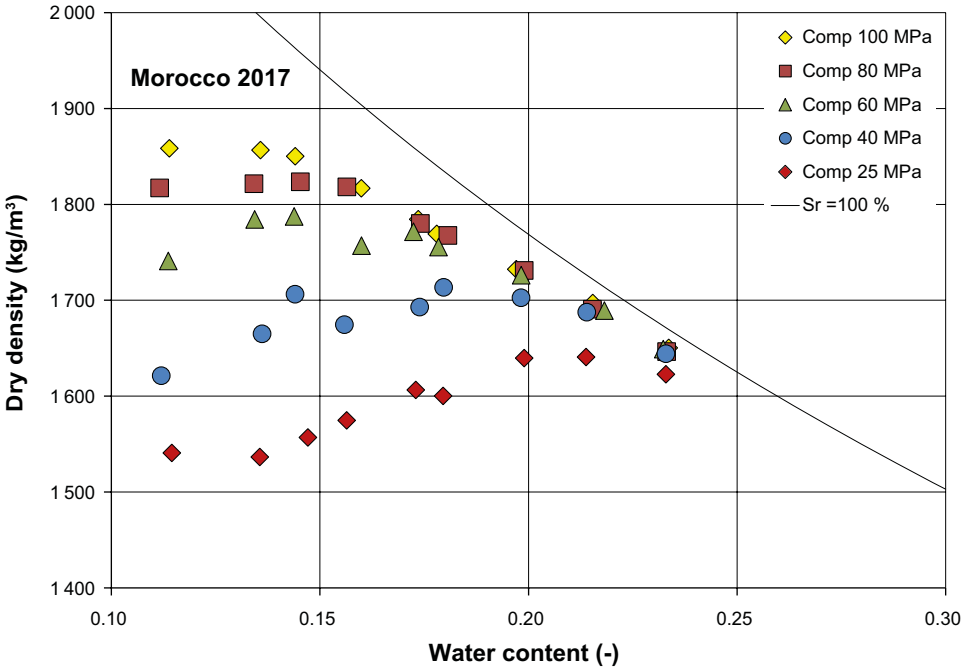

Figure R-4. *Determined dry density as function of both water content and compaction pressure for the bentonite Morocco 2017.*

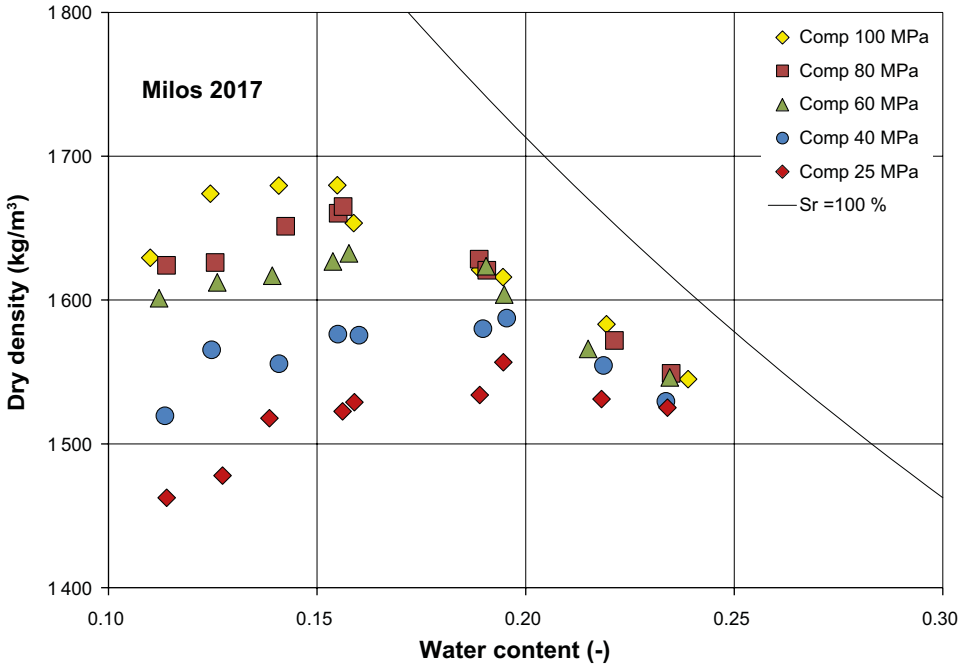

Figure R-5. *Determined dry density as function of both water content and compaction pressure for the bentonite Milos 2017.*

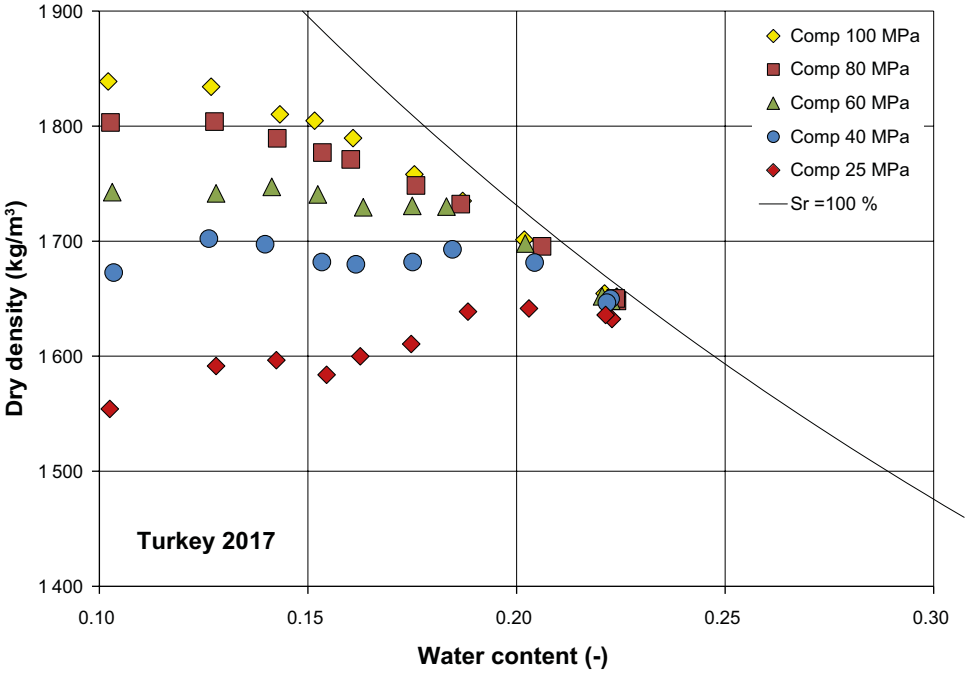

Figure R-6. *Determined dry density as function of both water content and compaction pressure for the bentonite Turkey 2017.*

Arkitektkopia AB, Bromma, 2020

SKB is responsible for managing spent nuclear fuel and radioactive waste produced by the Swedish nuclear power plants such that man and the environment are protected in the near and distant future.

skb.se